Strength and Reliability of Aluminium Stiffened Panels

By

Matthew Collette

Submitted for the degree of Doctor of Philosophy

June 2005
School of Marine Science and Technology
Faculty of Science, Agriculture and Engineering
University of Newcastle
Newcastle upon Tyne

THESIS CONTAINS

VIDEO CD DVD TAPE CASSETTE

School of Marine Science and Technology
Armstrong Building
University of Newcastle
Newcastle upon Tyne
NE1 7RU
United Kingdom
http://www.ncl.ac.uk/marine

Abstract

The objective of this thesis is to develop improved reliability-based structural design methods for stiffened aluminium panels in high-speed vessels. In recent years aluminium high-speed vessels have grown larger and are venturing into increasingly hostile operating environments. Designing such vessels requires structural prediction techniques capable of producing a light structure with high confidence in its strength and safety. However, current aluminium marine structural design methods are largely simple modifications of steel methods that do not account for all of the differences between aluminium and steel. This thesis presents new reliability-based design techniques for the ultimate strength and fatigue strength of aluminium stiffened panels. A review of recent aluminium high-speed vessels is made, along with their structural configuration and hydrodynamic loading. Structural reliability techniques are discussed. Existing prediction methods, including marine approaches and civil engineering design codes are compared to experimental results for the compressive collapse of aluminium plates and stiffened panels. A modified technique is proposed to model the compressive collapse of such panels. The tensile response of welded aluminium structures is investigated, including the influence of strain concentration in the reduced-strength region around welds. Reliability formulations are presented and discussed for ultimate strength predictions. A reliability based hot-spot S-N fatigue prediction method is developed for welded connections, including an analysis of the material and prediction uncertainty values and a comparison with existing design codes. Discussion of extending the fatigue prediction techniques to include through-life initiation-propagation fatigue models are presented, along with a simple trial application to butt welds. Conclusions from the techniques investigated are presented, and potential future developments are discussed.

Acknowledgements

The work behind this thesis was carried out at the University of Newcastle during the period of 2001 to 2005. During this period of time I was fortunate to receive support from many people across the globe. My supervisor, Professor Atilla Incecik, must come first in this list for his tireless support of my work which he provide regardless of the extensive other calls on his time. My compatriots at the School of Marine Science and Technology have provided much fruitful discussion and support as well; special thanks in alphabetical order goes to Jonathan Downes, Jonathan McGregor, Ana Mesbahi, Craig Rose, and Ben Webster. I would also like to thank my external examiner, Professor Jørgen Jensen, and my internal examiner, Dr. Yongchang Pu, for their suggestions and comments which have improved this thesis.

Without the funding and support of a Graduate Research Fellowships from National Science Foundation in the United States, I would not have been able to attend the University of Newcastle for this degree, and their support is gratefully acknowledged. Once in Newcastle, the Safety@Speed project allowed me to participate in discussions which high-speed vessel operators, builders, designers, and consultants across Europe; this exposure significantly enhanced this thesis. My thanks goes to the European Commission for funding this work under contract G3RD-CT-2001-00331, and all the participants in this project for their contribution to my understanding of aluminium design and the world of high-speed ferries.

Several people helped move my research forward. I would like to thank John Ayres, the head librarian at The Welding Institute, for his assistance during my visits to TWI. Dr. Andrew Hinkle from ALCOA helped locate and provide me with several published and unpublished reports on all aspects of aluminium design, and I am grateful for his efforts. I was also grateful for the opportunity to collaborate on a PRADS conference paper on aluminium panels with Professor Paik from Pusan University in Korea, Alexandre Duran, and Sjoerd van der Veen from Pechiney in France.

Last, but in no way least, I would like to thank my family and Karishma for all their support and encouragement over the last four years.

Table of Contents

Table of Figures

Table of Tables

CHAPTER

1

"To achieve the goal of producing environmentally friendly, low cost, high-speed transport, weight minimization of the hull is essential"

[1]

Introduction

1.1 Overview

Since the early 1990s, the marine industry has rapidly expanded its use of aluminium, primarily for the construction of high-speed commercial and military vessels. The quest for higher speeds and cargo capacity has lead to rapid development of new designs where weight savings is critical. In these applications, the higher strength-to-weight ratio of an aluminium structure gives it an important advantage over a traditional steel structure. In the space of just over a decade, aluminium high-speed vessels (HSVs) have evolved from 30m passenger-only vessels operating in protected waters, to vessels over 120m long, carrying both passengers and vehicles, and operating on exposed routes. This rapid increase in vessel size and capability has lead to an urgent need for new engineering tools capable of investigating the hydrodynamic and structural response of these vessels. Problems such as fatigue cracking and local structural damage has plagued many aluminium HSVs, increasing their operating costs and further underlining the need for new engineering tools capable of accurately predicting such phenomenon.

While the opportunities for research on aluminium HSVs are numerous, this thesis concentrates on developing methods to estimate the ultimate strength and fatigue strength of aluminium stiffened panels. Stiffened panels form the basic building block of the structure of most vessels, including HSVs. An understanding of their behaviour has been shown to be central to estimating the ultimate strength of the hull girder[2, 3], while service experience with aluminium HSVs has shown that the failures of these panels alone, either in buckling or fatigue, is also significant[4, 5]. In developing these methods, a structural reliability approach was selected. Structural reliability is a design technique where the probability of failure is estimated considering the uncertainty in the structural analysis and actual load carrying capacity of the structure, this probability is used to determine if the structure is

adequate. Reliability techniques have become increasingly popular in all fields of structural engineering, including the marine field[6, 7]. These techniques can offer increased confidence in the safety of a design. This is especially true in rapidly developing fields, such as HSVs, where previous experience with similar designs is limited, and thus traditional safety factor techniques or experience-based design codes may not be applicable.

The remainder of this chapter will present a brief overview of the aluminium HSV fleet at present, the current applied state-of-the-art in structural design, the shortcomings of the present marine structural design methods for aluminium, and the scope of work to be presented in the remained of the thesis. The remainder of the thesis is divided into five additional chapters, Chapter 2 discusses the properties of aluminium, and the established tools and approaches for structural reliability and hydrodynamic load determination . Chapter 3 presents the work on predicting the ultimate strength of stiffened panels under uni-axial loads. Chapter 4 discusses an aluminium reliability-based fatigue method based on the traditional S-N fatigue approach. Chapter 5 covers potential developments with fracture mechanics for fatigue life estimation. Conclusions and recommendations for future work are discussed in Chapter 6.

1.2 Current Fleet of Aluminium High-Speed Vessels

Aluminium has been used to build both high and low speed vessels for several decades now. In the middle of the 20th Century, many ocean liners were built with aluminium superstructures to allow increased superstructure volume for the same weight[8]. Aluminium was also used with hydrofoils and in a handful of experiments with conventional vessel applications, including the *Alcoa Seaprobe*, an all-aluminium 74m long deepwater drilling and research vessel[9]. However, in the last 10-15 years, the market for aluminium high-speed ferries has grown significantly, marking a new phase in the use of aluminium at sea. High-speed ferries are now in service in the Americas, Australia, Far East, Middle East, and Europe. In 2004, the total fleet of high-speed ferries was estimated at 1,700 vessels[10], though this total includes composite, steel, and hybrid vessels as well as all-aluminium vessels. While the fast ferry market has ceased to expanded as quickly as it did in the 1990s, there is still significant new building activity. Table 1 shows the total number of fast ferries delivered by year, again this includes vessels in all materials, although many of these vessel would be expected to be of aluminium construction.

Table 1: Fast Ferry Deliveries by Year

Year	*Total Deliveries*	*Large Vessel* Deliveries*
2000	*42*	*13*
2001	*43*	*11*
2002	*63*	*11*
2003	*49*	*10*

Compiled from January-February issue of *Fast Ferry International*, 2001-2004

***Large is defined as carrying at least 400 passengers or 100 cars**

While the origins of the fast ferries fleet can be found in the small coastal or harbour ferries 20m-30m in length, the upper size of these vessels has increased and vessels over 100m in length and capable of carrying passengers, cars, and trucks are common today. As can be seen from Table 1, roughly 20-30% of deliveries are currently vessels of significant size. At this size, most of these vessels would be built of all-aluminium construction, though some large fast ferries have been constructed of high-tensile steel. Large aluminium high-speed ferries come in many forms, an overview of the current and proposed large aluminium high-speed ferries is presented in Table 2. These vessel are typically able to carry 900-1000 passenger and 200-300 cars, or a mix of cars and trucks. These vessels are also capable of operating in comparatively exposed areas; recently delivered vessels are operating in environments such as the Irish Sea, Canary Islands, and the Alaskan coastline.

Table 2: Large All-Aluminium Fast Ferries as of 2005

Design	*Shipyard*	*Hull Type*	*LWL* meters	*Maximum Deadweight* Tonnes	*Operating Speed* knots	*Status*
TVM115	*Rodriquez*	*Monohull*	*96.2*	*700*	*38*	*In production*
MDV1200	*Fincantieri*	*Monohull*	*88*	*365*	*36-40*	*In production*
Auto Express 101	*Austal Ships*	*Catamaran*	*88.7*	*750*	*37*	*In production*
Auto Express 126	*Austal Ships*	*Trimaran*	*114.8*	*1000*	*40*	*In production*
Evolution 10B	*Incat*	*Catamaran*	*92*	*750*	*36-40*	*In production*
Evolution 112	*Incat*	*Catamaran*	*105.6*	*1000*	*40-45*	*Proposed*

Note: Data taken from manufacture's websites and vessel documents[11-15]

In addition to commercial ferry applications discussed above, aluminium HSVs have also generated interest among the militaries of the world. The initial interest from the military was in using commercial ferries to move troops around. The United States Marine

Corp experimented with an Austal 101m Auto Express vessel, the *Westpac Express*, in 2001[16] and found that it allowed them to transport troops to training exercise quicker and more effectively than their traditional airlifts. This vessel has continued to serve in this role, winning a 36-month charter contract in early 2002[16]. About the same time, the U.S. Army and the U.S. Navy were experimenting with a similarly-sized Incat catamaran based on the Evolution 10B design, the *Joint Venture*. Positive experiences with both vessels have lead to several follow-on projects. The *Joint Venture* has been complimented by a second vessel of similar design, the *Swift*. Unlike the *Westpac Express*, both of these vessels have been heavily modified from commercial service, and now include limited military features such as helicopter landing decks. These two vessels have participated in various training exercises and actual deployments, ranging from Norwegian Fjords to the Persian Gulf. The U.S. Army has also commissioned an additional transport catamaran the *Spearhead*, with discussions on potentially acquiring up to 17 similar vessels[17].

This interest has lead to several aluminium research vessels being commissioned by the Office of Naval Research(ONR) in the U.S. The largest is the X-craft, a 73m LWL, 50 knot all-aluminium catamaran designed to help evaluate the mission effectiveness and hydrodynamic, propulsion, and structural performance of this type of vessel[18]. Additionally, aluminium high-speed vessels are now being considered for combat roles in addition to transportation roles. A partnership including Austal Ships has proposed a variant of the Auto Express 126 design for the U.S. Navy's Littoral Combat Ship, and has won sufficient funding to construct a single-ship demonstrator. The competitor to this vessel is a monohull of high-tensile steel construction with an aluminium superstructure; indicating that whatever team wins the project competition, a significant use of aluminium in a naval combatant is again likely. Following on this interest, both Incat and Austal have established partnerships with U.S. Shipyards to allow them to build vessels for the U.S. Navy; they have also prepared design studies for a wide range of naval vessels based on their existing catamaran and trimaran commercial ferries.

With significant commercial and military interest in large aluminium HSVs, it is clear that a different category of structural design methodology is needed to design a large aluminium HSV today, compared to what was required to design a 20m-30m aluminium passenger-only ferry 15 years ago. The increase in length will result in an increased importance in global structural response over local structural response[1], requiring tools capable of predicting this type of behaviour. Commercial operators are interested in deploying these vessels on more exposed routes, and military deployments often require crossing entire oceans. Such operating environments are far rougher than the protected

routes common 15 years ago, placing higher demands on the structure. Additionally, as there is a strong competition between builders to offer vessels with the highest possible deadweight at the highest possible speed, there is pressure to reduce the structural scantlings to the minimum required for service to minimize lightweight. This provides motivation to develop advanced structural analysis tools to optimize the structural design as much as possible[1]. And finally, as the vessels carry more people and operate further offshore, the safety implications of a structural failure are also higher, further reinforcing the need for advanced structural design tools to guarantee the safety of this type of vessel.

The need for more advanced analysis tools has also been clearly demonstrated by the comparatively frequent incidents of structural damage in service for the large HSVs. An initial risk assessment of high-speed vessels carried out as part of the E.U. funded 5th Framework research project Safety@Speed determined that there was a substantial risk of structural damage to HSVs, especially local damage[19]. Conversations the author has had with operators and shipyards in both Europe and the U.S. has confirmed that aluminium HSVs frequently suffer local structural buckling and deformation, as well as extensive fatigue cracking in service. Unfortunately, for confidentiality reasons, the vessels involved cannot be referenced here, however typical fatigue crack failures may be available in the future when the Ship Structure Committee completes project SR-1434, "In-Service Performance of Aluminum Structural Details". An open-literature example of panel buckling experienced from global wave loading (slam response) on a large aluminium catamaran is shown below in Figure 1.

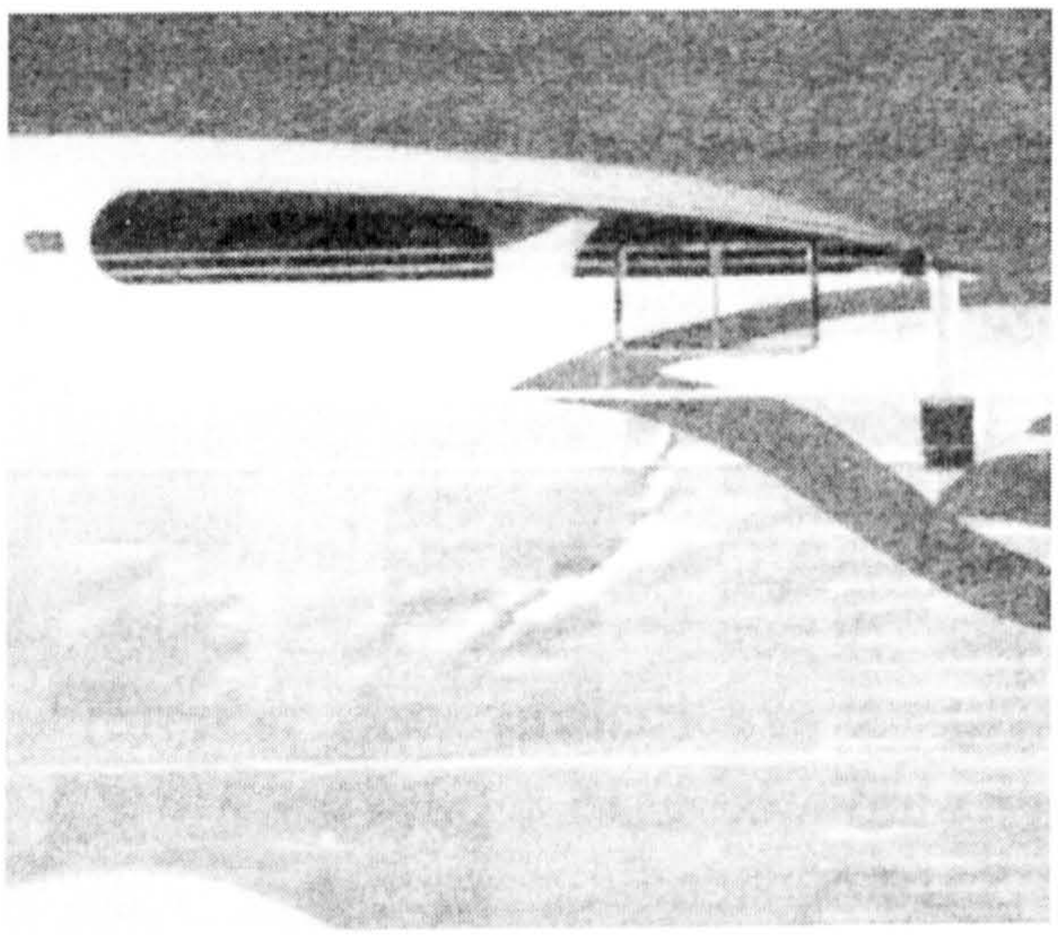

Figure 1: Failure of Aluminium Panels(From [5])

1.3 Applied State of the Art in Structural Design: Reliability-Based Design

The current technique of choice for both research and applications in advanced marine structural design has been the limit state design technique[20, 21]. In limit state design, the focus is on predicting the actual load capacity of the structure at which a failure will occur. This is termed the "limit state" of the structure. This is in contrast to allowable-stress design which preceded it, where the working stress in a structure is limited to a specific level, usually expressed as a fraction of the yield stress and determined by experience. In limit state design for marine vessels, typically three different types of limit states would be investigated. The same limit states apply for structure as a whole as well as various sub-units of the structure. The three types of limit states are listed below:

1. **Ultimate Limit State:** This is the load at which the structure collapses and can no longer serve its intended function. An example would be hull girder failure from global wave loads.
2. **Service Limit State:** The load at which the structure is damaged, though it can still accept additional loading. Repair is usually required to return the structure to an acceptable state. Examples would include fatigue cracking or permanent deformation of a stiffened panel.
3. **Accidental Limit State:** The load at which the structure fails in an accidental situation which is not within the normal operating conditions of the vessel, but which may be explicitly designed for when additional safety is required. Examples would include the structure's response in and after a grounding or collision incident. Some authors do not view accidental limit states as a separate category, instead seeing them as a subset of ultimate and service limit states.

Limit state design is usually coupled with some sort of probabilistic analysis to determine if the calculated strength is sufficient to guarantee safety in service. In its simplest form, such an analysis could compare the calculated limit state to the load expected with a specified return period, such as once in the vessel's lifetime. A more advanced approach might consider levels of confidence in the estimate of both the limit state and the applied loading, typically comparing a load and limit state estimate with a fixed probability of exceedance. Such an approach is termed characteristic value approach and is discussed by Hughes[21]. Reliability-based design represents a more complex probabilistic approach, where uncertainties in the limit state, the applied loading, and modelling of each phenomenon would be included, and an explicit calculation of the probability of failure in

service would be made. While reliability approaches require both more data and more effort by the engineer, they have become increasingly popular, and many experimental applications have been made to ship structures, including the work of Mansour et al.[6, 22] and a recent application to naval vessels by Ayyub et al[7].

From this body of previous work, a common series of limit states has emerged which must be evaluated in the structural design process, namely, overall hull girder collapse (*primary behaviour*), collapse of large stiffened panels (*secondary behaviour*), collapse of the plating between stiffeners (*tertiary behaviour*) and fatigue failures in the structure[6]. The first three limit states represent ultimate limit states, and the final limit state is a service limit state. These four limit states do not represent all of the limit states for the complex structure of a vessel, others such as the collapse of pillars or web frames are also significant, yet have not attracted as much research attention to date. However, the four limit states presented above are central to the design of the overall structure of the vessel and to the selection of the majority of structural members, such as shell plating and longitudinal stiffeners. Because of this significance, it does not seem unreasonable that they have been the focus of research attention to date.

The most catastrophic ultimate limit state is hull girder collapse, which addresses the maximum resisting load the hull girder can generate before it collapse, potentially severing the ship into two parts. Based on the severity of such a failure, ensuring adequate reserve in this limit state is one of the central tasks in structural design. This limit state is now being explicitly evaluated in the new classification society rules, such as the Joint Tanker Project rules from ABS, DNV, and Lloyd's Register[23]. Typically, in this limit state the hull girder would be loaded by a combination of horizontal and vertical bending, shear forces, torsion, and lateral pressures; though in some situations one of these load components can be viewed as dominate and the problem simplified. For steel, there are several methods capable of estimating the hull girder ultimate limit state, these methods have been extensively reviewed and compared over the past decade by the periodic International Ship and Offshore Structures Congress(ISSC)[24-27]. A brief overview of these methods will be presented here, roughly in order of complexity:

- **Empirical Formulae:** These approaches attempt to calculate the ultimate strength either by modifying the elastic yield moment by knock-down factors to account for buckling[28], or by assuming a stress distribution across the midship section at failure[29].
- **Beam-Column Progressive Collapse:** In these models, the midship section is broken up into elements consisting of a stiffener plus its attached plating and

plain plate elements. Stress vs. strain curves are computed for each element, treating the stiffener and attached plate as a combined beam-column. The hull girder ultimate strength is calculated by applying incremental curvatures to the midship section, and calculating the corresponding resisting moment by calculating the strain and hence the stress at each element in the midship section. Examples of this method include the approaches of Rutherford[3], Rahman and Chowdhury[30], Gordo and Soares[31], and Nielsen[32].

- **Idealized Structural Unit Method**: This approach is similar to the beam-column formulation, except that the structure is broken up into different sub-units, and typically the response of the structure is calculated in more complex terms than just axial stress-strain curves. This method could also be viewed as a simplified finite element approach, where the element have been replaced by "super-elements" to reduced the complexity of solving the problem. A discussion of this approach can be found in Chapter 13 of Paik and Thayamballi[20].
- **Non Linear Finite Element Analysis**: In this approach, the structure of the vessel is modelled directly with finite elements, typically non-linear shell elements. A typical model would include the structure between several adjacent transverse frames. The difficulty in such an approach is to make the model of the structure detailed enough so that initial imperfections and the correct failures modes will be captured, without making the model so large that solution becomes impossible. Hence, this method depends on the skill of the human analyst more so than the other approaches. Despite these difficulties, this method has been implemented successfully[33].

In evaluating the hull girder collapse limit state, determining the response of the local stiffened panels that comprise the hull girder is central to understanding the overall behaviour of the structure[2]. Additionally, the collapse of these stiffened panels is an important limit state in its own right[6, 21, 34], as they are major pieces of structure on their own. Local pressures, shear loading, and biaxial compression may be significant for the response of these local panels, especially those located near the neutral axis of the overall hull girder, and thus not as heavily loaded by global bending. Similar to hull girder collapse, a wide range of methods has been developed for predicting secondary behaviour, including empirical equations[35], beam column methods[21, 36], a variety of semi-analytical approaches[20, 37] and non-linear finite element analysis[38, 39]. Further review of these approaches can be found in the references above, as well as in the periodic ISSC reports.

The final limit state that is normally considered is fatigue cracking in the ship's structure[6, 40]. Fatigue cracking represents a significant repair cost for the owner, and is usually treated as a service limit state. However, such cracks also present the possibility of rapid hull-girder fracture should an undetected crack grow large enough, indicating that they are also related to an ultimate limit state. Typically, most design and reliability approaches to date have adopted the largely empirical stress-life, or S-N approach to fatigue life calculation, which is also used in the mechanical and civil engineering industries. Some authors have started to investigate fatigue by a crack-growth or fracture mechanics approach[41-43], though this remains more common in the offshore and aerospace design process than in the ship design process.

1.4 Limit State Design Applied to Aluminium

As an initial approach for reliability-based structural design of aluminium HSVs, developing approaches to address the four limit states, primary response, secondary response, tertiary response, and fatigue would be a logical starting point. The extensive work on these limit states for steel vessels forms a good starting point for such an approach, however, the details of the structural response will differ as aluminium behaves differently than steel. There are many differences between the two metals, and aluminium is available in a wide variety of different alloys and different tempers. The properties of aluminium are presented in detail in Chapter 2. Some of the key differences between aluminium and steel for structural response are summarized below:

- The stress-strain relationship for aluminium alloys can differ significantly from the elastic-perfectly plastic relationship normally assumed for steel. Furthermore, the stress-strain relationships can differ between different alloys of aluminium to such an extent that it needs to be accounted for in the structural design process, for example, in inelastic buckling[44].
- The equivalent yield stress, taken as the point in the stress-strain curve where the plastic component of the strain is 0.2%, is lower for many marine aluminium alloys than the yield stress of steel.
- Welding aluminium alloys can reduce the yield stress and change the shape of the stress-strain curve in the heat-affect zone (HAZ) around the weld. This effect varies between the different aluminium alloys, and between the different work-hardening and heat-treatment processes used to increase the strength of the alloys.
- The elastic modulus of aluminium is roughly 70,000 MPa, which is about a third as much as steel.

Given these differences, it is clear that the methods for estimating the limit state strength for steel structures cannot capture all of the significant aspects of the response for aluminium. In terms of hull girder collapse, the only methods available to the practicing naval architect today for aluminium construction are the non-linear finite-element method, or perhaps slightly modified ISUM methods to account for the lower elastic modulus of aluminium alloys. The situation is similarly bleak for the secondary response of stiffened panels, though at the same time as this thesis, work was underway to develop a regression equation for the axial collapse of aluminium stiffened panels[38]. Tertiary response of the structure has had slightly better coverage, with two PhD thesis on welded panels in marine alloys[45, 46]. For many of these applications, the naval architect is left using slightly modified steel approaches and hoping for the best. As the demand for larger, highly-optimized structures grows for aluminium HSVs, such an approach is becoming increasingly unsatisfactory.

The fatigue limit state has received much more attention, as fatigue cracks emerged as a problem immediately after the upswing in aluminium ferry construction in the early 1990s[47, 48]. However, these works have rarely addressed the reliability aspects of fatigue design, focusing more on different methods to predict the loading and mean strength of fatigue-prone locations. The prevalence of fatigue problems on aluminium HSVs has also raised the question of the adequacy of the existing marine approach to fatigue, which concentrates on designing the structure not to crack initially, but can give no information on the criticality of a crack once one exists, nor on the inspection and repair policy necessary to ensure safe operation of a vessel prone to fatigue cracking. To obtain such information, the influence of fatigue cracking on the structure's ultimate limit state must be quantified, requiring an approach that treats fatigue as more than a service limit state.

1.5 Objectives and Scope of this Thesis

Given the current situation with aluminium HSVs and structural design capabilities there are clearly many areas in the marine structural design process where improved prediction methods for aluminium would be beneficial. Developing methods in all such areas would take far more effort than is available within the scope of a single PhD thesis. For this thesis, it was decided to focus on developing strength and reliability methods for the response of stiffened panels, the secondary behaviour of the structure. Unlike the response of individual flat plates, there is little previous work in this area to guide naval architects. Additionally, a correct understanding of the response of the individual stiffened panels is required to estimating the overall hull girder collapse strength. Such stiffened panels also include many of the bracketed connections and welded joints that are prone to fatigue

cracking, and thus addressing the fatigue limit state is an integral part of determining stiffened panel response.

Even with the decision to focus on the secondary response of the structure, a further definition of scope is required to fit within a single PhD thesis. The general response of stiffened panels can be quite complex, as the loading may be any combination of biaxial compression, shear, and lateral pressure. Panels located in the cross-structure of a catamaran, for example, may be loaded in all these ways simultaneously. For this work, attention is restricted to cases with axial compression or tension. Additionally, aluminium structures can be assembled in many different ways, and recent developments, such as extruded sandwich panels, friction stir welding, and adhesive bonding, offer promise to develop lighter and stronger structures. To keep the scope manageable, this work will focus on traditional construction where extruded closed profiles and/or rolled plates are joined by MIG or TIG welding. These restrictions in scope are made solely to allow this work to be completed within a single PhD, and should not be taken as an indication that such load components or methods of construction are not considered important.

With the scope of the work established, it was then possible to develop a set of four objectives to guide the research behind this thesis. These objectives are:

1. To review and benchmark existing methods for predicting the compressive strength and reliability for secondary and tertiary response of aluminium structures.
2. To develop an improved approach to determine the tension and compression stress-strain relationship of aluminium stiffened panels, accounting for the differences between aluminium and steel.
3. To develop a reliability-based fatigue approach extending the existing S-N design approach.
4. To investigate a fracture-mechanics based approach for estimating the impact of fatigue on the panel's ultimate limit states.

The development of these objectives is addressed in five further chapters. Chapter 2 presents background information on aluminium, structural reliability methods and estimating the hydrodynamic of HSVs. The material in Chapter 2 does not represent new research, but forms a foundation for understanding the work that follows. Chapter 3 presents the work on ultimate compressive and tensile limit states, including a review of existing methods, and the development of the new compression and tension stress-strain curve approach. In Chapter 4, existing fatigue data in the conventional S-N approach is

used to develop a reliability-based design method for fatigue. Chapter 5 presents a study on using a through-life fracture mechanics model in place of the S-N model for fatigue, and Chapter 6 presents the conclusions and recommendations for future work.

CHAPTER

2

"If I have seen further it is by standing on the shoulders of giants"
From a letter of Isaac Newton to Robert Hooke

Background Material and Existing Tools

2.1 Introduction

The purpose of this chapter is to present background information and techniques that will support the research in the remainder of this thesis. While this information does not represent new research, and can be found spread throughout a number of reference books and articles, it was felt important to gather it in one place to aid in the understanding of the work in the chapters to follow. Three specific types of background information and tools are presented here. First, the metallurgical and mechanical properties of aluminium are presented. Aluminium is often treated as a weaker type of steel in marine structural design, a simplification which masks many of the important response characteristics of aluminium structures. To avoid this pitfall, the properties of the major marine aluminium alloys are presented in some detail. Second, the background to structural reliability theory is presented. While this thesis does not propose new approaches to reliability, it does examine methods to implement aluminium structural design via existing reliability techniques. For this reason it is important to understand those techniques. Finally, hydrodynamic load estimates are reviewed for high-speed craft. This is an area of active research, and certainly the "best" or "standard" approach for hydrodynamic loading on high-speed craft is much less well defined than the loading on large commercial vessels. The components of the loading on high-speed craft are reviewed, and potential approaches for determining each component are discussed. A simplified approach is adopted to generate lifetime loading for reference vessels used later in this thesis.

2.2 Aluminium In Shipbuilding

Aluminium has several advantages over steel for marine construction, though for marine structural applications the crucial advantages are lighter weight and better corrosion resistance. This is offset by higher material costs and generally lower strength and elastic

modulus than steel, especially the high-tensile shipbuilding steels. While aluminium alloys weigh approximately one-third as much as steel alloys, the lower equivalent yield stress and elastic modulus of aluminium means that scantlings have to be increased over steel scantling. Accounting for this geometric increase in scantlings, final aluminium structures tend to come out with a weight savings of roughly 50%[49].

Similar to the wide variety of iron and steel products, aluminium is available in many different alloys and tempers to suit needs ranging from electrical conductors to spacecraft[49]. The primary alloying elements used with aluminium are copper, manganese, silicon, magnesium, zinc, and lithium. Space is not available here to review all the properties of these various alloys and their combinations which can be found in several reference books[9, 49, 50]. For wrought alloys, there is an internationally-recognized four-digit classification system in place for identifying alloys by their chemical composition[49]. In this classification system, the 5000 and 6000 series alloys are the most common for marine applications. The primary alloying elements used in these alloys are magnesium and silicon. The resulting alloys combine reasonable cost, high strength, good corrosion resistance, and can be joined by welding. The focus in this section will be on these two type of alloys, and their uses in typical HSV structures. First the metallurgical properties of these two alloys will be presented, along with their typical use on board vessels. Then the base material and welded material strength characteristics will be reviewed. The information in this section has been complied form several reference books[49, 51, 52].

2.2.1 Alloys and Construction Techniques

2.2.1.1 5000 Series alloy

The 5000-series alloys is one of the most common aluminium alloys used in marine construction; it is typically used for shell plating. In the 5000-series, the primary alloying elements is Magnesium. The most common marine alloys within this series are 5083, 5086, 5456. A recently-developed alloy which is becoming popular is 5383 or "Sealium" which was developed by Pechiney. In these alloys, Magnesium is added to between 3.5% and 5.2% by weight, with 0.2%-1.0% of Manganese added as well. The resulting alloy has excellent corrosion resistance at moderate temperatures and good ductility, but fairly low strength. The strength of these alloys can be improved through cold-working, where they are in-elastically deforming during production, a process also known as strain-hardening. This raises the strength of alloy at the expense of ductility, which typically drops significantly. These alloys cannot be heat treated, and are often grouped with other non-heat treatable alloys in terms of behaviour.

An additional complexity is that the strain-hardening operations can reduce the compressive yield stress compared to the tensile yield stress as a result of the Bauschinger effect. For example, the U.S. Aluminium Association grade minimums for 5083-H116 are 180 MPa in compression, but 215 MPa in tension[53]. The 5000-series alloys that are high in magnesium, including the marine alloys, can suffer from age-softening, where the added strength from cold-working reduces over time. These alloys are typically stabilized in the mill after cold-working to account for this loss. Thermal welding of these alloys leads to a reduction in their strengths, as the area around the weld is partially annealed by the heat input of the welding process.

The amount of strain hardening is indicated in the alloy designation by the letter H followed by one, two, or three numbers. The first number indicates the steps performed on the alloy, such a work hardening, or work hardening plus partial annealing[49]. The second digit indicates the degree of work-hardening, and the final digit is used to differentiate different properties with the same amount of work hardening. For marine use, there are now two tempers which are acceptable for use. The most common is H116, which is a special temper roughly equivalent to the H22 or H32 temper in strength, but with an additional requirement to resist exfoliation corrosion[54, 55]. H321 is a similar temper that is now acceptable for marine use. This temper had been previously used in marine applications without the formal requirement of the exfoliation corrosion test. In the late 1990s, one mill in North America switched production processes for their 5083-H321 to a process that met the requirements of the specifications governing H321, but did not have sufficient exfoliation resistance for marine use. This change was not detected until many vessels were built with this plate, and then suffered severe corrosion and cracking in service. Estimates of the repair costs to replace this plate range between US $30-$50 million for roughly 200 vessels[54]. The ASTM standard governing H116 and H321 has now been updated to include exfoliation corrosion requirements for both tempers and make them marine-specific tempers[56]. Other tempers which may be encountered are -0 which indicates annealed material, or H111, which has similar properties but better dimensional characteristics[55]. These are quite weak compared to H116 and H321, and will rarely be used in HSVs.

2.2.1.2 6000 Series alloy

The 6000 series of alloys is also commonly encountered in marine construction. In this series, the primary alloying elements are Magnesium and Silicon, which are added so that Magnesium Silicide will be formed in the aluminium[49]. The most common alloy seen in marine construction is 6082, along with 6061, a slightly weaker version which is popular in

the North American civil engineering market. The 6000-series alloys are not as corrosion resistant as the 5000-series, but are much easier to extrude, making them attractive for producing structural shapes or integrated plate-stiffener combinations.

The metallurgy of this alloy is significantly different than the 5000 series, with heat-treatment, not cold-working, increasing the strength of the alloy. When produced, this alloy is heated to a high temperature so that the alloying elements are in solution. Then, the metal is quenched rapidly to a low temperature, leaving the Magnesium Silicide trapped in a super-saturated solution. The Magnesium Silicide will then precipitate from the aluminium which results in a stronger microstructure. When this precipitation occurs naturally over time it is referred to as natural aging. Alternatively, the quenched material can be raised to an elevated temperature for a short period of time, allowing a more rapid precipitation to occur. This process is referred to as artificial aging. By controlling the temperature and exposure time, the size of the precipitates can be controlled, allowing an alloy with optimum strength properties to be obtained. This results in an increase in strength, but a corresponding reduction in ductility. If the alloy is exposed to an elevated temperature for too long a time, the precipitates will grow in size, and the strength of the alloy will be reduced but its ductility increased. This is known as over-aging. Thermal welding of these alloys typically produces a significant drop in strength, as the added heat will over-age the metal. Heat-treatment tempers are indicated by the letter T followed by one or more letters. The common temper for 6082 or 6061 in the marine market is T6, which indicates an alloy that has been quenched and artificially aged. T4 is a weaker form that has only been quenched, with no aging. Additional numbers after the first number in a "T" specification generally refer to various stretching and stress-relief operations that are available for these alloys.

2.2.1.3 Alloy Use in Typical HSV Construction

At first glance, a typical HSV structure looks much like a conventional steel craft, with welded longitudinally stiffened plates supported by transverse web frames. Because of the different properties of the 5000 and 6000-series alloys, they tend to be used in different locations on HSV structure. 5000-series alloys are normally available in large plates, and with their increased corrosion resistance they are typically used for shell plating. Because the 5000-series is significantly harder to extrude than the 6000-series, the 6000-series are typically used for stiffeners and shallow beams. Thus the bottom and side shell plate often consist of 5000-series plate and web frames with 6000-series extruded stiffeners. 5000-series extrusions are sometimes used stiffeners, but at increased cost. Using 5000-series for

stiffeners may become more common with the advent of new marine-specific alloys and profiles, such as the 5383 Sealium discussed above.

Extruding aluminium is a relatively common and inexpensive process that is used in preference to hot-rolling to produce most aluminium beams and structural shapes[49]. Although standard sections are available, designing custom aluminium extrusions is quite inexpensive, with die and tooling costs typically measured in the hundreds or thousands of dollars, and minimum orders can be as little as 500kg of material[49, 57]. As a result of this situation, it is not unusual to see different aluminium companies or even shipyards offering semi-custom aluminium extrusion where a plate and one or two attached stiffeners are extruded as a single unit. An example of such an extrusion is shown in Figure 2. Such extrusions eliminate the need to locate and weld the stiffeners on the panel. The only joint required is a longitudinal butt weld where the sections join, which can typically be joined by automatic welding to form large flat decks very quickly and at reduced costs. Recently, some aluminium companies have begun to offer these types of decks preassembled with friction-stir welding used to join the individual extrusions[58]. Such extrusions are popular for internal decks and weatherdecks on HSVs, where the corrosion resistance of the 6000-series alloys is adequate. Custom extrusions can also be used to facilitate complex joints on the vessel, though this is less common. Sharp[9] gives and example of such an extrusion used on the *Alcoa Seaprobe*. Additionally, decks can be constructed with sandwich-panel type extrusions which eliminates the need for longitudinal stiffeners, although this complicates the joining process. Thus, while the side shell and bottom structures may be primarily 5000-series alloys, typically the upper and internal decks are 6000-series alloys.

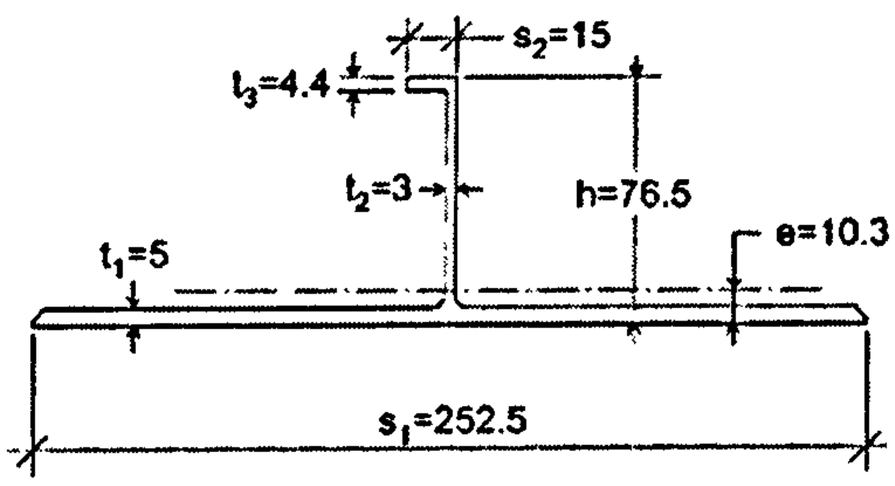

Figure 2: Aluminium Extruded Stiffener and Plate(From [59])

2.2.2 Base Material Properties

The material properties of the 5000 and 6000 aluminium alloys discussed above are significantly different than the properties of steel, and there are also important differences between the properties of the 5000 and 6000 series alloys. Perhaps the most fundamental material property for structural design is the stress-strain curve of the material. This curve

defines the limit of the material's elastic response, the material's ultimate strength, and the elastic modulus of the material, which governs elastic buckling. For steel, the stress-strain relationship can be idealized as elastic-perfectly-plastic, which means that the material stresses will increase linearly with strains according to Hooke's law until the yield stress is reached, and then will maintain the yield stress for any strain above the yield strain. While this simplification ignores the details of the behaviour near yield, it is accurate enough for most engineering work.

However, the response of aluminium significantly deviates from the elastic-perfectly-plastic assumption, following a much more rounded stress-strain curve that features neither a well-defined yield point nor a perfectly-plastic region after yield. To deal with this more complex stress-strain relationship, aluminium alloys are often described by a 0.2% offset proof stress, which can be viewed as an estimate of an equivalent yield stress for the alloy. This stress is determined by drawing a perfectly-elastic stress-strain relationship starting at a strain of 0.2% on the same plot as the aluminium stress-strain curve. The point at which the elastic line intersects the material stress-strain curve is termed the proof stress. This corresponds to point at which the plastic component of the strain is 0.2%. This is shown in Figure 3 as the heavy black line.

For more complex engineering approaches, the shape of the stress-strain curve may be significant in addition to the proof stress. In such situations, the non-linear stress-strain response of aluminium alloy can usually be approximated by the Ramberg-Osgood relationship, which expresses the strain on the curve for any stress as a combination of an elastic response and an inelastic response:

$$\varepsilon = \frac{\sigma}{E} + 0.002\left(\frac{\sigma}{\sigma_{0.2}}\right)^{n}$$

Where:

ε Strain

σ Applied stress

E Elastic modulus

$\sigma_{0.2}$ 0.2% offset proof stress

n Exponent

Equation 1

The exponent term, n, can be varied to represent different curve shapes. As the value of n rises, the curve flattens out and looks more like an elastic-perfectly-plastic curve.

Typical exponent values and minimum material properties for 5083-H116 and 6082-T6 alloys are listed below in Table 3, along with typical marine mild steel properties. The aluminium values have been taken from national code and recent papers in the area [38, 53, 60, 61], as not all national codes cover all alloys and temper combinations. The difference in

compressive and tensile proof stress for the H116 temper is taken from the U.S. *Specification*[53] . The elastic modulus for aluminium varies slightly from tension to compression, and with the alloying elements in each particular alloy[49]. However, these differences tend be small for the marine series alloys, roughly between 69,600 MPa and 71,700 MPa in compression and about 2% less in tension[49]. Based on this small difference, a standard value of 70,000 MPa has been used be throughout this thesis, which follows the approach of British Standard BS8118[61] and several previous studies in marine aluminium[38, 45]. The Ramberg-Osgood exponent in the table has been estimated from a mix of several previous experimental results[45, 62]. The exponent does show significant variation test to test[45, 62], and can change with the direction and type of applied loading as well[49], so these must be viewed as typical exponent values. The minimum elongation values have been taken from BS8118[61] and previous studies[38].

If a single Ramberg-Osgood relationship is going to be applied throughout the entire stress-strain curve, the minimum elongation cannot be selected independently from the remaining material properties. To check that the minimum elongations given are compatible with the selected values for proof stress, elastic modulus, ultimate stress, and exponent, the calculated stress at the failure strain was compared to the ultimate stress listed in the sources consulted. This comparison is shown in the last two column of Table 3, and as can be seen the agreement was quite good. The stress-strain curve corresponding to each of these values is shown below in Figure 3, along with the offset elastic line for establishing the 0.2% proof stress.

Table 3: Typical Minimum Material Properties

Alloy	*0.2% Proof Stress Tension MPa*	*0.2% Proof Stress Comp. MPa*	*Elastic Modulus MPa*	*Elongation at failure*	*Ramberg Osgood Exponent*	*Calculated Tensile Failure Stress*	*Code Tensile Failure Stress*
5083-H116	*215*	*180*	*70000*	*12%*	*12*	*302*	*305*
6082-T6	*260*	*260*	*70000*	*8%*	*30*	*294*	*290-310*
Mild Steel	*235*	*235*	*208000*	*20-30%*	*Infinite*	*--*	*--*

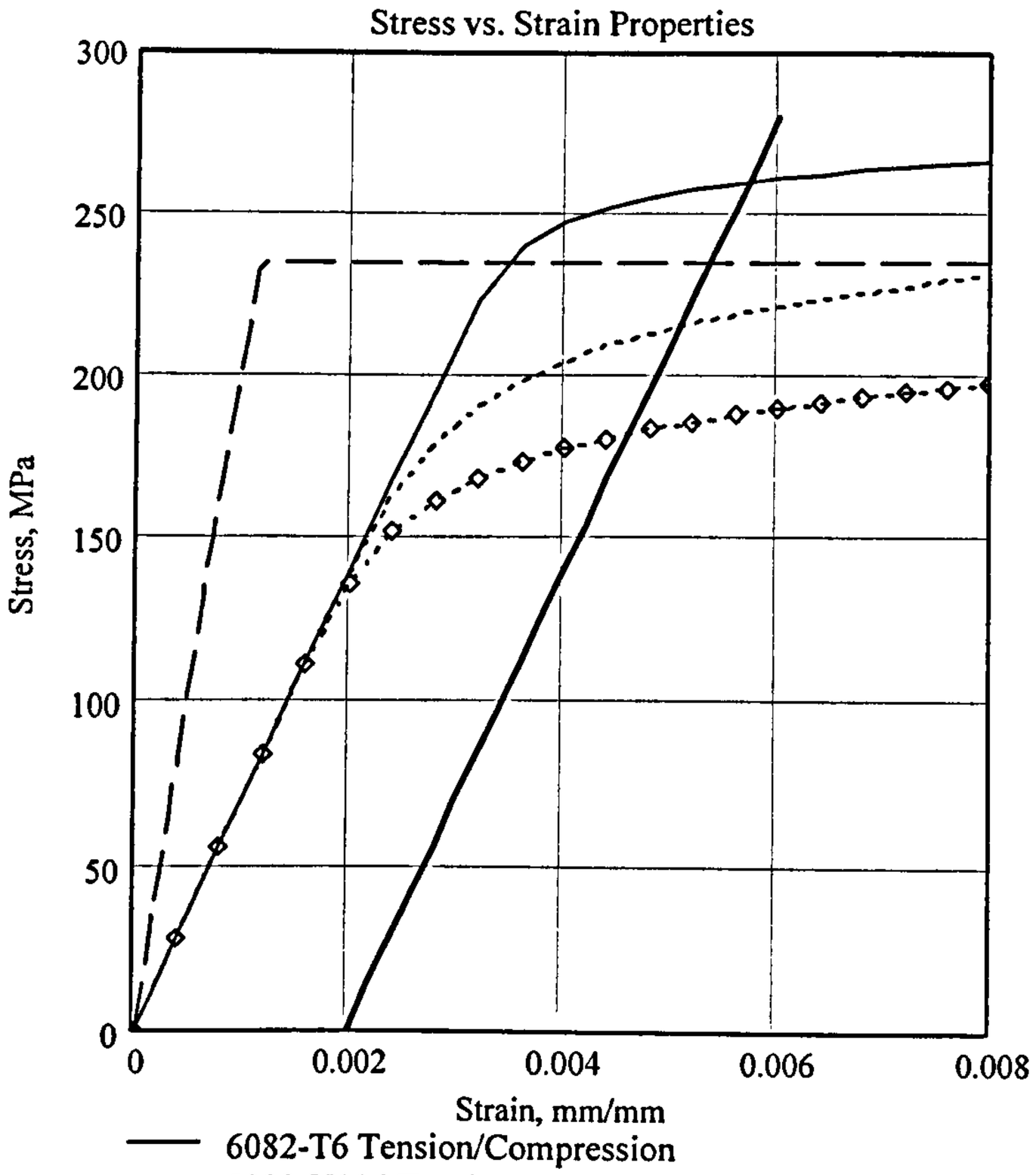

Figure 3: Stress-Strain Curve for Aluminium and Steel

The difference between aluminium and steel can clearly be seen in this plot. The elastic modulus of steel is about 3 times greater than that of aluminium, thus the steel stress-strain curves rises much more rapidly than the aluminium curve. This difference in elastic modulus also effects elastic buckling, where the elastic modulus alone determines the buckling stress, with no influence from yield stress. Thus, in the elastic response, aluminium plates and columns will behave in a much more slender manner than steel structures of equal dimensions, and have significantly lower buckling strength.

The curved nature of the aluminium stress-strain curve can also be clearly seen. A consequence of this curve response is that the aluminium alloy's response has significantly departed from the elastic region by the time the proof stress is reached. In terms of stress, this departure increases as the exponent term in the Ramberg-Osgood equation decreases. For the two alloys shown here, it is clear that the departure happens proportionately earlier for the 5083 alloy. This indicates that there is a loss of stiffness in the response of aluminium before the proof stress is reached, and that the tangent modulus of the material at the proof stress is significantly less than the elastic modulus. For the 5083-H116 alloy in tension, this

departure starts around 150 MPa, roughly 30% below the proof stress of 215 MPa. For the 6082, the departure is much later, around 230 MPa vs. a 260 MPa proof stress. After the proof stress is reached, the aluminium alloys stress-strain curves continue to rise by a significant amount. The lower the Ramberg-Osgood exponent is, the steeper the rise of the stress-strain curve after the proof stress. The differences in the stress-strain response between the 5083-H116 alloy and the 6082-T6 alloy are sufficiently different that the inelastic buckling strengths need to be evaluated separately. In the U.S. Aluminum Association approach, the inelastic buckling response is segregated by temper, with the artificially-aged precipitation-hardened alloys, which tend to have higher Ramberg-Osgood exponents, treated separately from the strain hardened or annealed alloys[49]. A final difference between steel and aluminium which must be noted is the fracture strain of each alloy, which is less for aluminium than it is for steel, though the elongation are sufficient that the material is still considered ductile. However, the lower limit of strain for aluminium is enough in some cases to influence plastic deformation capacity[63]. The material properties presented in Table 3 will be used throughout this thesis when more specific material properties are not available from experimental tests.

2.2.3 Welded Material Properties

The properties of aluminium need to be revisited if the alloys are to be welded. As described in Section 2.2.1, the marine aluminium alloys gain a large part of their strength from either cold-working or precipitation hardening. Exposure of the material to high temperatures in operations such as welding will remove some of the benefit of these treatments, resulting in a reduction to the proof stress, and potentially the ultimate stress. As the metallurgy of these two alloys differ, the effects of welding also differ. For the 5000-series alloys that have been strain-hardened, the heat input of welding is sufficient that the metal is raised above it recrystalzation temperature, and the effects of the strain-hardening are lost[52]. The resulting weld has a proof strength near the annealed strength of the alloy, though it has the ability to strain-harden significantly. For the 6000-series, welding has a different effect. Near the weld, the temperatures will be high enough that the Magnesium Silicide will go back into solution, and the weld metal and adjacent area may then naturally age after welding, recovering some strength[52]. However, at a further distance from the weld, temperatures will not have been high enough to achieve this solution, and the precipitates will overage and coarsen, resulting in a significant loss in strength[52].

As the temperature that the base metal reaches varies with distance from the weld, the mechanical properties of the alloy will differ with distance as well. For structural design

work it is customary to replace this actual property distribution with a simpler constant-property distribution using the minimum strength in the joint, but assuming it is effective over a smaller distance. This distance in terms the heat-affected zone(HAZ). This approach was proposed by Hill et al. in 1960[64], and is shown graphically in Figure 4. Note that 6000-series welds often show a partial recovery near the weld centreline as discussed above, and this graph may take a "W" shape for these alloys.

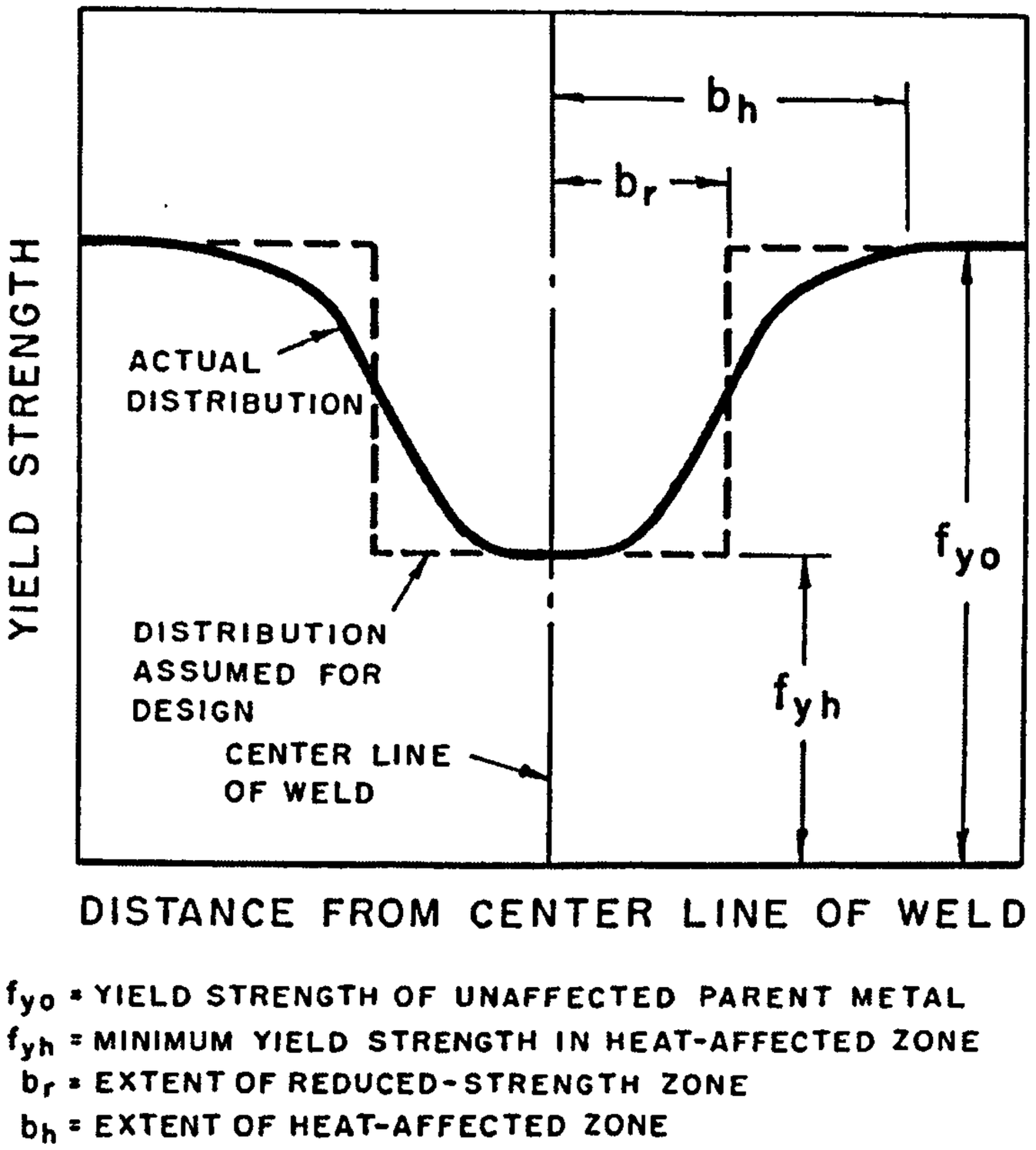

Figure 4: Effective HAZ Breadths[64]

The breadth of the HAZ assumed varies code to code, the U.S. Aluminum Association assumes a breadth of 25mm on every side of the joint, while BS8118 and Eurocode 9 have variable HAZ widths depending upon joint geometry and welding process. For thickness and processes used in marine applications, these codes typically yield HAZ breadths on the same order as the Aluminum Association's 25mm. Typical strength in this idealized HAZ are presented below in Table 4. These are taken from two recent numeric studies from Norway and Korea[38, 62] on the response of aluminium stiffened panels, with input from the DNV rules[65]. As the strain-hardened H116 temper has been annealed by welding, the HAZ proof stress will be the same in tension and compression. The variation in the Ramberg-Osgood exponent was assumed to be proportional the change in proof stress of the material[62].

Information on the change in failure strain in the HAZ is difficult come by. Measuring the elongation in four locations in the HAZ of 6082-T6 weld, Hval et al.[66] reported 3-4% gains in ductility near the weld, and 2-3% losses in ductility away from weld, though at 14% elongation, their base metal had significantly more ductility than the code minimums for this alloy. In a similar study of several specimens[67], where the HAZ was treated as a single block, the HAZ ductility increased on some specimens and decreased on others. Matusiak and Larsen[68] noted that the HAZ in 6082-T6 welds was generally less ductile then the weld metal or the base metal, though the properties varied throughout the HAZ. Mindlin[69] showed similar results for a comparison of butt welds in 5083-H113 plate, welds transverse to the applied loading had 9%-15% elongations over a two inch gauge length, while welds in parallel with the applied loading achieved 16%-22% elongation. In this thesis, the HAZ elongation at failure will be assumed to be the same as the base metal.

Similar to the base metal properties, both the calculated and code-specified ultimate tensile strength are listed in Table 2 for comparison. The calculated tensile strength for the 5083-H116 alloy is about 10% low, this might be a result of the minimum elongation not occurring simultaneously with the minimum proof stress. Raising the proof stress by 20 MPa would increase the failure stress to the code minimum. There is a wide variation in material properties for the 6082 alloy, depending on the thickness of the material and the type of joint, and the U.S. Aluminum Association recommends a further 10% reduction to these strengths for limit-state design for welds that receive only visual inspection[49]. The difference between the base and HAZ properties are shown graphically in Figure 5.

Table 4: Typical Minimum Material Properties in the HAZ

Alloy	*0.2% Proof Stress MPa*	*Elongation at failure*	*Ramberg Osgood Exponent*	*Calculated Tensile Failure Stress MPa*	*Typical Code Failure Stress MPa*
5083-H116	*144*	*12%*	*8*	*240*	*270*
6082-T6	*138*	*8%*	*16*	*173*	*162-200*

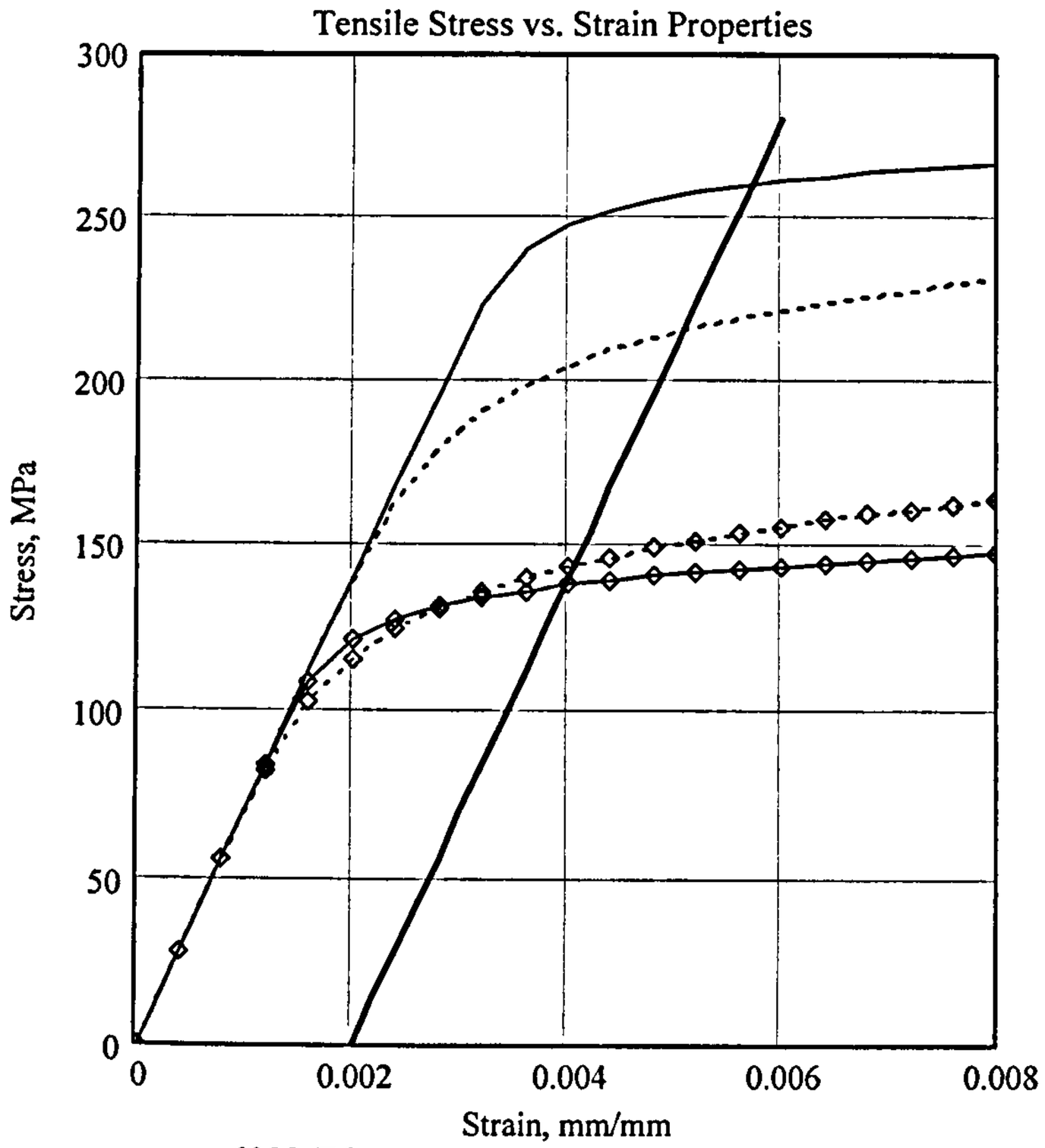

Figure 5: Tensile Stress-Strain Properties, Base and HAZ Metal

The estimate of proof stress for HAZ material depends on the geometry of the specimen used to determine the proof stress. Unless the entire tensile specimen is composed of HAZ material, the results will vary with the length over which the deformation is measured. Typically, the strain is measured by the total deformation over the gauge length, assuming uniform distribution of strain within the gauge material. However, if HAZ and base material are mixed in bands perpendicular to gauge length, such as a butt weld, this will not be the case. As the HAZ material tends to be weaker than the base material, a disproportionately high amount of deformation will occur in the HAZ material. Extending the gauge length by including more base material tends to reduce the overall strain, requiring more strain in the HAZ to obtain the 0.2% overall plastic strain required to determine the proof stress. For example, using a two inch gauge length in place of a ten inch gauge length can reduce the measured proof stress of a transverse butt weld by 25%[49].

This non-uniform distribution of strain in a welded connection is of more than passing interest to the structural design of HSV structures, which have many welds. Hval[66, 70] terms this distribution of strain "strain localization", it is also known as strain

concentration. Because the fracture strain of aluminium is low to start with, if the strain is further concentrated into a small part of the structure, the overall behaviour of the structure may begin to appear brittle, not ductile[66, 68, 70]. This can be clearly seen in the published tensile tests of transverse butt welds in aluminium. As typically the test specimen includes base material on each side of the weld as well as the weld itself, the overall specimen exhibits fracture at very low strains for a metallic material. Feng and Li[71] reported the failure strain of GMAW tensile specimen in 6082-T6 was on the order of 4%-4.5%, while the initial parent metal was 12.4%. Likewise, Strombeck et al.[72] showed a reduction from 15.6% to 3% in 6061, using an electron beam weld with a smaller HAZ than conventional welds. Matusiak and Larsen[68] showed that the overall ductility of a specimen containing a transverse weld could be significantly altered by altering the angle of the weld across the specimen. Their results are shown in Figure 6.

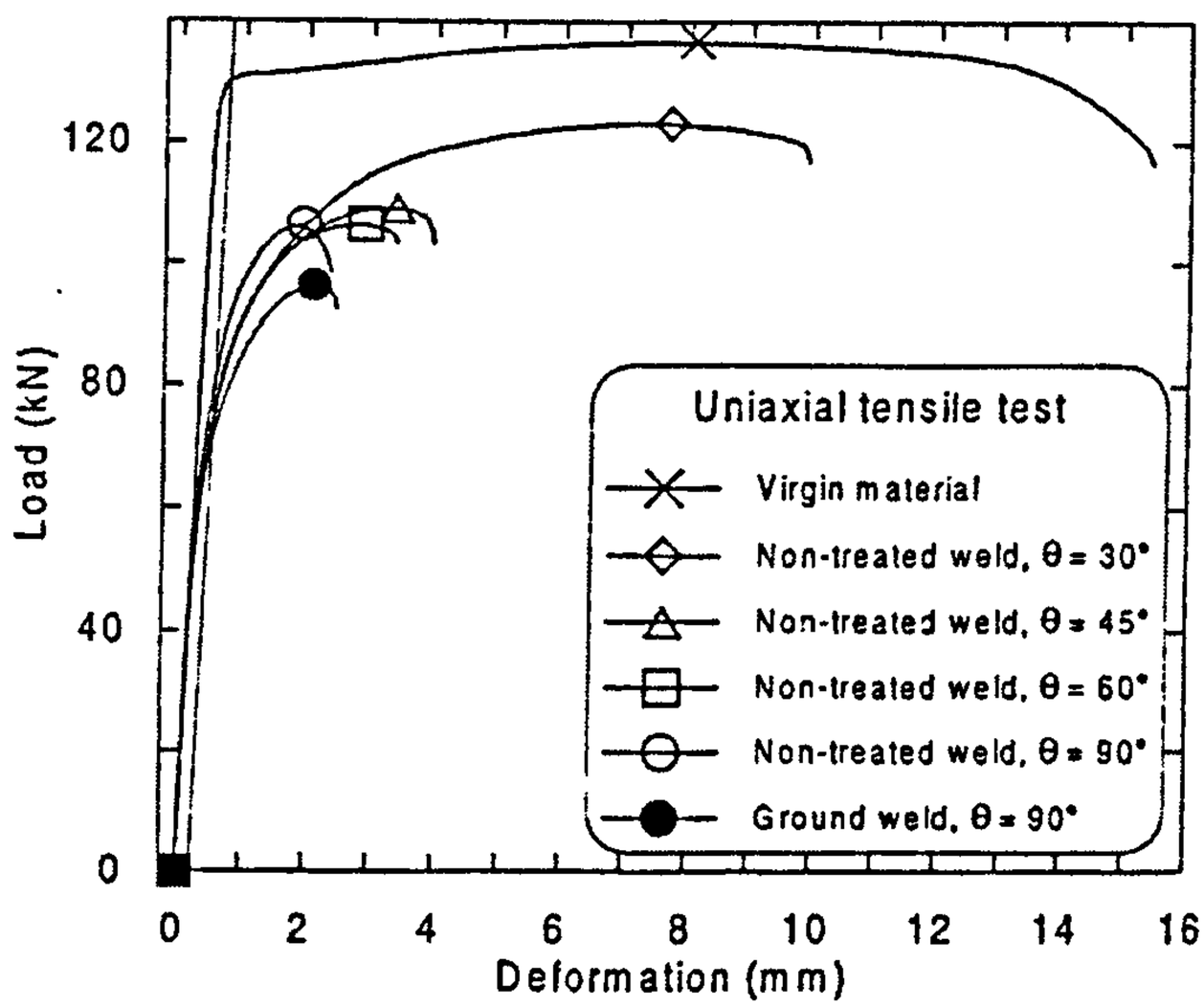

Figure 6: Deformation of Butt Weld Tensile Specimens vs. Weld Orientation[68]

This raises the potential for failures in the HAZ near the welds of large aluminium structures with little deformation. Hval et al.[70] examined this for large 6082-T6 aluminium framework structures typical of offshore process models, including both small and large scale specimen tests and numeric modelling. Hval et al. concluded in these types of structures, the plastic straining is localized in the weld regions, with significant effect on both the strength and deformation capability of the resulting member. In a smaller study on the plastic rotational capability of aluminium I beams, Moen et al.[63] studied both non-welded 6082-T6 beams and beams with a welded vertical web stiffener. All of the welded I-beam failed by fracture in the HAZ of the weld in the tension flange, without any local buckling. In contrast, the non-welded beams mostly failed by combined local and overall buckling, with only one failing by tensile fracture, and this only after significant local buckling. Moen

et al. concluded that such welds should be avoided as both strength and ductility of the beam are reduced. Based on these studies, it is clear that strain concentration could be a failure mode of concern for HSV structures. The typical HSV alloys loose a significant amount of their strength when welded, and HSV stiffened panels tend to be long compared to the length of the HAZ at the ends of the panels. Thus, inelastic strains would be expected to occur first in the HAZ, and even when the HAZ is under a high amount of strain, the overall strain in the panel may appear quite low. To develop their ultimate resisting moment, ship hull girders may require their tension and compression flanges to achieve fairly high strains, raising the risk of fracture in the HAZ. This mode of failure will be investigated further in Chapter 3.

2.3 Reliability Methods

The second area of background material for the remainder of the thesis is structural reliability. Structural reliability, which combines limit-state design and probabilistic analysis, has been an area of research for over 50 years now since the landmark paper on the subject by Freudenthal[73]. Reliability-based structural design methods such a load and resistance factor design (LRFD) have become common in many civil engineering codes, and are growing in popularity in the marine industry. Compared to conventional allowable stress or safety-factor design methods, reliability approaches attempt to determine or estimate the probability that a structure will fail by explicitly considering the uncertainty in the load and strength variables and the engineering approach used to model the structure's behavior. Adopting such an approach has several advantages. Mansour et al.[22] state that a reliability-based approach can result in a lighter structure with a more consistent level of safety. Furthermore, the sensitivity of the design's safety to the load and resistance variables can be quantified, uncertainties can be treated more rigorously, and design requirements can be adapted as new information on uncertainties come to light.

Structural reliability is perhaps best introduced by making a comparison between conventional structural design techniques and reliability-based structural design techniques. In both techniques, the goal is to ensure that the structure's capacity is greater than the loading it is expected to experience. However, in all practical structural engineering applications, neither the loading nor the structure's capacity are perfectly known. To make up for this uncertainty, conventional design techniques apply a safety factor to either the loading or the structure. For example, if a structural member is thought to be able to withstand 180 MPa of stress, and the maximum loading expected in service is 50kN, it may be designed so that the maximum stress under 50kN of load is only 120MPa, representing a safety factor of 1.5. This factor accounts for the fact that the actual loading may be higher

than 50kN, or that the actual capacity may be lower than the predicted 180 MPa. Reliability-based design takes a different approach; the stochastic properties of both the structure's capacity and applied loading are explicitly modelled, and then the probability that the structure will fail is determined. The reliability is defined as one minus the probability of failure. Continuing the example above, using reliability-based design, the loading might be represented as a normally-distributed variable with a mean of 50kN and a coefficient of variation (COV, defined as the standard deviation divided by the mean value) of 0.2, while the capacity might be defined to follow a log-normal distribution, with a mean of 180 MPa and a COV of 0.05. Then, using a reliability calculation technique, the probability that the loading would exceed the capacity would be determined. The probability of failure determined this way would be the basis of accepting or rejecting a design.

In this work, the process of determining reliability will be split into three separate steps. First, the limit state equation must be written. This is an equation of stochastic variables that determines when the structural member has failed. The traditional formulation of the limit state equation is to return positive values when there is still reserve strength left in the structure, and negative values when the structure has failed. The second step is to determine the mean value and stochastic distribution associated with the variables in the limit state equation. Much of the material in this thesis covers this step. The final step in the process is to determine or estimate the probability of failure. There are many approaches for this step, mainly because the exact determination of the probability of failure is often impractical. The techniques used in each of these three steps will be reviewed in turn in the following sections.

2.3.1 Limit State Equations

The limit state function relates the basic strength and loading variables, indicating when the structure has failed. In the general case, the limit state equation can consist of both deterministic variables, whose values are known, and stochastic variables, which can take on a range of values characterized by a probability distribution. The simplest limit state equation involves a single resistance and loading variable:

$$G(X) = R - S$$

Where :

$G(X)$ Limit state equation

X Vector of random variables, in this case R and S

R Strength of the structure

S Load applied to the structure

Equation 2

In the general case, both the load and resistance could be represented by more than one variable. Many limit states in marine design have a single strength variable from which several loads are subtracted, accounting for the various load components acting on the structure, such as still water loads, wave loads, and transient responses[6, 74]. There is also no firm requirement that the limit state function must be an explicit function; it is possible to use implicit formulation such as the results of finite element analysis, with stochastic inputs[75]. Downes and Pu[76] investigated a global hull girder collapse limit state by linking reliability procedures to a beam-column progressive collapse analysis program. Such approaches may become more common in the future, as engineers seek to incorporate advance strength prediction methods directly into reliability analysis. These approaches also allow the engineers to study the sensitivity of the design's reliability to the basic stochastic parameters such as material properties and geometric tolerances.

2.3.2 Modelling of Loading and Strength Variables

The second step in determining reliability is to assign mean values and uncertainties to each of the variables in the limit state equation. Determining the mean strength of aluminium structures is discussed at length in Chapters 3, 4, and 5, and will not be covered here, while loading is discussed in Section 2.4. This section will concentrate on presenting the types of distributions typically used to model strength and loading variables in the limit state equation. Four of the most commonly used distributions are the Normal, Lognormal, Weibull, and Gumbel distributions. The Normal and Lognormal distributions are often used to represent material properties or strength estimates[77], the advantage of the lognormal distribution is that it excludes negative values. The Weibull distribution has been shown to be a good fit for the distribution of the individual peak values of wave induced bending moments in a ship's hull[78, 79], while the Gumbel distribution is often used to represent the distribution of the extreme load in a vessel's life[78]. Each of these distributions is defined by a probability density function (PDF), which determines the probability of any particular value in the distribution occurring. The PDF can be integrated to yield the cumulative distribution function (CDF), which determines the total probability of any particular value and all values less than this value in the distribution occurring. The cumulative distribution functions for the Normal and Lognormal distributions are not easy to evaluate, and are usually found via suitable transforms of the standard normal distribution tables. The properties of these distributions are given below in Table 5 and Table 6.

Table 5: Properties of the Normal and Lognormal Distributions

Distribution	*Normal*	*Lognormal*
Parameters	μ_x, σ_x	λ_x, ς_x
Range of x	$-\infty < x < \infty$	$0 \le x < \infty$
Probability Density Function, $f_X(x)$	$\frac{1}{\sigma_x\sqrt{2\pi}}\exp\left(-\frac{1}{2}\left(\frac{x-\mu_x}{\sigma_x}\right)^2\right)$	$\frac{1}{\varsigma_x x\sqrt{2\pi}}\exp\left(-\frac{1}{2}\left(\frac{\ln(x)-\lambda_x}{\varsigma_x}\right)^2\right)$
Cumulative Distribution Function, $F_X(x)$	$\int_{-\infty}^{x} f_x(x)dx$	$\int_{-\infty}^{x} f_x(x)dx$
Mean	μ_x	$\exp\left(\lambda+\frac{1}{2}\varsigma^2\right)$
Variance	$\sigma_x^{\,2}$	$\left(\exp\left(\lambda+\frac{1}{2}\varsigma^2\right)\right)^2\left(\exp(\varsigma^2)-1\right)$
Source	*Eq. 4.1-4.2[80]*	*Eq. A60-A63[81]*

Table 6: Weibull and Gumbel Distributions

Distribution	*Weibull*	*Gumbel*
Parameters	α, β	x_n, σ
Range of x	$0 \le x < \infty$	$-\infty < x < \infty$
Probability Density Function, $f_X(x)$	$\left(\frac{x}{\alpha}\right)^{\beta}\frac{\beta}{x}\exp\left(-\left(\frac{x}{\alpha}\right)^{\beta}\right)$	$\frac{1}{\sigma}\exp\left(-\frac{(x-x_n)}{\sigma}\right)F(x)$
Cumulative Distribution Function, $F_X(x)$	$1-\exp\left(-\left(\frac{x}{\alpha}\right)^{\beta}\right)$	$\exp\left(-\exp\left(-\frac{(x-x_n)}{\sigma}\right)\right)$
Mean	$\alpha\Gamma\left(1+\frac{1}{\beta}\right)$	$x_n + C\sigma$ $C \approx 0.5772$
Variance	$\alpha^2\left(\Gamma\left(1+\frac{2}{\beta}\right)-\left(\Gamma\left(1+\frac{1}{\beta}\right)\right)^2\right)$	$\frac{\pi^2}{6}\sigma^2$
Source	*Eq. 3.38-3.39[78]*	*Eq. 3.51-3.54[78]*

2.3.3 Determination or Estimation of the Probability of Failure

Once the limit state equation has been determined, and the mean value and stochastic distribution assigned to each variable in the distribution, the probability that the limit state equation is less than zero must be determined. This final step is often the most complex, as the limit state equations may involved several (or perhaps hundreds[76]) of variables. Additionally, the variables may be statistically correlated, further adding to the complexity of this task. In many cases, an exact determination of the probability of failure is impractical, so approximate methods are needed. This section will review several techniques for predicting the probability of failure. Direct solution methods will be briefly reviewed, followed by estimation techniques including Monte Carlo simulation, first-order reliability methods (FOR), second-order reliability methods, and response surface methods. The primary focus will be on the FOR and Monte Carlo techniques, which will be used later in this thesis.

2.3.3.1 Direct Solutions

For certain simple limit states, it is possible to determine the probability of failure by integrating the joint probability density distribution of the variables in the limit state over the failure region specified by the limit state equation. This process is demonstrated graphically for a simple two-variable limit state equation such as Equation 2 , in Figure 7. The joint probability distribution of the resistance (R) and load (S) variables is plotted in the centre of the figure, and the limit state equation is plotted as a straight line. The probability of failure can be determined by integrating the joint probability density distribution over the region where the limit state is less than 0, the failure domain on the left side of the figure.

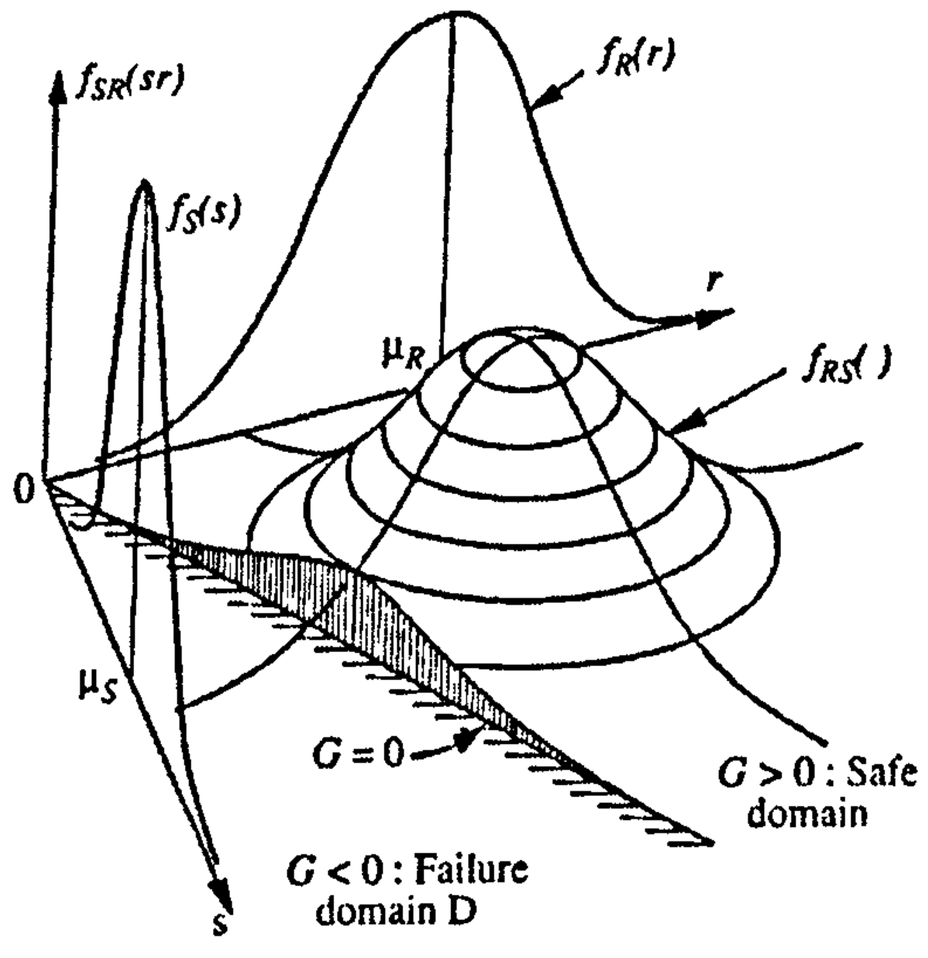

Figure 7: Determining the Probability of Failure[81]

If the load and resistance variables are assumed to be independent, the integration of the joint density distribution can be replaced by a simpler convolution integral based on the marginal probability distributions, and the probability of failure determined directly:

$$p_f = \int_{-\infty}^{\infty} F_R(x) f_S(x) dx$$

Where:

p_f Probability of failure

$F_R(x)$ Cumulativedistribution function of strength

$f_S(x)$ Probability density function of load

Equation 3

For problems involving correlated variables, or more than two variables, it is usually not straightforward to apply the direct approach. As this includes most structural limit states of interest, alternative approaches must be used. Each of these approaches attempts to simplify the fundamental problem shown in Figure 7.

2.3.3.2 Monte Carlo Simulation

A simple, but computationally-intense, method of estimating the probability of failure is to simulate the limit state equation many times and count the number of times the limit state equation indicates failure. The estimated probability of failure can be determined by the observed failures divided by the number of total observations:

$$p_f \approx \frac{n_f}{N}$$

Where:

p_f Probability of failure

n_f Numberof failuresobserved

N Numberof trials

Equation 4

Such an approach is known as Monte Carlo simulation, and is fairly straightforward to implement via computer programs where a large number of simulations can be performed quickly. For structural reliability problems, where expected probabilities of failure are quite small, often on the order of 10^{-3} to 10^{-5}, it is clear that a large number of trials will be necessary, especially as confidence in the accuracy of the estimate rises as the number of observed failures rises.

To implement Monte Carlo methods requires a large pool of random number to generate the values of the stochastic variables in the limit state equation. For practical implementations, computer-based pseudo random number generators are used for this purpose. These are not truly random numbers, but rather a finite-length sequence of numbers generated by an equation that have similar statistical properties to truly random

numbers. The standard generators most widely used are linear congruential generators. However, care must be taken in the choice of generator, as many library or "standard" generators are particularly poor implementations that will be marred by short periods (sequence lengths), and poor multi-dimensional distribution properties, as discussed in Section 7.1 of *Numerical Recipes in C*[82]. All of these type of generators are marked by serial correlation between successive calls, which means that a very small return value is followed by a smaller-than-average return value[82]. While it is hard to tell what impact these shortcomings would have on reliability analysis, it was decided to use more advanced generators in this work, even though they are slower. Most of the numerical work done was done based on the generator "ran2" in *Numerical Recipes in C*[82]. This generator achieves a very long period ($\approx 10^{18}$) by combining two linear congruential sequences, and uses as shuffle table to break up serial correlation. No significant difference was seen in the simulation results when other advanced linear generators were used, including the open-source tt800 generator[83]. All of these generators produce uniformly-distributed numbers between 0 and 1, which then must be transformed into the distribution of each stochastic variable. This transform can be done via the inverse cumulative distribution function. For the normal and lognormal distribution where the cumulative distribution function is difficult to work with, the Box-Muller transform technique was used[81].

At some point the Monte Carlo simulation must be stopped, however, it is difficult to know for sure how many simulations are enough to guarantee sufficient accuracy. In this work, the simulation was stopped when the results passed two different tests. The first was a simple running plot of the estimated probability of failure against number of simulations, as recommended by Melchers[81]. This should show the estimated probability of failure converging to the actual value as the number of simulations increase, which was observed in practice. However, in this technique, the estimate tends to bounce around actual probability of failure, so a second criteria was introduced which directly estimates the coefficient of variation(COV) of the estimated probability of failure:

$$COV(p_f) \approx \frac{\sqrt{\frac{(1-p_f)p_f}{N}}}{p_f}$$

Equation 5

Where:

p_f Probability of failure

N Number of trials

This approach is recommended by Haldar and Mahadevan[75], and is based upon the assumption that each simulation can be treated as a Bernoulli trial, and that the number of failures should follow the binomial distribution. A COV of 0.03 was used as a stopping

criteria, although in practice usually a lower COV was obtained in all cases bar those with very low probabilities of failure. There are several techniques which can be used to increase the efficiency of the Monte Carlo simulation by reducing the number of simulations required, such as importance sampling and directional sampling[81]. These techniques rely on additional assumptions about the limit state function. Therefore, they were not used in this work as the primary function of the Monte Carlo technique was to confirm the accuracy of other simplified methods.

2.3.3.3 First Order Reliability (FOR)

The first-order reliability techniques emerged out of efforts to find a simple method of estimating the probability of failure for linear limit state functions of several variables, initially assuming the variables follow normal distributions. The techniques have proven quite powerful for handling more complex cases involving non-normal variable, non-linear limit state functions, and correlated variables. Only a brief review of these techniques will be presented here, more information is available in the texts on structural reliability[80, 81]. For the two-variable limit state equation shown in Equation 2, if the variables are both normally distributed and independent, the probability of failure can be directly determined via:

$$p_f = \Phi(-\beta), \beta = \frac{\mu_Z}{\sigma_Z} = \frac{\mu_R - \mu_S}{\sqrt{\sigma_R{}^2 + \sigma_S^2}}$$

Where:

Φ Standard normal CDF

β Safety Index

μ_Z, σ_Z Mean and standard deviation of response (R - S)

μ_R, σ_R Mean and standard deviation of resistance

μ_S, σ_S Mean and standard deviation of loading

Equation 6

Initial efforts consisted of attempting to extend the validity of this approach to cases with many variables by using linear approximations of the failure surface at the mean values of the stochastic variables. These were used to estimate the mean and standard deviation of the response distribution, and hence the probability of failure. Such formulations had the disadvantage that for mechanically equivalent but mathematically re-arranged formulations of the limit state function different probabilities of failure would result[80]. This shortcoming was fixed in the Hasofer-Lind method, also referred to as the advanced first-order second moment method(AFOSM)[80]. In this approach, the problem is first transformed by reducing each of the stochastic variables into their standard normal form, where they have a zero mean value and standard deviation equal to one by the transform:

$$X' = \frac{X - \mu_X}{\sigma_X}$$

Where :

X' Transformed value

X Original Value

μ_X Mean value

σ_X Standard deviation

Equation 7

With the problem formulated in this reduced space, the safety index β, is defined as the least distance from the origin of the reduced space to the surface of the limit state function in the reduced space. The corresponding point on the limit state function is known as the checking point, design point, or most probable point of failure. This is shown graphically for the two-variable problem in Figure 8. As can be seen from this figure, the strict relationship between β and the probability of failure from Equation 6 will only be valid for linear limit state functions. For non-linear limit state functions, a linear estimate is constructed about the checking point, which means that the probability of failure is only an estimate.

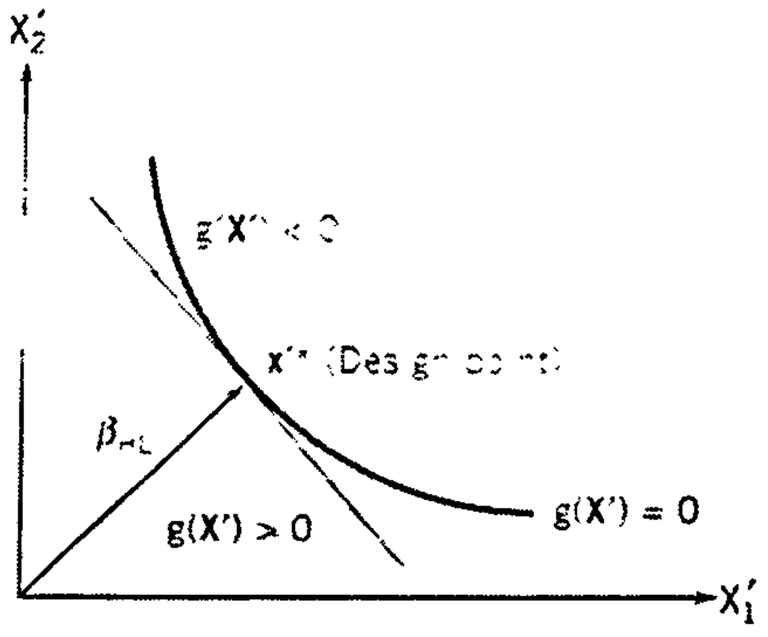

Figure 8: Definition of Safety Index, Hasofer-Lind Approach[80]

This approach can also be extended to include non-normal variables. A technique to allow such variables is the two-parameter transform, or tail-transform. This replaces the non-normally distributed variable with a normal distribution at a particular point, selected so that cumulative distribution function and probability density function of the original variable and the equivalent normal distribution are equal at this point. This requires that[80]:

$$\mu_X^N = x - \Phi^{-1}\left[F_X(x)\right]\sigma_X^N$$

$$\sigma_X^N = \frac{\phi\left\{\Phi^{-1}\left[F_X(x)\right]\right\}}{f_X(x)}$$

Where:

ϕ Standard normal PDF

Φ^{-1} Inverse standard normal CDF

$f_X(x)$ Non - normal PDF

$F_X(x)$ Non - normal CDF

μ_X^N, σ_X^N Mean and standard deviation of equivalent normal distribution at point x

Equation 8

More advanced Rosenblatt transforms are available for correlated variables, and other supplemental techniques may be required for highly-skewed distributions in certain cases[80], but are not developed here.

The final requirement for implementing the Hasofer-Lind approach is that the design point must be determined, this can not be found via a close-form equation. As the design point is defined as the point closest to the origin, this is fundamentally a minimization problem, and there are several potential approaches. A common approach which is both efficient and reasonably robust is the Rackwitz and Fiessler algorithm[84]. This procedure uses the Newton-Rahpson approach as part of its iterative scheme. The approach consists of several steps:

Step 1: Calculate the starting checking point, X*, for the stochastic variables, X, in the limit state equation. The individual value of X* are labelled x_i * and the standard deviation is σ_i Mean values are normally a good starting point.

Step 2: Evaluate the value of the limit state function at the current checking point $G(X)=g_0$

Step 3: Calculate the value of the partial derivative of the limit state equation with respect to each of the stochastic variables. These partial derivatives are labelled g_i'

Step 4: Transform the non-normal distributions into equivalent normal distributions at the current checking point via Equation 8. Simpler formulations are available for log-normal variables[80].

Step 5: Calculate the current value of the safety index, β, and directional cosines, α, for each variable as shown:

$$x = \sum g_i'(X^*)x_i^*$$

$$\mu_x = \sum g_i'(X^*)\mu_i$$

$$\sigma_x = \left[\sum \left\{g_i'(X^*)\sigma_i\right\}^2\right]^{\frac{1}{2}} \qquad \textit{Equation 9}$$

$$\alpha_i = \frac{g_i'(X^*)\sigma_i}{\sigma_x}$$

$$\beta = -\frac{x - g_0 - \mu_x}{\sigma_x}$$

Step 6: Calculate the next checking point

$$x_i^{*(m+1)} = \mu_i - \alpha_i \beta \sigma_i \qquad \textit{Equation 10}$$

Step 7: Check if the algorithm has converged yet, based on the change in the checking point and the change in the predicted safety index, β.

$$\left|\frac{x_i^{*(m+1)} - x_i^{*(m)}}{x_i^{*(m+1)}}\right| < \varepsilon$$

$$\left|\frac{\beta^{(m+1)} - \beta^{(m)}}{\beta^{(m+1)}}\right| < \varepsilon \qquad \textit{Equation 11}$$

For the current work, the value of epsilon was set at 0.001. If convergence is not achieved, Steps 2-7 are repeated. Typically on the order of 5 iterations are required for convergence. As this approach is using the derivatives of the limit state surface to search for the minimum value, it is possible that it will not converge[80]. Additionally, it is possible that for certain rough or irregular limit state functions, it could converge to different minimum values depending on the starting point used[81]. In the use of this method in this thesis, some difficulty in convergence was experienced for highly non-linear limit state equations, however, modifying the starting point of the algorithm removed these problems. Finally, it must be remembered that value of safety index, β, determined in this manner can only give an estimate of the probability of failure via Equation 6 for non-linear limit states, though often this estimate is quite good. Limit states which are initially linear may become

non-linear when transformed into the reduced space used to determine β if non-normal variables are used via the two-parameter transform[80].

2.3.3.4 Advanced Evaluation Options

For situations where the FOR approach is not deemed adequate, there are more advanced methods for estimating the probability of failure. The first among these are the second-order reliability methods (SORM) which improves on the FOR approach by including the curvature of the limit state equation near the checking point. There are various approximating methods for including this curvature, including asymptotic approximations and quadratic approximations. Further details can be found in standard books on reliability estimation[80, 81]. An alternative, but related, approach is the response-surface approach where the limit state function is sampled at several points, and replaced with an mathematical surface, which is then used to compute the probability of failure. This approach is useful when the limit state cannot be expressed analytically but is only available via an implicit method, such as finite-element analysis. Thus a limited number of implicit (and potentially computationally-intensive) limit state function evaluations can be made to fit a surface, and then the equation of this surface can be used to determine the probability of failure. Additional information can be found in references on reliability[81] [80]. Haldar and Mahadevan have also published a book on using finite element analysis with reliability techniques which includes a discussion of response surface techniques[75].

2.4 Loading

Determining the loading on high-speed craft is one of the most pressing of current research challenges. As sufficient time was not available in this thesis to look at both the strength and loading side of the response of aluminium HSVs, only a brief overview of the topic will be presented here, along with a description of the loading approach taken to estimate loads for use in the reliability formulations later in this thesis. Initially, the types of loads and related structural response will be presented for HSVs, followed by a more detailed review of the prediction options for global loads, and an approach for predicting the long-term load distribution on the hull girder.

2.4.1 Sources of Loading on HSVs

The sources of loading on ship structures, including HSVs, are numerous and often act in combination. For typical HSVs, the components of the load will include[85, 86]:

- **Hydrostatic shell pressure:** Seawater pressures applied normal to the shell when the vessel is at rest in still water.

- **Hydrostatic bending moments and shear forces:** Arising from the difference in weight and buoyancy distribution along the ship's length.
- **Dynamic Shell Pressures:** Created by the relative motion between the vessel and the surrounding fluid. For HSVs these pressures will be non-linear, and will often include slamming components over the forward part of the vessel.
- **Global Wave-Induced Response:** Arising from the summation of the local wave-induced pressures, including global bending, shear, and torsion loads. HSVs will also experience dynamic whipping responses following a slam, and have the potential for exhibiting a springing response at certain combinations of hull girder stiffness and forward speeds. Because aluminium has a much lower elastic modulus than steel, aluminium HSVs are especially at risk for springing[87].
- **Vehicle Loads:** The internal decks of car and truck ferries will need to resist tire loading which will influence the plating and stiffener spacing selection.
- **Machinery Vibrations:** Local vibrations from machinery such as waterjets, propellers, or engines can contribute significantly to local fatigue loading.
- **Internal tank loading:** Acceleration loads and sloshing loads from tank contents which impact the tank boundaries.
- **Pressure pulses from propulsion:** When external propellers are used, cyclical pressure pulses from the propeller blades can lead to fatigue failures on the local shell plate and in the propulsion struts.
- **Residual stresses:** Residual stresses are also present in the structure from welding and assembly operations.

In the traditional load and structural response classification, these loads and the resulting structural response are divided into three hierarchal levels[34]. The primary loads and stress are the resultant loads that act on the entire hull, such as vertical bending moment or shear forces. Secondary loads and responses cover the response of grillages and panels bending between out-of-plane supports, such as a double-bottom section bending between bulkheads or a stiffened panel bending between frames. Tertiary loads and responses are those of un-stiffened plate elements. Of course, this breakdown is solely of value for the engineer calculating the loads, the actual stress at any point in a ship's structure is a complex, time-varying combination of all of these loads. To make matters worse, for HSV analysis, all of these loads can be significant, depending on the location of interest and relative length of the vessel in question[86]. For example, consider a stiffener connection in a hypothetical longitudinally-stiffened bottom panel in a forward auxiliary machinery space on a high-

speed vessel. The stress in the stiffener connection will be composed of the global response stresses from vertical bending, horizontal bending and torsional loading, which will likely include non-linear effects from bow slamming. Additionally, the local shell pressure will cause the overall bottom grillage in the space to deflect between bulkheads, and the stiffener in question to deflect between web frames. This shell pressure will also probably include non-linear effects from slamming if the space is forward in the vessel. Furthermore, the machinery in the space will be transmitting high-cycle vibratory loading to the surrounding structure when operational. On top of all of these dynamic loads, there will undoubtedly be additional residual stresses from both the welds on the stiffener itself, and longer-range assembly residual stresses from welding building modules together.

Given the complexity of the total load estimation on HSVs, it was decided to limit the scope of loading in this thesis to wave-induced loads. This is in line with most of the recent research on HSV loading. Additionally, these loads can be discussed in a more general sense than vibration loading or propeller pulse loading, both of which are heavily dependent on the local details of the structure and the exciting sources. However, it must be remembered that the total structural performance of a HSV will also be dependent on its response to local loading situations. For the wave-induced loads, a range of different prediction methods are available to estimate the loading:

- **Model and Full-Scale Measurements:** Measuring the wave loads from models in towing tanks and wave basins, and full-scale measurements on ships in service is an excellent way of determining the loads on the vessel with high confidence. However, it is very expensive and time-consuming, making such techniques more useful for final design verification than exploratory research. Full-scale measurements significantly reduce the number of load scenarios that can be safely evaluated, though full-scale measurements have been used to investigate particular aspects of the response[5].
- **Fully Non-Linear Numerical Hydrodynamic Techniques**: Time-domain models such as the 3-D Large Amplitude Motions Program (LAMPS), or non-linear strip theories can be used to predict loads with very good accuracy, but are very time-consuming in terms of model set-ups, run times, and output verification.
- **Partial Non-Linear Techniques:** Quadratic strip theory, such as that of Jensen and Pedersen[88] can include many of the sources of non-linearity that are significant for typical ocean-going vessels, such as bow flare slamming, while continuing to solve the problem in the frequency domain, as opposed to the time domain of the fully non-linear models discussed above. Such approaches have been used

previously to investigate the non-linear effects of whipping and springing on the rate of fatigue damage accumulation in HSVs[87, 89].

- **Linear Techniques:** By assuming that the response depends linearly on the wave height, linear theories significantly reduce the complexity of the sea-keeping problems. This is significant as it allows the extensive body of predictive techniques developed for linear response of an object to random excitation in other fields, such as signal processing, to be applied to estimating the response of the vessel in waves. Combined with oceanographic descriptions of sea-states in terms of power spectrums, linear techniques allow the vessel's response to be quickly determined for a wide variety of sea-states, and allows a straightforward prediction of the peak and extreme values associated with the response. Typically, the linear assumption is fairly good for most conventional ships. This assumption is more valid for the vessel motions than the loads where non-linearites are usually observed, for example in the difference responses for sagging and hogging. Linear prediction methods include both three-dimensional panel methods, and strip theories which divide the hull into transverse strips ignoring the interaction between strips. These strip theory assumptions can break down at high forward speeds, attempts to fix this shortcoming have lead to a group of 2 ½ -dimension codes, which are based on strip theory but account for forward motion. An example of which is the procedure presented by Faltinsen and Zhao[90].
- **Simplified Methods:** Several authors have proposed empirical or quasi-empirical load estimation techniques, which are very simple to use, and attempt to include some of the non-linearities that linear theory leaves out. Recent working include those of Jensen and Mansour[91] and the extensive work performed by Sikora in the United States[92-94]. Classification society rules also fall into this category, though they often only predict a peak value, not the entire load spectrum. For HSVs, some of the methods which are used in this category are impact-based theories originally developed for smaller planning boats.

The combination of high forward speed and the potential non-linear events such as bottom and bow flare slamming has made load predictions on HSVs difficult, and has resulted in damage in service in some cases[5]. Determining the loading on HSVs is thus still an area of active research. Further information on the state-of-the-art in load prediction options can be found in the discussion of the Loads committee in recent ISSC publications[25]. By focusing on linear and simplified methods, it was possible to develop

long-term load spectrums for the global response of typical HSVs for use in this thesis. The techniques and approaches used for this purpose will be presented in the next section.

2.4.2 Lifetime Loading Distribution

To investigate the reliability of an aluminium stiffened panel, the long-term load distribution on the panel must be known. For aluminium panels, both the panel's ultimate strength and the panel's fatigue strength must be determined, so it is necessary to estimate the load spectrum applied to the panel, not just the peak load value. To determine this spectrum, the "Lifetime Weighted Sea Method"[21] will be used in this thesis. In this approach, the load is first predicted in each operational condition that the HSV is likely to encounter. Then, the response in all the possible operating conditions are combined to give the long-term load spectrum which can then be used for design. In this section, a brief review of the techniques available for estimating the response of a particular load component in a particular condition will be presented first. This will be followed by a technique for combining the contribution of all conditions to determine the lifetime load spectrum of this load component. Finally, a brief discussion on combining several different types of loads is presented. More in-depth coverage of these operations can be found in Jensen[78] or Hughes[21].

2.4.2.1 Estimation of the Response in Each Condition

To determine the long-term load spectrum of a particular load component, it is first necessary to determine the load in each operational condition. Initially, the linear approach to determining this loading will be presented, followed by options for including non-linear effects. As its name implies, the linear approach attempt to solve a linearized version of the equations of motions for the vessels, making the assumption that both the motions of the vessel and the incident wave amplitudes are small. To the wave exciting forces the resisting mass, damping, and restoring forces acting on the vessel are added, and the motions are determined. These later quantities are difficult to estimate, as both the motion in the fluid and the free surface must be considered. To simplify this calculation, the vessel can be divided into transverse cross-sections, and the free surface problem is solved for each cross section, assuming that the effect of flow between sections is small. This has been shown to be a fairly good assumption for typical commercial hull forms, but must be questioned for high forward speeds. Alternative approaches include using a three-dimension panel approximation of the hull form, or extending the strip theory approach to account for some of the interaction between sections, the so-called 2 ½-dimension approach that has been used previously[90, 95].

Linear solutions are typically performed by changing from the time domain to the frequency domain, resulting in a response amplitude operator (RAO) for each response of interest. The RAO shows the response, linearized by wave height, for incoming waves of various frequencies of encounter. A sample vertical bending moment RAO is shown in Figure 9.

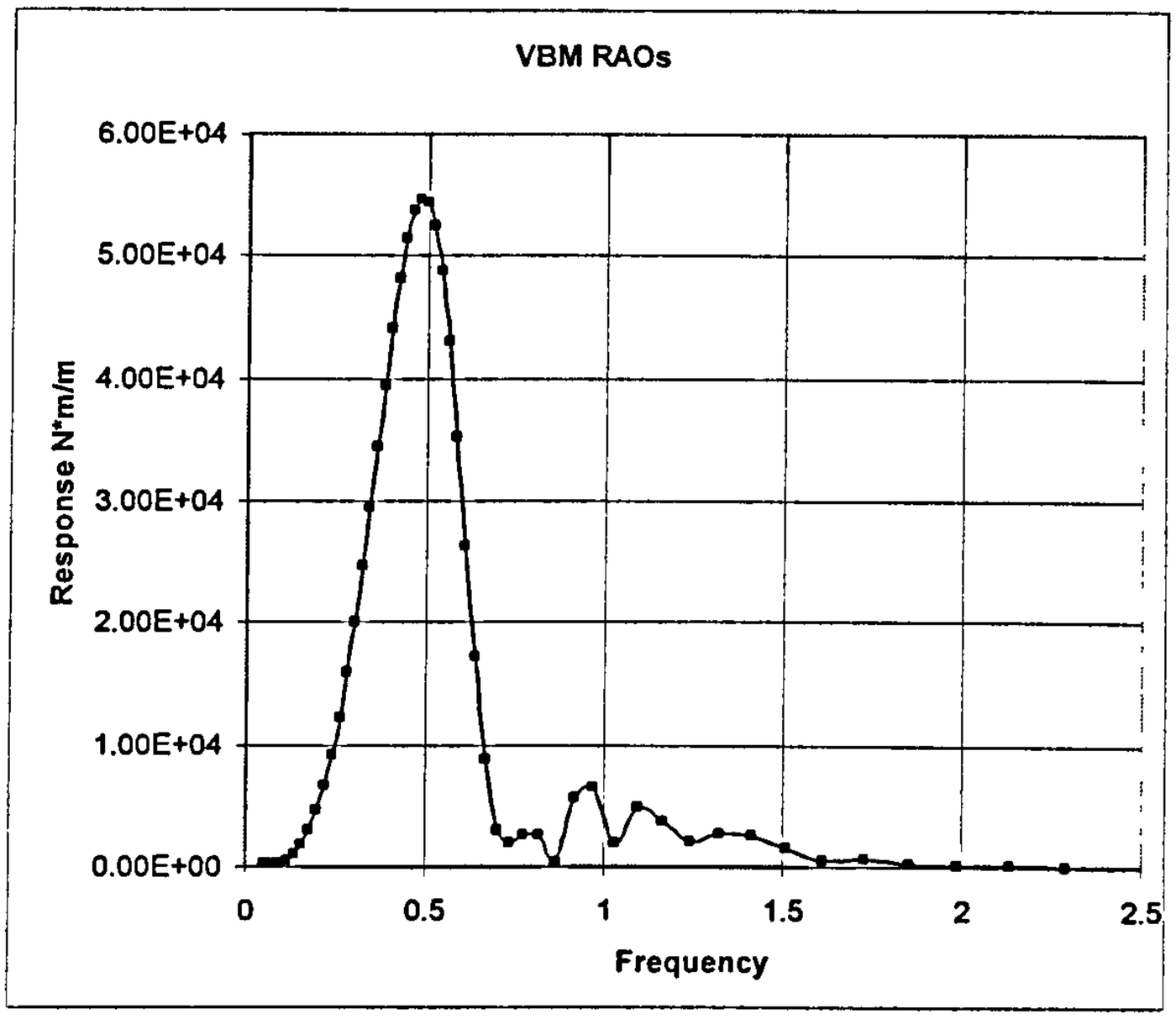

Figure 9: Sample RAO

With the RAO determined, it is straightforward to calculate the response in a complex sea-state composed of many different wave lengths, and hence frequencies. Such a sea state can be represented by a spectral density function or sea spectrum. This requires that the sea state is assumed to be restricted to a given location and a short duration, such that all of the amplitude components are constant. The spectral density is typically measured in m^2sec plotted against frequency, similar to the RAO shown in Figure 9. The sea spectrum can be thought of as a representation of the amount of energy contained in waves of various frequencies in the sea state, and the summation of all of these wave components results in the complex wave elevation profile observed at sea. Using theories of linear superposition originally developed for electronic instruments and communications[34], it is possible to determine the response spectrum for a given ship in a given sea state, from the RAO and the sea spectrum. The response spectrum is given by:

$$S_R(\omega) = RAO(\omega)^2 S_W(\omega)$$

Where :

$S_R(\omega)$ is the response spectrum at frequency ω *Equation 12*

$RAO(\omega)$ is the RAO at frequency ω

$S_W(\omega)$ is the wave spectrum at frequency ω

As can be seen, the RAO does not need to be recalculated for each sea state of interest, as a result of the assumption of linear response. This allows many potential cases to be examined quickly. The moments of the response spectrum are typically calculated in place of the of the spectrum itself, although care must be taken to be sure that both the wave spectrum and the RAO are expressed in the frequency of encounter experienced on the vessel, or a variance-preserving transform is applied to the integral used to determine the moments. With the moments of the response spectrum determined, statistical information on the response can than be determined from the response moments. The assumption of linearity in the response means that the load level at any point in time will follow a Gaussian distribution. If this linear assumption is combined with the assumption that load response is a narrow-banded response, then the distribution of the individual peaks of the response will follow the Rayleigh distribution, and the probability that any individual response, F_p, will be higher than the a given response, r, can be computed from the zero moment of the response spectrum (area) m_0:

$$F_p = \exp\left(-\frac{1}{2}\left(\frac{r}{\sqrt{m_0}}\right)^2\right) \qquad \textit{Equation 13}$$

While this approach is fairly straightforward to implement, the linear assumption made at the beginning of the approach means that the method cannot predict all of the significant aspects of the response, such as the difference between hogging and sagging bending moment responses. To include such non-linearites, one alternative is to return to the time domain, and carry out non-linear numerical calculations there. The disadvantage of such an approach is that the load estimations must now be based on statistical analysis of the predicted motions and loads which are then sensitive to the length of time the model has been run for and the details of the wave elevation trace used in the numeric simulations. An alternative approach is to return to the distribution of the load, and assume that the non-linearities induce only a small deviation from the Gaussian response, and thus by modifying the skewness and kurtosis of the distribution the non-linear effects may be included[78]. Jensen and Mansour[91] developed a closed-form expression for the long-term loading on ships, including estimating the skewness of the response based on the bow flare, speed, heading, and sea state in question. Using Gram-Charlier series or Hermite transformations,

the statistical properties of the peak loads may be obtained without resorting to time-domain analysis[78, 91]. Jensen and Pedersen[88] presented a second-order strip theory that includes the dominant non-linear effects, and can be used in a similar fashion.

An important note about including non-linearities in this way is that the springing, or a whipping and subsequent ringing response after a slam, are not included unless the hull form is modelled as flexible in the hydrodynamic formulation. These responses are typically at a higher frequency than the wave encounter frequency, and can combine with the wave-induced bending moment to result in a higher bending moment. They can also contribute additional load cycles for fatigue damage, and may make the load spectrum more broad banded. Many load prediction techniques have been extended to include flexible hulls[87, 88, 95]. Sikora presented empirical formulation to include whipping and ringing[92-94, 96], as did Jensen and Mansour[91].

2.4.2.2 Combination into Lifetime Load Response

Following the approaches discussed above, it is possible to estimate the response of a given load component in each particular operating condition. However, any vessel will experience many such conditions over its lifetime, and a technique is needed to combine all of the conditions in a logical manner. The goal of such an approach is to do this combination once, so that the resulting load spectrum can then be fitted by a single probability distribution which can then be used for the structural design work. The method presented in this section is based upon the "Lifetime Weighted Sea" method presented by Hughes[21] which is similar to the discussion in Section 4.4 of Jensen[78]. This attempts to determine the overall load profile on the vessel, which can then be used for both fatigue analysis and hull-girder ultimate strength analysis.

The approach taken combines the response in each condition via weights for the relative time of exposure in each condition. This requires knowledge of the probability of the vessel encountering each condition. There are five main variables than need to be considered when defining each condition, ship loading condition, ship speed, ship heading relative to the waves, wave height, and wave period. For HSVs in this work, it was assumed that the difference between loading conditions was small enough to be neglected in the analysis. Ship speed and heading are clearly related to wave height; in higher wave heights the vessel may slow down and adopt a particular heading relative to the waves. The relationship between speed, heading, and wave height is typically represented through an operational profile, which list the probability of each speed, heading, and wave height combination occurring. The wave environment is typically represented through a scatter

diagram, which lists the relative probability of significant wave heights and periods occurring.

HSVs typically operate under restrictions where the vessel is only allowed to sail in certain sea states. Additionally, some HSVs are fitted with an accelerometer to warn the crew when the loads on the vessel are becoming excessive. Thus, both the scatter diagram and the operational profile must be modified to account for these restrictions. Typically this could consist of removing most of the high sea-states from the scatter diagram, and keeping a few near the upper limit of the vessel's operational profile. If caught out in one of these sea states, the vessel could be assumed to slow down to minimize the loading. An initial study in this area undertaken by the author has shown the way these operational restrictions are modelled, and how carefully the crew adheres to the requirements, may influence the load profile on the vessel significantly[97]. Thus, some care should be taken in the choice of scatter diagram and operational profile.

With the operational profile and scatter diagram determined, the lifetime load spectrum of a particular load response can be estimated by a weighted-combination of all the individual responses in the individual conditions. The computational procedure for doing this is shown below, making use of the assumption of linear response and a narrow-banded process. Non-linear effects can be readily included into the same framework by adjusting the probability calculations shown in the framework to include effects such as non-zero skewness, different kurtosis values, and non-zero bandwidth as discussed above. The calculation requires a scatter diagram listing significant wave height(Hs) and period(Tz) combinations, an operational profile, and the response amplitude operator(RAO) for each speed and heading combination. The calculation procedure contains three main blocks, first the statistical properties of the load response are determined in each condition, along with the probability of each condition occurring. These are recorded for future use. The second block determines the number of load cycles experienced in each condition. The third block calculates the response magnitude with various probabilities of exceedance, so that an analytical distribution can be fitted to the measured response for future use. In this approach, the Weibull distribution is used for this fitting, as it has been shown to be a good fit for the long-term loading on ships[79]. This approach was coded as part of the computer program created in this thesis which is explained in more detail in Appendix A, although in the end this code was not used for reference vessels in this thesis as the assumption of linear response was felt to be too restrictive.

BLOCK 1

- For each wave height in scatter diagram:

- Make a list of speed, heading, RAO, and probability values from operational profile at this wave height
- **For each** period in scatter diagram at the current wave height:
  - Find the sea-state (Hs/Tz) probability of occurrence from the scatter diagram
  - Generate a wave spectrum for this sea state
  - **For each** speed/heading/RAO combination in this sea state:
    - Find the net probability of occurrence of this condition
    - Calculate the response spectrum by Equation 12
    - Calculate the area and first four moments of the response spectrum
    - Record the net probability and moments in a table of Hs/Tz/Speed/Heading combinations

BLOCK 2

- **For each** row in the Hs/Tz/Speed/Heading table:
  - Find the total time spent in this row by multiplying the net probability by the lifetime operating hours
  - Find the average zero-cross period from the area and second moment of the response spectrum. For a narrow-banded process, this is the same as the peak rate:

$$T_Z = 2\pi\sqrt{\frac{m_0}{m_2}} \qquad \textit{Equation 14}$$

  - Find the number of response cycles in this table row by dividing the operation time in this row by the zero-crossing period, and append this to the table row
- Find the total number of cycles by adding up the cycles in each row

BLOCK 3

- Iterate to find the load response levels with an overall probability of exceedance, F of 10^{-1} and 10^{-8} by root-solving the total probability of a given response determined by the weighted average of the probabilities in each condition:

$$F(r) = \frac{1}{N_{Z\_Total}} \sum_{i=1}^{Num\_Conditions} N_{ZI}\left(1.0 - \exp\left[-\frac{1}{2}\left(\frac{r}{s_{ri}}\right)^2\right]\right)$$

Where:

r : Load level to determine cumulative probability at

N_{ZI} : Number of peaks in the current condition

N_{Z_TOTAL} : Total number of peaks

s_{ri} : Standard deviation of the response specturm in this condition, $\sqrt{m_0}$

Equation 15

- Generate the probability of exceedance for 20 evenly spaced response blocks between the response at probability of exceedance levels of 10^{-1} and 10^{-8} via Equation 15
- Fit these 21 points with a Weibull distribution, using a minimization routine to minimize the sum of the square of the difference between the natural log of the calculated response exceedence probability and that of the Weibull distribution.

A final point which should be made in regards to this approach is the fitting of the Weibull distribution. By fitting evenly between 10^{-1} and 10^{-8} cumulative probabilities, the approach here is attempting to obtain a distribution that will be equally applicable for fatigue strength, which depends on the more frequent loads, and ultimate strength which depends on the highest value of load in the vessel's lifetime. It is useful to plot the actual probabilities and the Weibull fit over the entire probability range, to be sure that the fit is good in both regions before proceeding. An alternative approach would be to use separate Weibull distributions for fatigue and ultimate strength, and adjust the fitting routine so that the best fit is in the region of most interest for each type of response. For fatigue calculations, DNV specifiy that stress ranges should be determined at approximately 10^{-4} probability of exceedance. These stresses contribute the most to the lifetime fatigue damage, so errors in fitting the Weibull slope parameter using 10^{-4} as a reference probability level cause smaller errors in the resulting fatigue damage calculations[98]. Heggelund et al.[95] showed that fitting the Weibull distribution over different stress ranges could lead to a 10% difference in calculated fatigue damage for a high-speed catamaran, while Jensen and Mansour[99] showed the including whipping in the long-term load spectrum for an FPSO meant that a single Weibull distribution was not longer a good fit for the lifetime bending load spectrum.

2.4.2.3 Load Combination

The final subject which must be touched on is load combination. In this thesis, attention was restricted to global vertical hull girder bending moments. In the general case, it is necessary to combine several sources of loading. If the complete RAOs are available and the structural response is adequately modelled by linear response, it is possible to use the phase information in the RAOs to logically combine the different load components. However, this may not always be the case, and more empirical load combination procedures may be required. For fatigue analysis on conventional craft, DNV[98] assumes low correlation between vertical and horizontal bending moments, combining these with a correlation coefficient and a root-sum-of-squares approach. For combining local lateral loads and global bending, a simple linear combination is recommend taking maximum of 60% of the local plus the global load, or 60% of the global load plus the lateral load. Information on applicability of these approaches for HSVs is currently limited.

Such load combination factors can also be used to combine the various parts of the global response where they are not combined in the load prediction methodology, such as whipping and wave induced bending. Such an approach allows linear RAOs to be used to generate the response in each condition, or indeed the long-term response, and then for the non-linear effects to be incorporated after, via simplified approaches if necessary. This is the basic structure of Jensen and Mansour's simplified approach[91], and Mansour[100] discusses the use of such combination methods in a reliability-based setting.

2.4.3 Reference Vessels

For use with the structural reliability approaches introduced later in this thesis, loading information was determined on two reference vessels broadly representative of large HSVs. Attention was focused on vertical bending moment loading, and the other components of loading discussed in Section 2.4.1 were excluded. This simplification was made to reduce the complexity of the load estimate, not because the other sources of loading were assumed to be unimportant. Indeed, for the relatively short overall length of current HSVs, local loads are expected to be significant in determining the final scantlings. With this approach, the load determined can be viewed to be representative of the load experienced by the top deck of a HSV near centreline. Typically this is a passenger-only deck, and hence the lateral loading, machinery loading, and horizontal bending moments would all be expected to be small. Two vessels were considered, a nominal 120m catamaran which loading data was previously published for, and a hypothetical monohull. Each of these will be presented in turn.

2.4.3.1 120m Catamaran

The long-term stress distribution at several locations in a nominal 120m catamaran was presented at the 3rd International Forum on Aluminium Ships by Heggelund et al[95]. The catamaran's overall dimensions were based on Stena Line's HSS 1500 design, and the detailed section shapes of the hull were taken from a series of high-speed hullforms tested by Blok and Beukelman[101]. A modified version of the VERES program, a 2 ½-dimensional strip theory modified for high-forward speed effects was used, this modification included the effects of hydro-elasticity. A course global finite element model was constructed to estimate the dynamic response of the hull structure. The vessel's speed was assumed to be 31.6 knots, and a DNV scatter diagram Sc2, with a 10% probability of exceeding a 4m significant wave height, was used. 6700 operating hours a year were assumed, which at over 18 hours a day seems high for most ferry HSV operations. No speed reduction was used at higher wave heights in the scatter diagram. The long-term stress distribution in the deck was fitted with a Weibull distribution, the Weibull parameters are shown in Table 7.

Table 7: Long-Term Nominal Loading in Deck, Heggelund et al.[95] Catamaran

Weibull Scale Parameter MPa	*Weibull Shape Parameter*	*Number of Cycles*
1.32 MPa	*0.93*	*1.6-1.8*10⁸*

2.4.3.2 150m Monohull

To complement the catamaran presented above, and investigate a longer HSV, a hypothetical monohull was also created. The vessel was had a design length of 150m, based on model 5, from Table Two of Blok and Beukelman[101]. This yields a much larger vessel than vessels typical of today's HSVs, with a total displacement just over 5,400 metric tons. The vessel's required section modulus was estimated by the DNV HSLC Rules[102], again considering global loading only. The design speed of the vessel was 40 knots, and the same DNV scatter diagram, Sc2, used in the catamaran study was used for this vessel. Satisfying the global bending requirements leads to a required deck section modulus of 21.5m³ While a detailed structural design was not completed for this vessel, given its length and speed, it would be important to check that the vessel's moment of inertia is sufficient to prevent springing.

Long-term loading for this vessel was estimated by the approach developed by Jensen and Mansour[91], using the Microsoft Excel spreadsheet that accompanied their article. The default scatter diagram in the sheet was modified to the DNV Sc2 scatter diagram. Additionally, a 5m significant wave height was assumed to be the highest

operational condition at full speed. For wave heights above this level, the operational speed was assumed to drop to 5 knots, representing a survival condition. The distribution of headings within each sea state was estimated based upon profiles published by Sikora et al.[94]. For the lower wave heights, bow quartering, beam, and stern quartering seas were all assumed to be equiprobable at 25% probability, and head or stern seas were assigned a 12.5% probability. In survival conditions, bow quartering seas were strongly favored, with beam seas and stern seas excluded. The operational time per year was assumed to be 4,000 hours and the vessel's lifetime was estimated at 20 calendar years. A bow flare coefficient of 0.25 was used, as estimating this from the data in Blok and Beukelman's paper was difficult.

Based on this approach, the Jensen and Mansour spreadsheet was used to estimate the long-term vertical bending moment, both with the non-linear contribution included and excluded. In the Jensen and Mansour model, the non-linear hogging stresses are not directly calculated. These would be expected to be less than their linear values. Therefore, simply doubling the non-linear response amplitude would probably overestimate the stress range experienced by the hull girder for fatigue calculations. It is difficult to determine if the non-linear estimate is a better prediction than a purely linear prediction for fatigue response. For comparison purposes, both the linear and non-linear response, converted into stress at the deck, are listed below in Table 8, and can be compared in the reliability formulations later in this thesis. The difference is fairly small here, which may be a result of the fact that the vessel operates in lower sea-states than the conventional vessels that the method was originally developed for, and thus bow flare slamming may be less of an issue. The expression for the skewness of the response distribution in Jensen's and Mansour's formulation is linearly based on wave height and the relationships were originally derived for much larger container ships.

Table 8: Long-Term Nominal Loading in Deck, 150m Monohull

Weibull Scale Parameter MPa	*Weibull Shape Parameter*	*Number of Cycles*
3.36 (Linear)	*1.26*	*$3.2*10^7$*
3.60 (Nonlinear)	*1.21*	*$3.2*10^7$*

2.5 Conclusion

This chapter reviewed supporting tools and data from areas that will not be researched themselves in this thesis, but will be used to support the areas of research in the chapters which follow. The metallurgical and mechanical properties of the 5000 and 6000

series aluminium alloys used in typical HSVs were reviewed. The response of aluminium was compared to steel; aluminium has a much lower elastic modulus than steel, and a rounded stress-strain curve. The shape of the stress-strain curve changes with alloy. Both the 5000 and 6000 series alloys gain their strength from treatments which are partially removed by welding. The HAZ around welds is therefore an area of reduced strength. This reduced strength can lead to the phenomenon of strain concentration, where the strains in a welded aluminium structure build up disproportionately in the welds, leading to a more brittle overall response from the structure.

The fundamentals of reliability analysis were reviewed. Typical distributions used to model load and resistance variables were presented, followed by a discussion of the various solution techniques for limit state equations. Direct Monte Carlo methods were reviewed, including the need for good-quality random numbers, and techniques to verify convergence. The FOR approach was reviewed and an algorithm presented to rapidly estimate the safety index, β, of a given limit state equation. More advanced reliability techniques, including second-order formulations and response surface orientations were briefly noted. The loading on HSVs was also investigated, the total loading was shown to be composed of many different types of loads, including hydrostatic, hydrodynamic, vehicle, and machinery-related loads. The hydrodynamic loads were focused on, and methods for predicting these loads were reviewed. A calculation method for the "Lifetime Weighted Sea Approach" was presented, and then vertical hull girder bending loads were presented for two reference vessels, a 120m catamaran from the literature, and a new hypothetical 150m high-speed monohull. The techniques presented in this chapter for material response, reliability calculations, and vessel loading will be referred to from later chapters to support the analysis of aluminium stiffened panels.

CHAPTER

3

"To obtain a safe and economic structure, the limit-state-based capacity as well as structural behaviour under known loads must be assessed accurately"
[20]

Ultimate Strength: Analysis and Extension of Existing Tools

3.1 Introduction

One of the most significant limit states in reliability-based design of ship structures is the ultimate strength of the individual stiffened panels that comprise the vessel's structure. The strength of these panels determines the overall strength of the vessel's hull girder[2]. Additionally, the failure of any one of a vessel's stiffened panels is a significant structural collapse in its own right. Therefore, it is not surprising that the ultimate strength of stiffened panels has received considerable attention in the design of steel vessels. Most of this attention has focused on the behaviour of these panels in compression, as their tensile failure can be closely approximated by the stress-strain curve of the steel alloy used to fabricate the panel. However, few aluminium-specific methods have been investigated in the marine industry.

Therefore, it was decided to perform an investigation of suitability of the existing tools for predicting the ultimate strength of ship-type aluminium stiffened panels; as well as possible extensions to these existing tools to account for the aluminium-specific aspects of the response. While examining the response of stiffened panels is the ultimate goal of this chapter, it is impossible to completely separate stiffened panel response from the response of the individual plate components of the panel or the response of the overall hull girder. To address these interactions, sections are included on the strength of un-stiffened plates, and the influence of stiffened panel behaviour on overall hull girder response. Additionally, the use of these ultimate strength predictions in reliability formulations is discussed. Parts of the work presented in this chapter have been previously presented in a Safety@Speed internal report[103] and at the FAST 2003 conference[104]. The literature review is presented in the following section. The response of plates and stiffened panels are presented in Sections 3.3 and 3.4 respectively, dealing with both compression and tensile response and the various

prediction methods. The impact of the performance of plates and panels on the overall hull girder is investigated in Section 3.5, while reliability formulations are discussed in Section 3.6. Section 3.7 presents the conclusions regarding ultimate strength behaviour.

3.2 Literature Review

A literature review was conducted at the start of the research into ultimate strength to identify prediction methods and test data that would be useful in reviewing and extending ultimate strength prediction methods to aluminium. As the ultimate strength of stiffened panels plays such a central role in the overall ultimate strength of ships, there is an extensive body of research on the subject. However, at present there is substantially more information on steel structures, typical of large ocean-going vessels, than on aluminium structures. Furthermore, many of the aluminium methods share their approach with techniques initially developed for steel; so it makes sense to include works relating to both materials in this review. Therefore, the review below presents a selection of the significant papers in steel structures along with the papers on aluminium construction in chronological order, so that both the overall development of the field and the details of the current approaches to aluminium are covered.

In addition to the papers cited below, there are several useful books on the ultimate strength of stiffened panels that are good overviews of the topic and contain further reference material. While focused on steel, Paik and Thayamballi's[20] *Ultimate Limit State Design of Steel Plated Structures* is an excellent overview of the ultimate strength prediction for stiffened panels and overall structures. For buckling collapse of any metal structure, Galambos[105] *Guide to Stability Design Criteria for Metal Structures* is an excellence reference. For aluminium-specific works, Sharp's[9] *Behaviour and Design of Aluminum Structures* and Kissell and Ferry's[49] *Aluminum Structures: A Guide to Their Specification and Design* are excellent overviews of all areas of structural design, including ultimate strength in compression and tension. These two works are excellent for explaining the background of the formulations found in the U.S. Aluminum Association's[53] *Aluminum Design Manual*, which includes the Associations' *Specification* which serves as a design code for aluminium structures in the United States. In a similar vein, Mazzolani's[50] *Aluminium Structural Design* is also an excellent reference work, some of which serves as the background for parts of the European Eurocode 9[60] civil engineering design code for aluminium structures. The Eurocode 9 is also based in part on a preceding British standard, BS 8118[61], which is also a valuable source of information on aluminium design.

Concern over predicting the ultimate strength of ship hulls and their components has been expressed by naval architects for well over one hundred years; Rutherford and

Caldwell[3] mention historical calculations and discussion of the ultimate strength of ship hulls as far back as 1852. In the first half of the twenty century, several surplus destroyers were tested to collapse to investigate their overall strength and the buckling strength of their plate components[106, 107]. In a roughly contemporary timeframe, both the shipbuilding and aircraft industry developed an interest in the ultimate strength of aluminium plates and panels. The U.S. National Advisory Committee for Aeronautics (NACA), the forerunner of the present NASA, published a series of reports on the compression behaviour of aluminium plates and stiffened panels typical of aircraft structures[108-110]. At the same time, aluminium was in widespread use for the superstructures of large ocean liners, as the lower topside weight allowed more passenger space for the same vertical centre of gravity as a steel superstructure. To address the strength of these such superstructures, Muckle carried out a series of compressive collapse tests on un-stiffened plates[111], these test results were further analysed by Snaith[112]. Clark and Rolf[113] presented design formulas for the buckling of plates, columns, and beams for aluminium in civil engineering applications, summarizing several NACA publications and internal research carried out at the ALCOA company. These approaches were further extended to reliability-based LRFD equations by Chapuis and Galambos about 15 years later[114, 115].

In 1965, Professor Caldwell published a paper titled "Ultimate Longitudinal Strength"[28], which is often viewed as the start of the present analysis of the ultimate strength of ship hull girders. Caldwell's approach was to start with the standard plastic bending moment capacity of the hull girder, and adjust it by a series of reduction or knock-down factors that account for the buckling of the structure in compression before it reaches its full yield stress. Such an approach is highly simplified, and implicitly assumes that buckled panels do not undergo any further reduction in strength as the applied strain increases after they fail. Despite its simplicity, Caldwell's approach gives an understanding into the fundamental issues which are associated with predicting ultimate strength, including the importance of the compression response of the ship's panels.

Determining the compressive response of steel stiffened panels became a major area of research, driven both by the marine field and the civil engineering field, where unexpected compressive stiffened panel failures occurred in four different box-girder bridges in Vienna, Milford Haven, Melbourne, and Koblenz between 1969 and 1971[116]. Several experimental test programs were carried out on steel stiffened panels, ranging from small-scale models to full-size panels several stiffeners wide and several frame bays long. Murray reported on test from Monash[117] while Horne et al. reported on work from Manchester[118, 119] . Faulkner[120] reported on an extensive test program on tee and flat

bar stiffened panels while Smith[121] reported on the test results of several large ship-type grillages four to five frame bays in length, under both axial compression and compression and lateral pressure. There have been several other test programs, mostly smaller than those listed above. A listing of these programs can be found in several of the papers developing empirical methods from test data[35, 116].

Several analysis techniques for the compressive collapse of stiffened panels were developed along with these experimental programs. Faulkner presented analysis methods for both un-stiffened plates[122] and grillages[123, 124] for predicting the ultimate strength value. Murray developed a similar method with a slightly different approach[125], as did Hughes[21], who also included lateral pressure. These methods share a common approach of idealizing the stiffened panel as a series of identical beam-columns, each beam-column consisting of a stiffener and attached plating. Each method proposes corrections for the buckling of the plate and the potential for inelastic buckling of the entire beam-column out of plane, and in these details the methods differ. The use of various finite element and finite difference computer programs for the analysis of the non-linear collapse of stiffened panels became common at this time, with several alternative formulations proposed. Using such an approach, Smith[2] developed estimates for the entire stress-strain curve of stiffened panels in compression taken from the hull of a naval frigate. Smith then proposed a novel method for estimating the ultimate strength of the midship section of the vessel. The midship section was divided into small panels, and a stress-strain curve was generated for each panel. Then, by assuming the panels acted independently, and that plane cross-sections of the vessel's hull girder remain plane, Smith demonstrated the moment-curvature response of the midship section could be traced by applying incremental curvatures to the cross section, and integrating the response of the individual panels about the instantaneous neutral axis.

This approach has been implemented by many authors since Smith's paper, including a program developed by Adamchak for the U.S. Navy[126] based upon beam-column analysis to develop the compressive stress-strain relationship of the stiffened panels in the hull. Dow et al.[127] presented the result of Smith-type analysis applied to several experimentally tested box girders and the *Albuera*, a British frigate experimentally tested to collapse. The stress-strain curves for the elements of these structures were determined from a incremental non-linear finite-element approach also developed by Dow[128].
Rutherford[36] presented another beam-column analysis for determining the compressive stress-strain curve of stiffened panels. Chen[129] investigated using nonlinear finite element analysis to determine the ultimate strength of ship hulls, while Udea et al[130] developed the idealized structural unit method(ISUM) which uses an approach similar to finite elements,

except the elements represent a much large piece of the structure, typically entire plates or stiffener-plate combinations. These approaches reduces the computational complexity of the problem significantly, allowing more complex structures to be tackled with the same computing power.

While most of the marine work at this time focused on steel vessels, similar work was being carried out for aluminium in other fields in the early 1980s, albeit on a smaller scale. Little[131, 132] modified an approach he developed for steel for the analysis of aluminium plates in compression, including the effect of initial deformations and the non-linear stress-strain curve of aluminium. These approaches are based on an energy minimization technique. The compressive strength of such plates was investigated experimentally Mofflin[45], who also evaluated several numeric methods, including Little's work discussed above. Clarke and Swan carried out compressive collapse tests on stiffened aluminium panels[133, 134] and performed numerical simulations of the results with Dow's method for stress-strain curves. This was done by replacing the actual aluminium panel with an fictitious steel panel selected to have the same plate elastic slenderness parameters.

Further work on the response of steel structures took place in the late 1980s and early 1990s. Herzog[116] summarized the steel plate and stiffened panel tests to date, and proposed regression formulae for predicting the ultimate strength of such structures. Rutherford and Caldwell[3] investigated the actual collapse of the VLCC *Energy Concentration,* using the Smith approach and Rutherford's beam-column formulation. Several other beam-column formulations for Smith-type approaches were also proposed about this time, one proposed by Gordo and Guedes Soares was based on Faulkner's equations for the strength of plates and stiffened panels[31, 135, 136]. Rahman and Chowdhury[30] develop a method based on Hughes' ultimate strength approach and aspects of Adamchak's compressive stress-strain curve. Nielsen developed a beam-column methodology as well[32]; Yao and Nikolov[137, 138] also developed a similar methodology with a different approach to generating the stress-strain curve. Dow[139] presented the experimental results of a collapse test on a 1/3 scale model of a frigate, which was then used as the bases for an ISSC benchmark study lead by Jensen[24]. This study compared several different approaches to estimating the compressive stress-strain curve of the components of the hull girder and the overall moment-curvature relationship of the hull girder. This included several beam-column Smith-type approaches, finite element analysis, and the ISUM approach. The results showed significant scatter between the methods, both for the response of the panels and the overall response of the hull girder. Research into the response of steel panels and steel has continued, with increasing focus on the effects of corrosion and local

damage on the response. This work has limited applications to aluminium and will not be reviewed here, however references and discussion can be found in the report of Committee III.1 of the International Ship and Offshore Structures Congress[25-27] and a recent review article by Yao[140].

The increased use of aluminium in high-speed vessel construction in the early 1990s and the development of the Eurocode 9 design code lead to an increased amount of research into aluminium plates and panels during this time period. Hopperstad et al.[141] tested plate outstands in compression, and compared the results to non-linear finite element predictions with the ABAQUS program, as well as comparing Mofflin's experimental plate tests to ABAQUS results, with good agreement observed. Kristensen[46, 142] investigated the response of un-stiffened simply-supported aluminium plates with ABAQUS, examining axial compression, biaxial compression, shear, and combined loading cases. Several different alloys were used, and the effect of HAZ around welds was investigated by modelling including various HAZ locations and widths. Herrington and Latorre[143] carried out experimental and numeric tests on an aluminium panel of "floating frame" design where the transverse frame is not attached to the shell plating, but only to the stiffener flanges. Under lateral pressures, such construction performed well, although potential fatigue problems were mentioned by the authors. Tanaka and Matsuoka[144] experimentally investigated the strength of aluminium panels formed from extrusion with variable thickness. Zha et al.[62, 145, 146] experimentally investigated the compressive strength of flat-bar stiffened panels that were sized to fail primarily via stiffener tripping. Aalberg et al.[59] performed similar tests on extruded panels from 6082 aluminium, with both L-shaped stiffeners and closed stiffeners. Abildgaard et al.[147] examined the strength of welded aluminium plates, in both compression and out-of-plane loading, comparing the results to finite element predictions with LS-DYNA.

Several other purely numerical studies have also been published recently. Rigo et al. [39] published a sensitivity study on the ultimate strength of aluminium panel based on a benchmark study carried out for the Ultimate Strength Committee of the 15th ISSC. Using the same extrusion cross-section as Aalberg et al.'s experimental work, several different finite element codes were compared to predict the compression collapse, with good agreement. A sensitivity study was then carried out to investigate the effects of the volume of the HAZ, the locations of the HAZ including transverse welds at mid and quarter span, residual stresses, initial out-of-plane deformations, and material properties. The location and size of the HAZ seemed most significant, especially for transverse welds at mid-span, with the other factors having smaller impacts on ultimate strength. Paik and Duran[38] performed a parametric

analysis of tee-stiffened panels and un-stiffened plates with 5000-series aluminium, fitting empirical regression equations to the results. Xiao and Menzemer[148] investigated the response of plate elements via the ABAQUS software, by numerically testing stub H-columns in compression, comparing the results with Mofflin's test and the U.S. Aluminum Association *Specification*, with good agreement observed. Setta et al.[149] proposed an initial-yield ultimate strength model based on a Perry-Robertson approach, with good agreement shown between the proposed models and the tests of Zha and Moan[62] and the test program carried out by Tanka and Matsuoka [144]. It is clear that the performance of aluminium panels has received increasing attention in the last 15 years and the recent work has begun to shed some light on the issues which influence the design of these panels. However, there are still many unanswered questions for the designer.

3.3 Response of Plates

While the objective of this thesis is to develop structural analysis methods for the response of stiffened panels, it is logical to start the analysis of ultimate strength behaviour one level lower, with the individual plate elements of the panel. The response of these elements is traditionally considered the tertiary or lowest level of structural response for ship-type structures[34]. As such, accurate predictions of the response of individual plates is crucial in developing accurate response predictions for the higher levels of structural response. Additionally, investigating response of individual plates, while still a highly-complex undertaking, is simpler than investigating the response of stiffened panels and the overall hull girders. In this section, the response of individual plate elements in compression and tension will be developed. As discussed in the introduction, attention is focused on the axial compression and tension behaviour of these structures. The response of plates to each of these types of loads will be investigated in turn.

In traditional steel vessel design, the compressive response of plates is the critical response requiring analysis. In compression, buckling typically prevents the individual plate elements from reaching their full yield strength. Thus, understanding the buckling behaviour of thin-walled structures is essential to understanding their compressive strength. Such buckling has been the subject of study for over 100 years now, with the elastic buckling equation for a simply-support plate being determined by G.H. Bryan in 1891[21]. In this section, the compressive response of aluminium plates will be investigated. Previous experimental results of the compressive collapse of aluminium plates will be presented first, followed by four options for predicting the ultimate strength of these plates and an analysis of their performance. A similar investigation and comparison will then be made for methods capable of predicting the entire load-shortening curve of the plate's compressive response.

After examining the compressive response, the tensile response of welded plates will be investigated to see if the strain concentration effect in the HAZ discussed in Chapter 2 will be of significance for the response of plates typical of HSV construction.

3.3.1 Experimental Results

There have been several experimental investigations into the buckling performance of aluminium plates in both the marine and aerospace industries, complemented by extensive theoretical studies. The first major study of note for marine structures was a series of plate compressive collapse tests carried out by Muckle in the United Kingdom[111]. This work was carried out in the late 1940s, sponsored by the Aluminium Development Association in the U.K. Unfortunately, the alloys used by Muckle are no longer in production, and the focus of the tests were for transversely-framed vessels made of riveted construction. As a result, the experimental results are of limited interest for the HSVs of today. The alloys tested by Muckle were the British N6 and N5 alloys, where the primary alloying element is 5% and 3% Magnesium, making the alloys roughly equivalent to today's 5000-series aluminium. The plates were tested in uni-axial compression, with the loaded edges of the plates clamped between a pair 6"x4"x3/4" steel angles and the longitudinal edges left free. The principle dimensions varied in the test program was the thickness to length ratio. Such a test set up is broadly representative of the response wide plates loaded in compression, typical of transverse framing common for ship construction in the 1940s, but unusual today as the buckling strength of such construction is significantly less than longitudinal framing. Indeed, the theoretical discussion presented in the paper concentrates on plates where the width of the plate exceeds eight times the length of plate.

Muckle tested forty plates of the N6 alloy in the work-hardened condition, and 5 were tested in the annealed condition. Five specimens of the N6 alloy were tested in both the work-hardened and annealed condition. Muckle also made limited tests on plates made of the clad Duralumin alloy, which is roughly equivalent of today's 2000-series alloys, with an additional external coating to improve corrosion resistance. A further group of tests were also performed on wide riveted plates with longitudinal riveted seams running parallel to the applied loading, with clinker, in-and-out, and joggled riveting arrangements. Extensive theoretical discussion of buckling is also presented, which is further extended in Muckle's book on aluminium ship structures[8], and a further paper by Snaith[112]. While Muckle's work is of significant historical interest, the alloys, aspect ratios, and boundary conditions make Muckle's experiments of limited use to validate methods designed for welded, longitudinally-framed HSV structures typical of today.

Experimental results for long plates in the aerospace alloys 2014 and 7075 was reported by the U.S. National Advisory Committee for Aeronautics (NACA, presently NASA). Andersen and Anderson[110] tested thin (1/16" or 1.6mm) plates with breadth to thickness ratios ranging from 15 to 60. The configurations had simply supported longitudinal edges, partially clamped loading edges, and were in configurations so that at least 5 buckling waves could form over the length of the plate. These test results were complemented by test results for a plate with one longitudinal edge left free, determined by testing of short cruciform sections of 2014 alloy by Stowell[109]. Similar to the Muckle tests, these tests do not correspond well to modern HSVs, the alloys are not in the same series as the alloys used on HSV, the sheets were thinner than the plating used on HSVs, and thus may not have had the same initial imperfections as thicker sheets. Despite these limitations, these tests were used to form the basis of the plate buckling strength method adopted by the U.S. Aluminum Association in their Aluminum Design Manual, which has proven successful for a wide range of structures.

One of the largest and most relevant experimental programs into the compressive collapse of aluminium structures is a series of 76 plate compressive collapse tests carried out by Mofflin[45, 150] at the University of Cambridge. This test investigated two of the most common alloys for HSV construction, the 5083 and 6082 series alloys. The tests were especially comprehensive, with the influence of out-of-plane deflection, longitudinal welds, and transverse welds separately investigated. The 76 plates tested covered a non-dimensional plate slenderness, β, range of 0.86 to 5.47. β is defined as

$$\beta = \frac{b}{t}\sqrt{\frac{\sigma}{E}}$$

Where :

b Plate width

t Plate thickness

σ Yield stress(steel) 0.2% offset proof stress(aluminium)

E Elastic modulus

Equation 16

Note that the definition of β used in Mofflin's work has been multiplied by 1/1.92 compared to the definition of β used in the present work, the figures that follow have been adjusted to conform with the β used elsewhere in this thesis. This corresponds to b/t ratios between 20 and 85. The plates were all approximately 6mm thick, and were four times as long as their breadth. They were tested in a 1MN compression testing machine. This testing machine used a series of "fingers" to support the long, unloaded edges of the plate during the testing. These devices restrained the out-of-plane deflection of the plate, while allowing rotation and the plate to pull in its own plane. The transverse edges were partially clamped to ensure

good load transfer. However, the effect of this clamping on the ultimate strength of the plate was estimated by Mofflin as less than 5%, as the plates were quite long, and the rotational restrain was only partial.

Each test specimen was cut from a group of nine large plates, which were also used for material property tests. The 5083 plates were supplied in the –M temper, this is basically an "as-milled" temper, with no requirement for a specific proof strength. The 6082 plates were in a fully heat-treated temper (TF), with a 0.2% offset proof stress of about 290MPa. Several samples were taken from each of these large plates, and the material properties were determined by compression tests, which should properly account for any difference between tensile and compressive properties in the 5000 series alloys. Overall, the results were fairly consistent within each plate, with variations less than the 3% for proof stress, and 10% for elastic modulus. One of the 5083 plates had a much larger variation in proof stress, between 115 and 160 MPa in the same plate. A part of one of the 5083 plates was fully annealed, to reduce it to a -0 temper before plates were cut out of it for testing. After annealing, the 0.2% offset proof stress was only 91 MPa, well below the grade minimum of 125 MPa for this alloy. This situation is not unique, in the A.R.E. panel tests review below, one particular stiffener made out of 5083 alloy suffered a similar problem. While there was some variation in elastic modulus, Mofflin adopted the standard value of 70,000 MPa for his analysis of the result.

Mofflin's test programme included analysis of the effects of welding and initial out-of-plane deformations. To simulate longitudinal welds, TIG welding passes were made at the edge of the panel without adding any filler metal. The heat input was equivalent to that required to produce a fillet weld with a 3mm or 4mm leg, thus giving two different heat input values. To simulate the effects of transverse welds at mid-length of the plate, a MIG welding pass was made on top of the plate with a weld metal area equal to that of a single-vee full penetration butt weld. The weld metal was then removed before compressive testing. Measurement confirmed that residual stress had indeed developed in the plate, roughly as expected by prediction techniques. No welds were placed at the transverse (loading) edges of the plate. Initial out-of-plane deflection was introduced after welding, and took the form of a "bump" in the centre of the plate, extended over roughly the middle third of the plate's length. Two different deflections were used, corresponding deflections of 0.001 and 0.005 of the plate width.

Mofflin's experimental results are an excellent data source to validate methods for predicting the behaviour of aluminium HSV structures. The alloys, boundary conditions, and fabrications techniques used match those conventionally assumed for HSV analysis.

Additionally, both ultimate strength values and stress-strain curves are available for the plate results. As these data are quite extensive, they will not be presented in this thesis at this time. After the presentation of the various prediction methods, the data required for each comparison study will be presented as required. Readers are referred to Chapter 3 of Mofflin's thesis[45] for a complete description of the test results.

3.3.2 Compressive Ultimate Strength Prediction

When investigating plate behaviour, the first question is often how much does buckling reduce the ultimate compressive strength of the plate? Several methods have been proposed for predicting the ultimate compressive strength of the plate, usually taking the form of an equation or group of equations that relate the ultimate compressive strength to the yield stress. These methods, in general, do not give information about the stress-strain behaviour of the plate in compression, simply the maximum compressive stress which the plate is capable of resisting. In this section, four different methods will be presented, and then compared with each other and with the experimental results from Mofflin's program.

3.3.2.1 Faulkner's Approach

The first method is not an aluminium method, but rather a steel method originally proposed by Faulkner which has shown good agreement with experimental results and has been widely adopted in the marine industry[20, 122, 136]. It takes the form of an equation based on β, the plate slenderness

$$\frac{\sigma_m}{\sigma_0} = 1.0 \text{ when } \beta < 1$$

$$\frac{\sigma_m}{\sigma_0} = \frac{2}{\beta} - \frac{1}{\beta^2} \text{ when } \beta \geq 1$$

Equation 17

Where:

σ_m Mean stress in plate at failure

σ_0 Plate yield stress

β Plate slenderness ratio

Faulkner's approach is included in this comparison as it is a method that naval architects may be familiar with, and comparing it to aluminium-specific methods may highlight the difference between aluminium and steel behaviour. As is clear from the form of the equation, this approach cannot account for the different shapes of the stress-strain curve between alloys. Faulkner[122] extended this method to account for the residual compressive stress induced by welds on the longitudinal edges of the plate for materials that follow an elastic-plastic stress-strain curve. However, as this extension was designed for

steel, it does not address welds at the transverse (loaded) edges of the plate, nor variations in the yield stress of the plate . When implemented for aluminium, the 0.2% offset proof stress was used in place of the yield stress, and Faulkner's steel welding correction was not added to the formulae.

3.3.2.2 Paik and Duran's Approach

An aluminium-specific approach following a similar structure has been proposed by Paik and Duran[38]. The equation is based on the results of non-linear finite element analysis of 25 plates made of the new Sealium (5383-H116) alloy with the ANSYS finite element package. The reduced strength in the HAZ around welds was included, as was initial deformations equal to 0.009b, but no residual stresses. Their approach modifies the slenderness value, β, for the plate based on the relative volume of HAZ material to base material:

$$\frac{\sigma_m}{\sigma_{eq}} = 1.0 \text{ when } \beta' \le 0.46$$

$$\frac{\sigma_m}{\sigma_{eq}} = -0.215\beta' + 1.1 \text{ when } 0.46 < \beta' \le 2.2$$

$$\frac{\sigma_m}{\sigma_{eq}} = -0.083\beta' + 0.81 \text{ when } \beta' > 2.2$$

σ_{eq}

Where :

σ_m Mean stress in plate at failure

σ_0 Plate yield stress

$$\beta' = \frac{b}{t}\sqrt{\frac{\sigma_{eq}}{E}}$$ *Equation 18*

$$\sigma_{eq} = \frac{P_p}{ab}$$

$$P_p = (a - 2b_p')(b - 2b_p')\sigma_0 + 2\left[ab_p' + \left(b - 2b_p'\right)b_p'\right]\sigma_{0\_HAZ}$$

a Plate length

b Plate width

b_p' Width of HAZ

σ_0 Base material 0.2% offset proof stress

σ_{0_HAZ} HAZ material 0.2% offset proof stress

Note that this equation follows the form of the equation first presented at the RINA Advance Materials conference[151], not the journal paper where the predicted strength was non-dimensionalized by the proof stress of the HAZ, not the base material. The use of the HAZ strength in the journal paper is believe to be an error. This equation is capable of representing the effects of welding at the boundaries of the panel, though not in the middle

of the panel. It will also account for the rounded shape of a 5000 series stress-strain curve, though it may not be accurate for the 6000 series alloys which have a different stress-strain curve.

3.3.2.3 U.S. Aluminium Association Specification

The U.S. Aluminum Association has published a *Specification for Aluminum Structures* as part of the *Aluminum Design Manual*[53], which includes methods to estimate the compressive strength of various types of plate structures. Flat plates supported on all edges are covered in Section 3.4.9 of the *Specification*. The *Specification* divides plate buckling behaviour into three different types of response, based on the breath to thickness ratio of the plate. Stocky plates are allowed to reach the full yield stress, while plates of intermediate slenderness buckle inelastically and highly slender plates buckle elastically, with allowance for post-buckling strength. The three different zones of the response are shown graphically in Figure 10 below, taken from Kissell and Ferry's[49] book on aluminium design which explains the basis of the *Specification*. The general form of the mean strength (without partial safety factors) equations are given in Equation 19 for plates where post-buckling strength is recognized.

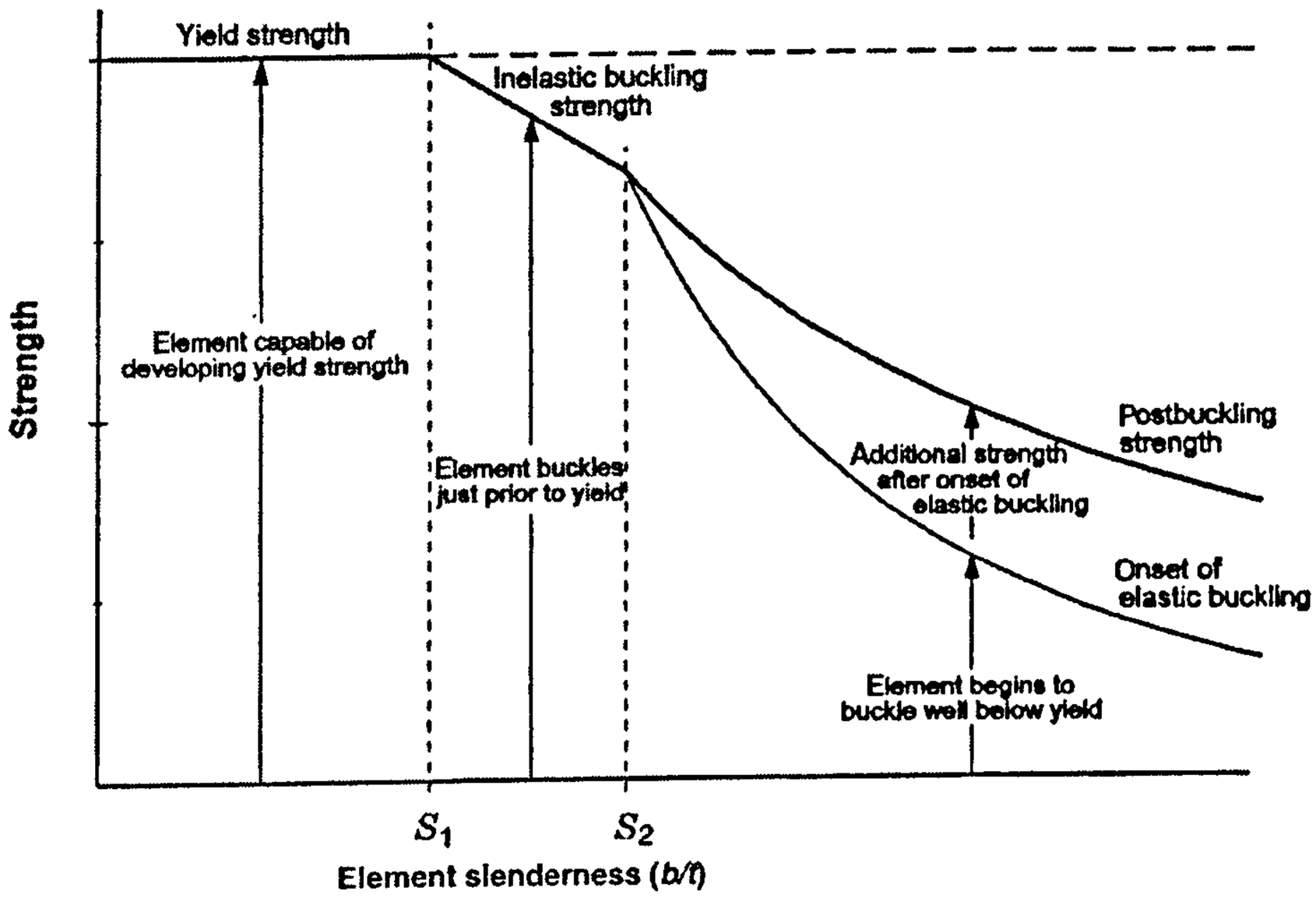

Figure 10: Aluminum Association Buckling Approach(reproduced from[44])

$$\sigma_m = \sigma_{0.2} \text{ when } S < S_1$$

$$\sigma_m = B_P - D_P\left(k\frac{b}{t}\right) \text{ when } S_1 \le S \le S_2$$

$$\sigma_m = \frac{k_2\sqrt{B_P E}}{k\frac{b}{t}} \text{when } S > S_2$$

Where:

Equation 19

σ_m Mean stress in plate at failure

$\sigma_{0.2}$ Plate compressive proof stress

B_P, D_P, k_2 Code material constants

S, S_1, S_2 Actual slenderness and intersect points

$$S = \frac{b}{t}$$

k Edge support constant

The slope and intersects of the inelastic and post-buckling range are computed separately for each alloy, and different equations and constants are used for alloys whose stress-strain curves have different shapes, thus accounting for the effect of different alloys. The strength curve is linear with respect to the b/t ratio for inelastic buckling, and the post-buckling curve varies with one over the b/t ratio. The influence of welding is addressed in Section 7.1.2 of the *Specification*. Where the area of the heat-affected zone from longitudinal welds is greater that 15% of the cross-section area of the plate, a reduction in plate strength is made based on the ratio of the area of heat-affected material to the area of base material, and the strengths of the two materials. Welds at the transverse edges of the plate may be ignored, provided that the final strength calculated does not exceed the proof strength of the heat-affected material. Transverse welds in the middle of plate cannot be explicitly handled by the code, the only option is to treat the entire plate as if it was made of heat-affected material.

3.3.2.4 Eurocode 9

The fourth and final method reviewed for plates is the Eurocode 9[60]. Eurocode 9 is the European Committee for Standardization (CEN) standard design code for structural design with aluminium, and includes a formulation for flat plates in compression. Two strength calculations are made, the first is an overall yielding calculation, where the cross-sectional area of the plate is first reduced to account for buckling and longitudinal welds, and the failure load is taken as the remaining area multiplied by the proof stress of the material. The second calculation is a local squashing calculation based on the ultimate

strength of the material at the least-favourable cross-section of the plate. The area of the least-favourable section is reduced to account for transverse welds and any bolt holes or other cut outs that may be present. The relative thickness reduction for welding is prescribed by the code, and the thickness reduction for buckling takes the form:

$$\frac{t_e}{t} = 1 \quad \text{when} \frac{\beta_{EC9}}{\varepsilon} \leq C_1$$

$$\frac{t_e}{t} = \frac{C_2}{\frac{\beta_{EC9}}{\varepsilon}} - \frac{C_3}{\left(\frac{\beta_{EC9}}{\varepsilon}\right)^2} \quad \text{when} \frac{\beta_{EC9}}{\varepsilon} > C_1$$

Where:

$$\beta_{EC9} = \frac{b}{t}$$

$$\varepsilon = \sqrt{\frac{250}{\sigma_0}}$$

Equation 20

t_e Effective plate thickness

t Plate thickness

σ_0 Material proof stress, MPa

C_1, C_2, C_3 Code - prescribed constants

The code-prescribed constants vary with the type of alloy, and whether the plate is welded or not. Thus, the effect of different stress-strain curves for different alloys and the effects of welding are incorporated in the formulation. In calculating the effective thicknesses, Bulson's[152] advice was followed, and the effective thickness reductions for buckling and HAZ effects were not taken as additive, rather, the largest reduction was taken as governing.

3.3.2.5 Comparison of Methods

These four prediction options were compared to each other and to Mofflin's experimental data. As a baseline comparison, the ultimate strength predicted by each method for non-welded 5083 and 6082 alloy plates was plotted as a function of the plate slenderness ratio, β. The material properties assumed in the comparison were typical values, as shown below in Table 9, and the predicted ultimate strengths are shown in Figure 11 and Figure 12. For the 5083 plate, Paik and Duran's approach is more conservative for stockier plates, though this may be influenced by the fairly high initial deformations included in the finite element models that this approach is based upon. The remaining methods agree well, even though Faulkner's approach was developed for steel, not aluminium. In the slender region, where the buckling would be expected to be initially elastic, Faulkner's approach is slightly more optimistic than either of the aluminium design codes. For the 6082 plate, Paik

and Duran's approach is more conservative, though as noted above this approach was based on a 5000 series alloy with a different shape of material stress-strain curve than the 6000 series. The difference is the most pronounced in the low-slenderness region where inelastic buckling occurs and the shape of the stress-strain curve would be expected to be more significant.

Following on this analysis, Mofflin's experimental data for plates without welds were extracted and plotted on top of the curves, as shown in Figure 13 and Figure 14. Note that in these figures, the lines for the Aluminium Association and Eurocode 9 predictions are for the typical properties list in Table 9. Both of these methods are functions proof stress in more ways than β alone, and the intersects between the different portions of the curve and the slope of the curves will change with the different proof stresses of the different experimental plates. However, these changes are generally small when plotted against β.

Table 9: Material Properties for Plate Comparison

Material	*5083-H116*	*6082-T6*
Proof Stress(MPa)	*180*	*260*
Elastic Modulus (MPa)	*70000*	*70000*

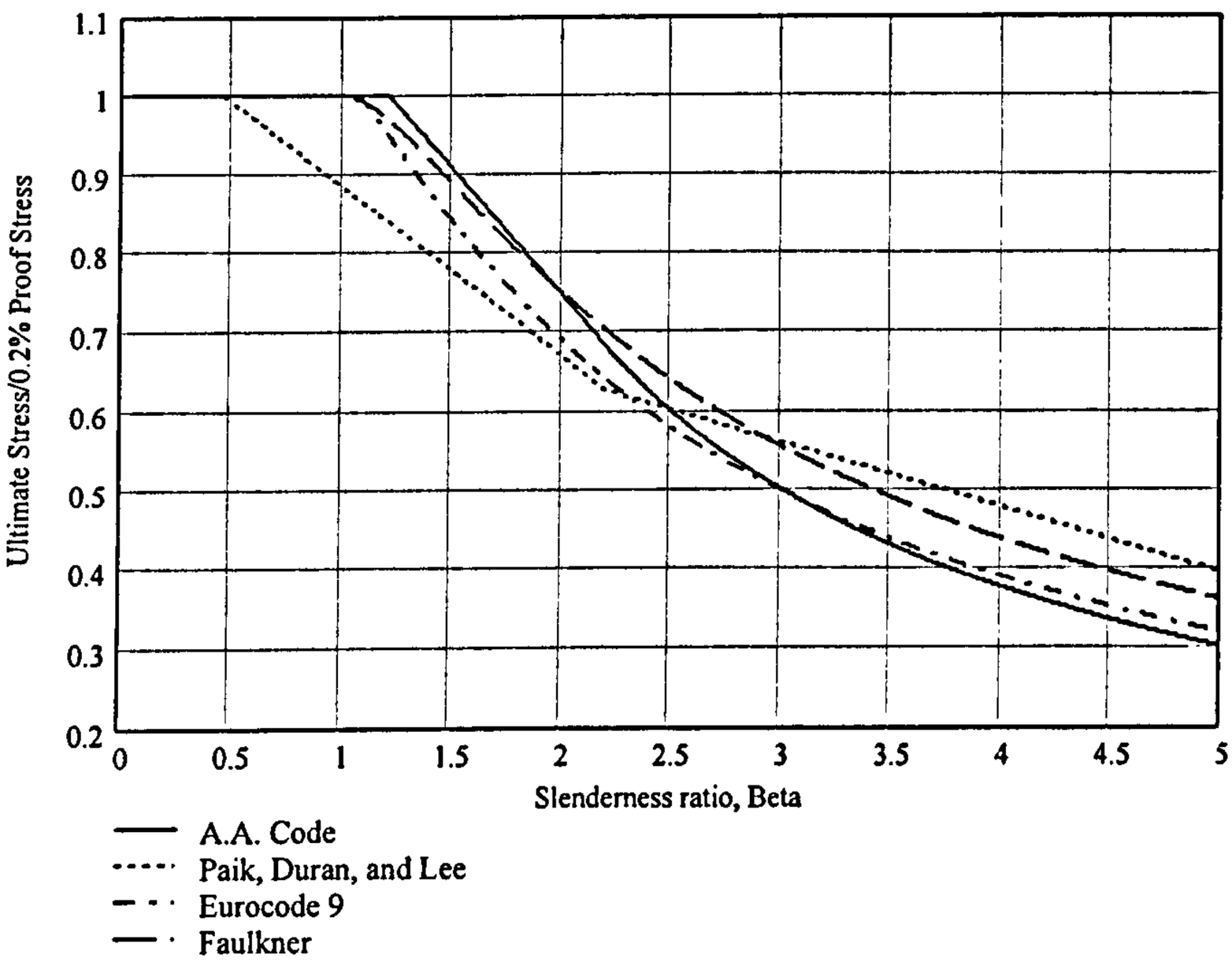

Figure 11: Comparison for 5083-H116 Plate, No Welds

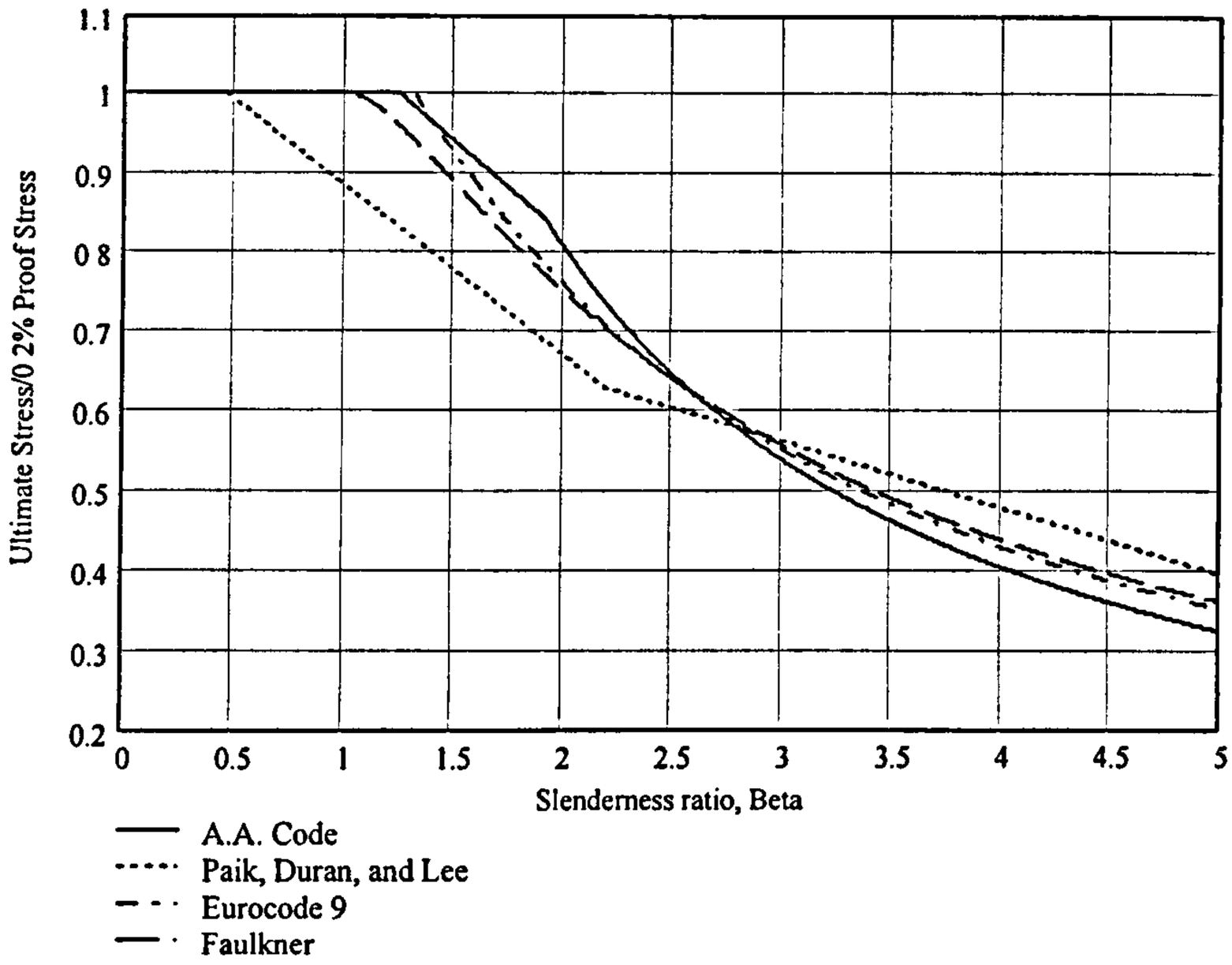

Figure 12: Comparison 6082-T6 Plate, No Welds

In general, the agreement between the test points and the prediction methods is excellent, and the natural scatter between the test points is as large as the difference between the prediction methods. Note that Paik and Duran's equation agrees better with the plates with large out-of-plane deflections, which were closer to the level of deflection (0.009b) used in the finite element analysis to develop the equation. The one exception is Paik and Duran's equation applied to the inelastic buckling region of 6082 alloy, where the approach seems conservative. This shows the influence of alloy on the plate response, and underscores the need to include the difference between alloys in the prediction method. This is further reinforced by the performance of Faulkner's method, which appears to agree better with the design codes and the experimental results for the 6000 series alloy than it does for the 5000 series alloy. The stress-strain curve of the 6000 series alloy is much closer to the elastic-plastic response of steel than the more rounded 5000 series alloy curve.

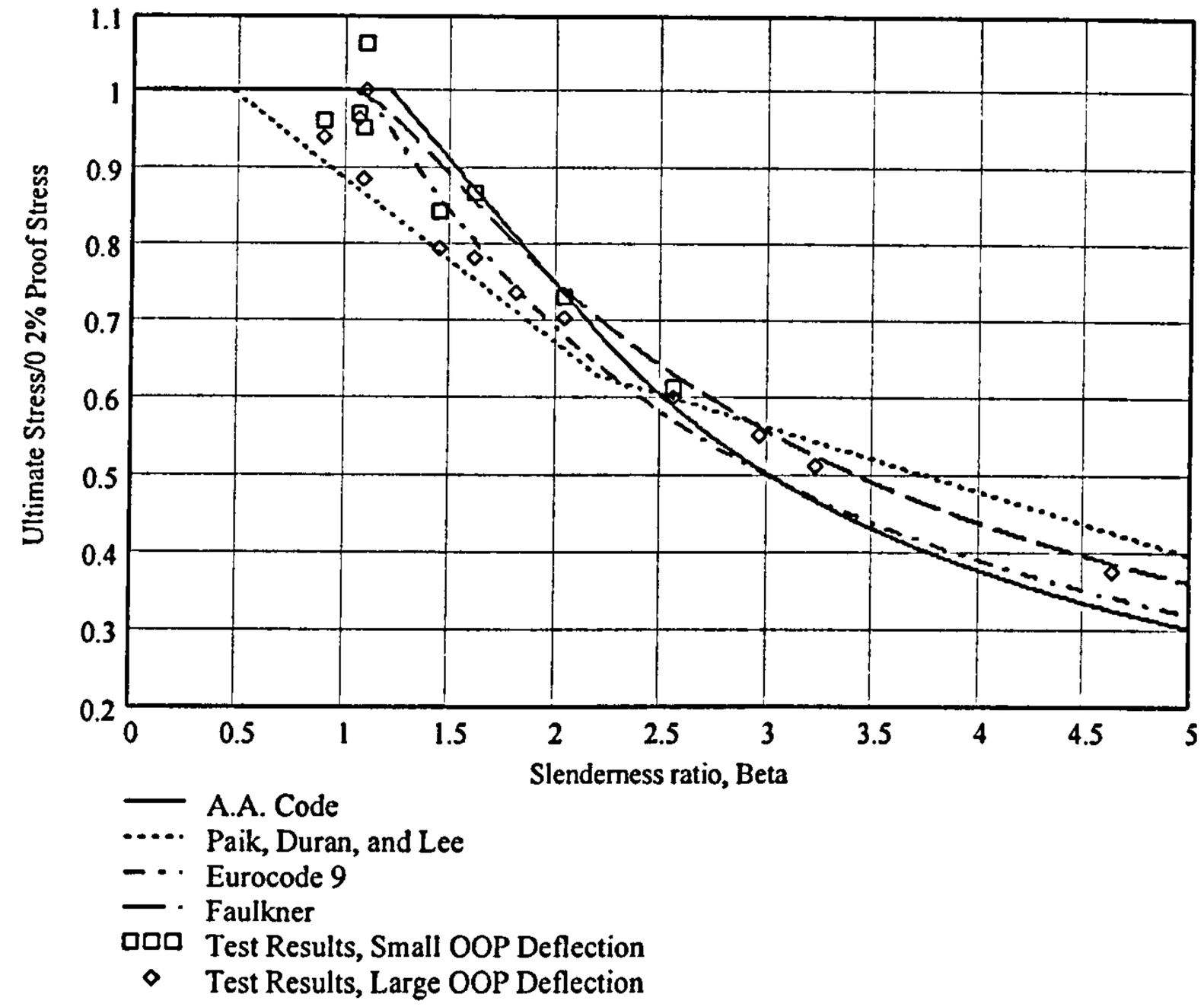

Figure 13: Comparison of 5083 Test Results and Methods, No Welds

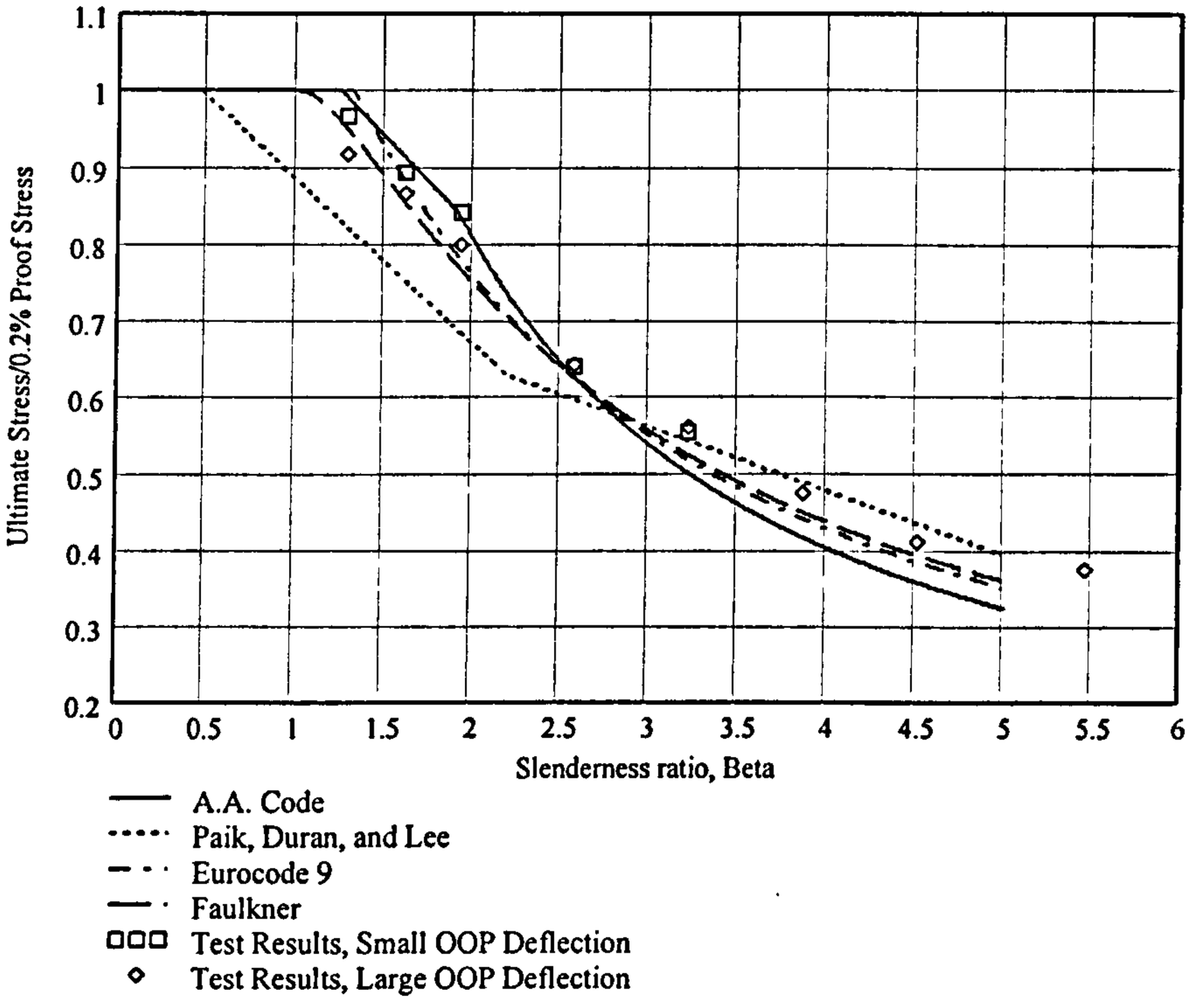

Figure 14: Comparison of 6082 Test Results and Methods, No Welds

With these encouraging results, the four prediction methods were applied to the remainder of Mofflin's experimental results, with the exception of plates with a transverse weld at mid-length, as none of the methods are capable of simulating such a weld. Previous studies[9] have shown that plates with such a weld behave in a similar fashion, but with

strengths lying between the predictions made assuming the entire plate consists of heat-affected material and the all-base material prediction. The results were divided by alloy, and within each result set by the size of the initial out-of-plane deformation, and the type of weld. The experimentally measured ultimate strength was expressed relative to the 0.2% offset proof strength of the plate, determined by Mofflin. The results of the four prediction methods were expressed as a bias relative the experimental result, where the predicted strength is divided by the experimental strength. With this approach, a bias of 1.0 indicates a perfect prediction, while a value over 1.0 indicates a optimistic prediction of strength. These results are presented in Table 10 and Table 11, along with the mean bias of the prediction methods, and the coefficient of variation (COV) of each method, defined as the bias sample standard deviation divided by the mean value.

Overall, the methods compare excellently with the test data, with mean bias very near 1.0 and small COV values, in all case less than 10%. It is interesting to note that for the 5083 plates, Faulkner's method slightly over predicts the strength of the plates, while it is nearly perfect for the 6082 plates. As mentioned above, the stress-strain response of 6082 is much more similar to steel than that of 5083, which may be reason for this difference. Furthermore, Paik and Duran's method developed for 5000-series material performs very well on the 5083 plates, but under predicts the 6082 plate strengths whose stress-strain curve is elastic for a proportionally longer time than the 5000 series alloys, as discussed in Chapter 2. This reinforces the need to consider the alloy-specific stress-strain behaviour when making predictions for aluminium structures.

3.3.3 Compressive Load-Shortening Prediction

If the entire load-shortening curve, or the corresponding stress-strain curve, of a plate is required, there are several methods which can be used to calculate the response. The most numerous of these methods seem to be numerical methods, such as using a general-purpose non-linear finite element program. This approach has been used by Kristensen and Moan[142] to investigate aluminium plates under complex circumstances, or by Paik and Duran[38] to develop a data set for their regression equation which was reviewed previously. Another option is to use a specialized numerical program based on a similar approach to finite elements, but adapted for the specific problem of the collapse of plates, such as those developed by Little[132]. As discussed above, these methods can produce very accurate results, however they are intensive in terms of time and effort. Another class of methods are the approximate approaches, where the complex buckling phenomenon is

replaced by a simpler model of what is happening in the plate. It is was decided to investigate applying and modifying such a method for aluminium plates.

Table 10: Comparison of Experimental Results and Predictions for 5083 Plates

Plate	OOP[1]	Weld[2]	b/t	β	$\sigma_{0.2\%}$ (MPA)	Exp./ $\sigma_{0.2\%}$	Faulk./ Exp.	Paik/ Exp.	AA/ Exp.	EC9/ Exp.
20SU5/7	S	U	20	1.09	208	1.06	0.94	0.82	0.94	0.94
25SU5/8	S	U	25	1.06	125	0.97	1.03	0.90	1.03	1.03
25SUA/9	S	U	25	0.90	91	0.96	1.04	0.94	1.04	1.04
30SU5/6	S	U	30	1.61	202	0.87	0.99	0.87	1.01	0.93
30SUA/9	S	U	30	1.08	91	0.95	1.04	0.91	1.04	1.05
40SU5/1	S	U	40	2.04	182	0.73	1.01	0.91	1.01	0.93
40SUA/9	S	U	40	1.44	91	0.84	1.07	0.94	1.05	1.02
50SU5/1	S	U	50	2.55	182	0.61	1.03	0.98	0.96	0.93
30SL5/6	S	L	30	1.61	202	0.77	1.11	0.94	1.06	0.93
30SW5/6	S	W	30	1.61	202	0.75	1.15	0.95	1.05	0.97
20BU5/7	B	U	20	1.09	208	1.00	0.99	0.87	1.00	0.99
25BU5/8	B	U	25	1.06	125	0.97	1.03	0.90	1.04	1.04
25BUA/9	B	U	25	0.90	91	0.94	1.06	0.96	1.06	1.06
30BU5/6	B	U	30	1.61	202	0.78	1.10	0.96	1.13	1.03
30BUA/9	B	U	30	1.08	91	0.89	1.12	0.98	1.12	1.13
40BU5/1	B	U	40	2.04	182	0.70	1.05	0.94	1.04	0.97
40BUA/9	B	U	40	1.44	91	0.79	1.14	0.99	1.12	1.09
50BU5/1	B	U	50	2.55	182	0.60	1.05	1.00	0.98	0.95
50BUA/9	B	U	50	1.80	91	0.74	1.09	0.97	1.06	1.01
60BU5/6	B	U	60	3.22	202	0.51	1.02	1.06	0.91	0.92
70BU5/8	B	U	70	2.96	125	0.55	1.02	1.03	0.91	0.92
85BU5/7	B	U	85	4.63	208	0.37	1.03	1.14	0.87	0.91
25BL5/8	B	L	25	1.06	125	0.98	1.02	0.89	0.97	0.94
30BL5/6	B	L	30	1.61	202	0.72	1.20	1.01	1.14	1.01
40BL5/1	B	L	40	2.04	182	0.64	1.15	1.01	1.15	0.94
40BLA/9	B	L	40	1.44	91	0.78	1.16	1.01	1.14	1.00
50BL5/1	B	L	50	2.55	182	0.54	1.17	1.09	1.10	0.94
60BL5/6	B	L	60	3.22	202	0.48	1.08	1.10	0.97	0.85
20BW5/7	B	W	20	1.09	208	0.88	1.13	0.87	0.91	1.02
25BW5/8	B	W	25	1.06	125	0.92	1.08	0.95	1.00	0.99
25BWA/9	B	W	25	0.90	91	0.99	1.01	0.91	0.92	0.96
30BW5/6	B	W	30	1.61	202	0.75	1.15	0.95	1.05	0.97
30BWA/9	B	W	30	1.08	91	0.93	1.07	0.93	0.99	0.97
40BW5/1	B	W	40	2.04	182	0.65	1.15	1.00	1.07	0.94
40BWA/9	B	W	40	1.44	91	0.73	1.24	1.08	1.16	1.07
50BW5/1	B	W	50	2.55	182	0.54	1.16	1.07	1.04	0.93
50BWA/9	B	W	50	1.80	91	0.70	1.15	1.02	1.08	0.95
60BW5/6	B	W	60	3.22	202	0.46	1.13	1.14	1.01	0.89
85BW5/7	B	W	85	4.63	208	0.34	1.14	1.24	0.97	0.88
						Mean	1.08	0.98	1.03	0.97
						COV	0.06	0.09	0.07	0.06

Notes:

1: Out-of-plane deflection, S corresponds to OOP/b ≈ 0.001, B corresponds to OOP/b ≈ 0.005

2: Weld on edge, U denotes no welding, L denotes light welding, W denotes heavy. For code calculations, the HAZ width was assumed to be 15mm for light welds, and 25mm for heavy

Table 11: Comparison of Experimental Results and Predictions for 6082 Plates

Plate	OOP[1]	Weld[2]	b/t	β	$\sigma_{0.2\%}$ (MPA)	Exp./ $\sigma_{0.2\%}$	Faulk./ Exp	Paik/ Exp.	AA/ Exp.	EC9/ Exp.
20SU6/2	S	U	20	1.2873	290	0.968	0.98	0.85	1.03	1.03
25SU6/3	S	U	25	1.6119	291	0.895	0.96	0.84	1.03	0.99
30SU6/4	S	U	30	1.9376	292	0.844	0.91	0.81	0.99	0.92
40SU6/5	S	U	40	2.5835	292	0.639	0.98	0.93	0.98	0.97
50SU6/5	S	U	50	3.2293	292	0.554	0.94	0.98	0.91	0.93
25SL6/3	S	L	25	1.6119	291	0.832	1.03	0.83	0.97	0.93
30SL6/4	S	L	30	1.9376	292	0.779	0.98	0.82	0.97	0.89
30SW6/4	S	W	30	1.9376	292	0.713	1.07	0.86	0.98	0.97
20BU6/2	B	U	20	1.2873	290	0.92	1.03	0.89	1.08	1.09
25BU6/3	B	U	25	1.6119	291	0.867	0.99	0.87	1.06	1.02
30BU6/4	B	U	30	1.9376	292	0.802	0.95	0.85	1.04	0.97
40BU6/5	B	U	40	2.5835	292	0.641	0.97	0.93	0.98	0.97
50BU6/5	B	U	50	3.2293	292	0.559	0.94	0.97	0.90	0.92
60BU6/4	B	U	60	3.8752	292	0.475	0.95	1.03	0.88	0.93
70BU6/3	B	U	70	4.5133	291	0.41	0.96	1.06	0.88	0.94
85BU6/2	B	U	85	5.471	290	0.374	0.89	0.95	0.79	0.86
25BL6/3	B	L	25	1.6119	291	0.827	1.03	0.84	0.98	0.93
30BL6/4	B	L	30	1.9376	292	0.742	1.03	0.86	1.02	0.94
40BL6/5	B	L	40	2.5835	292	0.637	0.98	0.88	0.99	0.89
50BL6/5	B	L	50	3.2293	292	0.523	1.00	0.99	0.96	0.90
20BW6/2	B	W	20	1.2873	290	0.855	1.11	0.78	0.85	0.94
25BW6/3	B	W	25	1.6119	291	0.773	1.11	0.84	0.95	0.97
30BW6/4	B	W	30	1.9376	292	0.702	1.09	0.87	1.00	0.98
40BW6/5	B	W	40	2.5835	292	0.573	1.09	0.94	0.98	0.99
50BW6/5	B	W	50	3.2293	292	0.474	1.10	1.07	0.98	0.99
60BW6/4	B	W	60	3.8752	292	0.419	1.07	1.11	1.00	0.95
85BW6/2	B	W	85	5.471	290	0.343	0.97	1.02	0.86	0.85
						Mean	1.00	0.91	0.96	0.95
						COV	0.06	0.10	0.07	0.05

Notes:

1: Out-of-plane deflection, S corresponds to OOP/b ≈ 0.001, B corresponds to OOP/b ≈ 0.005

2: Weld on edge, U denotes no welding, L denotes light welding, W denotes heavy. For code calculations, the HAZ width was assumed to be 15mm for light welds, and 25mm for heavy

An example of such an approach is the effective width approach. The axial stress distribution across the width of a long, simply-supported plate which has buckled is non-linear, varying from a maximum at the edge to a minimum in the centre of the plate, where the buckling deformation have reduced the axial stiffness. If the exact stress distribution is known, or the total resisting force of the plate is known, an average stress can be determined. This is shown in the upper part of Figure 15. The effective width approach replaces the actual width of the plate with a reduced width, chosen so that the edge stress can be assumed constant over the entire reduced width, and the same net axial force will be produced as in the actual plate. This requires:

$$b_e = \frac{\sigma_a}{\sigma_e} b$$

Where :

σ_a Average stress in plate

σ_e Edge stress

b_e Effective plate width accounting for buckling

b Plate width

Equation 21

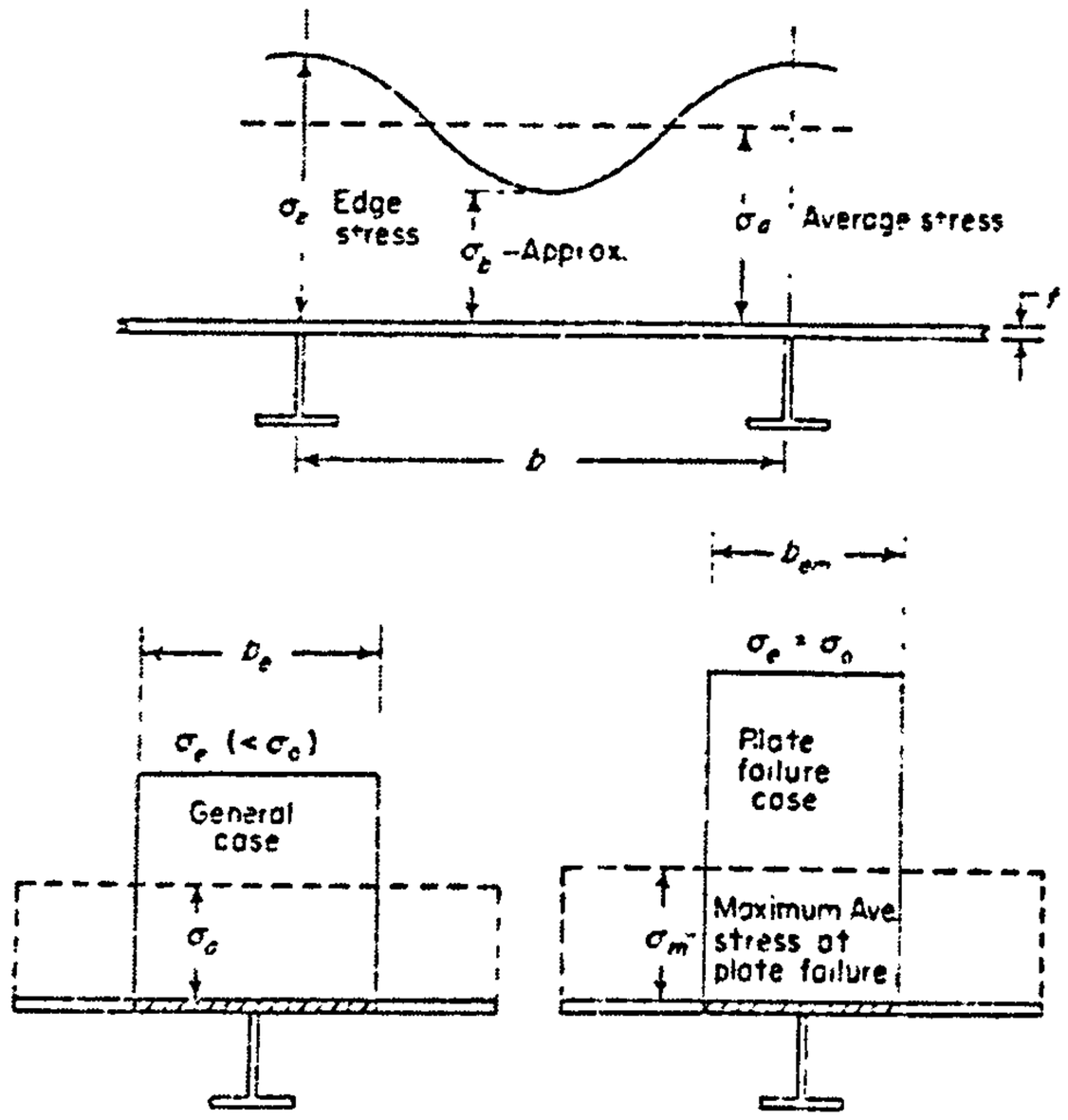

Figure 15: Effective Width (Faulkner et al.[123])

In such a model, assuming the elastic-perfectly-plastic stress-strain relationship typical of steel, the maximum strength of the plate will be reached when the edge stress reaches yield. Faulkner proposed that the stress-strain curve of a plate in compression for edge stresses between 75% and 100% of yield could approximated by Equation 17 if the value of β in the equation was replaced by an effective value of β, defined so that:

$$\beta_e = \frac{b}{t}\sqrt{\frac{\sigma_e}{E}}$$

Where :

σ_e Actual value of edge stress

All other variables as normal β

Equation 22

This approach was extend by Gordo and Guedes Soares[135] for the entire range of edge stress, by using the strain in place of the edge stress divided by the elastic modulus in the definition of effective β. This assures that the maximum stress occurs when the yield stress reaches yield, and is equal to the strength predicted by Faulkner's original equation.

Furthermore, the effective slenderness of the plate continues to grow after the edges yield, so that the plate's strength decreases after yielding of the edge strips. With such an approach, the stress corresponding to any strain for the plate could be determined by:

$$\sigma = b_e \sigma_e$$

Where :

b_e Effective breadth via Faulkner's equation, $\beta = \frac{b}{t}\sqrt{\varepsilon}$ ***Equation 23***

σ_e Edge stress, εE but not more than the yield stress

This model was further extended by Gordo and Guedes Soares to account for residual stresses and initial imperfections, and was shown to agree well with finite-element calculations.

It is initially attractive to adapt this assumption for aluminium, using the effective β ratio to determine a fictitious b/t ratio, however, with the non-linear stress-strain curve typical of aluminium alloys, one has to decide if the effective β is determined by the edge strain or the edge stress, with different values resulting from each approach. To shed more light on this decision, the stress-strain curve from eight of Mofflin's plate tests was plotted on a common set of axis. The plates selected were four un-welded 5083 plates with b/t between 30-60 and four un-welded 6082 plates with b/t between 30-60. Tests with the larger level of initial imperfections were selected, as these seemed more in line with measured results from ship-type aluminium panels[62, 133].

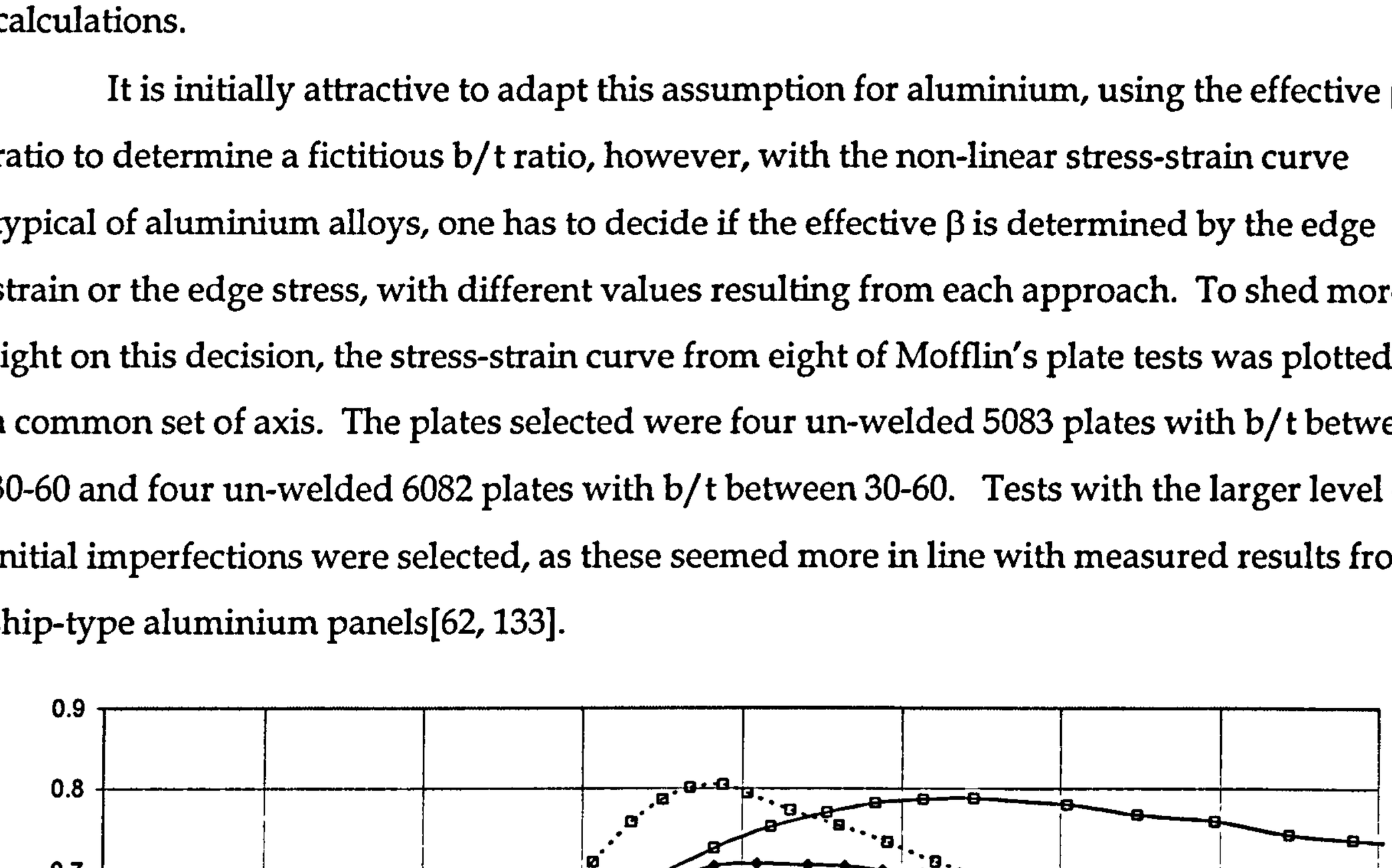

Figure 16: Stress-Strain Curves For Selected Mofflin Plates

From these curves, it was possible to determine the variation in effective width. When plotted against strain, the effective width appeared to be generally linear in the region of interest, namely where the edge stress is approaching the 0.2% proof stress. Based on this observation, the following formula was selected to model the effective width:

$$\frac{b_e}{b} = a - b\frac{\varepsilon}{\varepsilon_N}, \quad \frac{b_e}{b} \le 1$$

Where :

a, b Constants to be determined

ε *A*ctual strain

ε_N Reference strain

Equation 24

This method is limited to strains around the failure strain, as for large strains the effective widths will eventually become negative. In the analysis of Mofflin's plates, such strains were well beyond the region of interest. However, the constants a and b varied from plate to plate, and a method was required for determining them. Given the good performance of the plate strength prediction methods, especially the Eurocode 9 and the U.S. Aluminum Association *Specification*, it was decided to use the predicted peak strength as a rational way of determining the two constants. This was done by requiring the stress-strain curve for the plate to intersect the predicted strength at the failure strain, and for this point to be the maximum point on the stress-strain curve. Based on Figure 16, it seems reasonable to take the failure strain as equal to the 0.2% proof stress divided by the elastic modulus. Thus:

$$\frac{b_e(\varepsilon_f)}{b}\sigma_e(\varepsilon_f) = \sigma_{ult}$$

$$\left.\frac{d\left(\frac{b_e(\varepsilon)}{b}\sigma_e(\varepsilon)\right)}{d(\varepsilon)}\right|_{\varepsilon=\varepsilon_f} = 0$$

Equation 25

Where :

σ_{ult} Calculated ultimate stress

ε *A*ctual strain

ε_f Failure strain, $\varepsilon_f = \frac{\sigma_{02}}{E}$

$\sigma_e(\varepsilon)$ Edge stress at strain from inverse Ramberg - Osgood relation

Given the requirement to satisfy these equations, the constants a and b can be determined. This procedure was applied to the eight stress strain curves for the Mofflin plates investigated, and stress-strain curves were determined by the approximate method. These are shown in Figure 17 below. For each curve, the experimental failure load was used

to calculate the failure stress, so the peak of the stress-stress curve is guaranteed to reach the same height as the peak of the experimental curve, thus it is shape of the curve and hence the effective width assumption which is being tested in this comparison. The agreement in terms of curve shape is good, with the slope of the curve well approximated in both the pre-ultimate-strength and post-ultimate-strength regions. The post-ultimate-strength region of the 5083 plates was slightly underestimated in most cases, probably because the assumption of a linear variation in effective width is not correct in the post-ultimate-strength region. In this regard, the increased ability of the 5000-series alloys to strain harden over the 6000-series alloy may need to be incorporated into the effective width equation The primary error seems to come from the assumed failure strain, which is not always accurate, shifting the curve to one side of the experimental results. Several other relations were examined for the failure strain were examined, however they did not improve the consistency of the method. It should be noted that Mofflin reported up to 10% variation in the elastic modulus between plates, but used the standard value of 70000 MPa for his calculations, an approach followed here. The error in failure strain could be caused in part by this variation. Overall, the method appears to be an acceptable approximation given the simplicity of the effective width relation. The constants a and b were tabulated, based on the experimental failure stress, and are shown in Table 12 below. In general, the constant decrease with increasing b/t, and decrease with increasing n, the Ramberg-Osgood exponent.

Table 12: Effective Width Constants for Experimental Plate Results

b/t	5083 Plates		6082 Plates	
	a	b	a	b
30	1.38	0.44	1.179	0.31
40	1.09	0.30	0.946	0.25
50	0.93	0.25	0.82	0.22
60	0.97	0.31	0.69	0.18

To be of use in predicting the response of plates in HSVs the method must be extended to include welding, as plates in HSVs are typically welded along their edges where they are attached to frames, stiffeners or longitudinal girders. The effects of such welding need to be incorporated into the formulation, unfortunately, there is very little experimental data for plates welded this way. Kristensen's[142] numerical investigation into the compressive performance of aluminium plates revealed that the transverse welds seem to have the most significant effect on the strength reduction. Kristensen fitted exponential functions through his results in terms of the plate slenderness ratio, giving the plate ultimate

strength as a function of the stress in which the elastic and plastic components of the material strain are equal. Kristensen's formulas are shown in Equation 26.

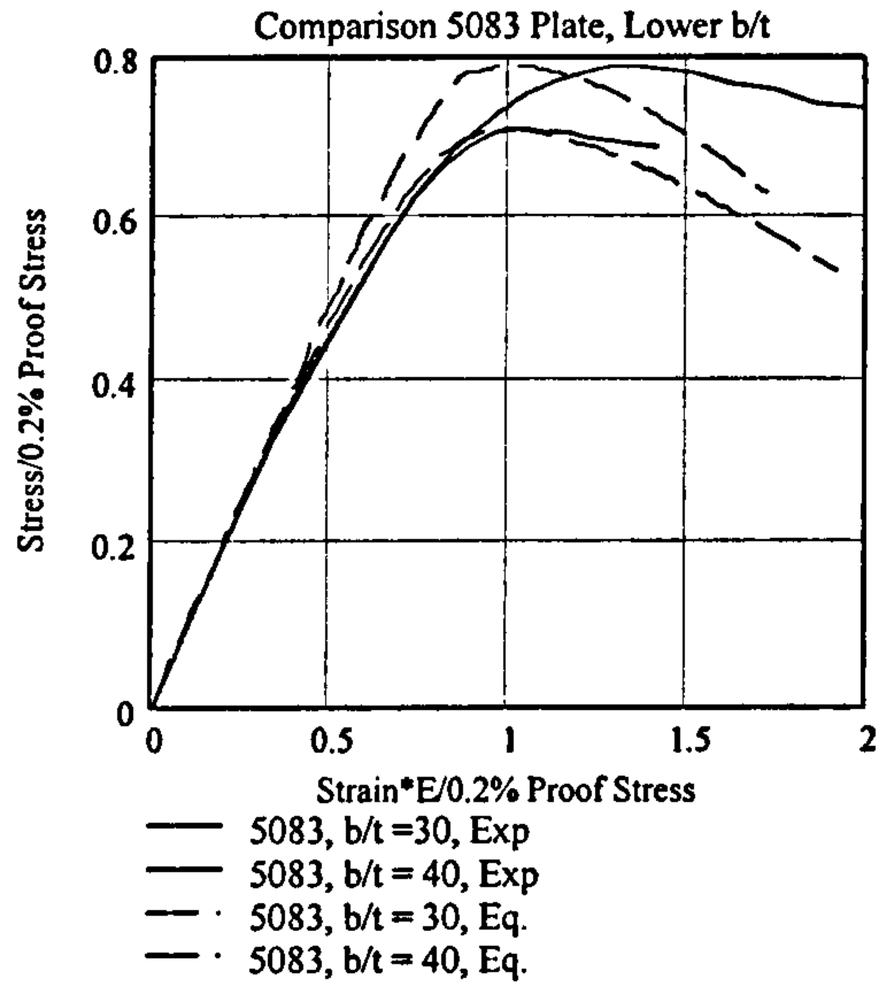

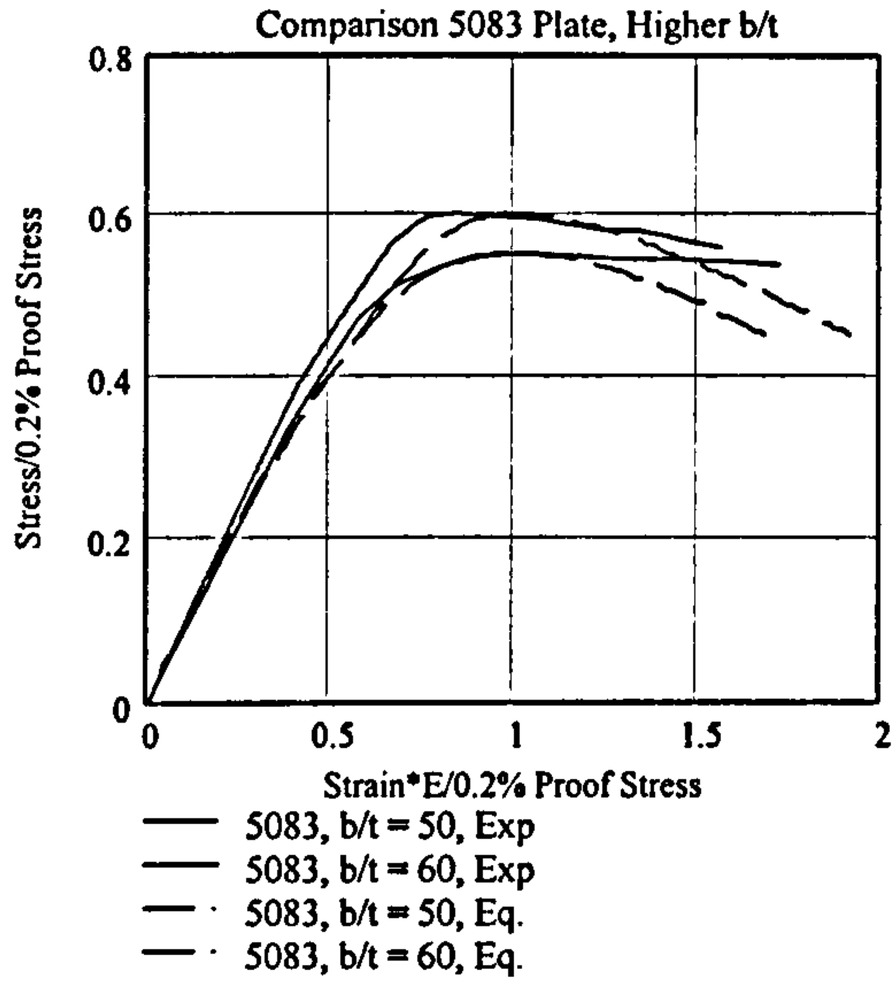

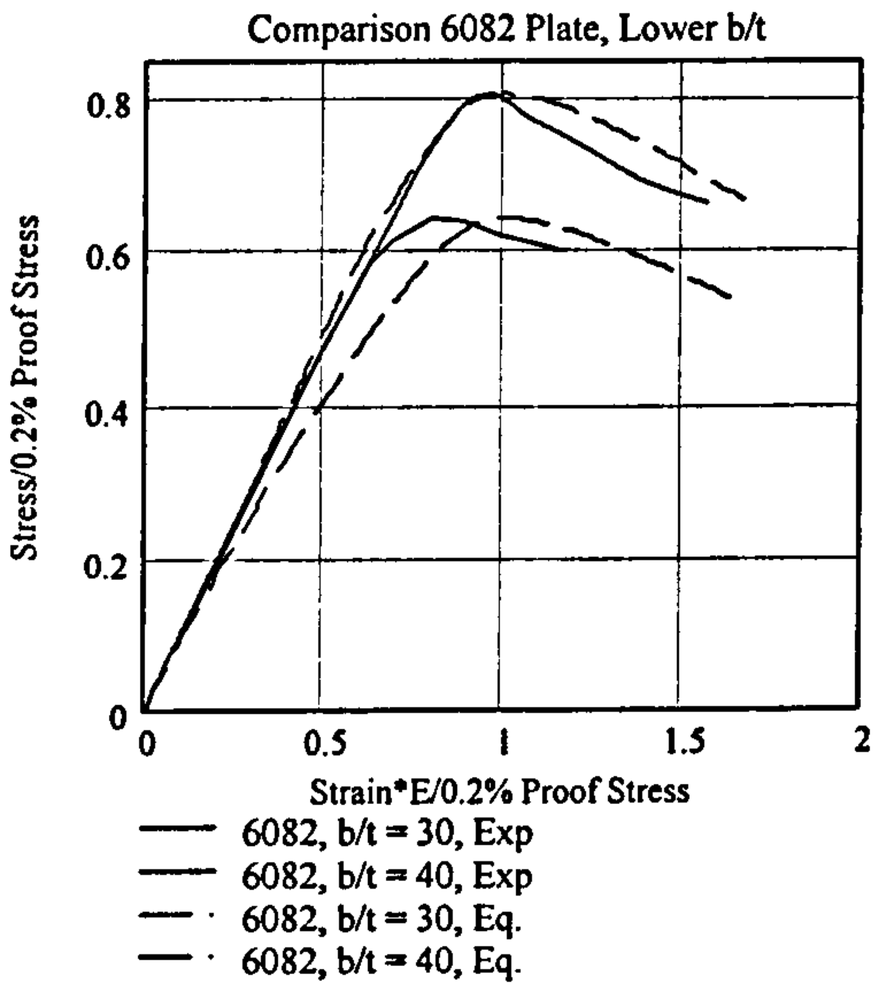

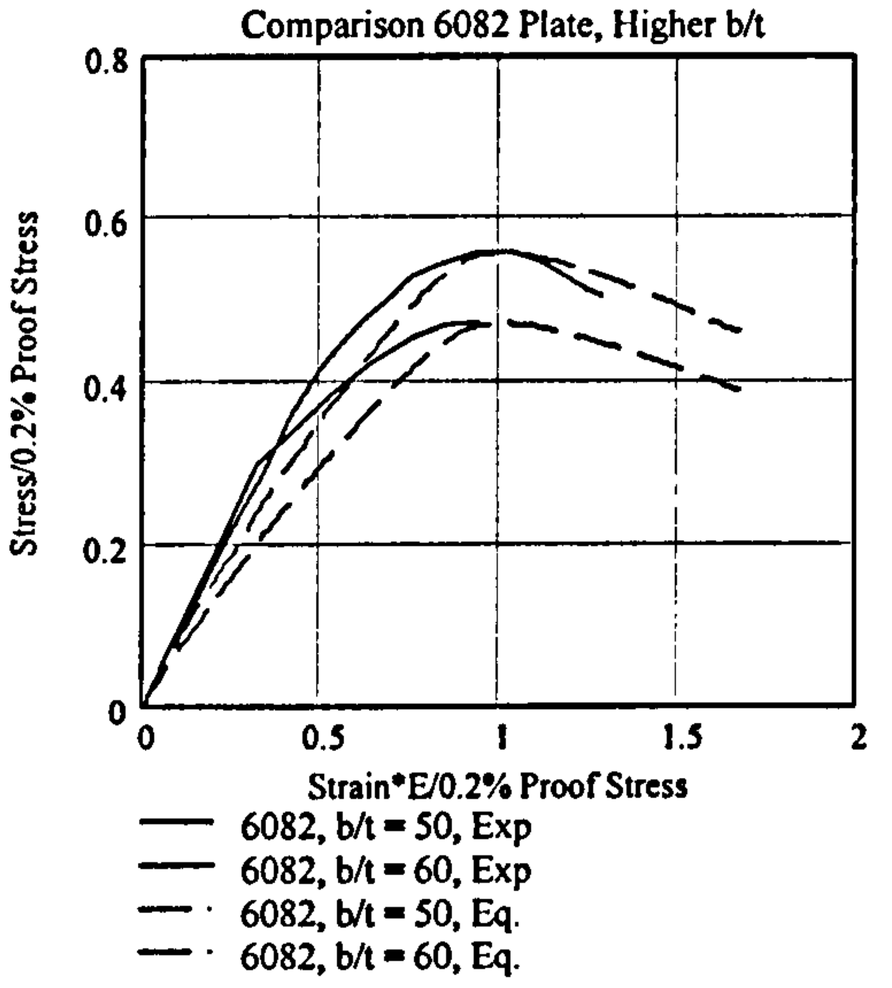

Figure 17: Comparison of Simplified Plate Load-Shortening Method

$$\frac{\sigma_m}{\sigma_{elpl}} = (1-K)\left(\frac{\sigma_m}{\sigma_{elpl}}\right)_{BASE} + K\left(\frac{\sigma_m}{\sigma_{elpl}}\right)_{HAZ}$$

$$K = \frac{b_{HAZ}}{25} 2\left(1 - \frac{\sigma_{HAZ}}{\sigma_{0.2}}\right)$$

$$\left(\frac{\sigma_m}{\sigma_{elpl}}\right)_{BASE} = 1.562 - 1.426\, e^{-0.9403\,\beta^{-0.8616}}$$

$$\left(\frac{\sigma_m}{\sigma_{elpl}}\right)_{HAZ} = 0.7495 - 0.7036\, e^{-3.387\,\beta^{-1.224}}$$

Equation 26

Where :

σ_m Predicted ultimate stress

σ_{elpl} Stress at which elastic and plastic strains are equal

$\sigma_{0.2}$ 0.2% offset proof stress of base material

σ_{HAZ} 0.2% offset proof stress of HAZ material

β Plate slendernes s

b_{HAZ} HAZ breadth in mm on each side of plate

This equation represents a fit to the lower bound of Kristensen's results, including several alloys, so it should be conservative. By taking the ratio of the ultimate stress predicted by Kristensen's formula for a welded plate to the ultimate stress of an unwelded plate (the second component of Kristensen's formula), the reduction in strength caused by welding can be approximated. This value is only valid at the ultimate strength point on the stress-strain curve. It is proposed to apply this reduction at all strain values in the compressive stress-strain curve by multiplying the ultimate strength reduction by the difference in edge stress at the strain level between the base material and HAZ material, divided by the difference in edge stress between the base and HAZ material at the failure strain. The final reduction to the stress predicted at each strain is given in Equation 27. This additional factor captures the strain-dependence of the HAZ reduction in an approximate way. At low stress and strain levels, where the HAZ and base material respond similarly, the numerator in this factor will approach 0, and no reduction will be observed as a result of the HAZ. At the failure strain, the reduction will be equal to Kristensen's prediction, and then increase as strain increases beyond the failure strain.

$$F_R(\varepsilon) = 1 - K\left(1 - \frac{\left(\frac{\sigma_m}{\sigma_{elpl}}\right)_{HAZ}}{\left(\frac{\sigma_m}{\sigma_{elpl}}\right)_{BASE}}\right)\frac{\sigma(\varepsilon) - \sigma_{HAZ}(\varepsilon)}{\sigma(\varepsilon_f) - \sigma_{HAZ}(\varepsilon_f)}$$

Equation 27

Where:

$F_R(\varepsilon)$ Reduction in stress at edge strain ε

$\sigma(\varepsilon)$ Stress in base material at edge strain ε, and failure strain ε_f

$\sigma_{HAZ}(\varepsilon)$ Stress in HAZ material at edge strain ε, and failure strain ε_f

This approach was applied to the b/t = 40 and b/t = 50 plates with heavy edge welds and large out-out-plane initial deformations, and the results are shown below in Figure 18. The ultimate stress used for the determination of the approximate load shortening curve was the measured maximum stress for the equivalent un-welded plate. The typical HAZ properties discussed in Chapter 2 were used to represent the HAZ, with 0.2% offset proof stresses of 144 MPa and 138 MPa for the 5083 and 6082 plates respectively. As can be seen, the HAZ correction is fairly accurate, though a bit conservative for these plates in terms of the reduction in ultimate strength, which is attributed to the fact that these plates were only welded on their longitudinal edges, not their transverse edges, while the formula above assumes welding all around. The current approach is less accurate in predicting changes to the shape of the compressive stress-strain curve, particularly for the 5083 plates where the curve tends to elongate.

The issues of strain concentration discussed in Chapter 2 and the potential for compression failure in the transverse HAZ must also be addressed. While the principle of strain concentration would apply to the transverse HAZ in compression as well as tension, the ultimate failure of the HAZ material in compression seems to be unlikely to effect these results significantly. Most significantly, because of buckling, the average ultimate stresses are lower in compression than they are in tension, for compression the structure generally does not reach the proof stress of the base material. With the b/t ratios examined here, only 50%-80% of the base material proof stress is reached. Additionally, ultimate compressive failures in the HAZ are expected to be broadly similar to bearing failure, and not marked by sudden fracture and the loss of load carrying capacity as tensile failure in the HAZ would be. Furthermore, ultimate bearing stresses in aluminium are normally on the order of 1.8 times the tensile ultimate strength[153] indicating a generally higher resistance to this type of failure.

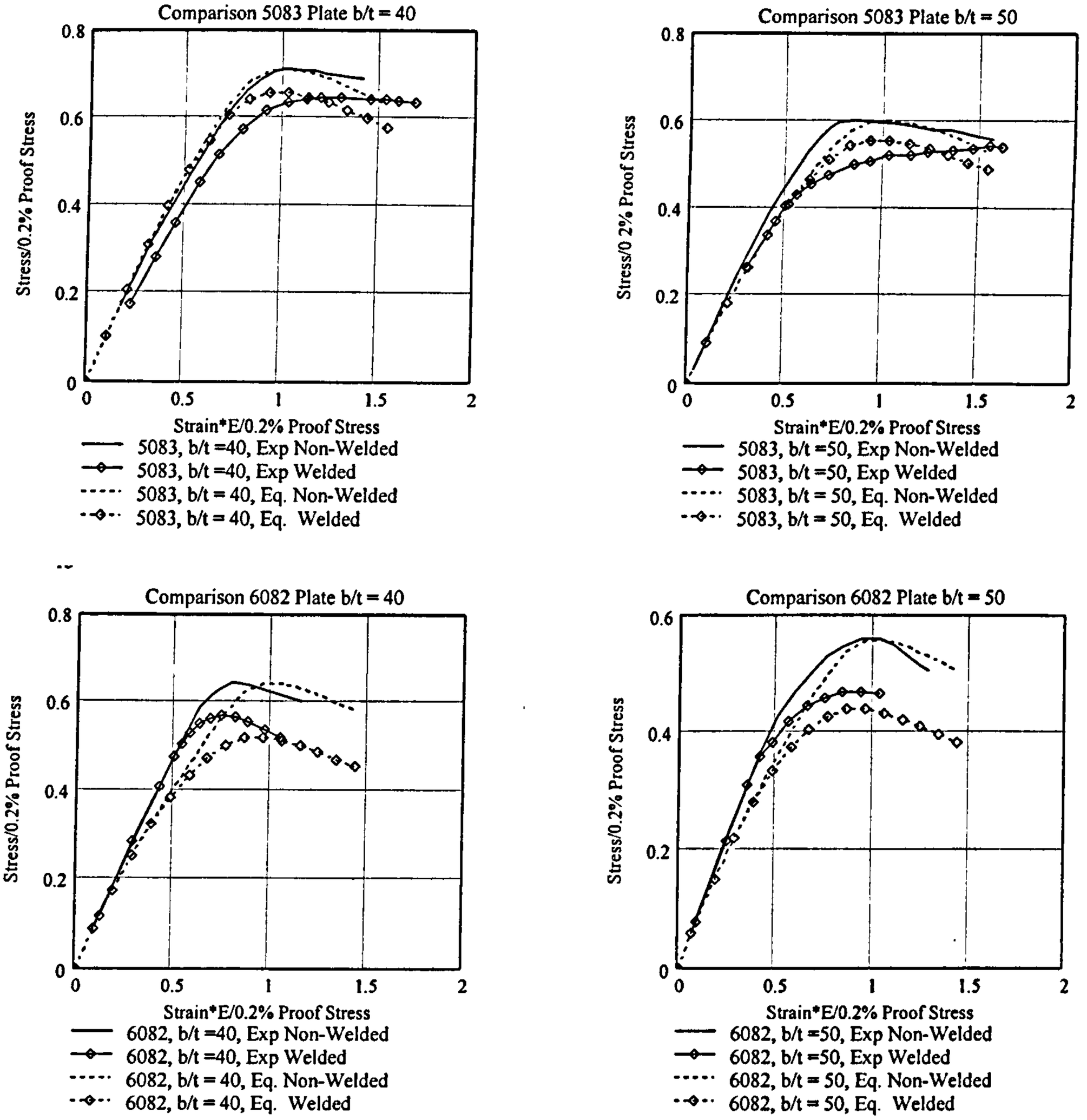

Figure 18: Reduction in Strength From Welding

3.3.4 Tensile Load-Shortening Prediction

While the tensile response of steel plates is typically no different than the material's stress-strain curve in tension, it is not immediately clear that the same situation applies to aluminium plates because of the potential for strain concentration, as discussed in Chapter 2. In typical ship construction, plates are welded on all four edges, the longitudinal edges are welded to stiffeners or deep girders, while the transverse edges are welded to frames. Taking a longitudinal section through the mid-region of such a plate, the distribution of the HAZ and base material is as shown in Figure 19.

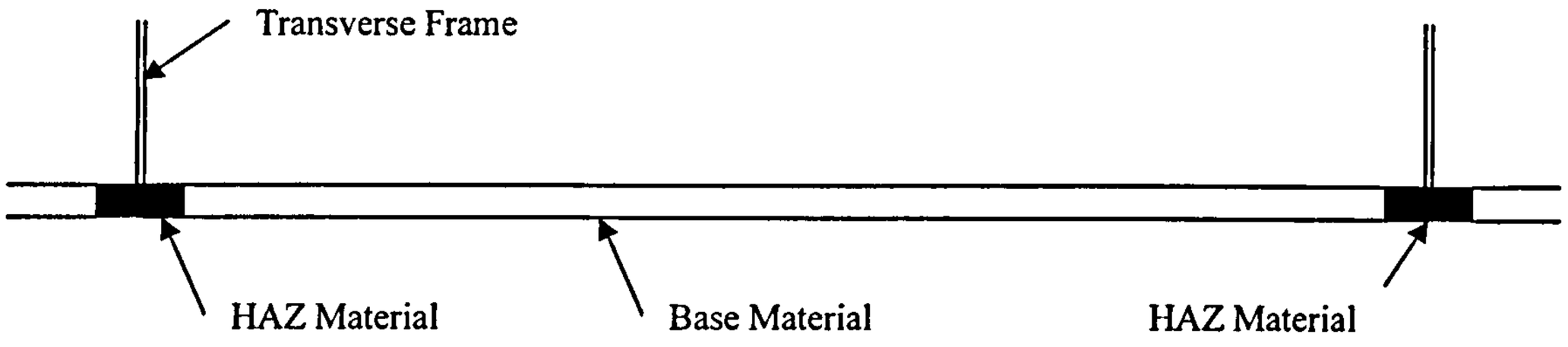

Figure 19: Longitudinal Section of Plate Showing HAZ Locations

This figure shows that the tensile response of these plates is likely to be influenced by strain concentration in the HAZ by the transverse frames. The effect of strain concentration was introduced in Chapter 2, and basically refers to the potential for a normally ductile material to exhibit overall brittle behaviour when there are large variations in the proof stress of the material over small distances. As the plate is loaded in tension, the HAZ material and base material will initially strain at equal rates. However, as the stress in the plate increases to the proof stress of the HAZ material, the HAZ regions will undergo large plastic strains while the base material remains elastic. As the length of the HAZ is small compared to the overall length of the plate, roughly 25mm-50mm total to overall length of 1000mm or even 1500mm, the overall strain of the plate will remain small even as the strain in the HAZ builds up to levels approaching failure. Finally, the HAZ may fracture at an overall plate strain much less that the material's failure strain.

To model this phenomenon, a straightforward model is proposed which treats the HAZ as an area with uniform reduced material properties relative to the base metal. This approach was initially proposed by Hill et al.[64] is widely established for structural analysis. In actuality, the material properties vary throughout the HAZ, however, the exact variation is dependent on the type of alloy and the details of the welding procedure used, making it difficult to incorporate into a design formulation. At the moment, such detailed data for the variation in properties is available in limited form for the 6000 series alloys[66], and the data that is available is mostly for butt welds, not fillet welds typical of the welds at the plate boundaries. A second assumption for the model is that transverse plane sections remain plane throughout the plate as it deforms. With these two assumptions, the response of a plate welded on all four edges can be viewed as an assembly of non-linear springs, each following the Ramberg-Osgood relationship for either the base material or the HAZ material. The plate and the idealisation are shown in Figure 20.

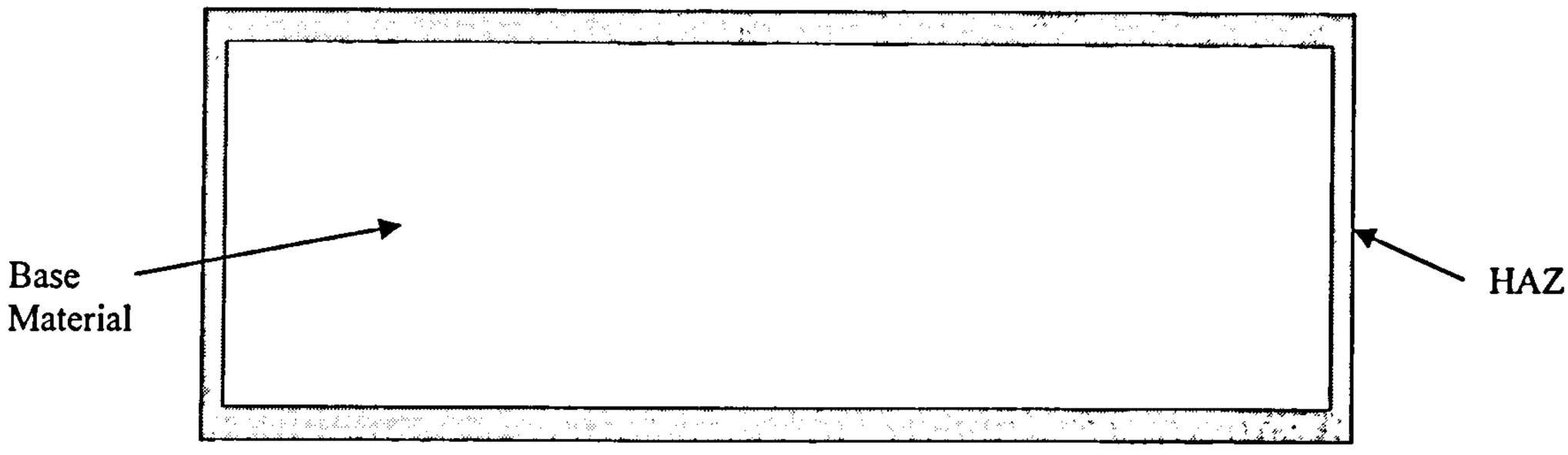

Figure 20: Tension Model of Plate

Numerically, solving such a model is straightforward. The force in the transverse HAZ must equal the total force from the base material and longitudinal HAZ, and the strains in the base material and longitudinal HAZ must also be equal. The only complication is that the stress-strain law does not have an analytical inverse relationship so a root-solving approach must be adopted. However, the stress-strain function is smooth and the overall behaviour is bounded by a plate made entirely of HAZ and a plate made entirely of base material, so a numerical solution is straightforward.

To test this model, trial applications were made to 5083-H116 and 6082-T6 plates, to determine the overall stress-strain curve of the plate. Additionally, the strain in the transverse HAZ was recorded, to see if fracture in the HAZ is a relevant failure mode. The material properties of the plates were taken as the tension grade minimums discussed in Chapter 2, and summarized in Table 13. The overall plate length was taken as 1000mm, and the breadth at 300mm, which were selected as roughly typical values for the larger size of HSVs. Determining the HAZ extent proved more problematic, as the actual HAZ extent will vary with the details of the welding process used and the thickness of the plate,

transverse frames, and longitudinal stiffeners. To make matters worse, assuming large HAZ breadths is a conservative approach for compressive strength calculations, however, for evaluating the risk of fracture from strain concentration, smaller HAZ breadths would be conservative. The values of HAZ breadth reported in the literature vary widely. Zha and Moan [62] report HAZ breadths in 6082-T6 materials ranging from 8mm to 30mm based on experimental measurements and design codes, their own experimental results for a stiffened panel assembled by fillet welds indicated HAZ of roughly 10mm. Additionally, reducing the width of the HAZ even further is possible with advanced welding techniques such as laser welding or electron-beam welding. While this improves the strength of the joint, it may reduce the ductility of the overall structure. In their numerical analysis, Zha and Moan used HAZ breadths of 12.5mm and 25mm to cover a range of potential situations, and that approach was adopted here as well.

Table 13: Plates for Tension Study

Material	*5083-H116*	*6082-T6*
Length	*1000mm*	*1000mm*
Breadth	*300mm*	*300mm*
HAZ Width	*25mm/12.5mm*	*25mm/12.5mm*
Base Material Proof Stress	*215 MPa*	*260 MPa*
Base Material n	*12*	*30*
HAZ Material Proof Stress	*144 MPa*	*138 MPa*
HAZ Material n	*8*	*16*

The tensile stress-strain curve was determined for each of these plates, and the results are shown in Figure 21, where the plate response is compared to the stress-strain response of the base material and HAZ material. The response of the plates lies between the base and HAZ material response, as expected. For the 6082 plates, it lies nearer the HAZ response while for the 5083 plates it lies near the base metal response. This is attributed to the difference in the exponent term in the Ramberg-Osgood stress-strain relationship between the two HAZ materials. With an exponent of 16, the HAZ material in the 6082 plate hardens slowly, so even as the strain builds up in the transverse HAZ in this plate, the stress levels do not rise quickly. For the 5083 HAZ, the exponent is 8, and the hardening is considerably more rapid. This can be seen in the higher slope of the 5083 HAZ curve compared to the 6082 HAZ curve. As the strain builds up in the transverse 5083 HAZ, the resisting stress rises more rapidly. Additionally, for 5083 material the base material curve lies closer to the HAZ material curve, which also influences the results. Even the simple model adopted here

shows that the tensile stress-strain response of welded aluminium plates needs to be explicitly considered, as it is significantly different from the response of either the base material or the HAZ material.

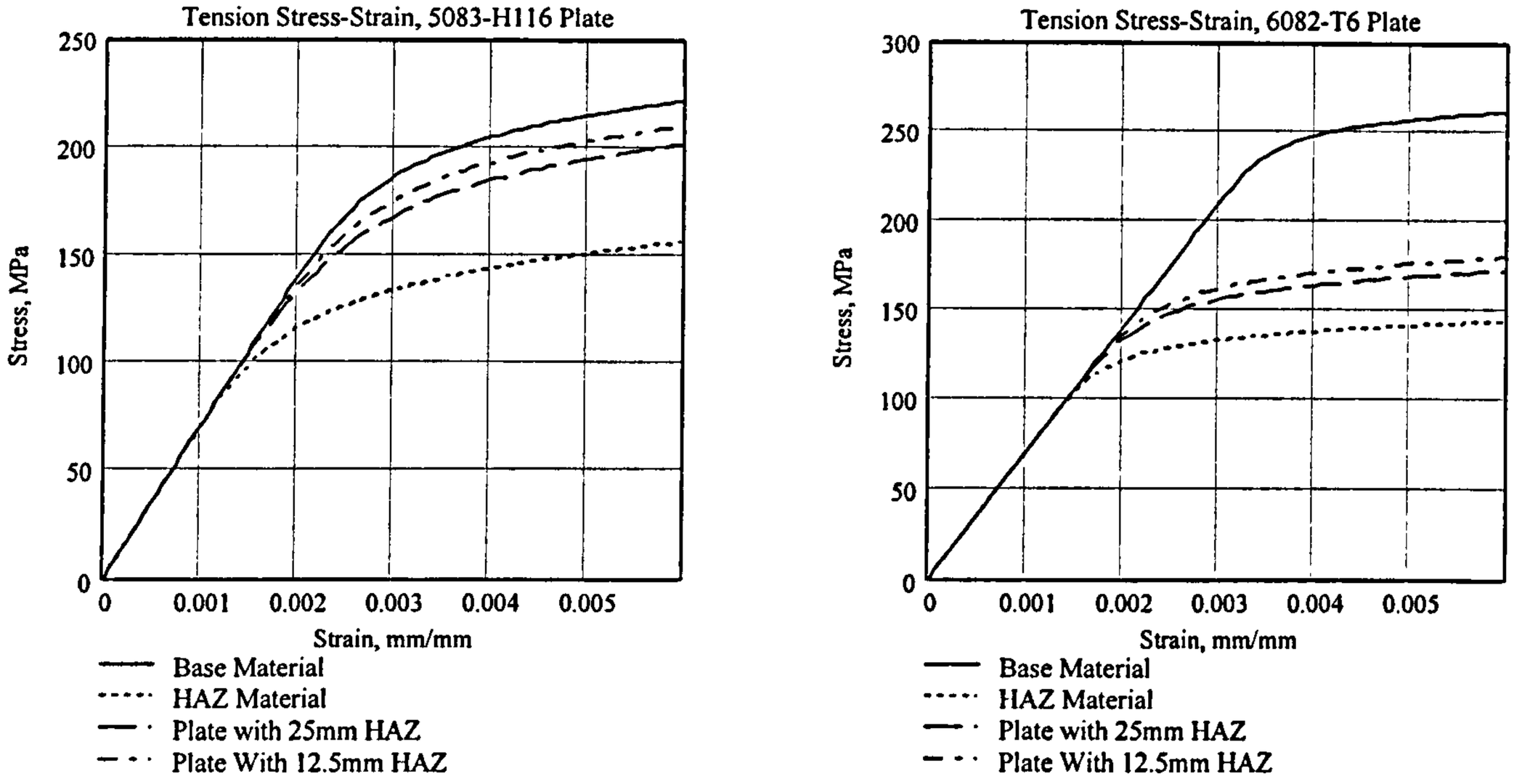

Figure 21: Welded Plate Tension Stress-Strain Curve

The results above show the effects of strain concentration in the transverse HAZ, however it is not clear if this region is in danger of fracturing. Examining Figure 21, it is clear that the strain in the transverse HAZ must be very large to develop the predicted tensile response. In both the 5083 and 6082 alloys, the tensile response curve lies above the HAZ material curve. However, as the transverse HAZ extends over the entire transverse edge, the stress in this transverse HAZ material must be equal to the overall tensile stress in the plate. To generate such stresses, the strain must be quite large, demonstrating the principle of strain concentration. To investigate this effect, the strain in the transverse HAZ was plotted against the strain in the overall plate, and the results compared to the grade minimum fracture strains. The results of this comparison are shown in Figure 22.

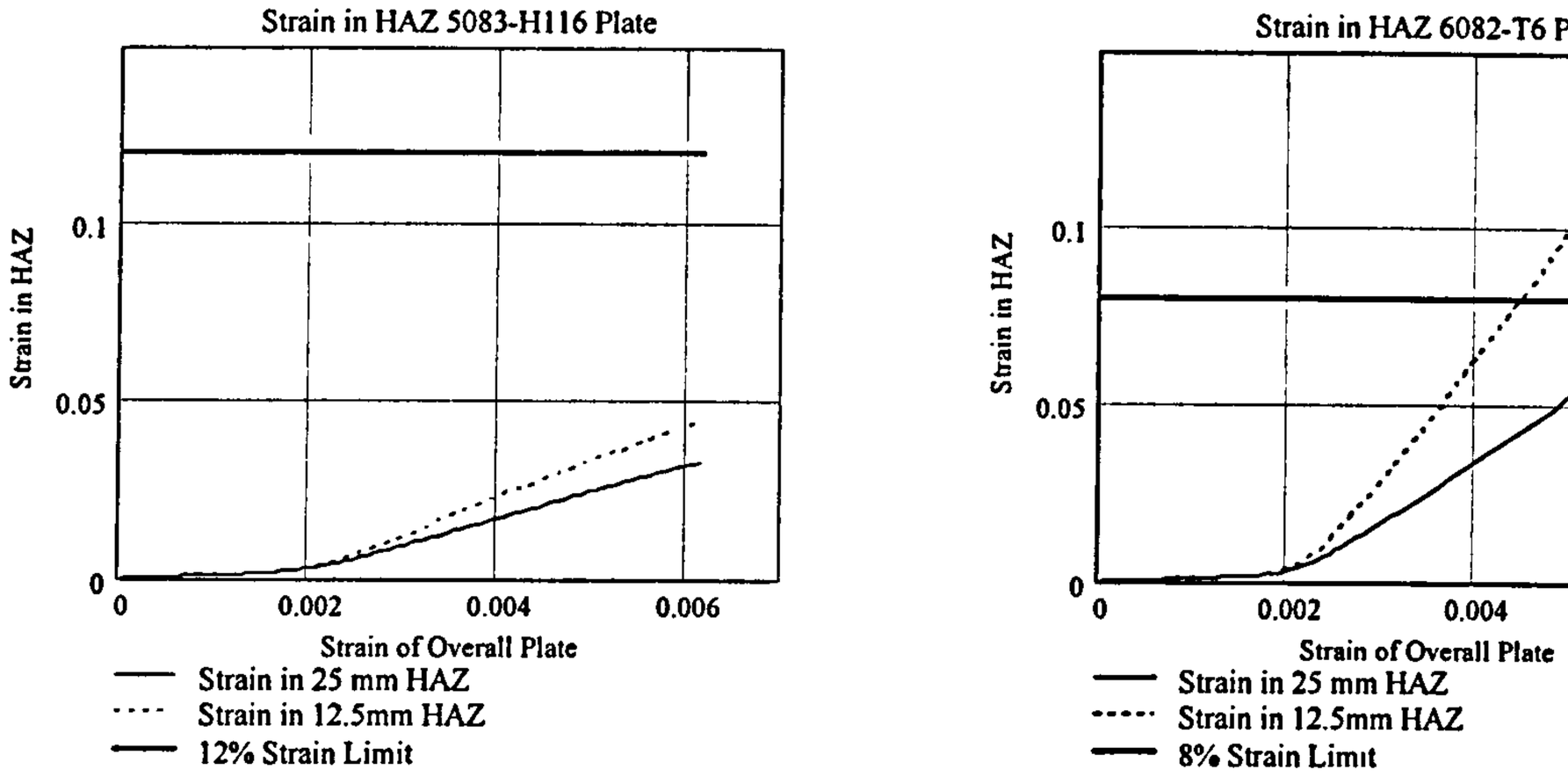

Figure 22: Strain in HAZ for Welded Plates in Tension

Here the difference between the 5083 and 6082 material is clear, with fracture a distinct possibility for the 6082 plate, but much more remote for the 5083 plate. The wider difference in HAZ to base metal proof stresses and the lower hardening exponent of the 6082 material means that the HAZ must carry a larger share of the strain in the 6082 material than in the 5083 material. This, coupled with a 50% lower maximum allowable strain means that fracture could occur at strains of roughly 0.0045 for a 1000mm long 6082 plate with 12.5mm HAZ at each end. At fracture, the plate has reached the specified ultimate strength of 6082 HAZ material, so there is no reduction in the ultimate strength of the plate in tension from what one would predict based on the HAZ material properties alone. However, if the plate is used in a beam-like assembly such as a ship hull girder, the ductility of the plate is important as well as its ultimate strength. For the entire assembly of individual plates and panels to develop its maximum resisting moment, individual components may be required to sustain strains greater than that corresponding to their ultimate stress, to allow other members of the structure to become fully effective. For consideration, the ultimate compressive strength of a 6082-T6 plate is predicted to occur at a strain of $\sigma_{0.2}/E$, or 0.0037, in the load-shortening procedure developed above. If the neutral axis is located closer to the compression flange than the tension flange of a hypothetical beam section, it is possible that fracture could be observed in the tension flange in the same region as the maximum resisting strength of the compression flange, potentially reducing the overall resisting moment. Thus, the effect of strain concentration should not be ignored when investigating structures such a the hull girder of a HSV. The potential for a fracture failure mode will be examined further in Section 3.5.

3.4 Response of Stiffened Panels

The stiffened panel is the basic building block of most ship structures[123], including aluminium HSVs, and thus an understanding of its behaviour is essential to understanding the overall response of the vessels structure. The response of such panels will be investigated here, following a similar approach to that taken for plates in the previous section. The stiffened panel typically used in HSV construction is longitudinally stiffened, consisting of plating and evenly-spaced stiffeners running in the fore-aft direction, supported periodically by transverse frames. A sketch of a stiffened panel with the principle dimensions labelled is shown in Figure 23, while a picture of an aluminium panel is shown in Figure 25.

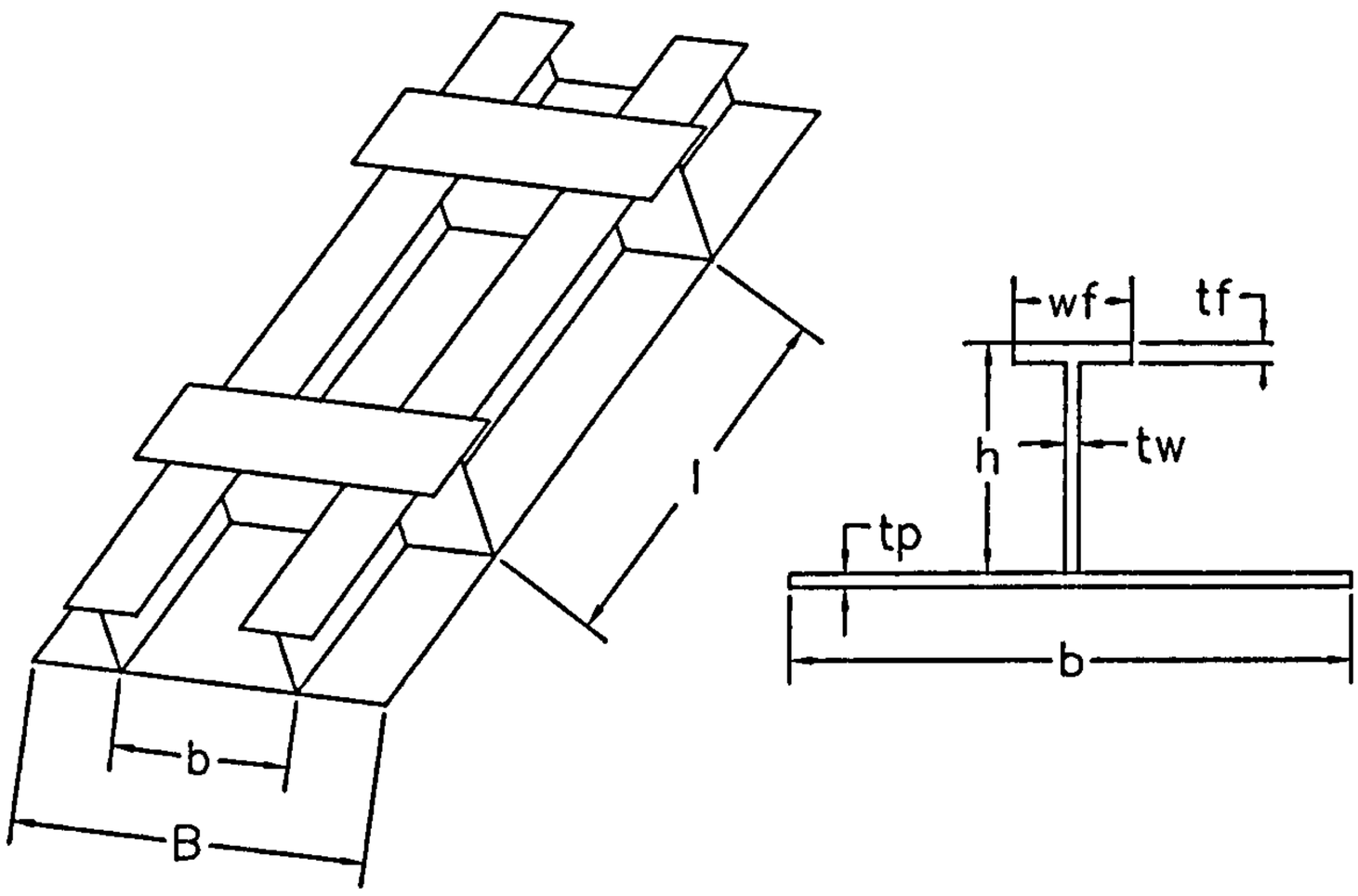

Figure 23: Stiffened Panel Dimensions and Nomenclature

The response of stiffened panels to axial compression is marked by several potential failure modes, combining aspects of plate response and column buckling. Paik and Thayamballi[20] have classified the potential failures into six different modes:

Mode 1: Overall collapse of stiffeners, plating, and transverse frames.

Mode 2: Biaxial compressive collapse of the plating between stiffeners

Mode 3: Beam-column type collapse of the plating and attached stiffener out of plane

Mode 4: Local buckling of the stiffener web

Mode 5: Tripping of the Stiffener

Mode 6: Gross Yielding

Dividing the failure modes in this manner is useful to gain insight into the type of behaviour that must be considered when determining the strength and response of the panel. However, it must be kept in mind that this division is fundamentally artificial and failures showing

interaction or combinations between these modes may occur as well [20]. Based on these six failure modes, it is clear that some of the key aspects of the response of stiffened panels in compression are:

- The plating and stiffener may buckle out-of-plate as a unit. This type of response can typically be modelled by treating the panel as a series of parallel columns, each column consisting of a single stiffener and a portion of the attached plating. This buckling may be elastic, and predicted by the Euler buckling equation, or inelastic, requiring a different approach, such as the tangent modulus approach.
- The plating may buckle as the panel is compressed, thereby providing less support to the stiffener and weakening the plating and stiffener combination as a column. This type of response builds on the plating response predictions developed in the previous section.
- The stiffener may fail itself, either from local buckling of the web or the stiffener flange, or in a tripping-type failure where the stiffener collapses sideways. In either case, after such a failure the stiffener has lost most of its effectiveness in stiffening the plate.

For typical ship structures, buckling of the stiffeners and transverse frames together(Mode 1) is quite rare as the transverse frames are normally strong enough to prevent such a failure. Hughes discusses the requirements on the transverse frames to prevent overall buckling in Chapter 13 of his book on structural design[21]. Likewise, the panels in HSVs are unlikely to be stocky enough to fail by gross yielding(Mode 6). However, the remaining failure modes are likely to occur for HSVs. Likewise, the tensile response of aluminium panels needs to be investigated. For steel panels, the tensile response of stiffened panels is similar to that of plates, and well approximated by the material's stress-strain curve. For aluminium panels, the potential for strain concentration to modify this response exists for panels as was previously shown for plates.

The investigation of the response of stiffened panels presented below will follow the same structure as the investigation into the response of plates. First, the previously published experimental test programs will be reviewed to assemble a data set to validate the prediction techniques against. Similar to the plate tests described above, these consist of compression tests only. Then, existing techniques for predicting the ultimate strength of stiffened panels will be presented, and their performance compared to the experimental results. These methods include both marine and civil engineering approaches, and range from simple regression equations to more complex methods which aim to directly address the failure modes discussed above. A similar presentation and comparison will be made with methods designed to predict the stress-strain curve of a panel in compression, including a modified method developed to account for some of the material-specific aspects of

aluminium panel response. Finally, a modified version of the plate tensile stress-strain curve method will be developed to model the tensile response and strain concentration effects in stiffened panels.

3.4.1 Experimental Results

3.4.1.1 Admiralty Research Establishment Panel Tests

The Admiralty Research Establishment (A.R.E.) in Dunfermline published the first set of ultimate compressive strength test results for ship-type stiffened aluminium panels in the 1980s. J.D. Clarke[134] presented the results of tests on five different panels at the International Conference on Steel and Aluminium Structures. Additionally, the original A.R.E. test report by Clarke and Swan was also released to the public [133]. The panels were of all-welded construction, with two complete frame bays. Three different tee-stiffened panels and one flat bar-stiffened panel were investigated, with one repeat test. All material was N8 aluminium alloy, which corresponds to the AA5083 series. Dimensions, material properties, residual stresses, and initial imperfections were measured. The dimensions and material properties of these panels are presented in Table 14. A typical panel set-up is shown below in Figure 24, while a picture of a panel on the test rig is shown in Figure 25.

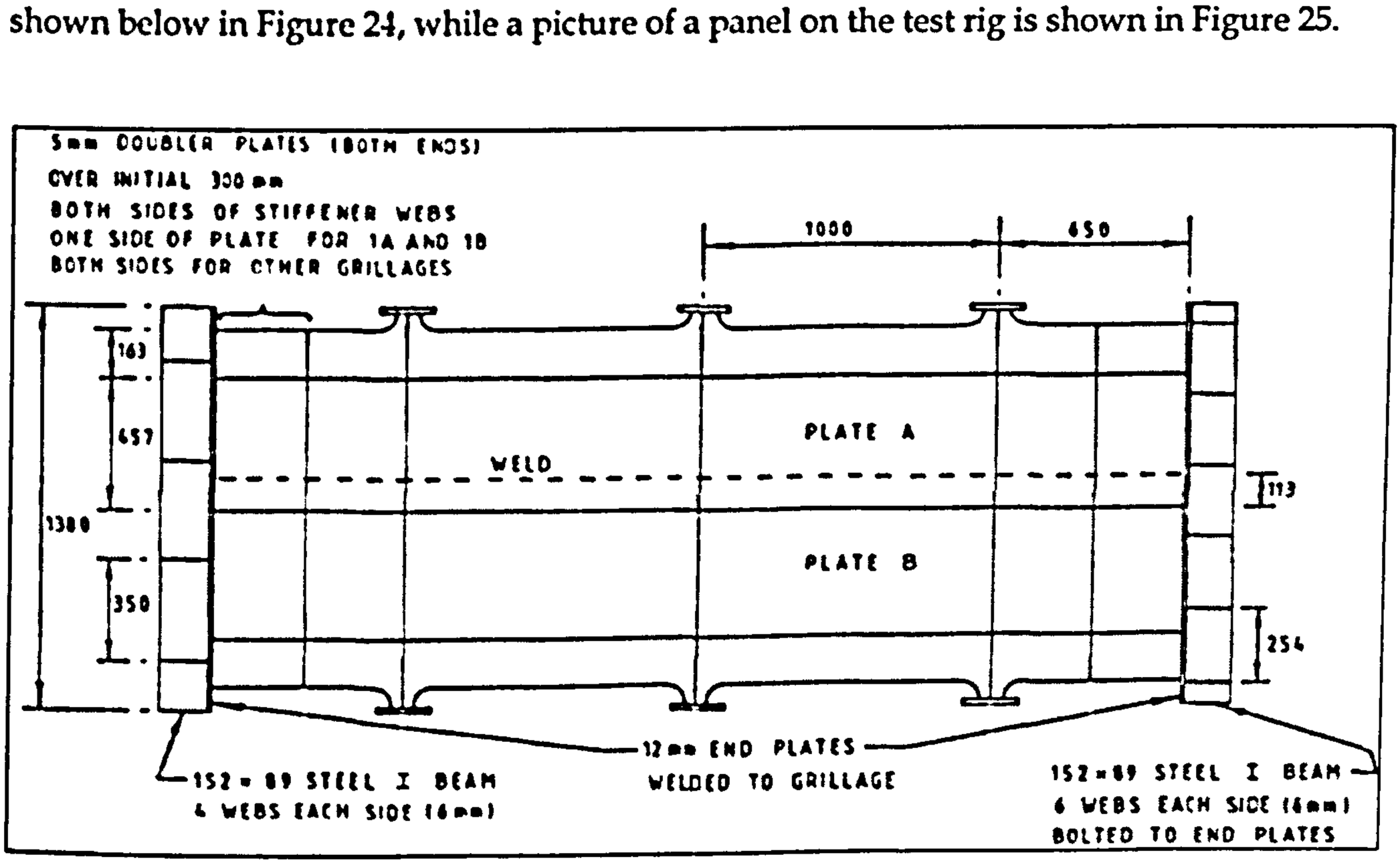

Figure 24 :A.R.E. Panels[133]

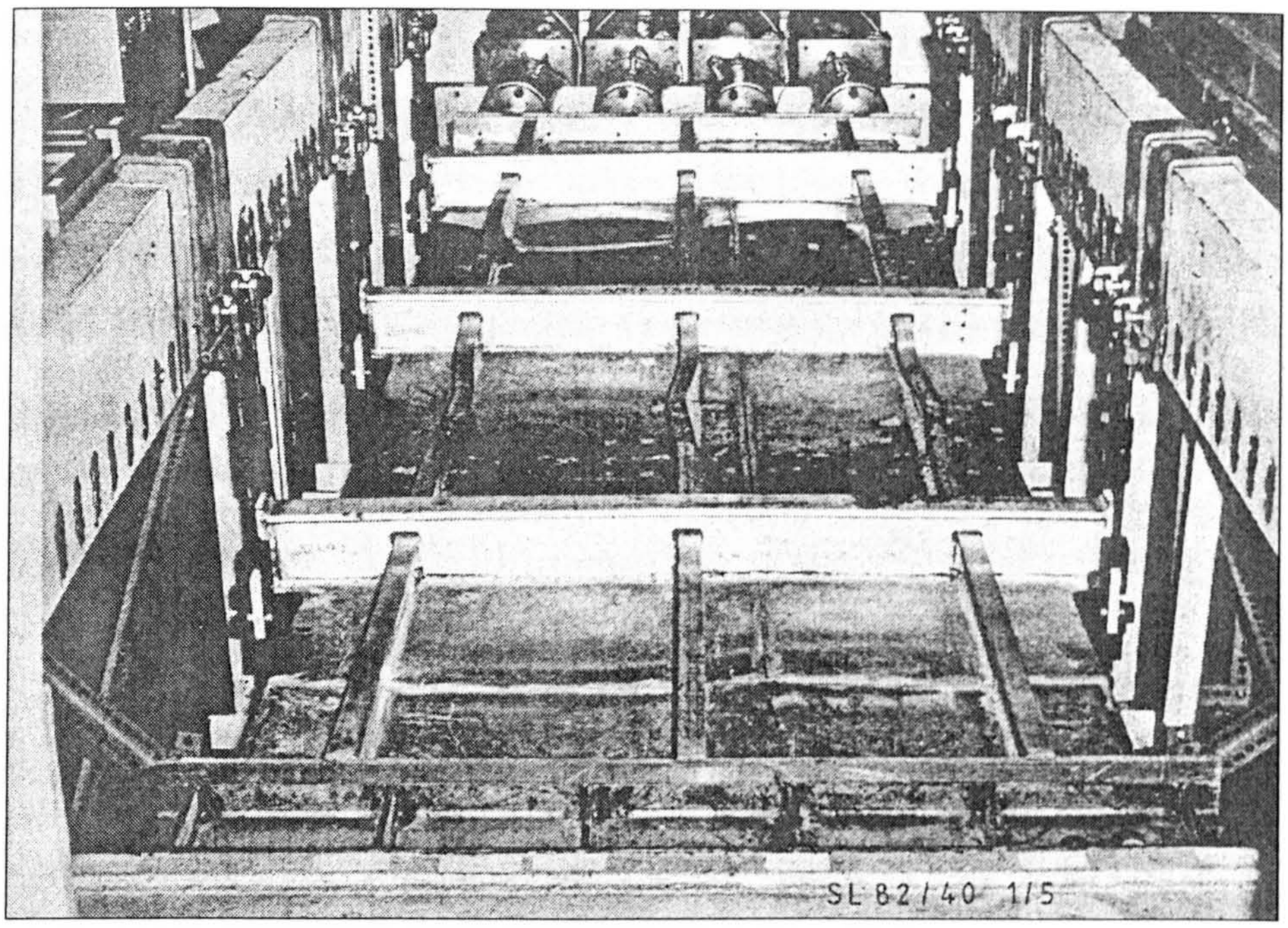

Figure 25: A.R.E. Panel 1B After Test[133]

After the initial condition of the panels were recorded, A.R.E. conducted displacement-controlled uni-axial compression tests to determine the entire load-shortening curve of the panels. Additionally, vertical plate and stiffener deflections, and plate and stiffener strains, were measured at several locations throughout the panel as the compressive load was applied. Clarke and Swan[133] present details of these measurements. While the panels were of two-bay construction, inter-frame buckling failure was assured by supporting the ends of the intermediate transverse web frames while leaving the longitudinal edges of the plate free. However, the free outboard edge of the plating was reduced in width so that the overall performance of the panel would be equivalent to that of 3 stiffener/plate combinations[133]. The effect of boundary conditions is further discussed below. Clarke and Swan[133] note that stiffener tripping, "only became noticeable in the post-buckling region and did not appear to influence the maximum load".

3.4.1.2 Zha et al. Panel Tests

Several years after the publication of the A.R.E. test results, Zha et al.[146] published the results of a second series of compression tests on ship-type aluminium alloy panels. The experimental program investigated 25 flat-bar stiffened panels, sized so that torsional buckling, or tripping, of the stiffeners was the dominate failure mode. The panels were constructed out of AA5083-H116 and AA6082-T6 alloys, and were of welded construction, with simply supported transverse ends and free longitudinal sides. Material properties and

initial deflections were measured. However, as the test program was conducted on a private contract, only typical values for these measurements have been published, and load-shortening curves and ultimate loads are only available for a sub-set of the panels. Additionally, many of the panels had intentionally-introduced eccentricities in the load application, which effects the ultimate strength prediction. The tests were conducted at the Norwegian University of Science and Technology in Trondheim, Norway. A sketch of the panel set-up is shown below in Figure 26.

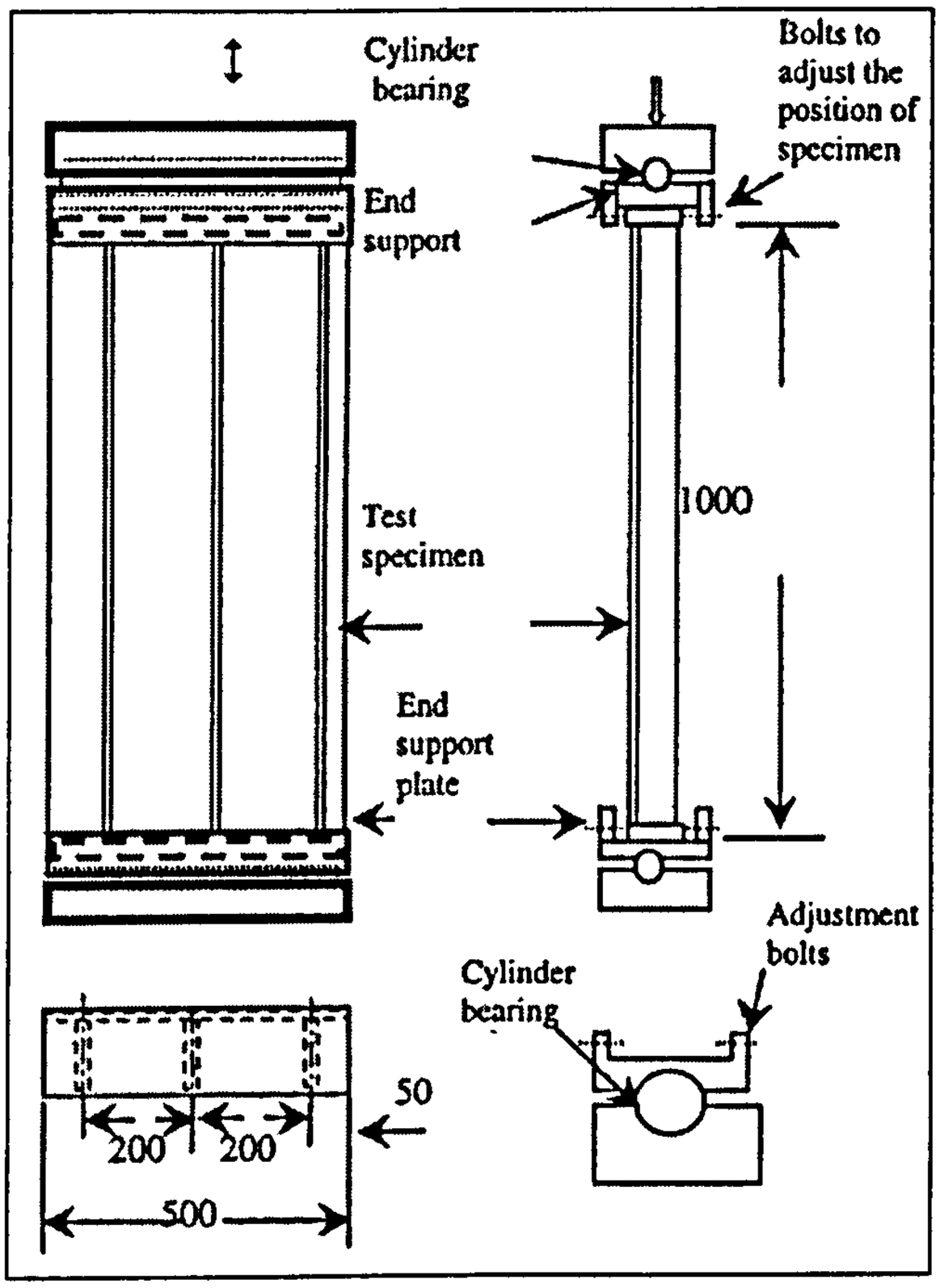

Figure 26: Zha et al. Test Panels[62]

After the initial publications of the experimental test results, Zha and Moan conducted further analysis of the experimental results and numerical studies, investigating effects such as residual stresses and the reduced material properties in the heat-affected zones (HAZ) adjacent to welds. The studies used the non-linear finite-element code ABAQUS to simulate the experimental results, and also to study a second set of panels of similar design but with no applied load eccentricity. These panels are also presented in Table 14. These studies were published in two further articles, [62, 145]. Additionally, Zha et al. investigated the accuracy of several aluminium and steel design codes in predicting tripping failures, including the Eurocode 9.

3.4.1.3 Aalberg et al. Panel Tests

At the same time Zha et al. were investigating the performance of flat-bar stiffened panels, Aalberg et al.[59] were conducting a similar test on extruded aluminium panels. These tests were also carried out at the Norwegian Institute of Science and Technology. The panels tested consisted of single-bay AA6082-T6 stiffened panels, with both open L-shaped and closed trapezoidal-shaped stiffeners. In addition to conducting the collapse tests, the resulting ultimate strength values were compared with the prediction of Eurocode 9. A vertical hydraulic test rig was used to conduct the tests, the test rig was capable of representing both simply-support and free boundary conditions along the lateral edges of the panels, while the transverse(loading) edges were simply-supported. Two different lengths of panel were tested, roughly 1000mm and 2000mm, with three stiffener and five stiffener panel widths tested. While the use of a closed-stiffener panel represents a type of construction that is easily employed with aluminium, the existing design equations investigated in this study can not handle such shapes, so these panels were not investigated further. Table 14 presents an overview of the geometry and material properties of the open-stiffener Aalberg et al. panels. While the stiffeners were extruded, not welded, the individual extrusions were joined by MIG welding. Tensile test were made on the stiffeners, plate, and HAZ around the welds. Additionally, initial imperfections were measured, while longitudinal bowing was still present, plate deformations from welding were much smaller than either the Clarke and Swan panels or the Zha et al. panels. No residual stress measurements were reported. The dimensions of the panel cross section are presented below in Figure 27 , along with a picture of the specimen on the test rig.

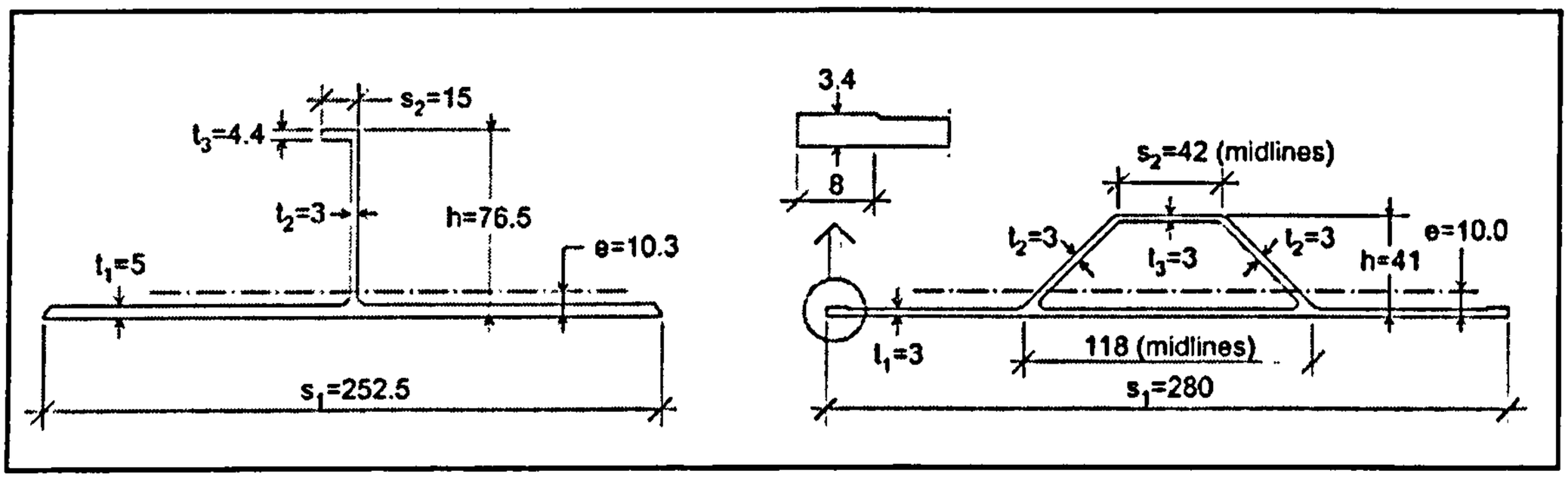

Figure 27: Aalberg et al. Panel Cross Section[59]

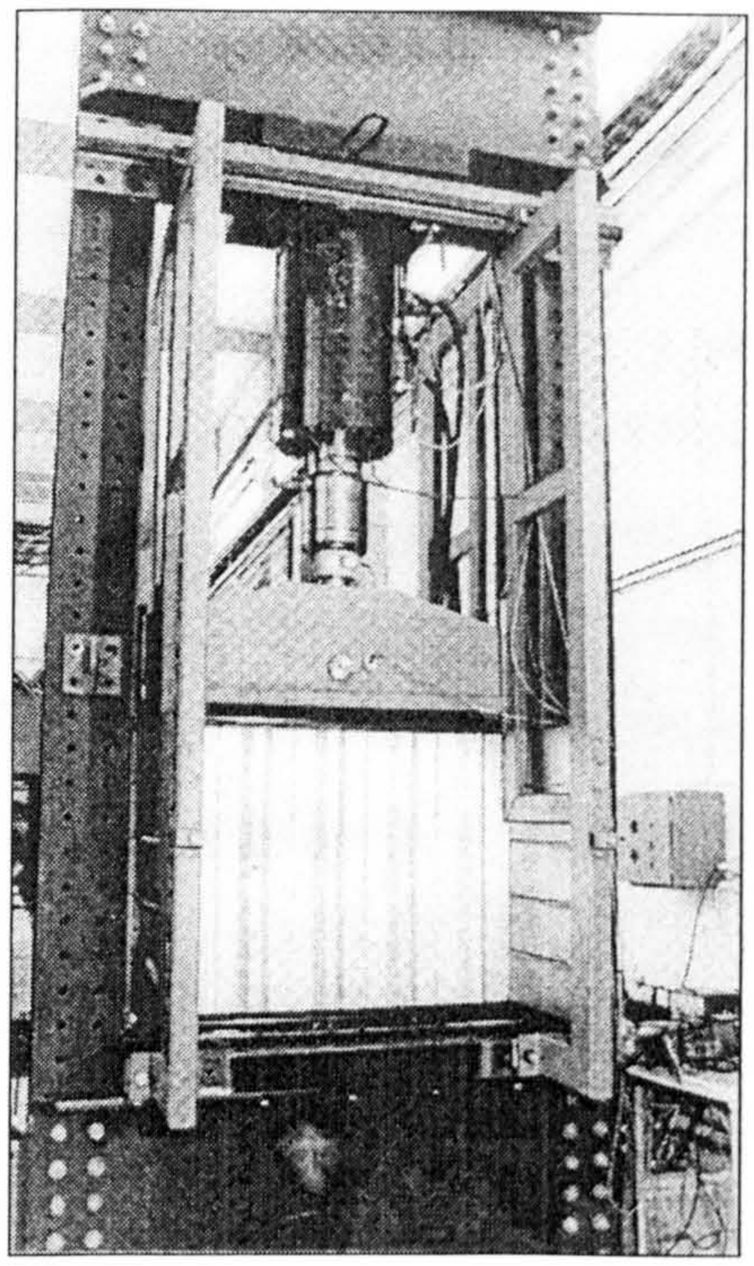

Figure 28: Aalberg et al. Test Rig[59]

3.4.1.4 Combination of Panel Test Results and Data Available

Compared to the steel panel test data, which numbers above two hundred panels tested[116], the aluminium test data available to date is very limited. Furthermore, not all of it is applicable to the current study. Some of the simplified ultimate strength methods can not handle eccentricity, so all of the physical panels tested by Zha et al., save panel A16 with negligible eccentricity, must be excluded from these methods. None of the methods can handle hollow stiffener shapes, so the hollow stiffener panels tests by Aalberg et al. must be excluded. It seems reasonable to include the Zha et al. finite-element panels, given the good agreement between this approach and the experimentally tested panels. Unfortunately, Zha et al. did not list the proof stress used for the AA6082-T6 panels in the finite element formulation, however, for the AA5083-H116 panels they used the minimum grade requirement of 215 MPa. Therefore, the corresponding minimum grade requirement of 260 MPa (255 MPa, t>6mm) was assumed for the finite-element panels made from AA6082-T6.

None of the test panels included transverse welds away from the ends of the panel. This lack of transverse welds means that the effects of the reduced material properties in the HAZ will not be fully explored in this study. This is unfortunate, as this effect may be significant. For example, the *Specification* of the Aluminum Association requires column elements with transverse welds located more than 5% of their length from their endpoints to be designed as if the entire column is heat-affected material[53], and recent finite element

studies have also shown that such welds can significantly reduce the ultimate strength[39]. It is however, important to emphasize that the effect of such welds on either the simplified methods or the beam-column method cannot be investigated with the approach of the current study as a result of the lack of experimental data.

A further complication is the different boundary conditions used in the various tests. The difference here lies predominantly in the boundary conditions on the longitudinal edges; though there is also a slight difference along the transverse frame boundaries, as Clarke and Swan tested multi-bay panels while the remaining tests were on single-bay panels. All three test series used different longitudinal boundary conditions. Clarke and Swan left the longitudinal edges of the plating free, but reduced the width of the outstanding plating so that the elastic buckling stress of the outstanding plate was the same as the elastic buckling stress of the plate between the stiffeners. While the total area of the resulting panels were only approximately 92% of the area of three complete stiffener/plate combinations, Clarke and Swan felt that the results obtained were reflective of three complete stiffener/plate combinations for inter-frame buckling[133]. For loads in the linear elastic region, Clarke and Swan recommend dividing the failure load by the fractional number of stiffener-plate combinations, based on the cross-sectional area of the test panel.

Aalberg et al. tested panels under two different boundary conditions, free edges and simple support. When the edges were left free, the outstanding plating was not reduced to match buckling stresses as Clarke and Swan did, and Aalberg et al. mention that for some of these panels large deformations appeared in the outstanding plate at load levels that were only 52% of the ultimate load, indicating that these results may underestimate the actual ultimate strength. However, for the simply-supported Aalberg et al. results the outermost plate panel width is only half that of the stiffener spacing, hence this plate panel will carry a much higher load than the plating between the stiffeners. Furthermore, Aalberg et al. noted that the maximum load occurred when this outermost panel buckled. Zha et al. tested panels with free longitudinal edges, but reduced the width of the outstanding plating proportionately more than Clarke and Swan. However, most of the panels tested by Zha and Moan failed in tripping without significant plate buckling, so it is uncertain how much effect this outstanding plate had on the results.

For the ultimate strength and stress-strain curves investigated below, the failure load per stiffener/plate combination or per area(stress) is often determined, thus, a consistent approach needs to be developed to determine the failure stress from the experimental results. The common assumption in ship design is that the stiffened panel behave as if they were simply-supported on their boundaries with heavier structural members, especially

when there is no lateral pressure on the panel. This assumption seems to be appropriate for the current study, given the experimental boundary conditions discussed above. In determining the experimental failure load per stiffener/plate combination, the following assumptions are made to reflect simply-support boundaries:

- In accordance with Clarke and Swan's recommendations, the reported experimental failure loads will be taken as the failure loads for three complete stiffener/plate combinations. When computing the load-shortening curve, the same assumption will be made except in the initial linear part of the load-shortening curve where the behaviour is clearly elastic.
- For the Aalberg et al. panels, only the simply-supported panel data will be used (Panels I-M) , for these panels, the published failure loads represent five complete stiffener/plate combinations. In all likelihood this represents an upper bound on the strength of the panel as these panels had stronger-than-actual outer plating bays. However, the free edge panels have weaker-than-actual outer plating bays, and are only three plate/stiffener combinations wide. The simple support panels are five plate/stiffener combinations wide, so hopefully the influence of the outer plating bays will be proportionally lower.
- For the Zha et al. panels, the failure load will be divided by the fractional number of complete stiffener/plate combinations in each test case, based on cross-sectional area (about 2.6 combinations for each panel). This approach should not be inconsistent with Clarke and Swan's approach, as for all of the Zha et al. panels the panel behaviour was virtually linear elastic until the ultimate load was reached, while the panels tested by Clarke and Swan showed significant deviations from the linear elastic response by the time the maximum load was reached. For the Zha et al. panels, this linear elastic behaviour can most likely be attributed to the fact that these panels failed suddenly by tripping with little or no previous flexural column or plate buckling.

It is believed that this these assumptions are reasonable and should be fairly accurate, however, combining tests with different boundary conditions does introduce another source of uncertainty in the results.

Table 14: Dimensions and Properties of Experimental Panels

Panel		Panel Length, l [2]	Plate Width, b	Plate Thickness , tp	Plate Yield, σyp	Height, h	Web Thickness, tw	Flange Width, fw	Flange Thickness, tf	Stiffener Yield, σys	Stiffener Type	Alloy	Number of Stiffeners	Average Yield Stress	Plate Slenderness, β	Overall Slenderness, λ	Collapse Load
		mm	*mm*	*mm*	*MPa*	*mm*	*mm*	*mm*	*mm*	*MPa*	--	--	--	*MPa*	--	--	*kN*
A.R.E[3]	1A	1000	459.6	5	282	76	4.3	38	7.9	162	T	5083	3	257	5.81	0.78	850
	1B	1000	456.1	5	264	76	4.3	38	7.9	162	T	5083	3	243	5.64	0.75	800
	2A	1000	455.7	7.4	162	76	4.4	38	8	178	T	5083	3	164	3.00	0.69	1070
	3A	1000	457.3	12.4	189	76	4.3	38	7.9	178	T	5083	3	188	1.93	0.86	1710
	4A	1000	456.8	7.7	161	78	9.4	0	0	87	FB	5083	3	148	2.86	0.78	760
Aalberg et al.	I	2035	252.5	4.9	255	71.3	3	14.9	4.4	265	L	6082	5	257	3.09	2.02	737
	J	2050	252.5	4.9	254	71.6	3	14.9	4.4	270	L	6082	5	257	3.12	2.01	693
	K	1073	252.5	4.9	254	71.6	3	14.9	4.4	270	L	6082	5	257	3.12	1.05	893
	L	1007	252.5	4.9	265	71.4	3	14.8	4.4	284	L	6082	5	268	3.20	1.01	899
	M	1007	252.5	4.9	265	71.4	3	14.8	4.4	284	L	6082	5	268	3.20	1.01	872
Zha et al.[1]	A16	1000	200	6	294	75	6	0	0	294	FB	6082	3	294	2.16	0.97	738
	N1[4]	1000	200	8	215	100	5	0	0	215	FB	5083	3	215	1.39	0.65	1011
	N2[4]	1000	200	5	215	100	5	0	0	215	FB	5083	3	215	2.22	0.59	458
	N3[4]	1000	200	5	215	80	5	0	0	215	FB	5083	3	215	2.22	0.77	467
	N4[4]	1000	200	5	215	80	3	0	0	215	FB	5083	3	215	2.22	0.90	287
	N5[4]	1000	200	5	215	60	5	0	0	215	FB	5083	3	215	2.22	1.10	406
	N6[4]	1000	200	8.5	255	100	6	0	0	260	FB	6082	3	256	1.42	0.69	990
	N7[4]	1000	200	6	260	100	6	0	0	260	FB	6082	3	260	2.03	0.65	785
	N8[4]	1000	200	6	260	75	6	0	0	260	FB	6082	3	260	2.03	0.91	734
	N9[4]	1000	200	5	260	60	6	0	0	260	FB	6082	3	260	2.44	1.15	487

Notes:

1: Only nominal dimensions, properties, and initial deflections available for the Zha et al. panels
2: Length includes distance to end bearings of the test rig, if reported
3: ARE Panels reported an elastic modulus of 69400 MPa, 70000 MPa used for all other panels.
4: Indicates a non-linear finite-element simulated collapse as opposed to a physical panel test

3.4.2 Compressive Ultimate Strength Prediction

Five simplified methods which aim to predict the ultimate strength alone are reviewed in this section. These methods consist of one or more closed-form equations which give the ultimate load or stress that a given panel can withstand. The first two methods, that of Paik and Thayamballi[35], and that of Herzog[116] are regression equations derived from experimental test results of steel stiffened panels. As these equations were not developed or verified for aluminium panels, there accuracy is in doubt, although they can account for aluminium's lower proof stress and elastic modulus. However, many classification societies use the same basic design formulas for aluminium structures as with steel structures in their existing rules, so it is worth investigating if the same approach could be made for limit-state formulations. The third method is an aluminium-specific regression

equation developed by Paik and Duran[151]. The remaining two methods are aluminium civil engineering codes, the Eurocode 9[60]from Europe, and the Aluminum Association's *Specification*[53] from the United States, both of which were developed for aluminium structures, but not specifically ship structures. These will each be reviewed in turn.

3.4.2.1 Paik and Thayamballi

Paik and Thayamballi[35] developed a simple, close-form equation for predicting the compressive strength of steel stiffened panels. This equation is intended for quick estimation of the ultimate strength of stiffened panels for preliminary design work, and reliability studies investigating the collapse of ship hull girders[29]. It is not intended for detail design of specific panels. Paik and Thayamballi decided the best way to proceed was to develop an empirical regression equation from the large published database of steel stiffened panel collapse tests. The equation developed took the form of a regression equation in terms of the plate and column slenderness of the panel. The plate slenderness is the same β as discussed in the previous section, while the column slenderness is defined as:

$$\lambda = \frac{l}{\pi r}\sqrt{\frac{\sigma_0}{E}}$$

Where:

λ Column slenderness

l Length of column

r Radius of gyration of column cross - section

σ_0 Yeild or 0.2% offset proof stress

E Elastic modulus of column material

Equation 28

Such an equation was originally proposed by Lin[154], however, new numerical constants were derived to include additional panels tested by Paik and Thayamballi. In addition to their own panel tests, Paik and Thayamballi included test data from Horne et al. [118, 119], Faulkner[155], Niho[156], and Yao[157] in their regression. The panels included were limited to panels with nearly simple-support boundary conditions, and average values of initial imperfections and welding residual stresses. Therefore, the regression coefficients obtained should implicitly include the effects of typical initial imperfection and residual stresses. The final equation derived by Paik and Thayamballi took the following form:

$$\frac{\sigma_U}{\sigma_0} = \frac{1}{\sqrt{0.995 + 0.936\lambda^2 + 0.170\beta^2 + 0.188\lambda^2\beta^2 - 0.067\lambda^4}} \le \frac{1}{\lambda^2}$$

Where:

σ_U Ultimate Stress

σ_0 Yeild Stress

Equation 29

Where the Euler buckling stress limit was a later addition to the formulation not present in the original paper, but does appear in later references to the equation[20, 38]. Paik and Thayamballi also compared the accuracy of the new equation with the data used to determine the regression coefficients. This comparison is summarized in Table 15 below, it is not clear if these results include the Euler buckling limit.

Table 15: Paik and Thayamballi Regression Performance(From [35])

Paik and Thayamballi Regression Equation			
Experimental Results	**# of Panels**	**Bias**	**COV**
Horne	38	0.979	0.132
Faulkner	43	1.011	0.162
Niho	7	0.956	0.123
Yao	7	0.921	0.066
Paik and Thayamballi	10	0.903	0.114

Note:

Bias is Mean of $\sigma_{uFormula}/\sigma_{uExperiment}$

COV is Coefficient of variation of the bias

When applying this formula to aluminium several issues need to be addressed. The lower yield stress and elastic modulus of aluminium should be accounted for in this formula, as the equation relies on the coefficients β and λ, which account for both the yield stress and the elastic modulus of the panel material. However, the initial imperfections and residual stresses are implicitly included in the coefficients of the equation. If initial imperfections and residual stresses reduce the strength of aluminium panels differently than steel, the current form of this equation will contain a bias. Finally, the database of panel collapse loads used to develop the regression coefficient did not contain many tripping collapses. While this mode of failure is undesirable in a structure, and should be avoided by design when possible, much of the experimental collapse data available for aluminium is for tripping failures. Therefore, applying this formula to the current aluminium collapse data will heavily test a mode of failure that had a relatively minor role in determining the regression coefficients for the equation.

3.4.2.2 Herzog

Civil engineers have also addressed the collapse of steel stiffened panels in compression. Herzog[116] proposed a regression equation for the ultimate compressive strength of steel stiffened panels based on a statistical regression of 215 panel collapse tests, including the Monash[117, 158, 159] and Horne et al.[118, 119] tests among others. Herzog modelled the stiffened panels as a series of independent, identical columns, ignoring lateral

constraints, and proposed the following equation for the mean collapse stress, where the variables are as in Paik and Thayamballi's equation:

$$\frac{\sigma_U}{\sigma_0} = 0.5 + 0.5\left(1 - \frac{\lambda}{2}\right)^2 \qquad \textit{Equation 30}$$

Where λ should be restricted to being less than or equal to two. To account for high values of plate breadth to thickness, this equation is multiplied by the factor R2 when the plate b/t is greater than 45:

$$R_2 = 1 - 0.007\left(\frac{b}{t} - 45\right) \qquad \textit{Equation 31}$$

Like the Paik and Thayamballi method above, average initial imperfections and residual stresses are implicitly included in the regression equation. To account for panels where non-average imperfections and residual stresses are present, Herzog adopted the following additional multiplier:

M=1.2	No or average initial imperfections, no residual stress
M=1.0	Average initial imperfections and residual stress
M=0.8	Average or large initial imperfections, large residual stress

When comparing the results predicted by this equation to the measured collapse stress for the 215 panels, Herzog reported a mean bias of 1.004, and a coefficient of variation of 0.135, using the same definition of bias and coefficient of variation as Paik and Thayamballi above.

As Herzog's regression equation contains the effects of initial imperfections and residual stresses in numeric coefficients, its applicability to aluminium is unknown, for the same reasons as Paik and Thayamballi's regression equation above. An additional cause for concern is that the coefficient R2 uses b/t, not β to account for plate slenderness. The b/t ratio is not independent of the material, in other words, an aluminium plate with the same b/t value as a steel plate will behave in a more slender manner. However, an "equivalent" steel b/t value can be determined for an aluminium plate by calculating the value of steel b/t that will yield a β value equal to the β value of the aluminium plate. This approach was used by Clarke and Swan when comparing their collapse test results to the predictions of an in-house computer program originally developed for steel[133]. Using this approach, the equivalent b/t is determined as:

$$\beta_{AL} = \beta_{STEEL}$$

$$\left(\frac{b}{t}\right)_{AL}\sqrt{\frac{\sigma_{0AL}}{E_{AL}}} = \left(\frac{b}{t}\right)_{STEEL}\sqrt{\frac{\sigma_{0STEEL}}{E_{STEEL}}}$$

$$\left(\frac{b}{t}\right)_{STEEL} = \left(\frac{b}{t}\right)_{AL}\frac{\sqrt{\frac{\sigma_{0AL}}{E_{AL}}}}{\sqrt{\frac{\sigma_{0STEEL}}{E_{STEEL}}}}$$

Equation 32

This leaves the question of what yield stress should be used for steel in the conversion. The 215 panels Herzog used to derive the regression equation had yield stresses between 193-440 MPa. Unfortunately, when conducting the current study, test data was not available for all of these panels, so the distribution of yield stress values within this range is unknown. A simple mean value yields 316.5 MPa, which when comparing with the yield stress values reported by Horne, does not seem to be far off the mark. Therefore, a value of 316.5 MPa for the yield stress of steel was used in determining the equivalent b/t. Collapse strength values for the aluminium panels were calculated both with and without the use of the equivalent b/t, and the results reported separately below.

3.4.2.3 Paik and Duran

Paik and Duran[151] revisited the regression equation originally developed by Paik and Thayamballi, and proposed a new set of coefficients for aluminium panels. These coefficients were derived from a parametric collapse study consisting of non-linear finite element collapse simulations on tee-stiffened aluminium panels for 5083-H116 alloy. The finite element models consisted of one full stiffener bay and a half-bay at each end with symmetric boundary conditions. One stiffener was modelled, and the plating was modelled to half a stiffener spacing on each side of the stiffener, with symmetric boundary conditions applied to the free edge. Thus, the finite element model approximates an infinite stiffened panel. Paik and Duran derived the equation using modified β and λ parameters to account for the HAZ. This follows their approach for predicting the ultimate strength of plates discussed above. The final form of the regression equation was:

$$\frac{\sigma_U}{\sigma_{eq}} = \frac{1}{\sqrt{1.038 + 1.099(\lambda')^2 + 0.093(\beta')^2 - 0.047(\lambda'\beta')^2 + 1.648(\lambda')^4}}$$

$$\frac{\sigma_U}{\sigma_{eq}} \leq \frac{1}{(\lambda')^2}$$

Where:

σ_U Ultimate compressive stress of stiffened panel

β' As in Paik and Duran plate regression equation

$$\lambda' = \frac{l}{\pi r}\sqrt{\frac{\sigma_{eq}}{E}}$$

σ_{eq} Equivlent yield stress accounting for HAZ

Equation 33

$$\sigma_{eq} = \frac{P_S}{b_p t_p + h_w t_w + b_f t_f}$$

$$P_S = (b_p - 2b_p')t_p\sigma_{0\_P} + 2b_p' t_p \sigma_{0\_HAZ\_P} + (h_w - b_s')t_w\sigma_{0\_S} +$$

$$b_s' t_w \sigma_{0\_HAZ\_S} + b_f t_f \sigma_{0\_S}$$

l Panel length

b_p, b_f, t_f Plate and stiffener flange width, flange thickness

b_p', b_s' Width of longitudinal HAZ in plate and stiffener web

h_w, t_w Stiffener web height and thickness

$\sigma_{0\_P}, \sigma_{0\_S}$ Base material 0.2% offset proof stress in plate and stiffener

$\sigma_{0\_HAZ\_P}, \sigma_{0\_HAZ\_S}$ HAZ material 0.2% offset proof stress in plate and stiffener

Where variables not defined are the same as their previous definition. In applying this formula, the equivalent plate slenderness was calculated as shown in Equation 18. This regression equation was derived from 5000-series tests only, so its applicability to 6000-series panels is not known. Paik and Duran reported good agreement when compared to Zha and Moan's panel test, however, most of these panels failed by tripping in the elastic region, so the strain-hardening properties of the alloys may not have been fully tested in these experiments.

3.4.2.4 Eurocode 9

Eurocode 9 is the European Committee for Standardization (CEN) standard design code for structural design with aluminium, and uses an ultimate-strength/partial safety factor approach for dimensioning stiffened panels. The format and style of the approach was intentionally made as similar to Eurocode 3, the steel structural design code, as possible[152]. The version reviewed here is the 1998 edition, specification ENV 1999-1-1: 1998 E. Section 5.11.2 of the Eurocode contains an ultimate strength formulation for simply supported stiffened panels. In light of the boundary assumptions discussed above in Section 3.4.1.4,

this section was used for all panels. Two explicit checks are made in this section, local squashing of the panel, and column buckling. The lowest failure load of these two failure modes governs the design of the panel. However, before these calculations can be made, the effect of local buckling of sub-members of the panel and the weakening effect of HAZ must be accounted for. Eurocode 9 adopts an effective thickness approach for both of these factors, where the thickness of each element in the section is reduced, if necessary, to account for local buckling and HAZ. This approach is similar to the approach for plates discussed previously. These reduced thicknesses are applied as specified by the code to calculate squash and column failure loads. An overview of the effective thickness approach in Eurocode 9 is given by Bulson[152].

After the effective thicknesses of the members in the section are calculated, the squash limit state is determined from the net effective area, the ultimate strength of the alloy, and a partial safety factor. Then the column-buckling ultimate compressive load is determined by treating the panel as a modified strut or column and determining its buckling load by the standard column approach. Unlike the two formulations reviewed above, the Eurocode 9 buckling calculation requires information relating to the overall panel dimensions in addition to the dimensions of a single plate and stiffener combination. This leads to some difficulty with the boundary assumptions discussed previously. To compare with the calculation methods used above, the effective thicknesses were calculated for a full plate and stiffener combination, and then applied uniformly to the entire panel, without applying any special treatment for the outermost strips of plating which may have different slenderness ratios. This leads to different predictions of strength than those previously reported[59, 146], but is believed to reflect the method in which this code would most likely be applied in preliminary design. In calculating the effective thicknesses, Bulson's[152] advice was followed, and the effective thickness reductions for buckling and HAZ effects were not taken as additive, rather, the largest reduction was taken as governing.

3.4.2.5 Aluminum Association

The U.S Aluminum Association has published a LRFD code for the construction of building-type aluminium structures[53], known as the *Specification*. The *Specification* does not explicitly address stiffened panels in compression. To apply the code to stiffened panels, the commonly used assumption that a stiffened panel can be idealized a series of identical, parallel columns consisting of a single stiffener and attached plate was used. The *Specification* include formula for columns that undergo local buckling of the sub-elements of the column, so this approach should be able to handle plate and stiffener buckling in the panel. With this assumption, the column formulae of the code were used to compute the

compressive strength of these columns. It is important to note that this approach is the authors' own approach, not that of the Aluminum Association.

Taking this approach, the strength of each column was taken as the lowest of three strengths. The first was the overall buckling strength of the column from Section 3.4.7 of the *Specification*. This section investigates a plate and attached stiffener as a column, and determines the buckling stress, either an elastic Euler buckling stress, or an inelastic buckling stress which is estimated by a straight-line relationship similar to the approach taken for plates which was presented in Section 3.3.2.3 of this thesis. The second was the weighted-averaged buckling strength of all the sub-elements in the column, such as plate between stiffeners, stiffener webs, and stiffener flanges, using Sections 4.7.2, and 3.4.8.1, 3.4.9 and 3.4.9.1 of the *Specification*. Finally, for panels in which the local elastic buckling stress of a sub-element was less than the overall buckling stress of the column, the interaction check between local and overall buckling in Section 4.7.4 of the *Specification* was also made. The presence of the HAZ around welds was accounted for in the calculation of the overall buckling stress using Section 7.1.2 of the *Specification*. The proof stress of the alloys in the base and welded condition were taken as the values presented in Chapter 2. In calculating the local strength of the plates, no post-buckling strength was included, as the overall "column" of a plate and attached stiffener is not buckling about an axis of symmetry. Furthermore, the ultimate strength of the assembly was limited to the proof stress in the HAZ for panels that contain transverse welds at their loaded edges, as required by Section 7.1.2 of the *Specification*. Given the ability of the 5000-series alloys to strain harden, this may be a conservative approach for ultimate strength calculations.

In addition to calculating the overall buckling strength by the approach of Section 3.4.7 of the *Specification*, a previously proposed approach by Sharp et al.[160] was also employed for comparison in overall buckling. This approach is used in the Aluminum Association *Specification* for calculating the buckling strength of a plate with one intermediate stiffener, and the commentary to the code mentions that the original approach is a potential starting point for multiple-stiffener panels. However, this equation is a lower-bound approach for lighter stiffened panels buckling in more than one half-wave, and as such it may be conservative for ship-type panels. Indeed, Sharp et al. originally recommended treating stockier stiffened plates as columns[160]. This concern is reinforced by the fact that the original aim for the formulation discussed by Sharp et al. is for comparatively light and slender structures, such as aluminium sheet structures for truck bodies[160]. This method was included for comparison with the column approach discussed above, the results from both methods are included in the results discussed below.

3.4.2.6 Comparison of Methods

The predicted collapse load by each of the four methods is shown below in Table 16. Along with the prediction results, methods are compared by a bias factor, defined as the predicted strength over the experimental strength, is reported. Thus, bias factor of one indicate a perfect prediction, while conservative predictions have biases less than one and non-conservative predictions have bias values greater than one. Additionally, the average bias and coefficient of variation of the bias are listed as well. These last two figures indicate how accurate the methods are, and how consistent they are in their predictions. As several of the tests were on virtually identical panels, such as A.R.E. panels 1A & 1B which had identical nominal dimensions and only small difference in material properties, calculating the bias from all the panel tests can double-count certain results. For this reason, the bias was also calculated by taking one value for each unique material/nominal dimension combination. Where multiple similar panels were tested, the average of all the similar test results was used as a single point. Both methods of calculating the bias are shown below in Table 16.

There are some small differences in the results presented in Table 16 from the results presented at FAST 2003[104], as a result of refinement of the methods used. These are:

- For the Paik and Thayamballi method, the restriction that the calculated ultimate strength must be less than the Euler buckling load has been included. This limitation was not in the original equation published by Paik and Thayamballi[35].
- For the Aluminum Association *Specification*, the material HAZ properties were updated to agree with the values presented in Chapter 2, in the previous work these strengths had been slightly lower. Additionally, the limitation that the failure stress can not exceed the proof stress of the HAZ material in panels with welds at their loaded edges was observed.

These difference have made only small impacts on the overall bias and COV of the methods.

Table 16: Performance of Simplified Methods

Comparison of Prediction Options																
Panel		Exp. Ult. Load	Eurocode 9 {ϕ}=1[a]		Paik and Thayam.		Paik, Duran, and Lee		Herzog				A.A {ϕ}=1[a]			
									Original[c]		Equiv. β[c]		Column		Sharp	
			Ult. Load	Bias[b]	Ult. Load	Bias[b]	Ult. Load	Bias[b]	Ult. Load	Bias[b]	Ult. Load	Bias[b]	Ult. Load	Bias	Ult. Load	Bias[b]
		kN	*kN*	--	*kN*	--	*kN*	–	*kN*	--	*kN*	–	*kN*	--	*kN*	--
A.R.E.	1A	850	739	0.87	674	0.79	1034	1.22	1045	1.23	424	0.50	513	0.60	128	0.15
	1B	800	705	0.88	652	0.81	984	1.23	981	1.23	444	0.56	507	0.63	127	0.16
	2A	1070	848	0.79	1006	0.94	1203	1.12	1227	1.15	1084	1.01	1020	0.95	249	0.23
	3A	1710	1734	1.01	2101	1.23	2008	1.17	2330	1.36	2258	1.32	2632	1.54	639	0.37
	4A	760	815	1.07	958	1.26	1110	1.46	1163	1.53	1038	1.37	990	1.30	236	0.31
Aalberg et al.	I	737	223	0.30	477	0.65	340	0.46	927	1.26	739	1.00	468	0.63	130	0.18
	J	693	217	0.31	476	0.69	340	0.49	914	1.32	725	1.05	467	0.67	128	0.19
	K	893	575	0.64	809	0.91	859	0.96	1120	1.25	889	1.00	769	0.86	128	0.14
	L	899	596	0.66	842	0.94	919	1.02	1178	1.31	919	1.02	793	0.88	126	0.14
	M	872	596	0.68	842	0.97	919	1.05	1178	1.35	919	1.05	793	0.91	126	0.15
Zha et al.	A16	738	593	0.80	691	0.94	613	0.83	810	1.10	752	1.02	600	0.81	318	0.43
	ZMN1	1011	594	0.59	867	0.86	798	0.79	860	0.85	860	0.85	718	0.71	463	0.46
	ZMN2	458	336	0.73	547	1.19	572	1.25	643	1.40	591	1.29	480	1.05	287	0.63
	ZMN3	467	315	0.67	466	1.00	466	1.00	548	1.17	503	1.08	498	1.07	241	0.52
	ZMN4	287	178	0.62	382	1.33	365	1.27	451	1.57	414	1.44	232	0.81	143	0.50
	ZMN5	406	261	0.64	367	0.90	316	0.78	440	1.08	404	0.99	413	1.02	171	0.42
	ZMN6	990	894	0.90	1113	1.12	993	1.00	1110	1.12	1110	1.12	835	0.84	668	0.67
	ZMN7	785	628	0.80	806	1.03	792	1.01	910	1.16	866	1.10	662	0.84	450	0.57
	ZMN8	734	568	0.77	646	0.88	579	0.79	734	1.00	698	0.95	600	0.82	318	0.43
	ZMN9	487	398	0.82	435	0.89	374	0.77	550	1.13	483	0.99	494	1.01	183	0.38

Summary of Results[d]

Panel	Mean	COV	Mean	COV	Mean	COV	Mean	COV	Mean	COV	Mean	COV	Mean	COV
A.R.E.	0.93	0.12	1.01	0.22	1.24	0.10	1.30	0.12	0.95	0.43	1.01	0.41	0.25	0.39
Aalberg et al.	0.52	0.37	0.83	0.18	0.80	0.37	1.30	0.03	1.02	0.03	0.79	0.16	0.16	0.13
Zha et al.	0.74	0.14	1.01	0.15	0.95	0.20	1.16	0.17	1.08	0.16	0.90	0.14	0.50	0.19
Total	0.73	0.26	0.97	0.19	0.98	0.26	1.23	0.14	1.04	0.22	0.90	0.25	0.35	0.50
Adjusted Total[e]	0.76	0.24	1.00	0.18	1.00	0.25	1.22	0.16	1.07	0.21	0.93	0.25	0.40	0.41

Notes:

a: Ultimate strength calculated with all resistance factors taken as equal to 1

b: Bias is defined as predicted result/experimental result

c: Original is with b/t formula, Equiv. β is with an equivalent steel b/t.

d: Mean is defined as the mean of the bias, COV is the coefficient of variation of the bias

e: Almost identical panels (ARE 1A & 1B, AAL I&J, K&L&M) averaged and only counted once

The methods generally performed well, as can be seen from the bottom of Table 16. Both of the civil engineering codes give conservative predictions with some variability, even with the partial-safety factors set equal to unity. The Eurocode 9 is significantly conservative for the Aalberg et al. panels, however this is due in part to the direction of buckling in the experimental tests, as discussed in the paper on these tests[59]. As mentioned above, these test results were also suspected of being optimistic, as the outer plating bay was considerably stronger than the plating between stiffeners. Most methods, including the steel and aluminium regression equations underestimated the panel strength significantly for the longer Aalberg et al. panels, though the methods improved for the shorter panels. Using the Aluminum Association code with the lower-bound buckling formulation of Sharp et al. appears overly-conservative for ship-type panels.

The steel equations have smaller overall biases, although their variability is higher than when applied for steel. In its uncorrected form, the Herzog equation is non-conservative, which would be expected. This initial bias is largely removed by using the equivalent β approach. Part of the variability in the A.R.E. prediction results may be a result of the very high plate slenderness ratio, β, (>5) of the first two panels, which is well beyond that normally used in steel construction. For the Herzog equivalent steel b/t method, the steel b/t for these panels is 148.7. The experimental data Herzog used to derive his method only included panels with b/t less than 75, so this panel falls far from range of validity of the formula. It also seems likely that the different experimental boundary conditions contribute to increasing the variability of the prediction results. Paik and Duran's formulation performs similarly, and has the advantage that the area of the HAZ is explicitly included in the analysis. Additionally, many of the panels were significantly different from the Tee panels this equation was developed from. From the limited data set available, there does not seem to be a strong difference between the 5000 series alloy panels and the 6000 series alloy panels. It is important to remember that none of the experimentally-tested panels had transverse HAZ in the mid-region of the panel, which can significantly affect the panel's strength.

Overall, the methods seem to have performed well, although the agreement is not as good as the agreement observed for the plate tests. This is felt to be largely a result of the more complex failure process of stiffened panels, as well as the combination of several test programs with different boundary conditions. Unfortunately, the tested panels are not very representative of panels likely to be used in HSV construction. Most of the panel were flat bar panels which are significantly inefficient compared to Tee or L panels from a weight point of view, and thus are unlikely to be used in weight-critical vessels. Additionally, the Zha and Moan panels, which were a significant proportion of the total panels, failed by stiffener tripping, which is failure mode that should be avoided by design in actual vessels. Given that the regression equations were the most accurate, the extra effort in applying the more complex design code formulations seems unnecessary, however, the bounds of the data sets used to formulate the regression equations must be observed, and for significantly different panels the more complex design code formulations may be required.

3.4.3 Compressive Stress-Strain Curve Prediction

In addition to the simplified methods that only predict the ultimate strength of the panel, methods have been developed which predict the entire stress-strain curve of the panel in compression. This additional information is required to estimate the progressive collapse

of the entire hull-girder, using a Smith-type progressive collapse approach. Such an approach has been discussed and implemented by several authors, including Smith[2], Rutherford and Caldwell[3], Rahman and Chowdhury[30], and Gordo et. al[136]. However, predicting the entire stress-strain curve is considerably more complex than simply estimating the peak load value. In this section, three potential methods for predicting the compressive stress-strain curve are examined. Two previously proposed steel methods for predicting the entire curve were examined, a proposal originally developed by Rutherford[36], and a later proposal by Rahman and Chowdhury[30], which is based on a simplified panel ultimate strength method originally proposed by Hughes[21]. Gordo and Guedes Soares[135] also proposed a steel compressive stress-strain relationship based upon Faulkner's formulations. Because of the approach taken by Gordo and Guedes Soares, the mechanics of this method proved adaptable for aluminium, so a modified aluminium approach was developed based on Gordo and Guedes Soares' structure. All three of these methods will be presented below, and then compared to a sub-set of the experimental stiffened panels discussed above.

3.4.3.1 Rutherford Approach

This methodology was developed by Dr. Rutherford[36] of Lloyd's Register of Shipping, and implemented as part of Lloyd's LR.PASS suite of programs for advanced analysis of ships. The methodology is based on the Imperial College[161] method of calculating the ultimate strength of stiffened panels. The Imperial College method models a single stiffener and attached plating as a combined beam-column, undergoing both compression and bending. The method checks for compressive failure in the plate or stiffener extremes, and tensile failure in the stiffener. The later can arise for certain deflected shapes and lateral pressures. Both initial deformations and residual stresses can be handled by the methodology. The Imperial College methodology was modified by Rutherford to include the effects of load eccentricity and the additional failure mode of stiffener tripping. Additional modifications were made to improve the prediction results for very stocky panels. A plastic mechanism load-shedding theory was developed to produce the post-ultimate-strength load-shortening curve. A broad outline of the procedure is presented in Appendix 1 and 2 of Rutherford and Caldwell[3], a more detailed overview is presented in Rutherford[36] though the presented post-ultimate-strength load-shortening curves in this source are for flat bar stiffeners only.

Rutherford[36] made extensive comparisons between the new methodology and experimental test results on steel stiffened panels. While comparatively few examples were found to test the entire load-shedding curve, over 100 experimental ultimate strength values

were available for comparison. The correlation is presented in Figure 29 below, as can be seen the predicted ultimate strength correlates very well with the experimentally-derived values.

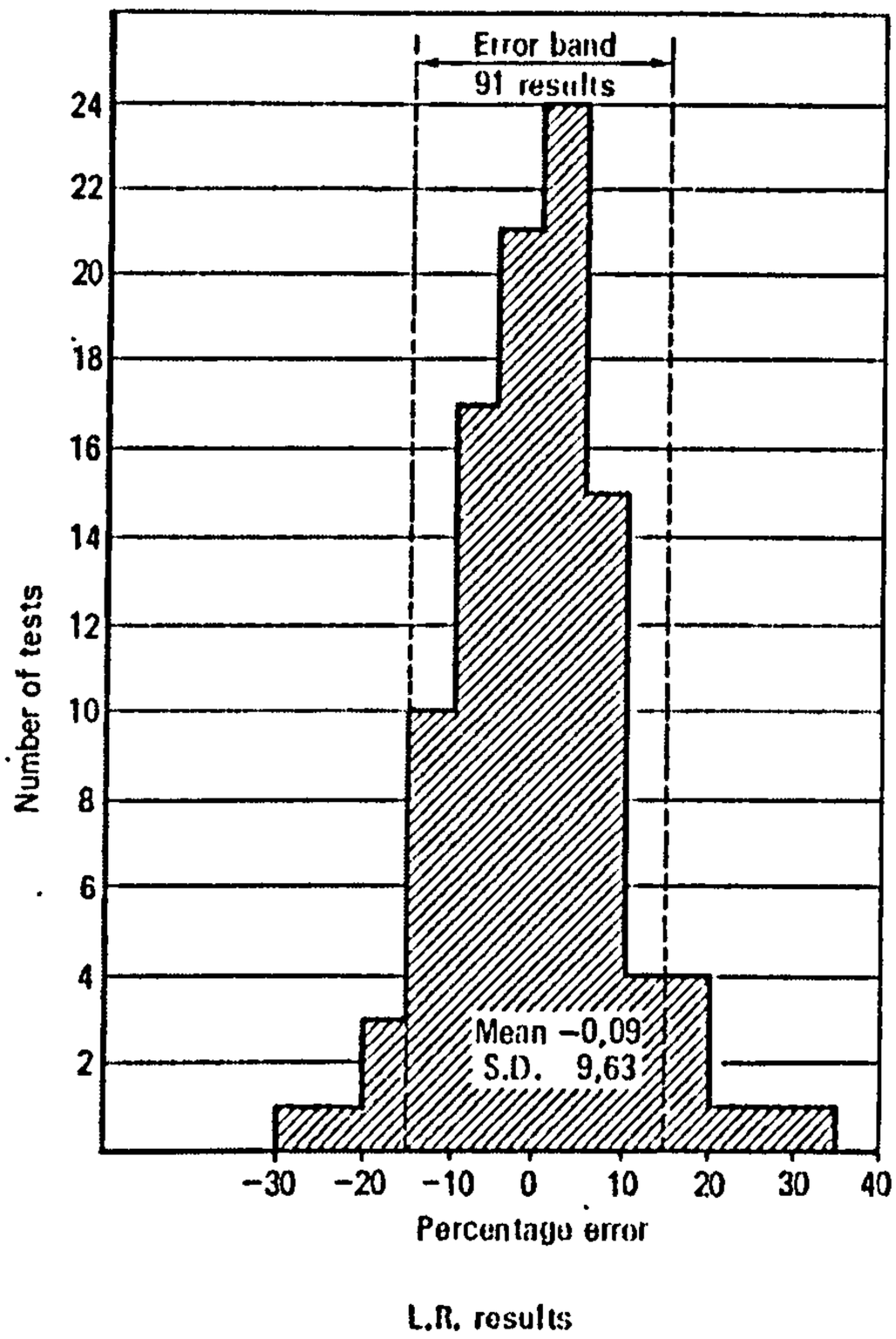

Figure 29: Comparison of Rutherford Methodology and Experimental Results (Rutherford[36])

While few experimental load-shortening curves were available for comparison, Rutherford and Caldwell[3] predicted the load-shortening curve of a VLCC bottom panel with finite-element analysis and compared this curve to the curve predicted by the simple Rutherford methodology, and good agreement was observed. Overall, by linking the Rutherford approach to a Smith-type progressive collapse analysis Rutherford and Caldwell were able to re-create the hull girder collapse of the VLCC *Energy Concentration* with high accuracy[3]. The Rutherford methodology appeared conservative in the 1994 ISSC benchmark[24]. This may be a result of the stress-strain curves being conservative, especially in the load-shedding region, however the ISSC report noted that the method was also originally developed for stocky commercial ship scantlings, while the benchmark was on a lighter frigate structure, which may also have influence the results. This is important to

keep in mind, especially as the aluminium panels tend to be more similar to frigate structure than to VLCC structure.

3.4.3.2 Rahman and Chowdhury Approach

Rahman and Chowdhury[30] presented an alternative methodology that shares the same conceptual origins as the Rutherford methodology. Similar to Rutherford, their methodology combines a pre-existing ultimate strength methodology with a plastic-collapse load-shedding model. However, both the ultimate strength methodology and the load-shedding methodology are different from those used by Rutherford. The ultimate strength methodology is a simplified version of that presented by Hughes[21]. In Rahman and Chowdhury's approach, stiffener tripping and combined compressive plate failure and stiffener tensile failure have been eliminated, leaving only two failure modes, stiffener compressive failure and plate compressive failure. The advantage of this approach is that the resulting equations are much more straightforward and easy to solve, and the authors state that failure by tripping can usually be excluded by appropriate design constraints.

Hughes[21] compared the ultimate strength theory to a range of panels tested a Monash University[125] under both pure compression, pure bending, and combined compression-bending. Good results were generally obtained. Rahman and Chowdhury also generated a stress-strain curve for the same VLCC bottom panel as Rutherford and Caldwell above, and the ultimate strength values agreed quite well. Rahman and Chowdhury combined the Hughes' ultimate strength method with a plastic load-shedding theory developed from a theory originally proposed by Adamchak[126]. In this theory, the load-shortening curve is divided into three regions, the stable zone on the way up to the ultimate strength, the no load-shedding zone around the ultimate strength, and the load shedding region. These three regions are depicted below in Figure 30.

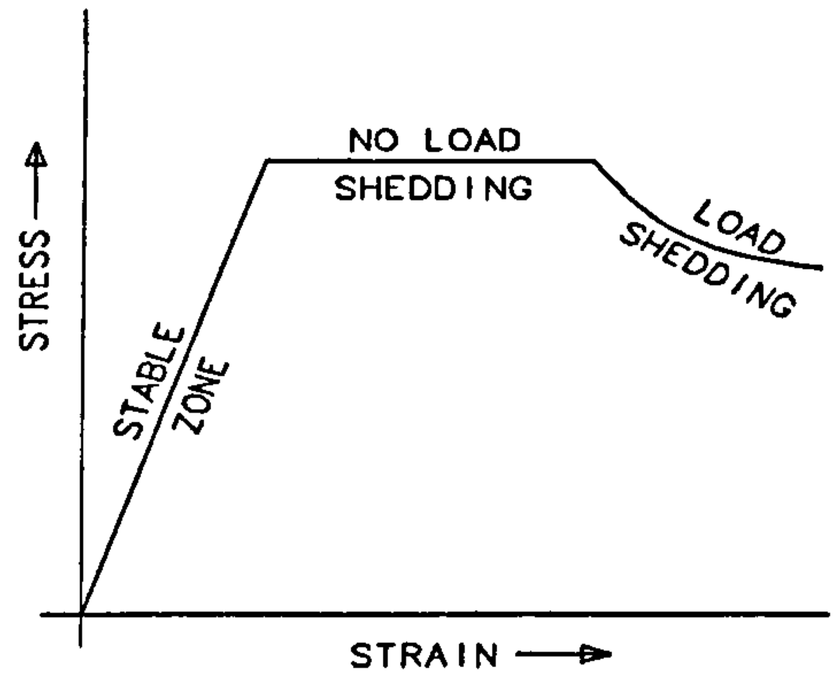

Figure 30: Three Regions of the Load-Shedding Curve, used by Adamchak[126] and Rahman and Chowdhury[30]

The relationship in the stable zone depends upon the type of failure mode predicted, if plate failure is predicted, this curve will include the effects of plate buckling, if stiffener failure is predicted, the curve is the elastic curve. Adamchak's proposed theory[126] was used to determine the no load-shedding region. In this region, the strain corresponding to the ultimate stress and the strain corresponding to the point at which the section reaches its fully-plastic moment are determined, and are connected by a straight line equal to the ultimate stress. A load-shedding relationship, based on plastic hinge theory, is then used to generate the load-shedding region.

Rahman and Chowdhury compared their method to several box-girder collapse tests, and a VLCC collapse first investigated by Rutherford and Caldwell[3]. Good agreement was observed in all cases, although they noted that in the VLCC collapse their methodology predicted a significantly higher strain at the ultimate moment than the strain predicted by Rutherford and Caldwell. Rahman and Chowdhury attributed this to the slower rate of load-shedding of their model. Comparing the Rutherford and Rahman and Chowdhury prediction for the bottom panel of the VLCC, it is clear that the no load-shedding region predicted by the Rahman and Chowdhury method is not at all present in the Rutherford prediction. This is something to keep in mind when comparing these two methodologies for aluminium panels.

3.4.3.3 Modified Gordo and Guedes Soares Approach

Gordo and Guedes Soares[135] proposed an approximate method for predicting the load-shortening behaviour of columns, extending both Faulkner's approaches for plates and Faulkner's approach for calculating the failure stress in stiffened panels, which was initially presented in the 1970s[123]. In Faulkner's approach, the ratio of the average stress at failure to the yield stress of a steel panel may be estimated by the equation:

$$\frac{\sigma_a}{\sigma_0} = \frac{\sigma_e}{\sigma_0}\left[\frac{A_s + b_e t}{A_s + bt}\right]$$

Where:

σ_a Average stress at failure

σ_e Edge stress at failure (εE)

σ_0 Yield stress

A_s Stiffner area

t Plate thickness

b_e Effective plate width accounting for buckling

b Plate width

Equation 34

The effective plate width can be calculated using Faulkner's effective plate width equation[122] and the ratio of the edge stress to yield stress is calculated using a Johnson-Ostenfeld interaction equation:

$$\frac{\sigma_e}{\sigma_0} = 1 - \frac{1}{4}\frac{\sigma_0}{\sigma_E} \text{ When } \sigma_E \geq 0.5\sigma_0$$

$$\frac{\sigma_e}{\sigma_0} = \frac{\sigma_E}{\sigma_0} \text{ When } \sigma_E < 0.5\sigma_0$$

Where :

σ_e Edge stress at failure (εE)

σ_0 Yield stress

σ_E Euler buckling stress, $\sigma_E = \left(\frac{\pi r_{ce}^{'}}{l}\right)^2 E$

l Length of panel

$r_{ce}^{'}$ Radius of gyration, $r_{ce}^{'} = \sqrt{\frac{I_{ce}^{'}}{A_s + b_e t}}$ *Equation 35*

$I_{ce}^{'}$ Moment of intertia of stiffener with attached plating of width $b_e^{'}$

$b_e^{'}$ Tangent effective width, $b_e^{'} = \frac{1}{\beta}\sqrt{\frac{\sigma_0}{\sigma_e}}$

A_s Stiffner area

t Plate thickness

b_e Effective plate width accounting for buckling

b Plate width

β Plate slenderness ratio

Where the tangent effective width is used in place of the effective width in the calculation of the moment of inertia as it represents the plate's ability to take additional loads over its current level, which is significant for the stability of the combined section[122]. This equation must be solved via iteration, as the ratio of edge stress to yield stress is used in the determination of tangent effective width. Gordo proposed modifying this approach so that it could be used to generate an entire stress-strain curve based on the assumption that at any strain level, ε, the ratio of the Euler stress to the yield stress could be determined by the following equation:

$$\frac{\sigma_E}{\sigma_0} = \frac{\varepsilon_0}{\lambda^2 \varepsilon}$$

Where:

ε_0 Current strain

ε Yield strain

λ Non - dimesional slenderness, $\lambda = \frac{l}{\pi r_{ce}^{'}} \sqrt{\varepsilon_0}$ *Equation 36*

And all other variables are as above, $r_{ce}^{'}$ is calculated using the effective width and tangent effective width corrosponding to this strain level

Taking this approach, the ratio of the averaged stress in the plate stiffener combination to the yield stress is determined using the Johnson-Ostenfeld interaction equation from above, and the actual edge strain at the loading in question.

$$\frac{\sigma_a}{\sigma_0} = \Phi_{JO}\left[\frac{A_s + b_e t}{A_s + bt}\right]\frac{\sigma_e}{\sigma_0}$$

Where:

$$\Phi_{JO} = 1 - \frac{1}{4\frac{\sigma_E}{\sigma_0}} \text{ When } \sigma_E \geq 0.5\sigma_0 \qquad \textit{Equation 37}$$

$$\Phi_{JO} = \frac{\sigma_E}{\sigma_0} \text{ When } \sigma_E < 0.5\sigma_0$$

This approach uses what could be called a fictitious column at each edge stress level to account for the lost of stiffness through column action in addition to the loss of stiffness through plate buckling. If the fictitious column assumption is accepted, there is another theoretical argument against such a formulation, namely Faulkner's tangent effective breath equation:

$$b_e^{'} = \frac{1}{\beta}\sqrt{\frac{\sigma_0}{\sigma_e}} \qquad \textit{Equation 38}$$

In Faulkner's original papers, the application of this equation was restricted to edge stress between 75% and 100% of the yield[122, 123], and by its nature, this formula cannot be correct over all stress ranges. The theoretical definition of tangent effective width is tied to the slope of the load-compression curve of the plate.

$$b_e^{'} = b\left(\frac{d\sigma_a}{d\sigma_e}\right) \qquad \textit{Equation 39}$$

Clearly, after failure of the plate, the tangent effective width would become negative as in this region the plate sheds load as it is further compressed. However, Faulkner's equation will not become negative regardless of what edge stress is entered. Given that

Gordo's overall method gives good results for steel in terms of the load-shortening curve, it may be that the error in tangent effective breadth has an insignificant effect on the overall response in the load-shedding region-for example if the overall column slenderness is already rising rapidly.

This method has the interesting property that it can be more easily modified to model aluminium than either of the beam column methods reviewed previously. It was proposed to create an aluminium-specific method by making the following modifications to the method:

- Replace the elastic-perfectly plastic edge stress-strain relationship with the Ramberg-Osgood relation
- Replace Faulkner's effective plate width equation with the aluminium specific equation developed previously
- Replace the Johnston-Ostenfeld interaction equation with the U.S. Aluminum Association column curve, using a linear formulation in the inelastic region

Such an approach would address the differences in material response, plate buckling and inelastic column buckling between aluminium and steel. The resulting method only address flexural buckling, tripping and stiffener web failures are not addressed at this stage. Assuming that the strength of the plate has already be determined by the approach from Section 3.3.3 above, the stress corresponding to a given strain can be calculated by the steps shown in Table 17 .

Table 17: Aluminium Column Method for Determining Stress at Given Strain

1	*Calculate the edge stress corresponding to this strain via the Ramberg-Osgood relation*	σ_e
2	*Using the plate prediction method above, determine the average plate stress and the plating effective width at this edge stress*	$b_e = \frac{\sigma_a}{\sigma_e} b$
3	*Determine the tangent effective width at this edge stress via Faulkner's equation at the 0.2% offset proof stress*	$b_e^{'} = \frac{1}{\beta}\sqrt{\frac{\sigma_{0.2}}{\sigma_e}} b$
4	*Calculate the moment of inertia of the stiffener with the attached plating width equal to the tangent effective width*	$I_{ce}^{'}$
5	*Calculate the radius of gyration by dividing the moment of inertia by the area of the stiffener and attached plating width equal to the effective width*	$r_{ce}^{'} = \sqrt{\frac{I_{ce}^{'}}{A_s + b_e t}}$
6	*Calculate a nominal value of* λ_n	$\lambda_n = \frac{l}{\pi r_{ce}^{'}}\sqrt{\frac{\sigma_{0.2}}{E}}$
7	*Adjust* λ *for the current strain relative to the plate failure strain* ($\sigma_{0.2}/E$ *with the current plate method)*	$\lambda = \frac{\lambda_n}{\sqrt{\frac{\varepsilon_{fail}}{\varepsilon}}}$

8	*Calculate the ratio of the fictitious column failure stress via the Aluminum Association column curve (σ_{AA}) to the 0.2% yield stress*	$\Phi_c = \frac{\sigma_{AA}(\lambda)}{\sigma_{0.2}}$
9	*Determine the overall stress at this strain*	$\sigma = \Phi_c \sigma_e \frac{A_s + b_e t}{A_s + bt}$

This approach could be extended to include tripping, Gordo and Guedes Soares[135] presented formulations to incorporate Faulkner's[162] stiffener tripping into this approach. It would be possible to start with this approach and seek to modify it for aluminium in a similar fashion, although this has not be done here. Sharp[9] also presents methods for handling elastically-supported compression flanges, but most of these methods are for lighter sheet structures. Likewise, the potential for stiffener web or flange buckling has not been addressed, although with the ease of producing custom extrusions with aluminium, such a failure mode could occur if the stiffeners are not designed to preclude this type of failure.

The effects of welds on the compressive ultimate strength of the panel must also be considered. For welds in the plate, it is proposed to use the equations developed in Section 3.3.3, and incorporate the effect of welding into the effective breadth relation. There is likely to be additional welds located at the transverse ends of the stiffeners, where the stiffeners are attached to the frames, and longitudinally where the stiffener web is connected the plate. It seems reasonable to assume that the transverse welds on the stiffener have negligible effect on the overall performance of the stiffener as a column, as the column curves used already assumed pin-jointed behaviour at the loading edges. This is the approach which is taken by the Aluminum Association *Specification*. The reduced effectiveness of the longitudinal HAZ in the stiffener web can be incorporated by assuming that the stress in the HAZ is equal to the edge stress in the plate, and then the reduction in axial force at each strain can be expressed as:

$$\sigma_{a\_WELD}(\varepsilon) = \sigma_a(\varepsilon) - \frac{A_{HAZ}}{A_{TOT}}(\sigma_e(\varepsilon) - \sigma_{e\_HAZ}(\varepsilon))$$

Where:

$\sigma_{a\_WELD}(\varepsilon)$ Average axial stress accounting for welds

$\sigma_a(\varepsilon)$ Average axial stress without welds *Equation 40*

A_{HAZ} Cross - sectional area of the stiffener web HAZ

A_{TOT} Total cross - sectional area of the plate and stiffener

$\sigma_e(\varepsilon)$ Edge stress at strain ε in base material

$\sigma_{e\_HAZ}(\varepsilon)$ Edge stress at strain ε in the HAZ material

3.4.3.4 Analysis of Approaches

The three approaches were applied to a sub-set of the experimentally tested panels. As neither the Rahman and Chowdhury approach nor the modified Gordo approach consider stiffener tripping, the Zha and Moan panels which failed by tripping were excluded from the comparison. Likewise, the shorter Aalberg et al. panels were excluded, as Aalberg et al. stated that these panels failed by tripping as well. The panels which failed by tripping showed a very distinctive stress-strain curve, with almost linear elastic compression until tripping occurs, and then virtually elastic unloading, forming a curve with an inverted "v" shape, which is fundamentally different than the failure modes addressed by the Rahman and Chowdhury and modified Gordo approaches. The stress-strain curves for the remaining panels are presented below in Figure 31 - Figure 35, and the accuracy of the peak stress prediction is presenting in Table 18, where the bias is defined as the predicted ultimate strength over the experimental ultimate strength. From the table, it is clear that these methods are more varied in their prediction than the simplified methods, although the mean performances are encouraging. The modified Gordo method seems to work well for the A.R.E. panels while under predicting the Aalberg et al. panel. As discussed earlier, because of the test-rig boundary conditions, the physical Aalberg et al. panel is most likely stronger than its representation in the beam-column models. Note that the A.R.E. tests were two bays in length, the stress-strain curve is presented individually for both bays below, as in many cases the bay that did not fail would unload into the bay that did fail after the ultimate strength was reached. In the figures below, the modified Gordo method is shown as a series of alternative long and short dashes, while the Rahman and Chowdhury method is shown as a series of long dashes.

Table 18: Peak Value Performance of Compressive Stress-Strain Curve Methods

Panel	Method & Bias		
	Rutherford	Rahman and Chowdhury	Modified Gordo
A.R.E. 1A	1.26	1.31	0.78
A.R.E. 2A	0.87	0.98	0.84
A.R.E. 3A	1.46	1.40	1.09
A.R.E. 4A	0.99	0.84	1.19
Aalberg I	0.54	0.58	0.56
Mean A.R.E.	1.15	1.13	0.97
COV A.R.E.	0.23	0.23	0.20
Mean Aalberg	0.54	0.58	0.56
COV Aalberg	--	--	--
Mean Overall	1.03	1.02	0.89
COV Overall	0.35	0.33	0.28

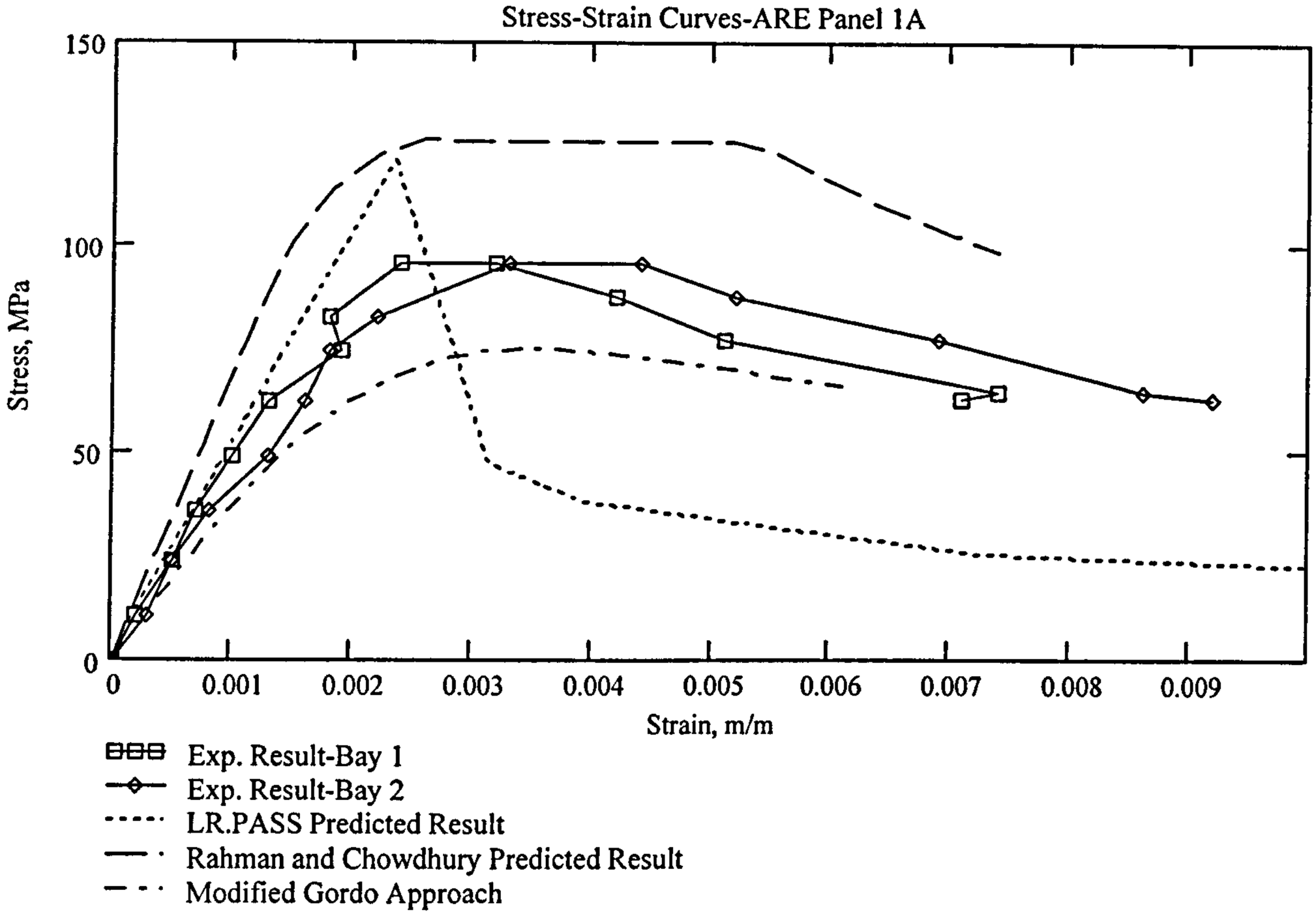

Figure 31: Stress Strain Curve A.R.E. 1A

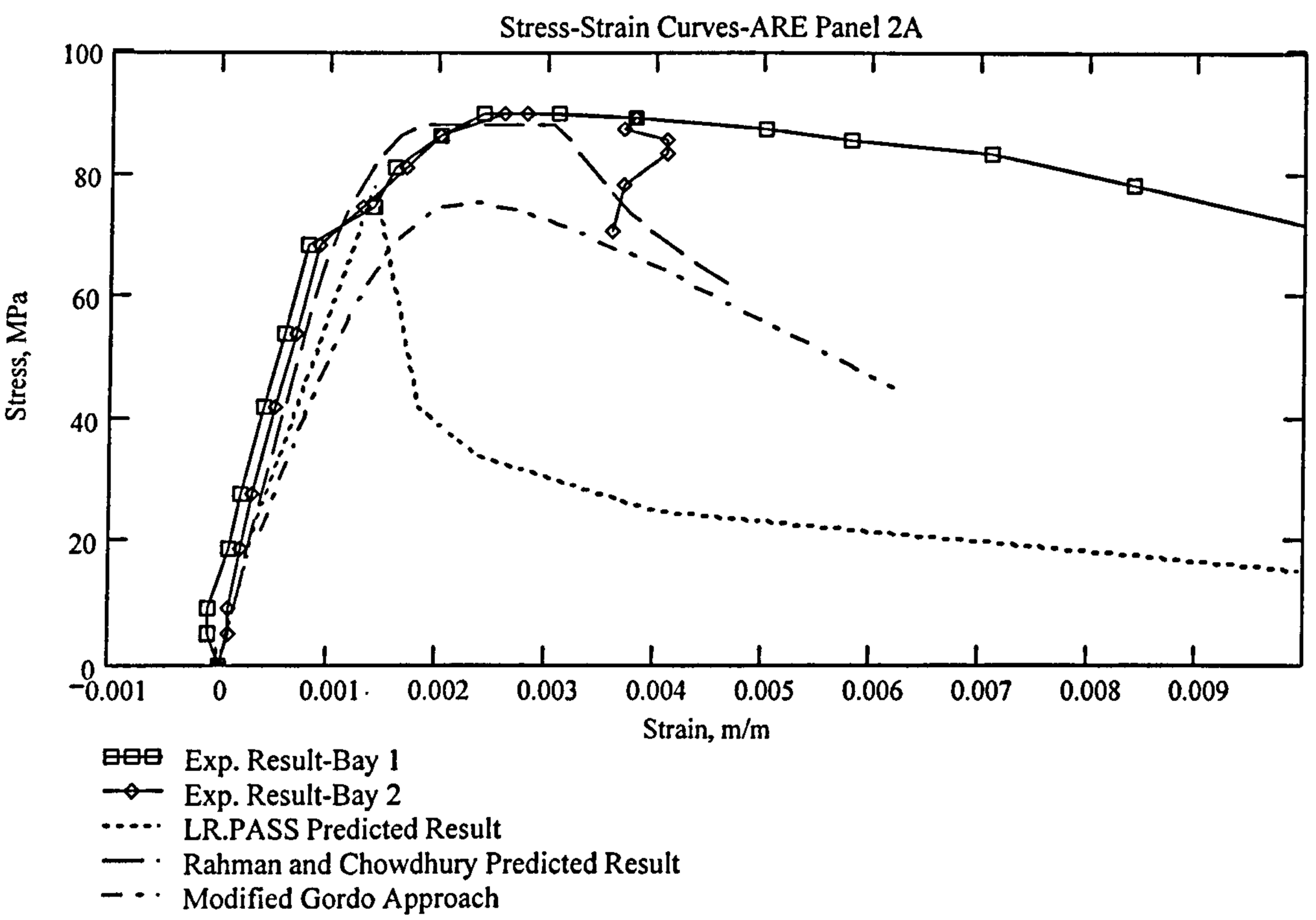

Figure 32: Stress Strain Curve A.R.E. 2A

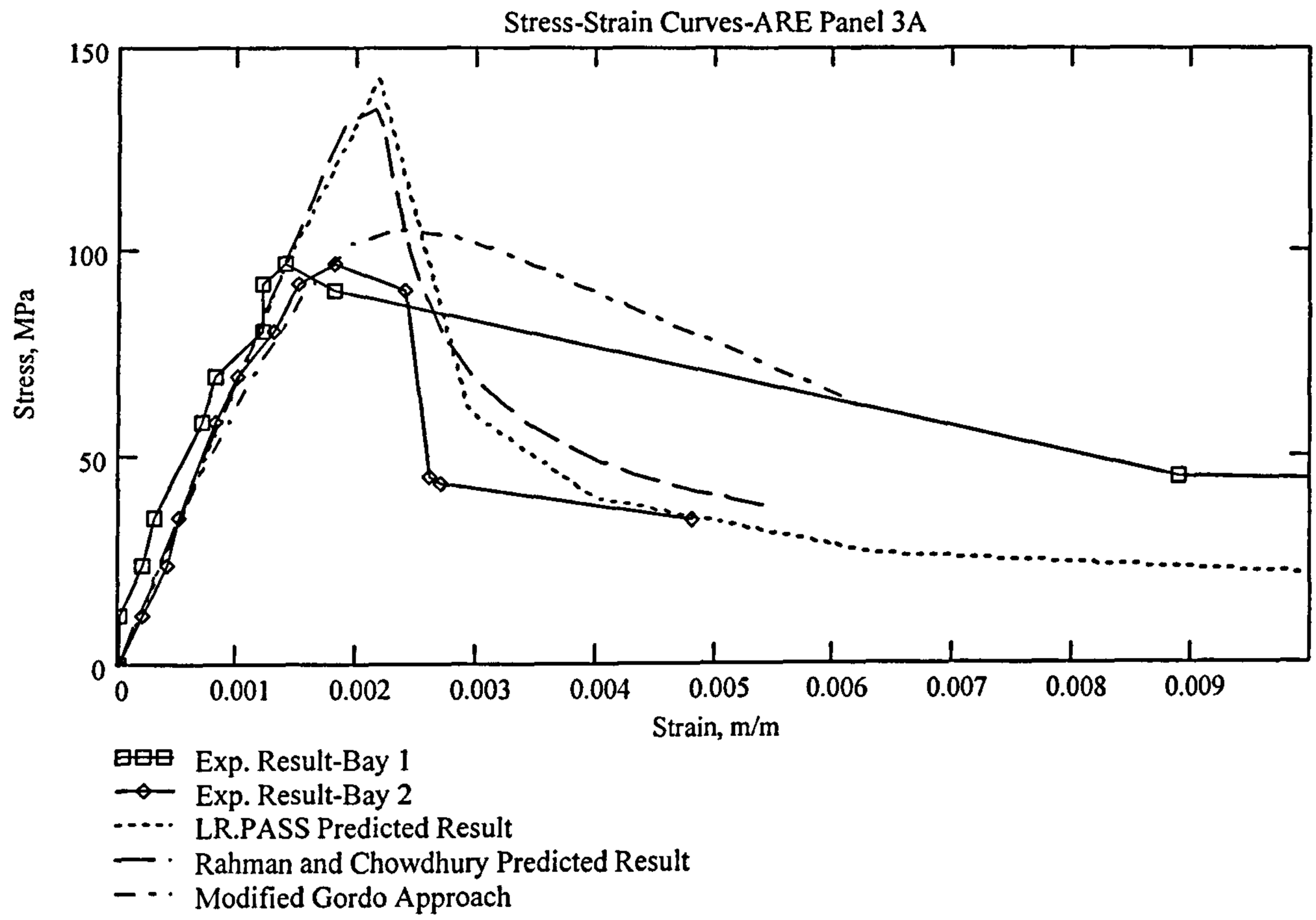

Figure 33: Stress Strain Curve A.R.E. 3A

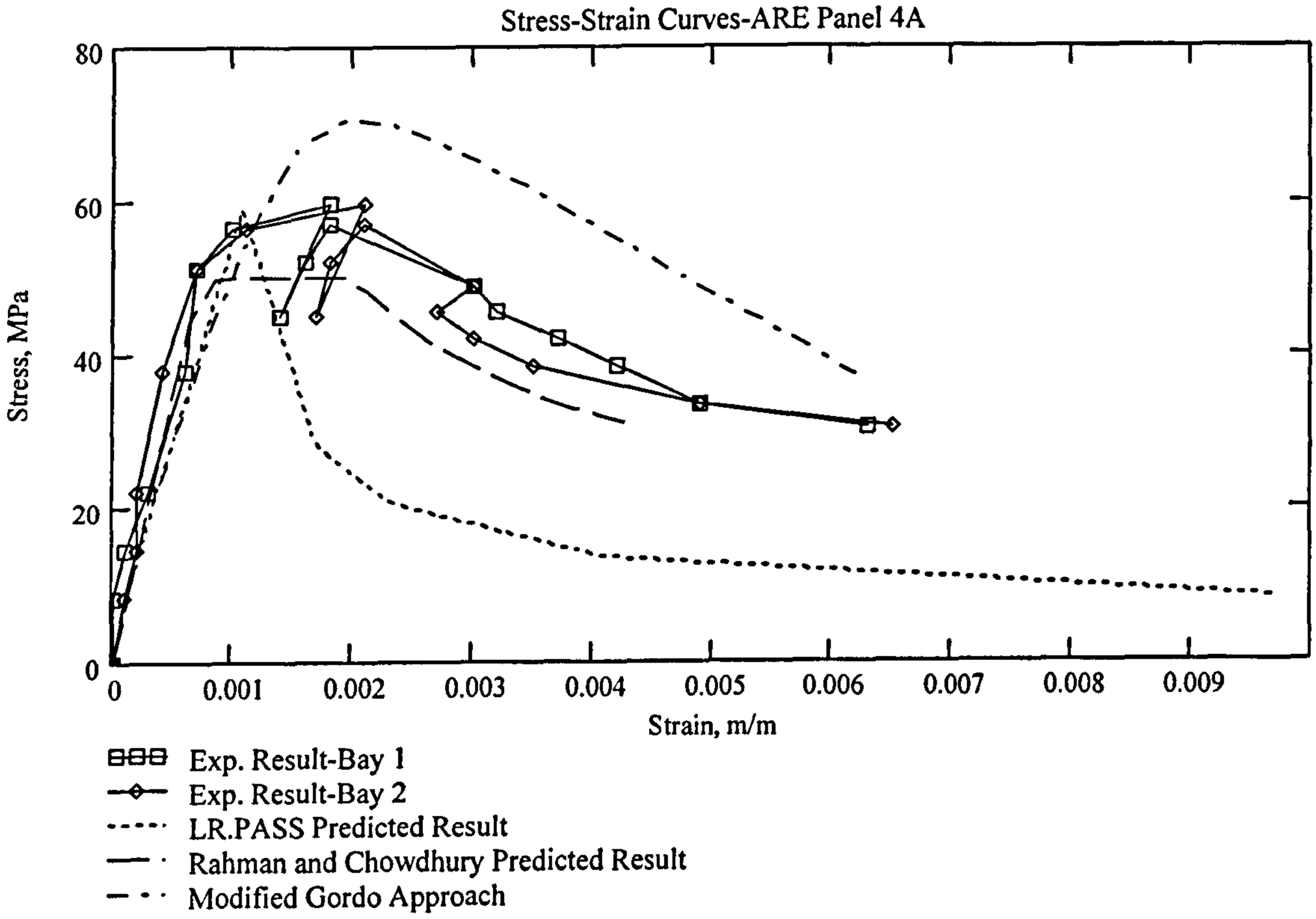

Figure 34: Stress Strain Curve A.R.E. 4A

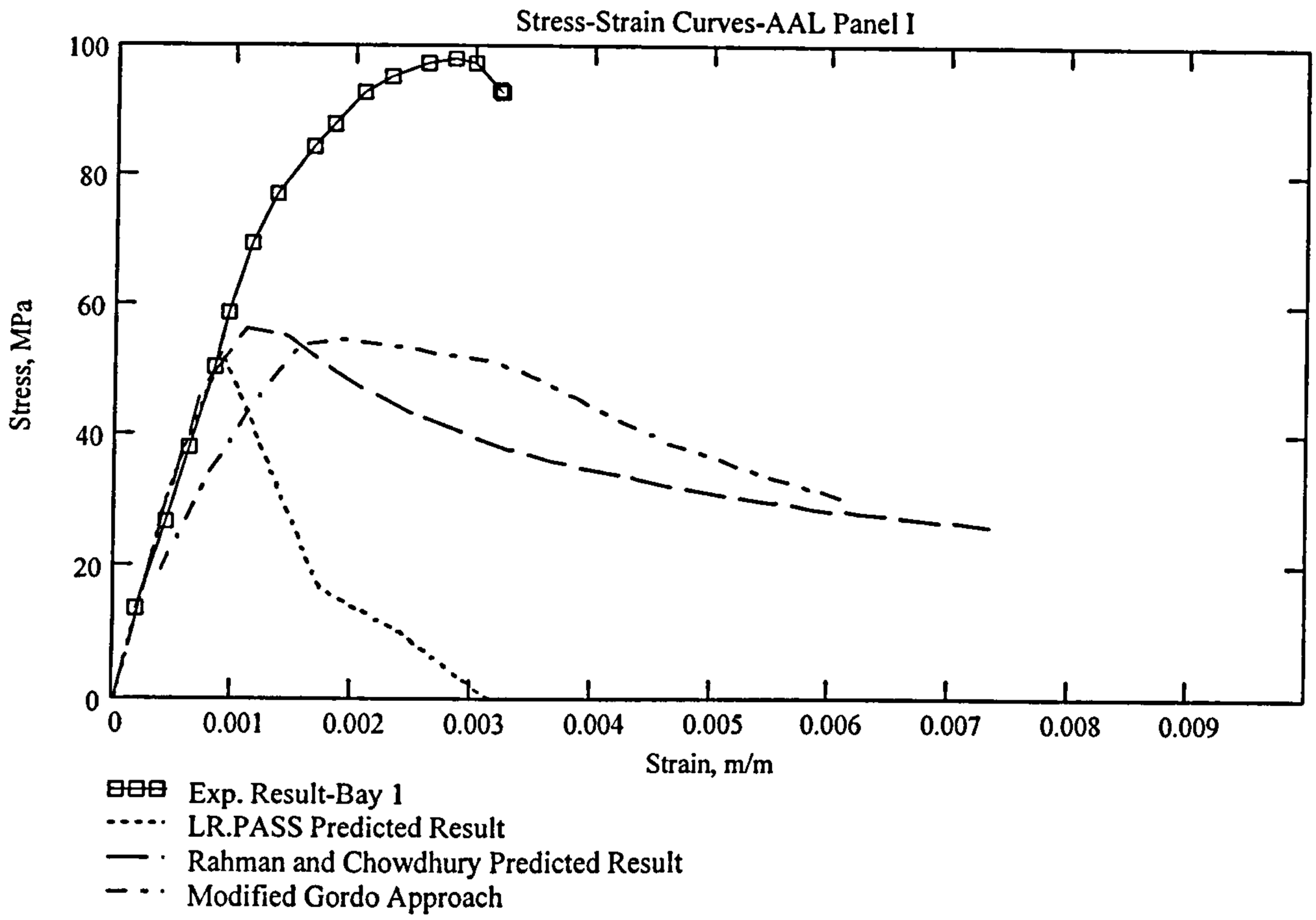

Figure 35: Stress Strain Curve AAL I

The agreement between the three methods and the experimental results can only be termed fair, as all three methods have trouble accurately estimating the ultimate strength of the panels in question. The Rutherford approach predicts the peak values as accurately as any of the other methods, but significantly underestimates the load-shedding portion of the curve. This is not a surprising results, as the method is now being pushed very far from its intended realm of application. Similar predictions were observed in the 1994 ISSC benchmark study[24]. The Rahman and Chowdhury method has a better shape to the stress-strain curve, with the exception of A.R.E. panels 2A and 3A, where the curve predicts a sharper load-shedding slope and a narrower ultimate strength plateau than the experimental results indicated. The shape of the modified Gordo stress-strain curve is perhaps the best fit of the three, the curve appears accurate with the exception of A.R.E. panel 2A, which had a very broad ultimate strength region. This may be a result of the newly proposed plate effective width equation, which appeared to be conservative for 5000-series plates in post-ultimate strength region. The ultimate strength predicted by the modified Gordo approach is variable, like the other two approaches. However, this may be a result the Aluminum Association column and plate curves which were used, it is interesting to note that over or under prediction of this method falls on the same side of the experimental results as the ultimate strength determined by the Aluminum Association *Specification* in Section 3.4.2.6. Also, the variability of the predictions made by the approach constructed from the

Specification was very high for the A.R.E. panels. The same approach could be tried with the Eurocode 9 plate response and column curves, which may perhaps yield more accurate results. This method was the only one to capture the shape of A.R.E. panel 3A's curve. This is a very unusual and weight-inefficient panel, in that the plating is 12.4mm thick, while the stiffeners are only 76x38x4.3x8 mm tees, far weaker than the stiffeners that would typically be used on such heavy plating. Overall, the modified Gordo method seems the most promising approach of the methods reviewed, however, further improvements would be valuable for all of the methods for wider use on aluminium. Certain common types of construction, such as 6000-series alloy stiffener welded to 5000-series alloy plate can not be handled by the modified Gordo approach, as the column curve used is only applicable to columns made of entirely 5000-series alloy or entirely 6000-series alloy.

3.4.4 Tensile Stress-Strain Curve Prediction

The tensile response of the stiffened panels is similar to the tensile response of plates, which was discussed previously in Section 3.3.4. The potential for strain concentration still exists in the transverse welds at the edge of the panels, this concentration may result in the panel behaving in a brittle fashion, especially for 6000-series alloys panels with small HAZ regions. The tension model for the stiffened plate is an assembly of non-linear springs similar to the tension model of the un stiffened plate, dividing the panel into the same three regions as the plate. The first region is the transverse HAZ at the frame/panel connection, the second region is the middle region of the panel, and the third region is the transverse HAZ at the frame/panel connection at the other end of the panel. The presence of the stiffener means that there may be base material present at the joint between the panel and the transverse frame, as it is common to leave the stiffener web un-welded in HSV construction. For example, a common technique for deck structures with tee-stiffened panels is to attach the stiffener to the frame by welding across the top of the flange only. Such a panel is shown in the upper part of Figure 36, where the HAZ regions are shown in heavy lines, and the base material as light lines. In the lower part of Figure 36 the equivalent spring model is shown. Each region has a spring for base material and HAZ material. For the transverse end regions, the HAZ material spring represents the plating, the stiffener flange, and the portion of the stiffener web that is heat-affected. The base material spring represents the remaining portion of the stiffener web. In the middle region, the HAZ material spring represents the longitudinal HAZ in the plating and stiffener at the weld which attaches the stiffener to the plate, while the base material is the unaffected portion of the plate, stiffener web, and the entire stiffener flange. This retains the assumption made for the plate in tension that

transverse plane sections remain plane, which may be violated in areas such as the stiffener flange and web, where HAZ and base material exist in the same transverse plane for short distances.

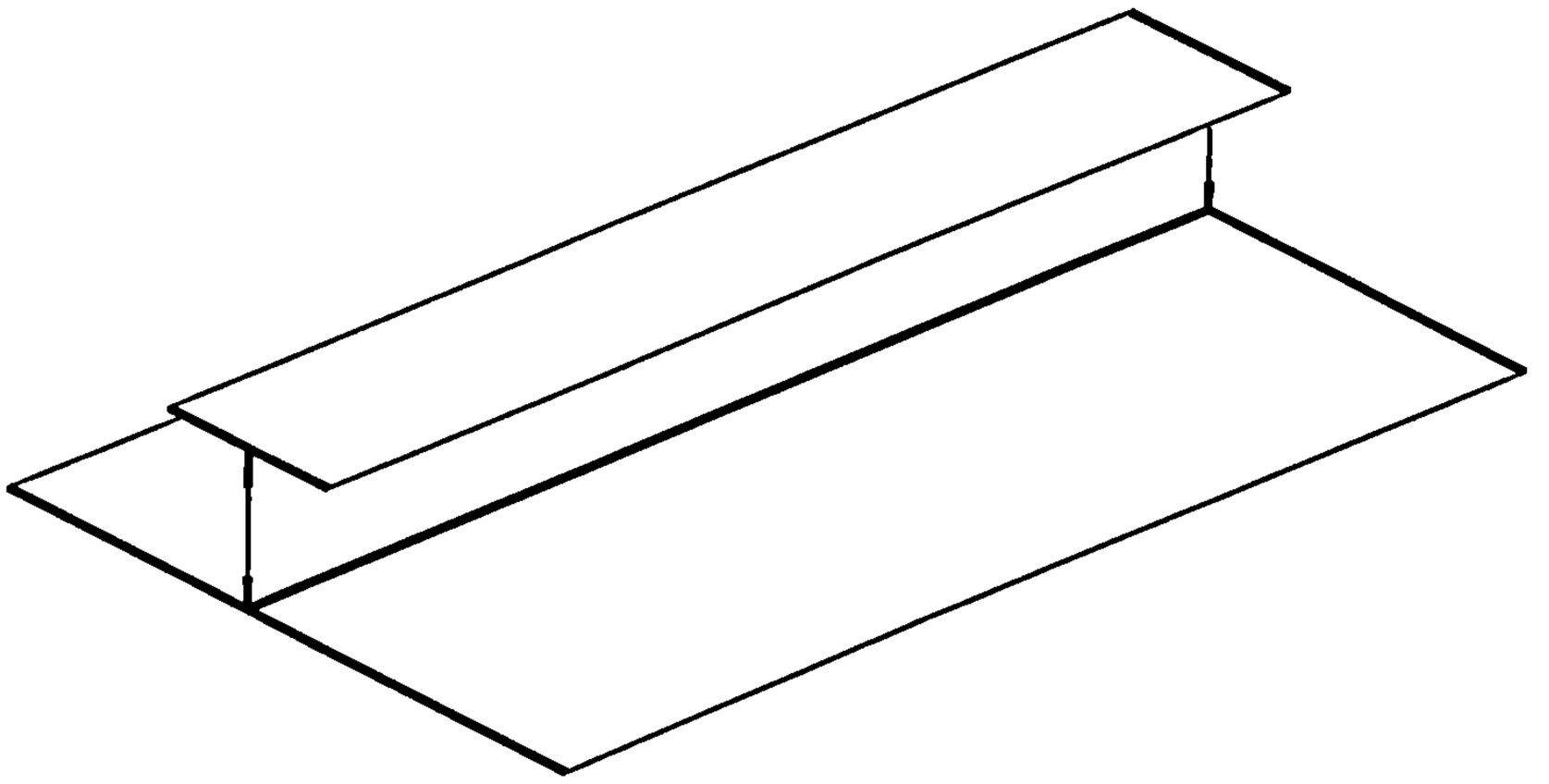

Distribution of HAZ Material (Heavy Lines)

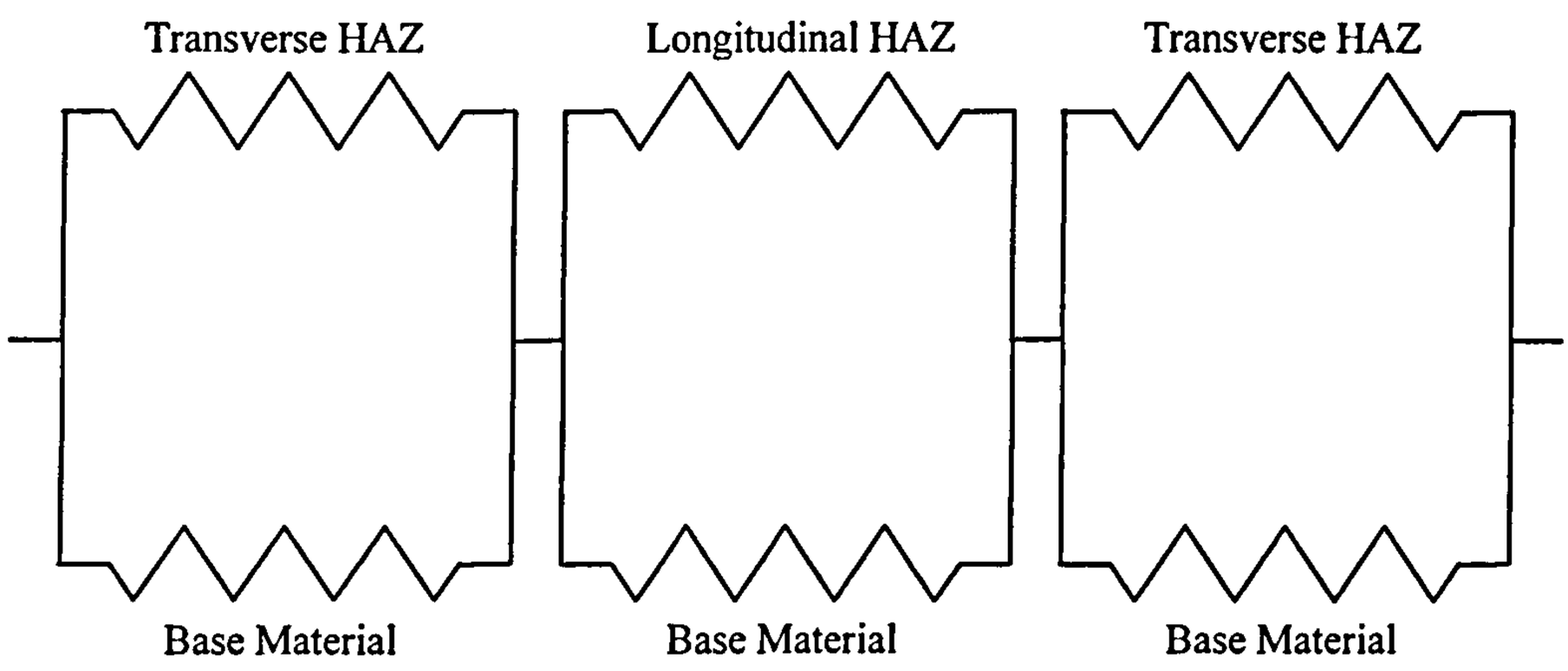

Numerical Model

Figure 36: Tension Model of Stiffened Plate

In a similar fashion to the plate study, the tensile response of two stiffened panels was selected for analysis, one of 5083 alloy and one of 6082. The properties of the panels are shown in Table 19 and the resulting stress strain curves in Figure 37 and Figure 38 . The response is very similar to the tensile response of the un-stiffened plate discussed in Section 3.3.4, however, the added base material in the end regions means that both of the curves lie closer to the base material curve, as this material stiffens the transverse HAZ region. The strain in the transverse HAZ region was tracked as the stress-strain curves were determined to investigate the potential of fracture as a failure mode. In the 5083-H116 panel, these strains were not high enough to risk fracture over the range of overall panel strains considered. However, for the 6082-T6 panels, fracture was indeed a possibility at overall

strains similar to the overall strains discussed in 3.3.4. Similar to the plates, the value of the ultimate strength in tension is not reduced, but the ductility of the panel is.

Table 19: Panels for Tension Study

Material	*5083-H116*	*6082-T6*
Length	*1000mm*	
Breadth	*300mm*	
Plate Thickness	*6mm*	
Stiffener	*70 x 40 x 4 x 6.1 mm Tee*	
HAZ Width	*25mm/12.5mm*	
Base Material Proof Stress	*215 MPa*	*260 MPa*
Base Material n	*12*	*30*
HAZ Material Proof Stress	*144 MPa*	*138 MPa*
HAZ Material n	*8*	*16*
Fracture Strain	*12%*	*8%*

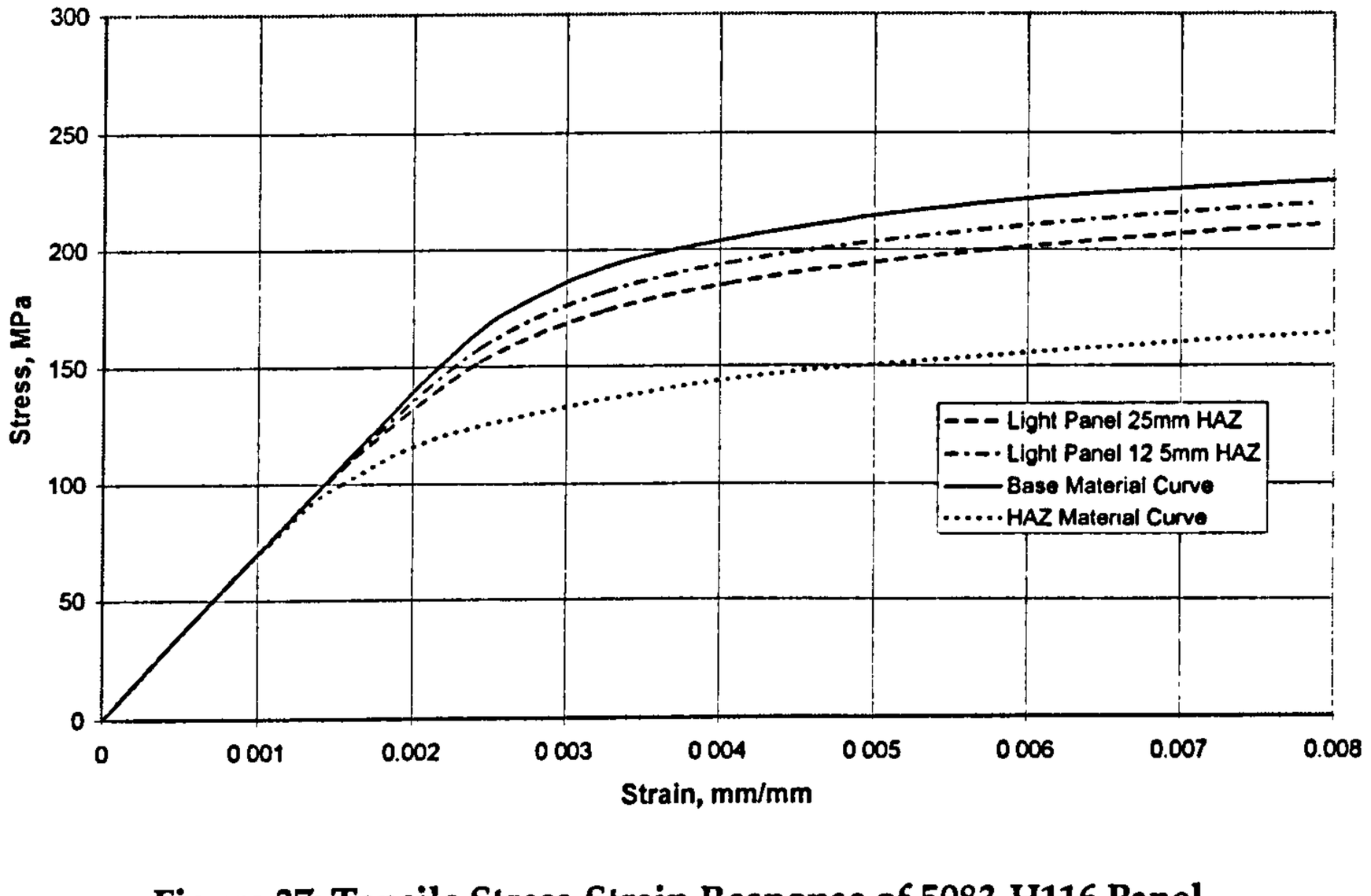

Figure 37: Tensile Stress-Strain Response of 5083-H116 Panel

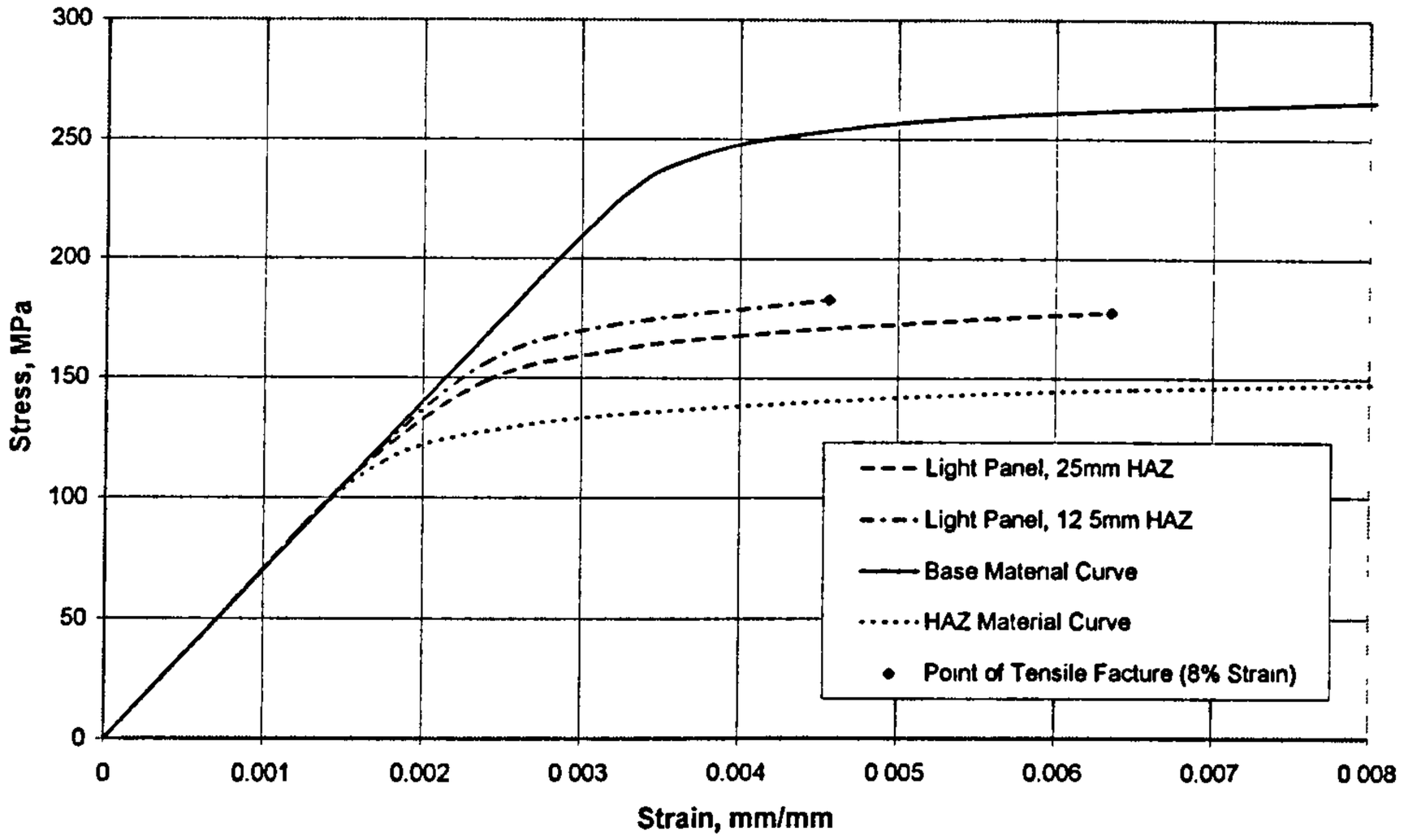

Figure 38: Tensile Stress-Strain Response of 6082-T6 Panel

The investigation of the tensile response of stiffened panels demonstrates that significant strain concentration is likely to occur in panels, as well as in plates. This strain concentration is likely to reduce the ductility of the panel, and should be borne in mind when investigating the response of structures composed of many panels, such as ship hull girders.

3.5 Effect of Panel Response on Overall Hull Girder Response

3.5.1 Overview

The investigation of the tensile response of plate and panels has raised the possibility that strain concentration effects may reduce the ductility of structure to the point where the ductility could effect the strength of structures composed of many such panels. To investigate the potential for strain concentration to effect the ultimate strength of aluminium HSV hull girders, the ultimate bending strength of two box girders, broadly similar to hull girders is considered in this section. The bending ultimate strength of two three-meter square box girder was investigated using a Smith progressive-collapse approach. The compressive and tensile and stress-strain curves for the elements of the girder were determined from the methods developed in Section 3.4.

The cross-section of the girders is shown below in Figure 39. The girders were designed to be representative of typically HSV hull forms. The lower flange and sides were assumed to be 5083-H116 alloy construction, and the upper flange 6082-T6 alloy construction. This reflects HSV construction, where bottom and side shell plating in contact

with seawater are often made from 5000-series alloys while the upper decks are often 6000-series alloys, as discussed in Chapter 2. As it is the 6000-series panels which show the most severe effects of strain concentration, it is expected that lack of ductility could be seen in the hogging response of the box girder, when the upper flange is in loaded in tension.

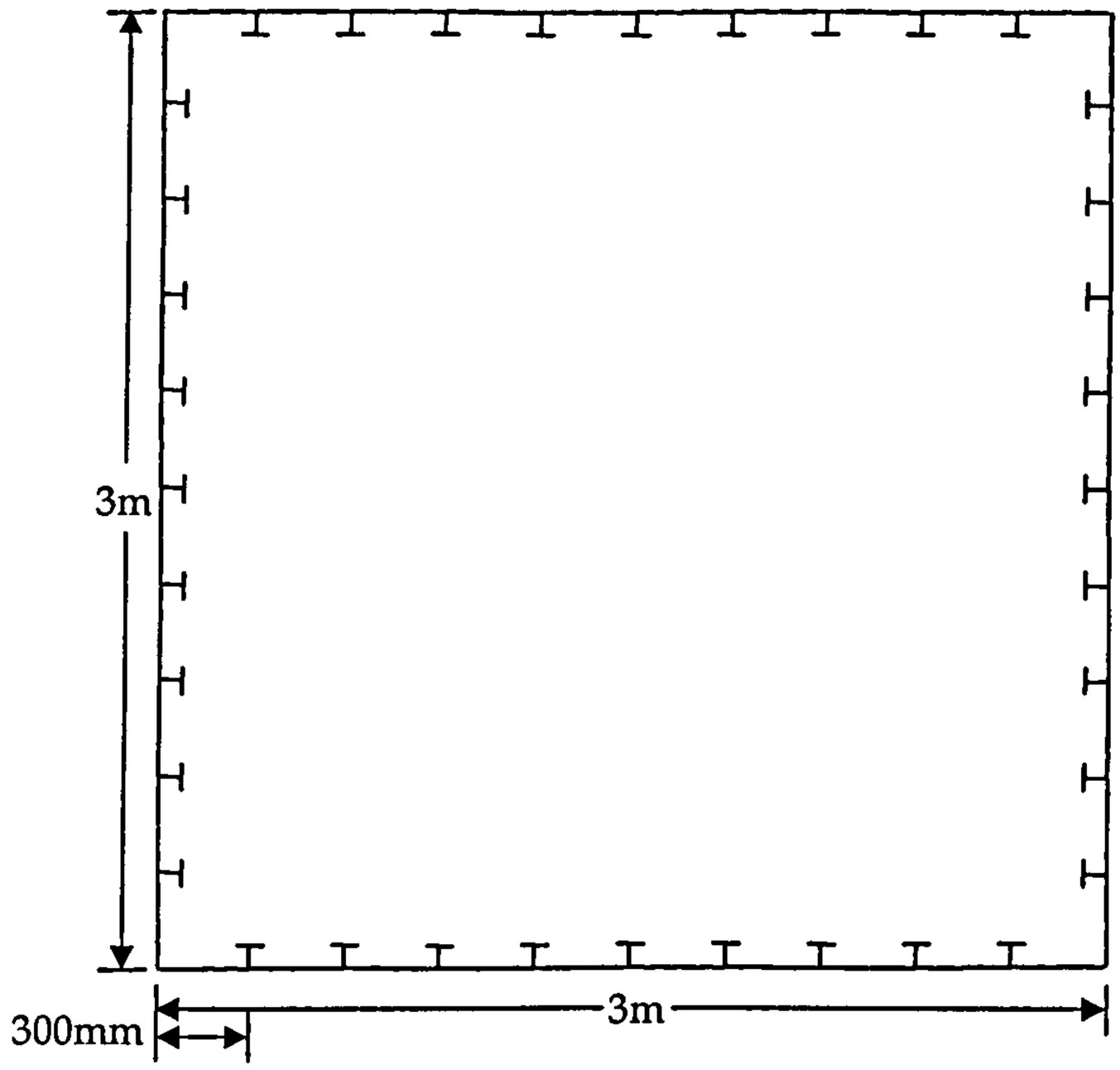

Figure 39: Box Girder Cross Section

The ductility of the tension flange is expected to be most influential when the bottom structure is stocky. This will raise the overall stress level in girder at which compressive collapse first occurs, moving it closer to the ultimate strength of the upper flange. Additionally, stocky bottom panels will pull the cross-section's neutral axis towards the bottom of the girder, increasing the strains in the tension flange. In this investigation, it was decided to investigate two girders which should bracket the range of structures expected to be seen in service. The stiffener spacing and panel length was kept constant between the girders, and the plating thickness and stiffeners varied to produce structures of different strengths. The first girder has identical scantling dimensions all around, which are capable of obtaining approximately 50% of the material's compressive proof stress. The upper flange is 6082-T6 alloy while the remained of the girder is 5083-H116. The second girder has bottom and sides capable of obtaining approximately 85% of the material's proof strength in compression. The upper flange is identical to the first girder, and again the bottom and sides are 5083-H116 alloy, while the upper flange is 6082-T6 alloy. The scantlings and elastic cross-

section properties of the girders are listed in Table 20 below, the material properties are identical to the properties used for the tensile response previously.

Table 20: Box Girder Properties

Girder	*Light Girder*	*Heavy Girder*
Panel Length	*1000mm*	
Stiffener Spacing	*300mm*	
Upper Flange Plate Thickness	*6mm*	
Upper Flange Stiffeners	*70 x 40 x 4 x 6.1 mm Tee*	
Side and Lower Flange Plate Thickness	*6mm*	*12mm*
Side and Lower Flange Stiffeners	*70 x 40 x 4 x 6.1 mm Tee*	*140 x 60 x 6 x 8.7 mm Tee*
HAZ Widths Considered	*25mm/12.5mm*	
Total Cross Sectional Area	*89985.6 mm²*	*165861 mm²*
Neutral Axis from Bottom	*1500 mm*	*1277 mm*
*Elastic Moment of Inertia**	*1.32 x 10^{11} mm⁴*	*2.31 x 10^{11} mm⁴*

*Note: Calculated in Smith approach from centres of individual elements, will be slightly conservative

3.5.2 Background to Smith Progressive Collapse Approach

The ultimate strength of two box girders will be determined by a Smith-type progressive collapse calculation. This type of calculation was briefly reviewed in Section 3.2, however it will be described in more detail in this section. The approach is an elegant combination of engineering beam theory and individual component response to determine the ultimate bending moment strength of ship-like structures without resorting to non-linear finite element analysis. The original method was implemented by Smith[2] in the late 1970s, and has since been used by several other authors. [3, 30, 31]. The approach starts by making three key assumptions about the collapse of a hull girder under a bending moment. First, it is assumed that the collapse will occur over one panel bay between adjacent transverse frames. Thus, it is only necessary to consider a cross-section of the hull girder consisting of the longitudinally effective material. Second, it is assumed that the strain distribution in the cross section remains linear throughout the bending response of the hull girder. Finally, it is assumed that cross-section can be divided into sub elements which respond independently to the local strain at their location. This final assumption takes advantage of the stiffened-panel type of structure typically used for ship hull, which can be fairly successfully idealized as a series of identical, closely-spaced column elements, as discussed in Section 3.4. These assumption are not always strictly true, for example Gordo et al.[136] comment that the

assumption of plane sections remaining plane may be violated when significant shear is present in the plates. However, under predominantly bending loading, this approach has been shown to agree well observed collapses of box girders and actual ships[3, 127].

With these assumptions in place, the Smith method consists of applying incremental curvatures to the cross-section of the ship's hull which as been divided into individual components whose tension and compression stress-strain curves can been determined by suitable methods, such as those presented in Sections 3.3 and 3.4 above. By calculating the resulting strain at each element the resisting force at each element can be determined, and by adding the contribution of all the elements in the cross section overall resisting bending moment at each curvature is found. If only vertical bending is considered, the method starts by assuming a curvature, C, of the hull girder, which is one over the radius of curvature of the section about its neutral axis. Invoking the assumption that plane sections remain plane as the curvature is applied, the strain at any particular element, i, can be found by:

$$\varepsilon_i = Cy_i$$

Where:

ε_i Strain in the *i*th element

C Applied curvature

y_i Distance of the *i*th element to the instantaneous netural axis

Equation 41

If the stress-strain curve of this element can be determined, then the stress corresponding to this strain can be found, and the total force produced by this element determined:

$$F_i = A_i\sigma(\varepsilon_i)$$

Where:

F_i Force in the *i*th element

$\sigma(\varepsilon_i)$ Stress in the *i*th element from strain ε_i

A_i Area of the *i*th element

Equation 42

The total moment is then simply the summation of the individual element forces multiplied by the distance to the instantaneous neutral axis of the section

$$M = \sum F_i y_i$$

Equation 43

The only complication applying this approach is that the location of the neutral axis is not known ahead of time. For the initial linear elastic response of the girder, it will be equal to the elastic neutral axis, however, as elements fail through buckling, or in the case of aluminium, as the tensile stress-strain response departs from the linear response, the neutral axis will shift and an iterative approach is required. Rutherford and Caldwell[3] developed an expression to estimate the shift in the neutral axis, however Gordo and Guedes Soares[31] noted that they felt this approach could lead to difficulty getting the method to converge to a

valid neutral axis. Gordo et al. recommended directly using the requirement that the summation of the axial forces about the instantaneous neutral axis must be equal to zero:

$$\sum F_i \equiv 0 \ @ \text{correct neutral axis location} \qquad \textit{Equation 44}$$

This approach was adopted here, by expressing the net axial force as a function of the neutral axis position for a fixed value of curvature, and using a numerical root bracketing approach to locate the root of axial force equation until the relative error in the neutral axis was sufficiently small. The neutral axis position and net force in the section was tracked along with the moment and curvature output, to ensure that this requirement was being correctly implemented. It is also possible to determine the moment-curvature relationship of a purely elastic beam by combining Equation 41 with Hooke's law and elastic beam theory, yielding:

$$M = CEI$$

Where :

M Total moment

C Applied curvature

E Elastic modulus of the beam material

I Elastic moment of inertia of the beam

Equation 45

This relationship can be plotted along with the moment-curvature results from the Smith approach, both as a check on the results from the Smith approach and as a method to determine when the section's response first becomes non-linear.

3.5.3 Application of the Smith Approach to the Box Girders

The Smith progressive collapse approach was applied to the two box girders to determine their ultimate sagging and hogging moment. The girders were divided into the 44 sub elements, 36 of the sub-elements consisted of a single stiffener and attached plating, while 8 of the element consisted of flat plate alone, these elements were located at the corners of the girder. The sub-elements in the section are shown in Figure 40. The stress-strain compression and tension curve of each stiffener-plate sub-element was determined using the modified Gordo compression approach and the panel tension approach presented in Sections 3.4.3.3 and 3.4.4 respectively. The stress-strain response of the individual plate elements that form the "corners" of the girder could be modelled several different ways. Gordo and Guedes Soares[31] note that such corners could be considered to follow the material stress-strain law perfectly, in other words no buckling effects, as the corners are presumably stiff. Alternatively, they could be modelled as un-stiffened plate elements, or neglected all together[31]. In this study, is was decided to assign these elements the same stress-strain curve as the stiffened plates. As the corner bay of plating in this girder is the same width as

the plating between stiffeners, it was felt that this bay would behave similarly to the other bays, although the side supported by corner is in fact probably a bit stiffer than the rest of the panel.

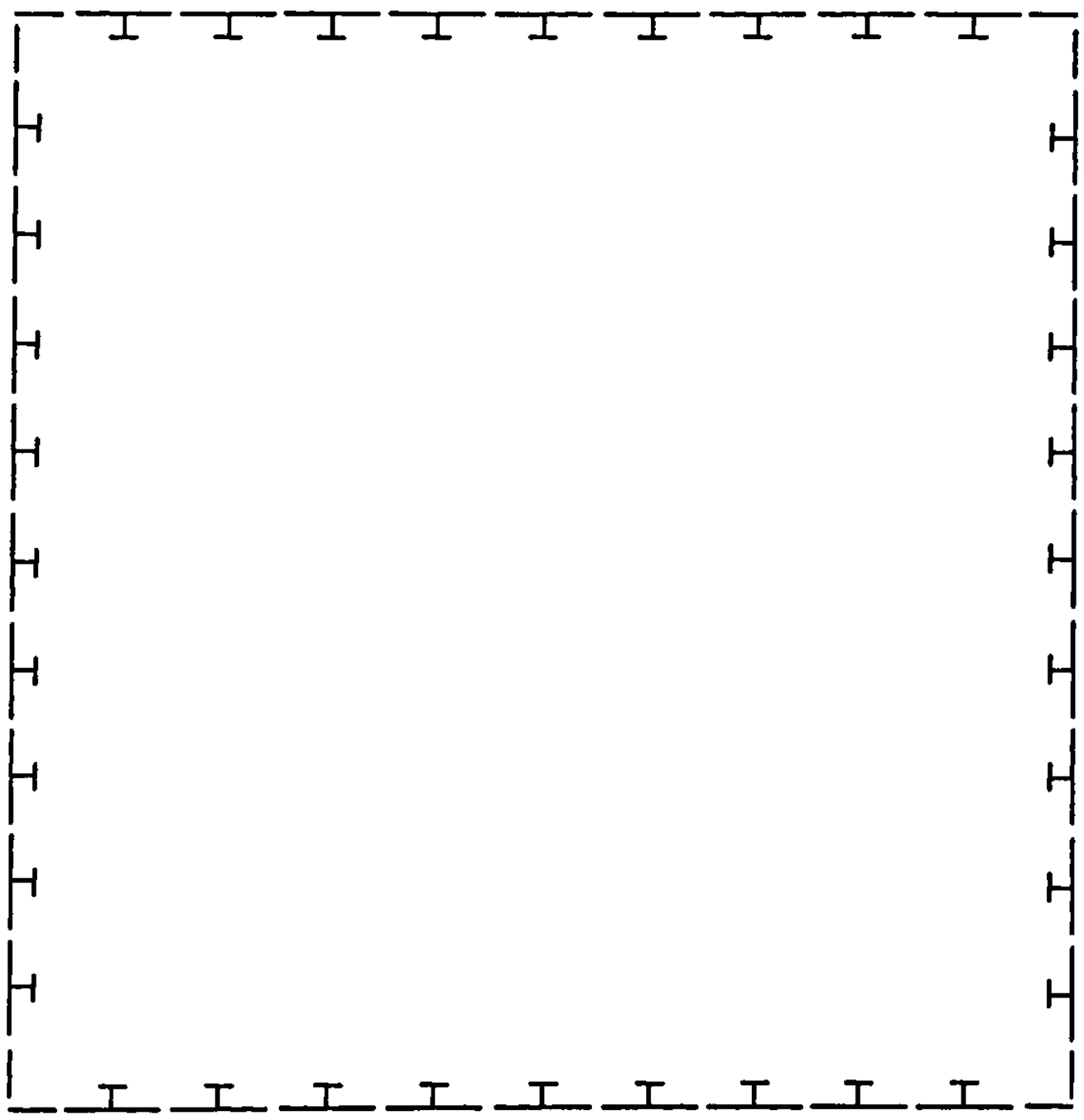

Figure 40: Division of Box Girders into Sub-Elements

The stress-strain curves for the individual elements are presented below in Figure 41 and Figure 42, divided by alloy type. Two complete curves were produced, one for 25mm HAZ and one for 12.5mm HAZ. Note that the HAZ breadth in the stiffener was assumed to be equal to the HAZ breadth in the plate, and that the transverse and longitudinal HAZ were assumed to be of the same breadth. An 8% fracture stain limit was observed for the 6082-T6 panels, and a 12% fracture strain limit was observed for the 5083-H116 panels. The later panels did not appear to suffer fracture at strain values obtainable in this cross-section. A perfectly-elastic response line is also included on each graph for comparison.

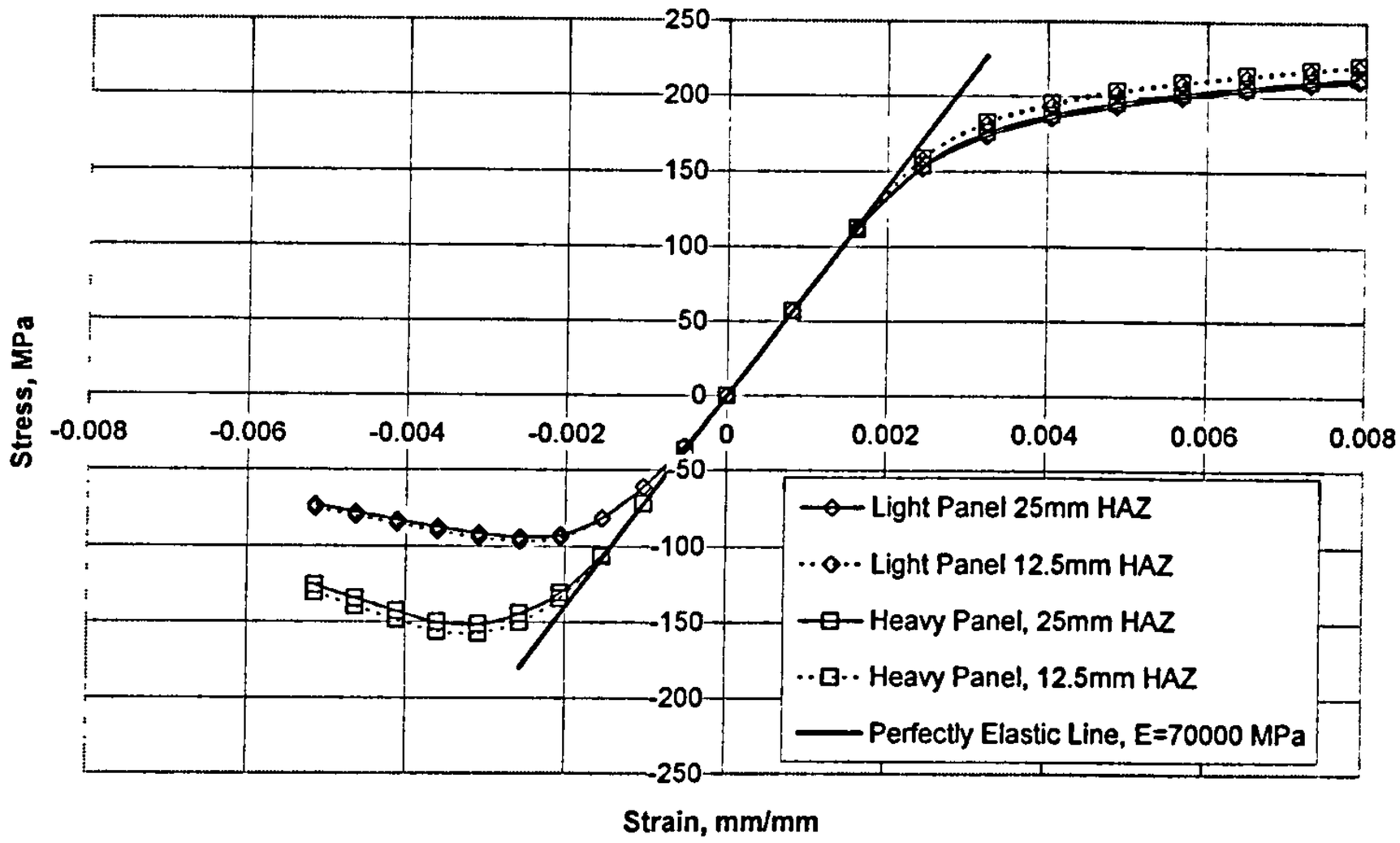

Figure 41: Stress-Strain Curve for 5083-H116 Panels

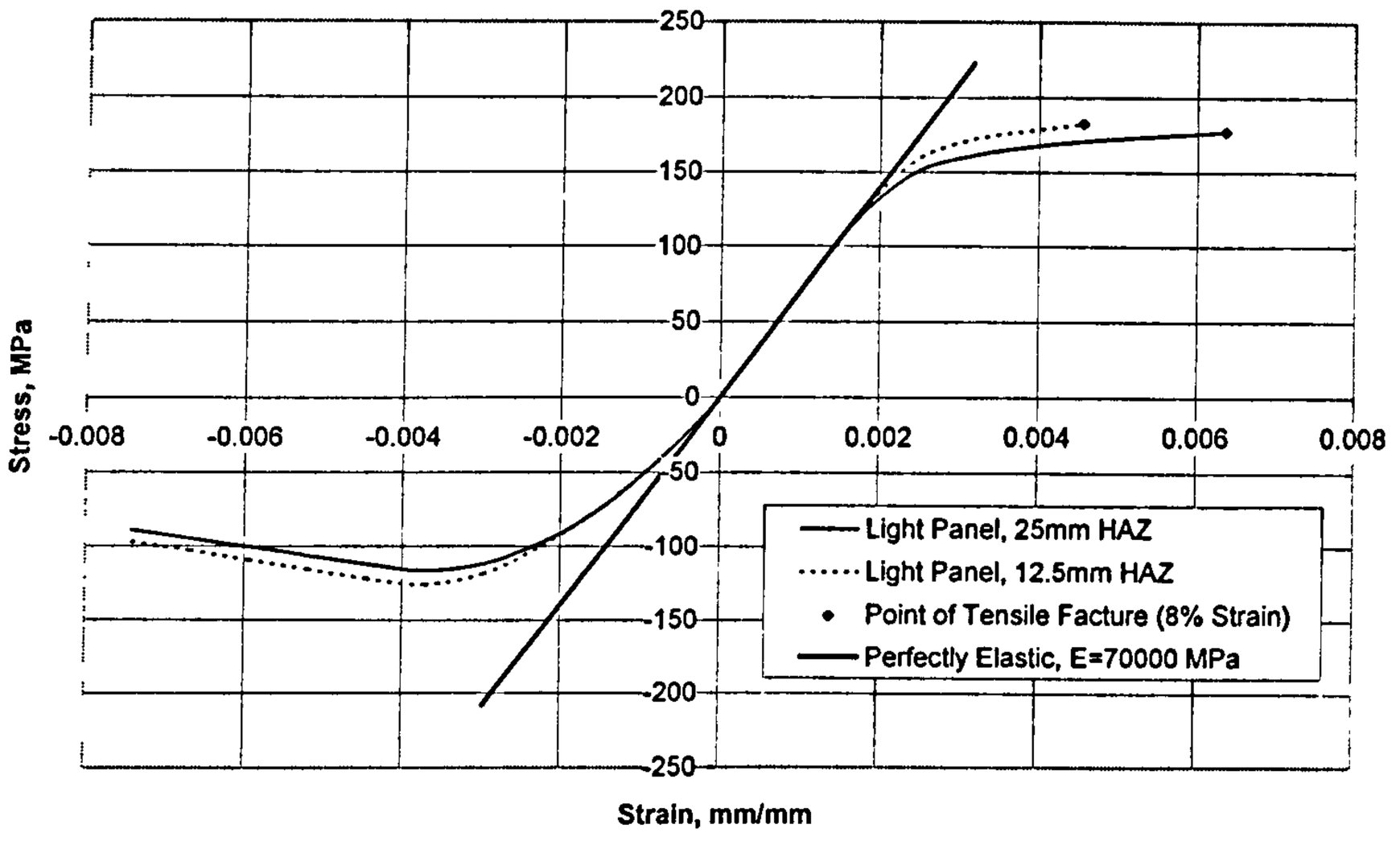

Figure 42: Stress-Strain Curve for 6082-T6 Panels

The panel response shows that the influence of the HAZ on the compressive strength is generally small, in the region of 10%. For the 5083-H116 panels, a similar reduction applied to the tensile response. Increasing HAZ also decreases the tensile strength curve for the 6082-T6 panel, however, it significantly prolongs the ability of the panel to deform, doubling the HAZ width results in just shy of a 50% increase in the fracture strain. The ultimate tensile strength is slightly reduced, as the increase HAZ breadth has reduced the continuous area of base material in the stiffener. It is also interesting to note that the compressive response of the lighter panels deviates almost immediately from the liner elastic line, while the tensile response and stockier panels have a significant elastic region in their curve. The compressive strength of the lighter 5083 panels is below 100 MPa while the

fracture stress of the 6082-T6 panels is above 150 MPa, making fracture unlikely to effect the ultimate strength of the lighter girder. However, the stockier 5083 panels fail at roughly the same compressive stress as the 6082-T6 panel in tension, raising the possibility of interaction between fracture and compressive collapse as failure modes.

The moment-curvature plot for the light box girder is shown below in Figure 43, sagging response is plotted on the left of the figure, represented by negative curvature and bending moments. The ultimate strength curve is smooth, initially following the linear elastic response which is also plotted on the figure. It is interesting to note that the hogging response follows elastic curve longer than the sagging response, even though the ultimate strength in hogging is less than in sagging. This is attributed to the compression stress-strain response of the 6082-T6 panels which almost immediately diverge from the elastic response line, as seen in Figure 42.

An investigation of the element strains in the 6082-T6 tension flange were approximately 0.002 when the ultimate hogging strength was reached, well below the fracture strain. As the bottom failed, the neutral axis rose rapidly towards the tension flange, moderating the increase in the tension flange strains in the post-ultimate strength region and preventing fracture in the post-ultimate strength region. In both sagging and hogging, the neutral axis moved between 350mm-and 400mm when the ultimate strength was reached, and almost doubled this movement in the load-shedding region. Doubling the HAZ width reduced the ultimate strength of the hull, though this was more apparent for sagging than hogging, and the reduction was roughly in line with the reduction to the individual panel's stress-strain curve. It is interesting to note that because of the much higher proof strength of the 6082-T6 upper flange material than the 5083-H116 lower flange material, this box girder is significantly stronger in sagging than hogging. The response of the lighter box girder is fairly similar to that of steel box girders and hulls[30], and shows negligible influence of strain concentration effects.

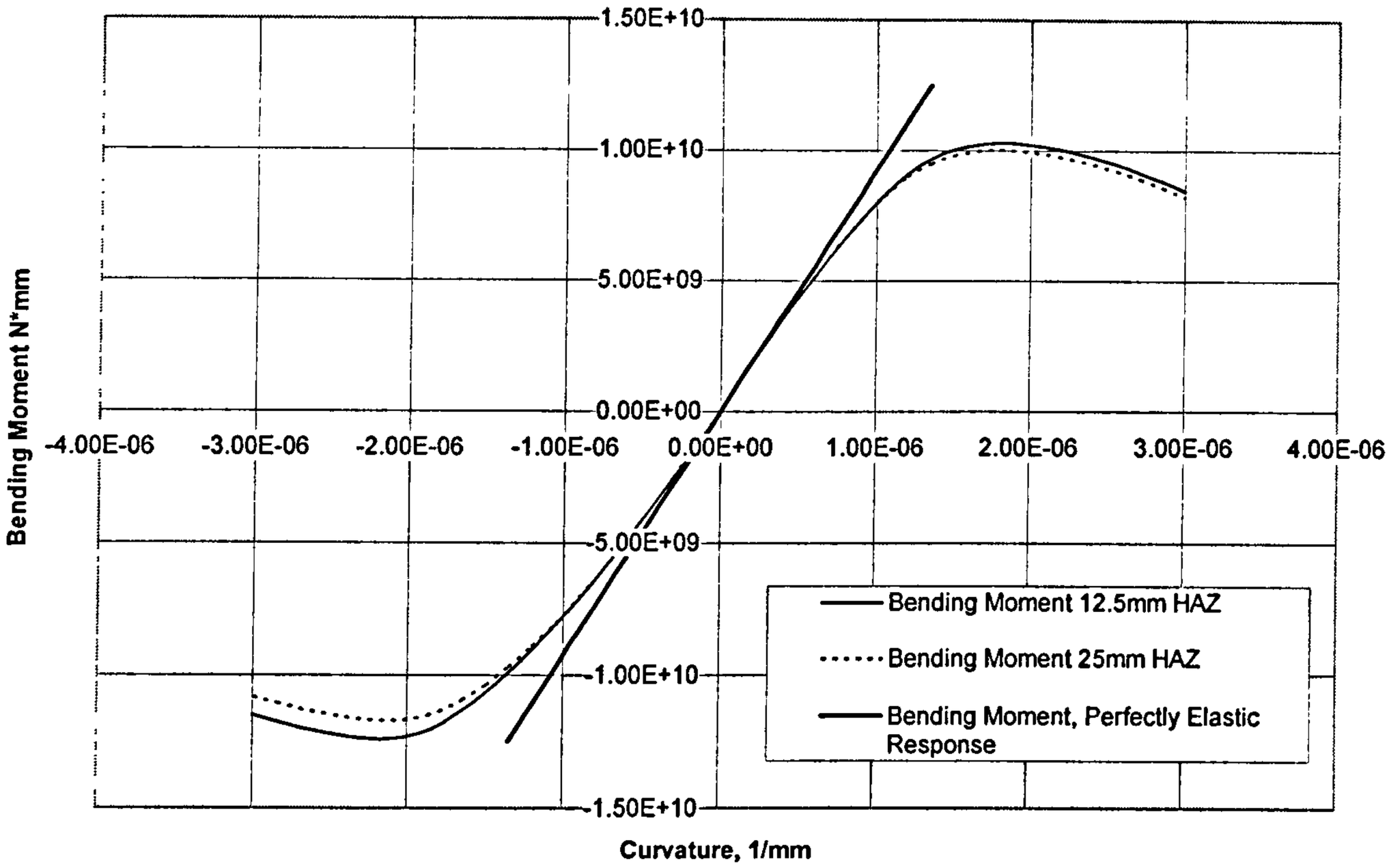

Figure 43: Moment Curvature Response of the Light Box Girder

The moment-curvature plot for the heavy box girder is shown below in Figure 44, and shows a different story than the light girder above. The sagging response is broadly similar to the light girder, but the hogging response of the heavy girder with the 12.5mm HAZ is marked by a sudden jump as the resisting moment curve begins to level out. Investigation of the element strains indicate that this jump occurs when the 6082-T6 tension flange fractures. After fracture, the stress of the 6082-T6 panels was assumed to go to zero, and the resisting moment continued increasing with increasing curvature, showing that the remaining structure still has reserve strength left. This indicates that the ultimate strength of this girder is determined by tensile fracture and compressive failure together, not compressive failure alone. This is further strengthened by the response of the 25mm HAZ girder, which parallels the 12.5mm HAZ girder and continues rising after the 12.5mm girder fractures. The hogging response of the 25mm HAZ girder is different, the higher fracture strain of the 6082-T6 panels in this girder mean that the ultimate strength is determined by the compressive collapse of the bottom flange. The strains in the top flange of the girder with 25mm HAZ were approximately 0.005 at ultimate strength, and 0.00538 where the curve terminates. As the fracture strain for these panels is 0.0065, fracture will not occur until further out in the post-ultimate strength region. The neutral axis movement for the heavy girder was much less pronounced than for the light girder, as compressive failure occurred much later in the response of this girder. This is also seen in the comparison of the moment-curvature response to the purely elastic response line, the heavy girder follows the elastic

response line proportionally longer than the lighter girder. Once the compressive flange neared failure, the movement of the neutral axis was much more pronounced, and a large downward jump was observed when the tension flange fractured for the girder with 12.5mm HAZ. In sagging, the response was similar to the lighter box girder although the computed ultimate strength was higher as a results of the stockier side shell panels which were also in the tension flange. For sagging, the ultimate strength reduced with increasing HAZ width, as for the lighter girder.

This example indicates the strain concentration has the potential play a significant role in the response of aluminium HSV hull girders, and should be included in the investigation of the their ultimate strength. It is emphasized that this type of fracture was only observed in a fairly extreme case, with small HAZ breadths, a very stocky compression flange, and the grade minimum elongation used for fracture. As discussed in Chapter 2, the actual elongation is often significantly superior to the grade minimums, and even small increase in the elongation would seem to be enough to avoid this type of failure. However, on the other hand, improved welding processes may reduce the HAZ below 12.5mm offsetting this. Zha and Moan reported experimental HAZ breadths of only 10mm for their experimental panels[62]. Additionally, larger vessels may have frame spacing greater than the 1000mm used here, making the HAZ proportionally smaller and further offsetting any increase in elongation.

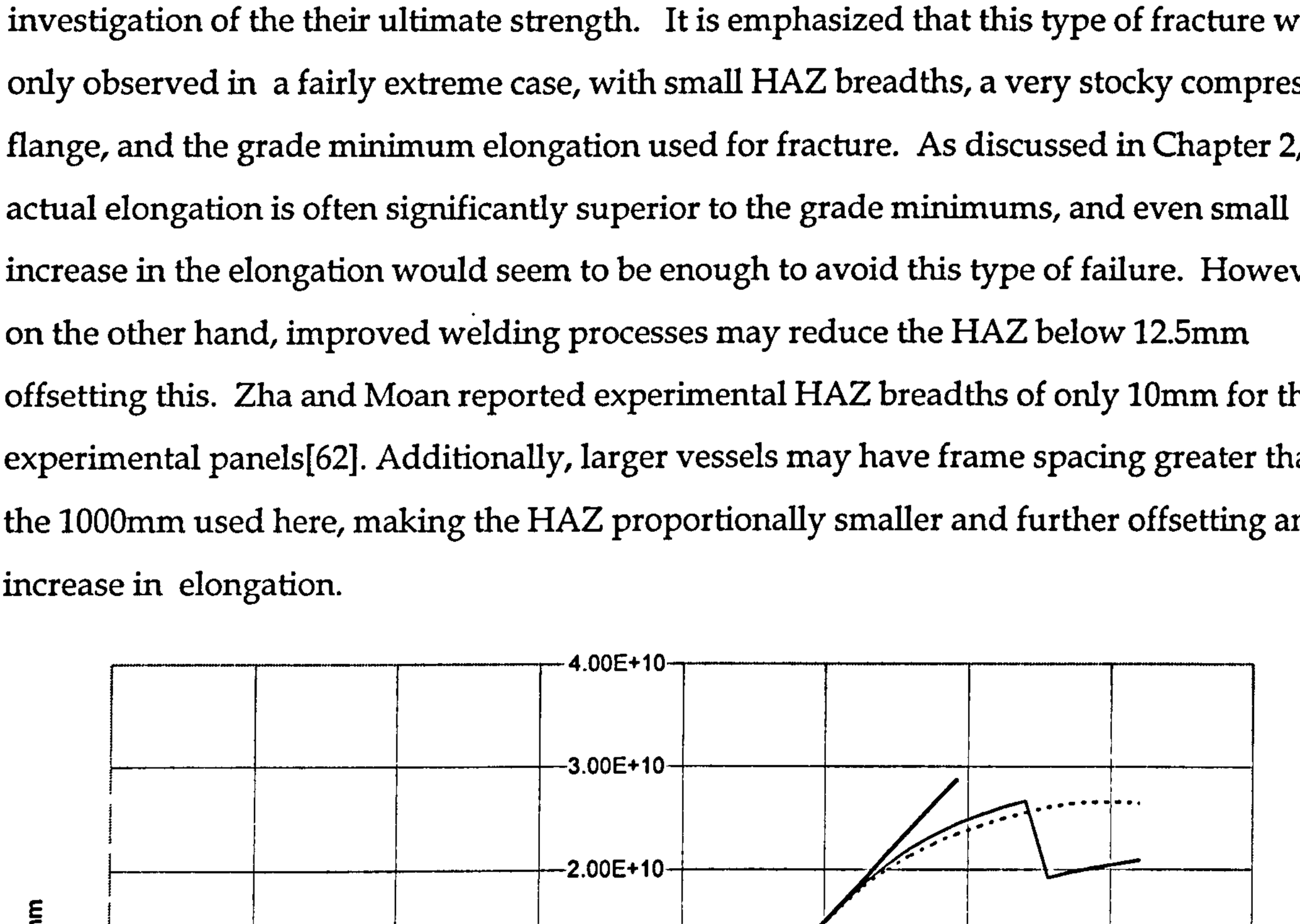

Figure 44: Moment Curvature Response of the Heavy Box Girder

A final point of interest is that although the sagging response is now weaker than the hogging response for the heavy girder, they are not as different as the difference in upper flange and bottom flange scantlings would suppose-the bottom flange has twice as thick plate and has stiffeners twice as tall as well. Part of this is a result of the stockier side shell, the upper portion of the side shell contributes in compression in the hogging case . However, this can also be partially attributed to the much higher compressive strength of 6082-T6 material than 5083-H116 material, 260 MPa against 180 MPa. Given the tendency of HSVs to be built with 5000-series alloys for bottom structure and 6000 series alloys for deck structure, it is also possible that the hogging strength of these vessel may be less than the sagging strength, even if the bottom structure appears stockier than the deck structure. Thus, it is clear that the material-specific characteristics of aluminium need to be considered when investigating the ultimate strength of aluminium HSV hull girders, and that some of the response assumptions which are acceptable for steel vessels may not apply to aluminium vessels.

3.6 Reliability Formulations

Determining the ultimate strength of aluminium plates and panels is an important step in the structural design process, but not the only step. After determining the ultimate strength, the designer is then faced with the question of "is this strength adequate for the intended service?" Structural reliability theory is one way of answering this question, and the determination of structural reliability with aluminium ultimate strength estimates will be reviewed in this section. Determining reliability is a three-step process, as discussed in Chapter 2. First, the limit-state function must be determined. This function indicates under which strength and loading combinations the panel will fail. Second, a mean value, stochastic distribution, and measure of uncertainty must be assigned to each of the variables in the limit state function. Finally, the probability of failure must be mathematically determined by one of the methods discussed in Chapter 2. All three steps in the process of reliability determination will be examined in this section, using a hypothetical deck panel on a high-speed vessel. Additionally, the accuracy of the first-order reliability (FOR) method for determining the probability of failure will be examined by comparing it to a Monte Carlo simulation.

3.6.1 Limit State Function

To determine the reliability of a hypothetical deck panel, a limit state function must be written to determine under what conditions the panel fails. As the limit state function is traditionally written so that failure is represented by a return value less than zero, a suitable

function would start with the ultimate stress that the panel could sustain, and then subtract the applied loading. Several previous authors have investigated limit state functions along these lines for hull girder stiffened panels. For this study, an adaptation of a limit state function used for steel naval ships by Assakkaf et al.[74] is employed, the principal change being that an additional uncertainty factor has been added to the panel strength:

$$g(X) = X_S \sigma_U - \sigma_{SW} - X_{Wave} \sigma_{Wave}$$

Where:

X_S Ultimate strength modelling uncertainty factor

σ_U Estimated ultimate panel strength *Equation 46*

σ_{SW} Still water bending stress at panel

X_{Wave} Wave bending stress modelling uncertainty factor

σ_{Wave} Estimated wave bending stress

Where the X variables are modelling uncertainty factors, and the σ variables are loading or strength variables. This equation produces negative values when the combined stress resulting from the still-water bending moment and wave bending moment exceeds the strength of the panel, indicating a failure. When combining still water bending moments and wave bending moments, a more rigorous approach is to use an additional load-combination factor, see for example the limit states in Mansour et al.[6] and the extended discussion in Mansour and Thayamballi[100]. However, the information required to determine such a combination factor is not readily available for HSVs. Assuming that the stillwater bending moment is fairly constant, this load combination factor was assumed to be equal to unity, and therefore was excluded from the equation.

There are a couple of additional assumption which are inherent in the limit state function which should be reviewed as well. In determining the applied stress in the limit state equation, typically the elastic section modulus would be used to convert from still water and wave loading. This is only valid if the panel in question in first panel to fail in the cross-section. If other panels fail before the panel in question, their failure will reduce the effective section modulus of the cross section, increasing the load on the remaining panels. In the example at hand, a deck panel is considered in compression, which typically would be one of the first panels to fail in a sagging mode, so the approach should be reasonably accurate.

A second assumption is that the ultimate strength of the panel can be adequately represented by a single stochastic variable. While this approach is widely used, it is also possible to construct an implicit limit state equation relating the basic panel properties such as dimensions and material properties to the applied loading via one of the strength prediction routines, and determine the reliability in this manner. Such an approach was

successfully implemented for the ultimate hull girder strength of a steel HSV by Downes and Pu[76], linking not only the calculation of the individual panel response but also a progressive collapse analysis to a reliability approach. This approach has the advantage that the influence of the fundamental parameters of the vessel's structural design can be directly assessed by the sensitivity factors determined in the reliability analysis. Additionally, the effects of load shedding from other panel in the cross-section will be captured in determining the actual bending moment at which the panels fail.

3.6.2 Mean Values and Uncertainties

Each variable in the limit state equation must have a mean value and uncertainty defined for it as well. This will be done for a hypothetical deck panel. X_s, the modelling uncertainty factor expresses the variability in the engineering method used to predict the panel's ultimate strength. Based on the performance of the simplified methods discussed in Section 3.4.2.6 above, it seems that a mean value of 1.0 is appropriate for this variable as many of the simplified prediction methods had biases less than 5% different than 1.0 in Table 16. Likewise, the result in Table 16 can be used to develop a method-specific COV for this variable, for most methods this seems to be roughly a COV of 20%. A normal distribution will be assumed for this factor. These values should be considered approximate, based on the limited number of panels used to benchmark the ultimate strength prediction techniques. Based on 120m high-speed catamaran study published by Heggelund et al.[95], a mean value of 125 MPa was taken for σ_u, this was estimated by Paik and Thayamballi's method as this section of the thesis was completed before the revision of this formula for aluminium. An additional measure of uncertainty should be included in this variable to account for the effects of variability in material properties, dimension tolerance, and fabrication of the panel. At present, published data on this topic for aluminium in the marine field is scarce. As a first approximation, data from the civil engineering field that was originally proposed by Galambos [115] and summarized by Kissell and Ferry[49] will be used. This data is based upon the work done to develop the LRFD specification for aluminium structures in the U.S. In this approach, the variability in material properties and dimensions of the structure are treated separately. For buckling-type failures, a mean value of 1.0 is assigned to each of these categories, with a COV of 0.06 assigned to material, and 0.05 to fabrication. A second-moment approach was used to combine these effects in the original work:

$$COV_\sigma = \sqrt{COV_M{}^2 + COV_F^2}$$

Where:

COV_σ COV of ultimate strength

COV_M COV of material properties

COV_F COV of fabrication influences

Equation 47

Using the recommend COVs, the overall COV works out to approximately 0.08. A few comments must be made on this approach, given that the mean value of the modelling uncertainty was taken as 1.0, an alternative approach would be to eliminate the modelling uncertainty factor and including the modelling COV in the second-moment approach which was used to determine the variation of the ultimate strength. Secondly, the COV of 0.06 for material seems low when compared to the variability of the proof stresses in the plate and panel experiments reviewed above. Some of this could be attributed to the loose N8 specification used in the U.K. for 5083 alloys in the 1980s, however, in two occasions, sampled of the N8 material failed to achieve even the minimum annealed strength specified for the alloy by a large margin.

The loading data is based on the 120m high-speed catamaran published by Heggelund et al.[95] which was presented in Chapter 2. The long-term bending moment distribution at a deck panel in the hull with a Weibull distribution with a scale parameter of 1.32MPa and a shape parameter of 0.93. Roughly 1.8×10^8 cycles were expected in the vessel's lifetime. The extreme value of wave bending moment was represented by Guedes Soares and Teixeira's[163] method from the Weibull long-term load distribution:

$$F_e(x_e) = \exp\left[-\exp\left(-\frac{x_e - x_n}{\sigma}\right)\right]$$

$$x_n = \alpha[\ln(n)]^{\frac{1}{\beta}}$$

$$\sigma = \frac{\alpha}{\beta}[\ln(n)]^{\frac{1}{\beta}-1}$$

Equation 48

Where:

$F_e(x_e)$: Gumbel cumulative distribution function at x_e

α: Weibull scale parameter

β: Weibull shape parameter

n: Numer of applied loading cycles

The still water bending stress was assigned a value of 10% of the wave stress as this was not published by Heggelund. Information on the uncertainty in the still water and wave loading on high-speed craft is generally lacking. The uncertainties for naval and commercial ships presented in Hess et al.[77] will be adapted, taking the COVs of both σ_{sw} and X_{wave} as 0.15, normally distributed. Lacking information on modelling bias, the mean value of X_{wave} can be taken as 1.0. The mean value and COV of σ_{wave} can be derived from long-term

loading prediction, as the COV of the Gumbel extreme-value distribution for the highest wave load in the vessel's life. The final parameters for the base case are presented below in Table 21.

Table 21: Base Case for Reliability Study

Parameter	*Mean*	*COV*	*Distribution*
X_s	*1.0*	*0.20*	*Normal*
σ_{ult}	*125 MPa.*	*0.08*	*Normal.*
σ_{sw}	*3 MPa*	*0.15*	*Normal*
X_{wave}	*1.0*	*0.15*	*Normal*
σ_{wave}	*32.3 MPa*	*0.07*	*Gumbel*

3.6.3 Determination of the Probability of Failure

The final step in the reliability analysis to calculate the probability that the panel will fail in service, expressed through a safety index, β. Typically, the FOR reliability approach is used for such limit states, and has been used in the past[74]. As discussed in Chapter 2, the disadvantage of the FOR-methods is that the safety index produced is only an approximation for non-linear limit states or limit states involving non-normal variables, such as this one. Previous experience has shown that FOR methods are often sufficiently accurate for slightly non-linear limit states. To investigate the accuracy of the FOR methods for the limit state considered in this study, the FOR results were compared to a Monte Carlo simulation for a sample stiffened panel. In this section, the Hasofer-Lind safety index was determined by the Rackwitz and Fiessler method[84], as outlined in Chapter 2, and a direct Monte Carlo simulation was used for comparison, also as outlined in Chapter 2.

Given the lack of firm data for several of the stochastic variables in the limit state equation, the base case listed in Table 21 and several variants were run through both the FOR method and Monte Carlo simulations. The variants involved doubling and halving the wave loading of the base case to vary the safety index, and doubling all the uncertainties of the base case. By taking such an approach, a wide range of potential mean value and uncertainty combinations can be evaluated. The results are summarized in Table 22, which lists the safety index, β, produced by the FOR method, and the percentage error in safety index between the FOR and Monte Carlo methods. Note that as β is non-linearly related to the probability of failure, the errors in the probability of failure will differ, and will normally be higher than the error in β, especially for high values of β. However, engineers typically

work with the value of β in place of the numeric probability of failure. In Table 22, positive errors indicate conservative FOR predictions. The FOR method appears quite accurate for cases when the wave loading is comparatively small, with errors increasing as the non-normally-distributed wave loading increases. Raising the uncertainties raised the error in the FOR prediction slightly. In all cases the errors were conservative, and less than 10% of the actual safety index.

Table 22: FOR Safety Index and (*Error*) Between FOR and Monte Carlo Predictions

		Uncertainties as % of Base Case	
		100%	*200%*
Wave Load as % of Base Case	*50%*	*4.21(1%)*	*2.10(1%)*
	100%	*3.49(2%)*	*1.73(3%)*
	200%	*2.07(7%)*	*1.01(9%)*

The directional cosines are listed below in Table 23. These indicate the relative significance of each variable in the limit state equation(in the reduced, standardized, space) to determining the value of the safety index. The increase in error in the FOR approximation with increasing loading corresponds to an increase in the directional cosine to the non-normally distributed wave loading variable. From the directional cosines, it appears that the modelling uncertainty factors are quite significant in determining the overall safety index. This indicates that correct assessments of these factors will be important in obtaining accurate probability of failure estimates, unfortunately, the current data seem largely lacking in this regard. Overall, the application of reliability theory to aluminium panels is straightforward. Using similar limit state functions to those already applied to steel vessel and the FOR method appears entirely adequate. The biggest obstacle will be in obtaining accurate measures of the uncertainty associated with the loading and material variability of aluminium HSVs.

Table 23: Directional Cosines for FOR Solution

				Variable				
				X_s	σ_{ult}	σ_{sw}	X_{wave}	σ_{wave}
Uncertainty as % of Base Case	*100%*	*Wave Load at % of Base Case*	*50%*	*0.99*	*0.07*	*-0.02*	*-0.10*	*-0.05*
			100%	*0.97*	*0.13*	*-0.02*	*-0.20*	*-0.11*
			200%	*0.88*	*0.23*	*-0.02*	*-0.36*	*-0.21*
	200%		*50%*	*0.99*	*0.07*	*-0.02*	*-0.10*	*-0.05*
			100%	*0.97*	*0.13*	*-0.02*	*-0.21*	*-0.10*
			200%	*0.88*	*0.24*	*-0.02*	*-0.37*	*-0.19*

3.7 Conclusions

This chapter reviewed the options for predicting the ultimate strength and reliability of plates and stiffened panels in the structure of an aluminium HSV. The ultimate compressive strength of steel plates and panels has been extensively studied over the years, a smaller amount of work has been performed on aluminium. Starting with un-stiffened plates, several potential methods of predicting their ultimate strength were reviewed and compared to a series of plate compression tests carried out by Mofflin. Most of the methods showed good agreement with the experimental results, however, the effect of different alloys was noticeable on the ultimate strength of the plates, indicating that predictions based purely on the plates geometry and proof stress may not be accurate. A simple effective-width equation was proposed to model the stress-strain curve of aluminium plates in compression, and good agreement was observed between this approach and the experimental data. In tension, the potential for strain concentration in the transverse HAZ region of aluminium plates was examined by a spring model. This revealed that 6000-series plates may have limited ductility in tension, and the this restriction may effect the response of structures composed of many such plates, such as aluminium HSV hull girders.

A similar comparison study was carried out for aluminium stiffened panels, investigating both methods to predict the ultimate strength of the panels and methods to predict the entire stress-strain curve. Although the experimental data sets available for comparison were quite limited, most of the methods to predict the panel's ultimate strength worked well, including several steel methods. The prediction of the compressive stress-

strain curve was more varied. Two steel methods were applied, along with a modification of Gordo's method to account for the differences between steel and aluminium. None of the methods proved consistent in predicting the peak ultimate strength value, though the modified Gordo method did appear to capture the shape of the stress-strain curve, notably better than the steel methods. The tensile response of stiffened panels was broadly similar to that of plates, and the potential for strain concentration to limit the ductility of the response was seen again. From the limited data available, no strong difference in the response of 5000 series alloys and 6000 series alloys could be seen.

A Smith-type progressive collapse analysis was carried out on two box girders to investigate if strain concentration effects in the tension flange would reduce the ultimate strength of the girder. For a girder where the compression flange failed before the tension flange began yielding, no influence was seen. For a girder with a stocky compression flange, the limited ductility of the tension flange did limit the ultimate strength for the case where the HAZ width was assumed to be 12.5mm. This failure mode appeared very sensitive to the HAZ width in the plate and the fracture strain of the HAZ, and it is not clear that this will effect HSV in service, however, in investigating their ultimate strength of aluminium hulls, it seems clear that the effect of strain concentration must be borne in mind. This is especially true if advanced welding techniques are used which further reduce the size of the HAZ, or if the panel length grows beyond the 1000mm used in this study.

A reliability formulation was proposed to estimate the reliability of an aluminium plate or panel in compression. Uncertainty values were developed and a sample application was made based on the 120m fast ferry discussed in Chapter 2. The accuracy of the FOR method for determining the reliability of this panel was tested against a Monte Carlo simulation for several potential loading and uncertainty combinations. The FOR method performed well with conservative safety index predictions that were always within 10% of the safety index estimated by the Monte Carlo simulation. The primary source of error appeared to be the non-normally distributed wave loading variable. Applying reliability techniques to panel ultimate strength predictions appears straightforward, though adequate data on the uncertainties associated with the variables in the limit state equation is currently lacking.

CHAPTER

4

"It is quite possible to spend a career designing aluminium structures without entering the imperfectly understood netherworld called 'fatigue' "
[49]

Fatigue Life: S-N Reliability Approach

4.1 Introduction

Fatigue cracking is a problem that has plagued the majority of modern aluminium HSVs. The fatigue cracks typically appear at welds and locations of stress concentration in the vessel's structure, often after only a few months of service. This problem affects vessels of all sizes, types, and operating profiles. During the research for this thesis, the author has personally seen fatigue problems on vessels ranging from harbour ferries barely over 10 meters in length, to large vehicle ferries over 100 meters in length. Compared with ultimate strength, the fatigue strength of marine aluminium structures has received considerable research attention, and numerous papers have been presented and published on the topic. Investigations into fatigue problems on HSVs have been ongoing for many years, with significant investigations being carried out 25 years ago[164]. Indeed, fatigue in general has been an increasing concern for the marine industry over the last 20 years. If one considers both steel marine fatigue and fatigue of aluminium aircraft structures in addition to fatigue of aluminium marine structures, the volume of research output of the last half century is truly astounding.

The aim of this chapter is to review the current situation in fatigue design for marine HSV applications, construct an aluminium-specific fatigue reliability method using the hot-spot stress approach, and analyze the accuracy and suitability of new the approach. The origins of this work are in the European Union 5th Framework research project Safety at Speed(S@S), which constructed a linked risk-cost model for the preliminary design of high-speed passenger vessels. Fatigue was identified as a significant component of the risk-cost relationship for these vessels, and the author constructed a reliability-based fatigue method for use in this project. The current study presented here builds upon this initial reliability method with further investigations into alternative reliability formulations and an investigation into the method's accuracy. Some of the work presented in this chapter has

been previously reported in Safety at Speed deliverable 3.2.4 [165] and in a paper to be published in the *Journal of Ship Research*[166]. After an overview of the fundamentals of existing fatigue approaches in Section 4.2, the current situation is presented in the literature review in Section 4.3 below. From the results of this literature review, the hot-spot S-N approach was selected as the most promising approach for a reliability method, the development of a new reliability method using this method is discussed in Section 4.4. The new method is applied to the 150m reference vessel from Chapter 2 and civil engineering design codes in Section 4.5, this section also contains an investigation into the accuracy of first-order reliability(FOR) methods in evaluating the proposed limit state equations.

4.2 Overview of S-N Approach

The current state of the applied art in marine fatigue strength predictions is the S-N, or stress-life approach, which has been selected for study in this chapter. The fundamentals of the S-N approach are briefly reviewed below. In the S-N approach, the fatigue life of a certain material or specific detail is determined in the laboratory, by applying a cyclically-varying load of constant amplitude to a specimen and recording the number of loads cycles until a crack of several centimetres in length appears. The number of applied cycles is the fatigue life or strength at that tested load level. When the results of several such experiments at different load levels are plotted on log-log axis of applied stress vs. cycles to failure, a S-N diagram results, as shown in Figure 45. In such a plot, the line representing the number cycles to failure normally appears linear, or piecewise linear.

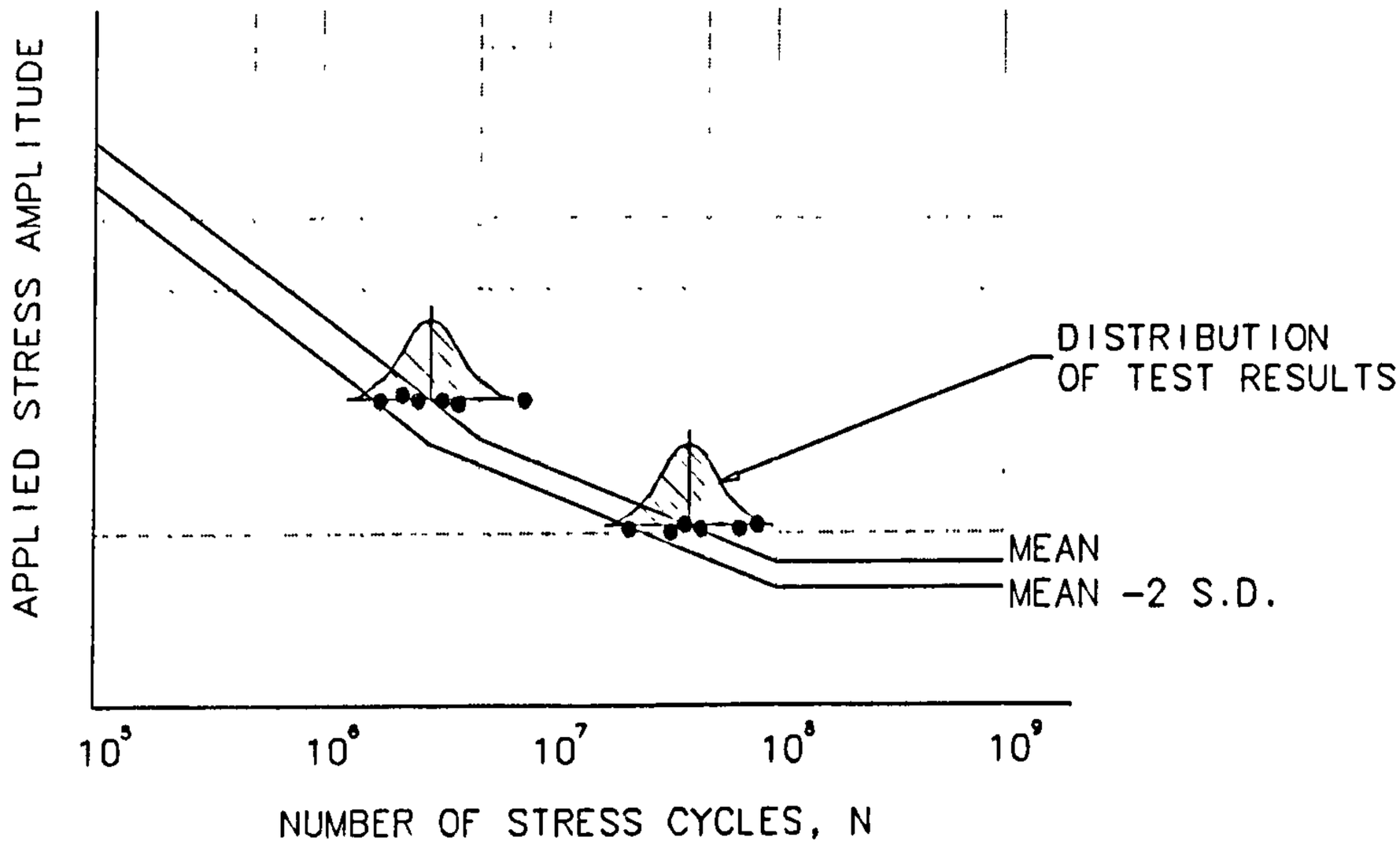

Figure 45--Typical S-N Curve Showing Mean and Design Lines

Often, several test specimens are tested at the same stress amplitude, and fail at different numbers of cycles. These test points can be used to form a probability distribution of cycles to failure at a certain stress level. These distributions are also shown, superimposed on the S-N curve in Figure 45. As the number of cycles to failure can vary greatly for a fixed stress amplitude, for design purposes, a S-N curve is typically plotted some distance off the mean values, for example a curve connecting the mean number of cycles of failure minus two standard deviations. This results in a curve where roughly 95% of specimens will survive to the number of cycles indicated. An overview of the statistical interpretation of S-N test results and S-N curves is given in Huther[167]. Within each linear portion of the S-N curve, the equation of the S-N line can be expressed as:

$$N = A(\Delta\sigma)^{-m}$$

or

$$\log(N) = \log(A) - m\log(\Delta\sigma)$$

Where :

N : Number of cycles to failure

A : Constant for S - N curve

m : Slope parameter

$\Delta\sigma$: Stress range

Equation 49

In many structures, including high-speed craft structures, the applied loading varies in amplitude cycle-to-cycle, a situation know as variable amplitude fatigue. To calculate the damage under this type of loading, researchers have developed cumulative damage rules. The most widely employed rule is the Miner-Palmgren Rule[85, 168]. In this rule, the damage is assumed to accumulate linearly. For example, if a specimen which can withstand 5×10^7 cycles at a certain stress level before failure is subjected to 3×10^7 cycles at that stress level, it is assumed to have used 3/5 or 60% of its fatigue life. Failure is assumed to occur when 100% of a specimen's fatigue life has been utilized. Expressing this failure criteria as a function:

$$D = \sum_{i=1}^{k} \frac{n_i}{N_i}$$

Where :

D : Cumulative fatigue damage, failure when D = 1

k : Number of blocks in the stress spectrum

n_i : Number of cycles in the ith stress block

N_i : Number of cycles to failure at the constant stress range of the ith stress block

Equation 50

This summation can be quickly applied if the load history can be expressed as a histogram of number of cycles vs. stress level. The assumption that the order in which the cycles are applied to the specimen will have no effect on the accumulation of damage is inherent in this methodology. Many authors have shown that this is not the case[168, 169], additionally, experimental results have shown that failure does not always occur when the summation reaches unity. However, more advanced cumulative damage rules have not yielded large enough improvements in accuracy and general applicability to offset their increased computational complexity. The S-N approach with the Miner-Palmgren damage rule is widely used for engineering fatigue life predictions. Versions of the S-N approach are employed by the major classification societies, including ABS, DNV, and Lloyds Register in their classification rules for ships, and several authors have used this approach in the analysis of aluminium high-speed craft[95, 170].

When applying the stress life approach to ship structural details, one has to choose between several different types of stress analysis and corresponding S-N curves. While all of these methods assume that fatigue cracks will start in the high-stress region of structural details, these analysis methods differ in where the defining stress range in the structure is calculated. To date, three main methods have been proposed:

1. **Nominal Stress Method:** In this method, the nominal stress in the region of the detail is calculated without including any stress concentration factor(SCF) caused by the detail itself. For example, in investigating a longitudinal bracket connection in a large vessel, the nominal stress would be the stress from global hull-girder bending, secondary panel stresses, and tertiary plate stresses, if applicable. Global SCFs, from sources such as hatch openings etc., would be included. The resulting stress range would be evaluated with a S-N curve developed by testing an identical longitudinal bracket connection in a laboratory. This method has several advantages, first, determining the nominal stress range is usually straightforward, and can be done with elastic theory, or coarse finite-element models. Second, the exact detail stress concentration factor, residual welding stress, and construction misalignment are built into the S-N curve, as an actual bracket connection has been tested. However, this method also has several drawbacks. Ideally, an exact copy of each of detail should be tested to generate a S-N curve. This is not economically feasible, so a range of reference details have been tested, and designers pick the closest detail to their detail for the fatigue analysis. It is not always possible to a get a perfect match in such an approach, and this introduces uncertainty in the analysis. Additionally, the

nominal stress approach cannot easily account for different fabrication quality in different shipyards, as these effects are implicitly incorporated into the S-N curve.

2. **Hot-Spot Stress Method:** In this method, the stress range is calculated at the toe of the weld in the detail being investigated, including the SCF from the structure of the detail, but not the SCF from the weld profile itself. This stress range is then compared to a base S-N curve for welded connections. This has the advantage that once S-N curves for typical welds are established, an infinite number of welded details can be investigated. Effects such as construction tolerances can also be investigated. Residual stresses from the welding may still be incorporated in the S-N curve, depending the fabrication procedure used to construct the test sample. The disadvantage of this approach is that the structural analysis is now much more complex. For most details, a fine-mesh finite-element approach is required, and because of the high stress gradient in most details, some sort of extrapolation procedure must be used to define the hot-spot stress. This extrapolation is sensitive to the element sizes used in the finite element model and the modelling technique. Many authors have investigated this extrapolation procedure, and several classification societies have developed guidelines for this type of analysis. For more information, see ABS[171] or Tveiten and Moan[172].

3. **Notch Stress Method:** This method is an extension of the hot-spot method, to include both the stress concentration factor of the detail, and of the weld profile itself. This allows a single S-N curve to be used for all welded joints in the same environment. This approach has been proposed by the classification societies Det Norske Veritas(DNV) and Bureau Veritas[85]. Ideally, this would allow both residual stress and the weld profile(with inherent variability) to be explicitly included in the analysis. However, there is still considerable uncertainty around each of these parameters which can make the applications of the notch stress approach difficult in practical applications. When these factors are unknown, DNV suggests default values which basically reduce the notch-stress approach to a hot-spot approach[85].

The S-N approach with the Miner-Palmgren damage rule is widely used in industry and it is logical to use it as the basis of a new reliability method. As can be seen, all three stress analysis techniques are currently in use, and the decision of which one to use will be made after the literature review, which is presented next.

4.3 Literature Review

To determine the current state-of-the-art for aluminium fatigue in the marine industry, a literature review was carried out. The shear volume of fatigue literature made it impossible to review every article published, this is especially true as many of the aluminium fatigue approaches are derived from steel fatigue approaches which have their own body of literature. In presenting this review, a decision was made to focus upon significant historical papers to show the development of the fatigue approaches in aluminium or steel, and recent aluminium-HSV specific papers to show the current situation in marine aluminium fatigue. Papers dealing with springing, whipping, and slamming effects on fatigue were included as well. To prevent repetition with the following chapter, work which mainly focuses on fracture mechanics approaches is excluded here. A short list of relevant design codes is also presented at the end of the review. In addition to the works reviewed below, several excellent review articles and reference books have been published in recent years. Fricke[173] gives an excellent overview of the current approaches for welded joints in the marine industry, while Maddox[174] focuses on current fatigue approaches for aluminium. For general fatigue reference, Stephens et al.[169] *Metal Fatigue in Engineering* is an outstanding reference book, along with Barsom and Rolfe's[175] *Fracture and Fatigue Control in Structures: Application of Fracture Mechanics* which focuses on the fatigue problem for engineering structures, including marine examples. For aluminium, Sharp et al.[176] *Fatigue Design of Aluminum Components and Structures* presents a wealth of aluminium data and experience along with the general principles of fatigue design, though it is not marine-focused.

Fatigue has been known as a specific failure mechanism for over 150 years. Some of the earliest engineering investigations into fatigue took place in the 1850s and 1860s, when August Wöhler studied fatigue failures in railway car axels[169]. In the years since then, both fatigue and fracture (the failure of engineering materials by uncontrolled crack propagation) have received extensive engineering study. In the marine industry, the rapid adoption of all-welded construction lead to several notorious failures of ships by fracture from crack-like defects. These fracture problems began appearing in the World War Two Victory ships and similar types. While improved material selection and detail design reduce the instances of catastrophic fracture, fatigue cracking began to emerge as one of the dominate structural design problems for large ships in second half of the 20th century. This increase in fatigue problems was driven in part by the growth in ship size, and the corresponding increase in cyclical global wave loading. Additionally, the increasing use of

higher-strength steels, with the corresponding increase in the stress range allowed(at least initially) by classification societies contributed to the increase in fatigue cracking.

By the 1970's fatigue problems were widespread in large steel commercial ships. At this time, approximately 70% of the structural damage in large ships (>200m in length) was fatigue related[79]. In response to this growing problem the Ship Structures Committee (SSC) commissioned a series of investigations into fatigue. The resulting reports were a major milestone in terms of both understanding and responding to the fatigue problem in the marine industry, and the general approaches and methodologies proposed still form the basis of several classification societies fatigue approaches. While the work focused on steel ships, the principles can be applied to aluminium as well. This work started with an extensive survey of ship structural details and fatigue cracks. Structural inspections took place on 86 ships, examining about 600,000 details and recording 6,856 failures[79]. The details were classified into a catalogue, by function and then construction style of the details. The results of these surveys were presented by Jordan and Cochran in two SSC reports, SSC-272[177] and SSC-294[178].

Following on these two reports, SSC-318[79] developed a fatigue design methodology. This report linked the different structural details classified by Jordan and Cochran to existing civil-engineering fatigue test data of similar structures. This provide a practical method for estimating the fatigue strength of a structural detail at the design stage without resorting to expensive testing. The study then presented a methodology to determine ship loading histories, examining the in-service measurement made on several merchant ships in the 60's and 70's. This resulted in the hypothesis that the Weibull distribution is a suitable approximation for the long-term fatigue loading of a ship's hull girder. Additionally, an in-depth investigation was conducted of the probabilistic nature of both fatigue strength assessments and fatigue loading, resulting in a design process which explicitly accounts for the uncertainty in the procedure, and allowing the designer to adjust for the degree of certainty required. This model was based on the assumption that the fatigue life of a structural detail could also be modelled by the Weibull distribution, this assumption allows the contribution of various source of uncertainty to be consider and a probability of failure estimated via a closed-form expression without using a more complex reliability approach such as FOR or Monte Carlo simulation. Finally, a simple design procedure is established, where the allowable once-per-lifetime stress range (corresponding to a loading with a probability of exceedence of 10^{-8}) can be determined for each fatigue detail, and then compared to the predicted hull girder stress under this loading to determine if the detail's fatigue strength is sufficient.

A contemporary approach to that taken by SSC-318 is the lognormal format, which was developed for offshore structures by API and presented by Wirsching[179]. In this approach a closed-form expression is developed for the safety index, β, by assuming the stochastic properties of fatigue life can be represented assigning the S-N curve constant A, the Miner-Palmgren damage summation Δ, and a stress modelling bias time, B, lognormal distributions. All other variables are assumed to be constant. With this approach, the safety index for any desired lifespan can be found directly:

$$\beta = \frac{\ln\left(\frac{\tilde{T}}{T}\right)}{\sigma_{\ln T}}$$

Where :

T : Desired life

$\tilde{T}$: Median life

$$\tilde{T} = \frac{\tilde{\Delta}\,\tilde{A}}{\tilde{B}^{m} f_0 E\left(S^m\right)} \qquad \textit{Equation 51}$$

$$\sigma_{\ln T} = \sqrt{\ln\left(\left(1+C_\Delta^2\right)\left(1+C_A^2\right)\left(1+C_B^2\right)^m\right)}$$

$\tilde{A}, C_A$: Median and COV of S - N intercept

$\tilde{\Delta}, C_\Delta$: Median and COV of Miner damage sum

$\tilde{B}, C_B$: Median and COV of stress modelling error

m : Slope parameter

$E\left(S^m\right)$: Expected mth moment of stress range

f_0 : Average frequency of stress history

While this model trades in some flexibility of by requiring lognormal distributions for the stochastic model and allowing only three stochastic variables, it has the advantage that the safety index can be determined directly from a closed-form equation. Additionally, Wirsching notes that the lognormal distribution is a good fit for the S-N data in the study of offshore structures. Jensen and Mansour[99] have adopted this model in a recent study of the response of FPSOs.

Fatigue and fracture concerns for aluminium were also moving into the marine environment during this time; though this was initially for liquefied natural gas (LNG) tanks, not high-speed vessels. Aluminium was a natural choice for these tanks, as aluminium has excellent material properties at the cryogenic temperatures required to liquefy natural gas. Several experimental and design studies were made into the fatigue and fracture properties of these tanks, including both spherical and the IMO type-B prismatic

tanks during this time[180-185]. While these references provide valuable material data and an early discussion of the fatigue problems for marine aluminium, the design and experimental methodologies employed do not seem to have been significantly extended into aluminium high-speed vessels. This is most likely as a result of the higher material, workmanship, and inspection standards employed in such tanks, and the higher level of design effort available for such project. This can make these approach un-economic for a typical HSV project.

During the same time period the U.S. Navy was also interested in aluminium for a naval combatants. In the 1970s, several material test programs were conducted on a un-welded aluminium and welded aluminium[186, 187]. The U.S. Navy went as far as to construct a 1/3 scale test model of a 300 ft aluminium destroyer (ASEM) which was tested under both static loads and fatigue loads for comparison to theoretical and scale-model predictions. Unfortunately, little of this program was published in open literature. Pohler, Stavovy et al [164] presents an overview of the program, while Birmingham, Marchica et al. [188] presents the development of the lifetime load distribution for the 1/3 scale test vessel, including horizontal and vertical bending, and the slamming-induced hull girder whipping contribution to the bending moment. An overview of the static test results is presented in Johnson and Beach [189] , which also contains partial references to the cyclical test results and "application guide" reports. However, the neither of the later appear on any of the Navy's publicly searchable databases.

One of the hardest steps in marine fatigue calculations is determining the long-term loading on the detail in question. The lifetime load distribution proposed by Birmingham, Marchica et al. [188] for the ASEM tests was further developed and extended for SWATH and Monohull vessels by Sikora, Dinsenbacher et al. [92]. The monohull calculation procedure presented allows the lifetime vertical bending moment spectrum to be developed from the overall dimensions of the vessel. The monohulls used in this study were largely destroyer-type naval ships, with the Mariner hullform, SL-7 hullform, and the hullform of one larger naval combatant also included. As such, most of the vessels investigated were fairly high-speed, making the results of interest to the current study. An operational profile and wave height probabilities are developed for the North Atlantic, including the effects of changing course or reducing speed in higher sea states. The Ochi 6-Parameter wave spectrum is used to represent the sea environment. A regression-based vertical-bending-moment RAO, non-dimensionalized by principle dimensions, is presented. This RAO was developed from model tests of several vessels by the U.S. Navy. With the RAO, operational profile, wave height probabilities, and Ochi spectrum, the lifetime vertical bending moment

spectrum from cyclical wave loads can be determined following an approach similar to that outlined in Chapter 2. To this spectrum, slamming and the resulting whipping cycles are added by empirical formulations derived from sea-test data. Phase effects and the log decrement of whipping cycles are also estimated from sea-trial data. The resulting lifetime vertical bending moment calculation can be used in fatigue damage calculations such as Miner's rule. Fatigue from secondary and tertiary loading is not examined. The methodology is extended for side force in SWATH hulls in the second half of the paper.

Sikora and Beach [93] further extended the approach of Birmingham, Marchica et al. [188] and Sikora, Dinsenbacher et al. [92], however, most of the new work presented in this paper is for conventional slow commercial vessels. The vertical-bending moment RAO first proposed in Sikora, Dinsenbacher [92] is verified against three slow, non-slender vessels, and good agreement is found. Operation profiles are added for slow commercial vessels, and wave height probabilities are extended to include the Pacific and the combined Atlantic, Mediterranean, and Caribbean Oceans, as well as the North Atlantic. Some of the regression formulas proposed in the original article are simplified, and new example calculations are presented for six vessels. The calculation procedure is explained in greater depth in this paper, which is valuable if the calculation procedure is to be re-created. The same basic methodology has been further refined and published in the last decade[94, 96] especially in regard to the non-linear effects.

Wirsching and Chen[190] published a summary of marine probability-based fatigue design approaches in 1988, further extending the work of SSC-318 and Wirsching[179]. While the examples presented and most of the references refer to offshore structures, the methods are also applicable to ships, and the design methodology presented by Munse in SSC-318 above was one of the methodologies reviewed. The paper reviews the basics of fatigue, including the S-N curve, and briefly touches on casting fracture-mechanics in a S-N format. Expressions for fatigue damage by Miner's rule under variable amplitude loading are developed. These expression are based on expected values, and the Weibull distribution of loads is examined further. Expressions are also developed for bi-linear S-N curves in terms of expected values.

Wirsching and Chen then present two different fatigue reliability models, the first is the Munse model from SSC-318, where the number of cycles to failure is assumed to be Weibull-distributed, and the key variable is p_f, the probability of failure. Then, the Wirsching/API model is reviewed, where the cycles-to-failure are assumed to be log-normally distributed, and the key variable is β, the safety index. After the two basic models are reviewed, numeric values for covariance and bias are presented from a variety of

sources(mainly offshore on onshore civil engineering). Values are given for S-N curves, stress analysis, and fatigue strength(material/joint capacity). Two design examples are given, the first is the extreme stress limit state for fatigue based on the design loading. This is the Munse approached discussed above. The second is an expression of the target damage sum from Miner's rule in term of beta, the safety index. A brief overview of the process of extending these relations from the single component to an overall system of components is also presented. Wirsching and Chen present and example of a simplified TLP tendon to demonstrate this concept.

Interest in aluminium HSVs and their fatigue problems started to increase in the 1990s, and several papers appeared on the fatigue aspects of these vessels. Allday [47] summarized the current situation with respect to fatigue, and gave practical design and construction advice for improving detail quality, and hence the detail fatigue life. In the September issue of Ship and Boat International, two overview-style articles appeared on fatigue, from Adley[48], and May and Baltrop[191]. In addition to reviewing the fundamentals of fatigue from a stress-life perspective, Adley provided data on how construction aids, such as lifting pad-eyes and tabs effected the fatigue life of ship structure. May and Baltrop also reviewed the fundamentals of fatigue, and commented that the lightweight structures of high-speed craft are inherently prone to fatigue damage, as the use of closely-spaced longitudinals increases the number of brackets and connections used, each of which is a fatigue hot-spot.

Olkinuora, Knuuttila et. al [192] presented an overview of the structural design process for a Finnish 40m aluminium high-speed missile boat at the first FAST conference in 1991. For this vessel, fatigue life and whipping stresses are the most restrictive structural design criteria. Olkinuora, Knuuttila et. al developed a computer-based design approach for the vessel. A non-linear time-domain strip theory was used to predict structural loading in 2m, 3m, and 4.5m head seas. Full-scale fatigue life tests were performed on structural details, including deck and bottom structure, and Olkinuora, Knuuttila et. al compared the resulting experimental fatigue life to the stress history predicted by the strip theory to ensure adequate fatigue life for the vessel. The results of a 2-day sea trial are also presented. This paper gives an excellent overview of the process employed, however, only limited results are presented. References are made technical reports which contain the calculations and further results, though some are in Finnish or confidential.

Interest in hydro-elasticity for HSVs and the related slamming, whipping and ringing effects lead to several papers in the mid 1990s. Talvia and Wiefelsputt [193] discussed recent research in slamming and springing loadings on high-speed monohulls, including 1:5 scale

model tests and a new design method for predicting the hull-girder natural frequency. Hermundstad, Wu et al. [194] investigated the importance of hydro-elasticity when calculating the global response of a high-speed monohull constructed out of steel. Calculations are made for several different hull girder frequencies, speeds, and structural damping values, however only head seas were considered. Hydro-elastic effects are accounted for by a hydro-elastic extension of 'high-speed' or 2 ½-D strip theory originally developed by Faltinsen and Zhao [195] The study demonstrates that hydro-elasticity will result in a different distribution of vertical bending moment, one with an increased standard deviation. For an operating environment off Japan, the increase is in the order of 5%-30%.

Friis-Hansen, Jensen, et al. [87, 89] also investigated the slamming and whipping loads on high-speed craft. The authors first examined methods to predict the dynamic characteristics of a monohull. Empirical formulas are developed to quickly estimate the lowest natural frequency of a high-speed monohull constructed out of Steel, Aluminium, and GRP. The authors examining spring first, employing an version of the quadratic strip theory originally developed by Jensen and Pedersen [196] and extended to include hydro-elastic effects by Jensen and Dogliani [197].

The springing analysis demonstrates that account for non-linear wave loads and hydro-elastic response significantly increases the lifetime fatigue damage up to one order of magnitude larger. Interestingly, the difference between the fatigue damage calculated for the hydro-elastic GRP, Aluminium, and Steel hulls is not large. However, the difference between any of the hydro-elastic hulls and the rigid hull is significant. Including non-linear wave loads causes a larger increase in fatigue damage for the 50m than for the 100m hull. The authors conducted a slamming study, using Friis Hansen's [198, 199] procedure for calculating the fatigue damage from slamming and whipping. While including slamming did increase the extreme values of bending moment, the effect of including slamming on fatigue damage was inconclusive. In some operating conditions, almost no increase in fatigue damage was observed, while in other conditions a significant increase was observed. As with springing, slamming loads increased the fatigue damage for the 50m hull more than for the 100m hull.

A major state-of-the-art summary work appeared in 1995 in the form of a Ship Structures Committee design guide for fatigue analysis.[85] This guide was designed to synthesize the state-of-the art fatigue analysis data for large steel commercial ships, and presented a recommended analysis method. The guide follows a three-level approach to fatigue, with the complexity of the analysis increasing from level one to level three. Level one consists of a catalogue recommended fatigue details with relative cost and fatigue

performance trade offs listed for a wide variety of details and ship types. In a level one approach, the designer simply selects an appropriate detail from the catalogue.

The level two and three approach are analysis methods for specific details. Both follow the same four-step process:

1: Establishment of long-term cyclical load distribution for the ship's lifetime

2: Determination of the corresponding long-term stress range distribution at the detail of interest.

3: Calculate the total fatigue damage

4: Estimate the reliability of the results

The methods differ in the level of analysis. The level two approach uses classification society rules for loading which are assumed to follow pre-determined statistical distributions, simplified closed-form equations and tabulated stress concentration factors to determine the stress range, and then the Miner's rule for fatigue damage. The level three approach follows the same outline with a higher level of analysis. Level three determines the loading by generating an operational profile for the vessel, listing the probability of encountering certain heading, speed, wave height and wave period combinations. A seakeeping analysis is then performed on each combination to determine short-term loading distributions, and the long-term loading distribution is then assembled from the short-term distributions. The loads are mapped to stresses by a transfer function that is determined by global and local FE analysis. Miner's rule is again used for damage accumulation. A brief overview of reliability is given. The level three approach represents what has become known as the "spectral" approach to fatigue predictions, and it has been used by most major classification societies. The section explaining levels two and three is quite detailed, and contains useful information on the selection of S-N curves and the comparison between various curves.

The report also includes three worked examples, one for level two and two for level three. Agreement between the different levels is questionable, and is not commented on in the report. An overview and comparison of classification society rules in presented in an appendix.

A second major fatigue work was produced by the SSC about the same time. While not focused on high-speed craft, a comprehensive overview of fatigue on large steel commercial vessels(primarily tankers) was published as part of the larger Ship Maintenance Project coordinated by the University of California Berkley. The full details of this study were published in two series of Ship Structure Committee Reports (SSC-386 and SSC-395), while Xu[200] gives an overview of the fatigue aspects of the project, which include S-N

curve fatigue prediction, fatigue reliability and inspections, and crack-growth estimation techniques. As tankers have grown in size, their flexibility has increased, in turn increasing the spectral bandwidth of the relevant fatigue loads, and wide-banded fatigue damage formulas were developed as part of this study. Extensive work on load-shedding around cracks was also performed, this is reviewed in the following chapter on fracture mechanics approaches.

Frediksen[201] gives an excellent overview of the fatigue problems in HSVs as part of the FAST 1997 conference. Fatigue failures were largely caused by a combination of high-cycle local loading and poor design/craftsmanship, occurring largely in the engine room or near other machinery. However, sharp corners in superstructure windows and in web frames were also identified as causing cracks, and global fatigue cracking is expected to increase as ship length increases. Four main contributing factors were identified, stress range, detail design, workmanship, and corrosion. A brief review of fatigue approach in the aircraft and offshore industry is also given, along with general design philosophy recommendations. The need for more aluminium S-N curves is also mentioned.

Violette et. al[170] presented an overview of fatigue for aluminium structures and a first-principles fatigue design approach at the Third International Forum on Aluminum Ships. The research work presented is part of Lloyds Registers' efforts to develop a fatigue design procedure for high-speed craft. A spectral approach for determining fatigue damage is proposed, using structural influence coefficients to construct the structural RAO. Structural influence coefficients relate the stress caused at a point of interest to the application of a unit force at a particular(localized) location on the hull girder. Approximately 1000-3000 structural influence coefficients are needed to define a typical hull adequately. The overall structural response to a given loading can be determined by the addition and scaling of the set individual structural influence coefficients for the hull. With the RAO, the response spectrum to a particular sea state can be determined, and expressions are developed to calculate the cumulative fatigue damage under Miner's rule, assuming the stress distribution follows the Rayleigh distribution in the short term. Corrections are made for the non-narrow banded processes, and the uncertainty in the analysis. Equations are developed to calculate the total fatigue damage for a given service life, accounting for the speeds and sea states encountered on a specific route. Violette also described the methods used by Lloyds to implement the calculation presented above. A sensitivity study is also conducted for a sample vessel, comparing the effects of route and speed have on cumulative fatigue damage for a fixed lifespan. Strong sensitivity is seen to both route selection and

operating speed, as well as number of stress cycles, implying that these variables need to be determined accurately.

Heggelund et al. [95] presented a methodology for fatigue life analysis at the Third International Forum on Aluminum Ships. The paper also included an example study on a 120m high-speed aluminium catamaran discussed in Chapter 2. The paper gives a brief review of fatigue loads and properties, and then concentrates on developing a methodology to determine the global load response for high-speed craft. The response spectrum is developed from a high-speed 2-D strip theory program, VERES. A modified version of this program is employed that accounts for the hydro-elasticity and resulting dynamic amplification of the structural response through an eigenmode analysis. The probability distribution of the response is investigated next, including a methodology for estimating the long-term distribution and Weibull parameters from calculated short-term response in specific sea-states. A brief overview of fatigue and Miner's rule is presented, with a detailed description of the notch (hot-spot) stress approach, as implemented by DNV. A formula is given to relate the cumulative fatigue damage to the parameters of the Weibull distribution and the number of cycles.

A case study is then made of a 120m catamaran. A rough global structural analysis is performed to get the eigenmodes, which are used to develop the structural response spectrum with the VERES code. Local structural models are made of two connection details to determine the stress concentration factors required to implement the notch stress approach. A fatigue limit state expression was developed for the details, and the Weibull parameters were estimated and cumulative damage calculated as described above. It was found that the cumulative damage was far in excess of unity, indicating that the operating sea states were too severe. It was found that the Weibull distribution had trouble matching the data, and a 13% variation in cumulative damage and Weibull parameters existed depending on how the Weibull parameters were estimated. The fatigue limit state was then calculated for butt welds and simple fillet welds typical of plate-to-plate and stiffener-to-plate joints. The effects of corrosion and fatigue limits were discussed. The fatigue limit states developed for the connections and the welds were then compared to estimated ultimate strength limit states. The ultimate strength limit state estimation was fairly crude, consisting of the yield stress multiplied by an empirical factor. It was found that the fatigue limit state was more restrictive in stress levels than the ultimate limit state was for the connection details. For the weld details, the fatigue limit state was about equal to the ultimate limit state. This indicates the fatigue will be the governing limit state for connections, and can be for the welds in the global hull structure. Finally, cumulative fatigue

damage was plotted vs. a significant wave height restriction to determine when the cumulative fatigue damage was less than one.

Tveiten and Moan presented further work on modelling the detail local stress distribution and fatigue life of typical aluminium ship details at the FAST 1999 conference[172]. Two primary structure types were investigated, a transverse fillet weld on an axial-load carrying member, and a longitudinal/floor connection. The procedure including both FEA modelling and physical testing of scale and full-size models. The paper investigated the various approaches to FEA modelling of fatigue stress hot spots, including the element type used and the extrapolation method used to predict the peak stress in the structure. A new extrapolation procedure based on using a singularity is presented and compared to currently used procedures. Comparison between the results of the study and established S-N curves is also made, with generally good agreement. Variable loading was also investigated, but the results did not compare well with previous studies, and more work is recommended.

At FAST 1999, Skjelby et al. [202] presented an overall procedure for calculating the fatigue performance of high-speed craft. The proposed methodology uses a stress-transfer function approach coupled with a stochastic analysis, similar to techniques used in the offshore industry. First, a transfer function is determined through a linked hydrodynamic and FEA model of the vessel. The pressure distribution over the hull is determined for unit waves at a variety of heading and speeds. Each of these load cases is applied to the FEA model, and the resulting stresses are the points of interest for fatigue are determined. The FEA model can be detailed enough to calculate the local stresses, or stress concentration factors can be used. When a sufficient number of headings and conditions are completed, a transfer function is assembled. Then, a wave scatter diagram and wave spectrums are determined for the operational area. When these are combined with the transfer function, a response spectrum is developed, which can then be analyzed for fatigue damage by Miner's rule. Unfortunately, no sample calculations or comparisons are presented.

The influence of non-linear hydrodynamic loading on the fatigue life of high speed craft was investigated by Donovan and Humphrey[203] This paper reviews the current state of the fatigue problem in high speed craft, before examining the effects of hydrodynamic non-linearities on the calculated fatigue life. A fatigue calculation is made for a typical high-speed craft by the current linear techniques developed for conventional vessels. This calculation is made for three European ferry routes. The fatigue damage for each route it broken down by sea-states, and it is demonstrated that a large portion of the fatigue damage calculated occurs in higher sea-states. Then, the results of a comparison of hydrodynamic

motions and loads predicted by linear and non-linear methods is presented. It is shown that the non-linear motions and loads predictions differ significantly from the linear predictions, and that the hull girder bending moment can be considerably higher. The authors review the procedure required to complete a fatigue analysis using non-linear hydrodynamic tools, concluding that the calculation time required is too long for practical applications. Two possible methods of simplifying the analysis are discussed, though no results or actual calculations are performed.

As the number, size, and speed of high-speed aluminium vessels increased, along with the fatigue problems, the Ship Structures Committee commissioned an investigation into the fatigue problem, which was summarized in SSC-410[86]. This report is a valuable state-of-the-art document for high-speed vessel fatigue problems, dealing with all aspects of the problem, including loading, fatigue strength, existing design codes, and recommendations for design. The investigation presented in this report is extensive, and address the fatigue approach of several different industries, including the civil engineering industry and the railway industry. Additionally, the report highlights areas, such as secondary loading and loading non-linearities, where practical design methods and design data are still lacking.

Polezhaeva and Malinowski[204] presented Lloyd's Register's work on determining the stress-life characteristics of typical aluminium structural details at FAST 2001. This paper presents the results of both full-scale and FEA model fatigue tests on three different common aluminium HSC structural details, a transverse fillet weld on an axial load-bearing member, a floor-frame intersect with a bracket, and a longitudinal-transverse connection made by welding the flange of the longitudinal to the top of the cut-out in the transverse floor. Physical tests were performed on all of the details. In the floor/frame connection, cracks were seen in all weld (bracket-floor and floor-frame), also surface cracks started at the bracket edge in the transition region of the soft-toe bracket. Some of these migrated to the weld, while others propagated through the bracket itself. For the longitudinal-transverse connection, cracks started in the weld, and a noticeable improvement was seen when the weld did not extend all the way to the flange edge on the longitudinal edge. This result agrees well with the data Adley presented in 1983 (Adley, 1983). FEA models were also constructed, largely using shell elements. Good agreement was observed between the physical tests and the FEA models.

A significant comparison study for steel fatigue for ships was carried out by the ISSC in 2000[205]. The study compared several different classification society fatigue life predictions and one direct calculation of fatigue life for a welded hatch landing pad on the

coaming of a container ship. The results were discouraging, with fatigue life predictions of the class societies varying from 1.8 years to over 20 years. The direct calculation approach gave a fatigue life of 5.3 years, which was also disappointing, as the detail was viewed as very good from experience, with a much longer fatigue life than 5 years. Differences were seen between the approaches in all aspects of the fatigue life, including loads, stress determination, and S-N curves. The conclusion was that the current state-of-the-art in fatigue life prediction is not satisfactory.

In addition to the mechanics of fatigue presented above, the use of reliability techniques for fatigue problems has also become a topic of research of late. There have been several attempts to develop new deterministic S-N fatigue design codes from reliability-based models of fatigue strength, using the partial safety factors approach as discussed in Chapter 2. Assakkaf et al.[74] and Ayyub et al.[40] detail the development of a partial-safety factors fatigue design approach for the U.S. Navy as part of a wider program of introducing reliability and risk-based design standards for naval construction. Folsø et al.[206] detail a similar effort for commercial ship classification rules, including a study of existing design to determine the safety margin in existing classification rules. Two sets of partial safety factors are derived, with a smaller margin of safety imposed on designs which have had a higher level of analysis.

Much of the research output has been developed into design codes for fatigue, with both marine classification societies and aluminium civil engineering codes now including fatigue checks. For the design of new structures, these codes use the S-N approach for evaluating fatigue. In the marine world, the classification societies have developed a fairly uniform structure in their approach to fatigue, though their predictions may not agree in final magnitude. Typically, fatigue is checked by computing the long-term stress range for many fatigue-critical locations throughout the vessel. The fatigue resistance of each location is specified, and a simple pass-fail criteria based on the Miner-Palmgren sum. Most societies have multiple levels of analysis, starting off with simple empirical formulations for the long-term loading, stress determination from simple elastic theory, and determining the S-N curve by picking a "closest match" detail from a catalogue of standard details. For cases where fatigue is critical, or the structural arrangement unusual, most societies also have a standardized advanced method where a spectral load approach is used, as discussed in Chapter 2, and typically the stress determination uses a hot-spot or notch-stress approach based on global and local finite element models of the vessel's structure. Relevant examples of these types of approaches can be found in the ABS Steel Vessel Rule[171], DNV Classification Note 30.7[98], or the new JTP Tanker Rules[23]. A similar approach has been

taken with the civil engineering design codes that cover aluminium structures. One of the first large proposed designed standards, covering joints in both aluminium and steel, with fatigue strength, defect acceptance criteria and other analysis techniques was published by the International Institute of Welding (IIW) in 1996[207]. In Europe, the Eurocode 9[60] features standard nominal-stress S-N curves for many configurations of plain material, welded joints, bolted connections, and adhesively bonded joints. Additionally, a hot-spot S-N curve is given for analysis of structures whose configuration cannot be matched with the standard configurations provided. The U.S. Aluminum Association *Specification for Aluminum Structures*[53] follows a similar approach, though it has fewer categories and S-N curves to choose from, and no hot-spot S-N curve.

While over 20 years have passed since Munse et al.'s[79] landmark report on fatigue, there is still no easy solution to the problem of fatigue life prediction. During the intervening two decades, research has focused on improving fatigue strength estimates, loading estimates, and stress modelling, but there is still much more work to be done. As can be seen from the variety of methods and conclusions presented above, the fatigue problem is very complex and several distinct phenomenon need to be accounted for to obtain accurate predictions. At the moment, the agreement between the different approaches is often poor, and the continuing occurrence of fatigue cracks in ships often only a few years after they enter into service has shown that the marine industry still needs a better fatigue approach.

4.4 Development of a Reliability-Based S-N Hot-Spot Approach

Based on the review above, it is apparent that the S-N approach is currently the state-of-the-art approach for fatigue applications. Not only has it received significant research attention, it is also the current approach favoured by major classification societies in their steel vessel rules, including ABS, DNV, and Lloyd's Register. Therefore, the S-N approach was selected as the basis for a new reliability-based fatigue method. The current S-N approach was originally implemented in the Safety at Speed project as part of a risk-cost model for the structural foundering of high-speed passenger ferries[165]. While this initial implementation satisfied the requirements of the S@S project, several potential areas for future work were identified during the creation of this model. The fatigue problem is notable for both the high level of uncertainty in the material data and the highly non-linear relationship between applied loading and fatigue life. The effect of these two factors on the accuracy of the simplified reliability methods commonly employed had not been evaluated. Additionally, it was felt that further comparison studies and the investigation of alternative

limit state equations would be beneficial. The development of the original method and these additional studies are described in this section.

To build a reliability-based S-N fatigue method for aluminium ship details, the hot-spot stress approach seemed to be the best stress technique to use. It was felt that the nominal stress approach was at a disadvantage because relatively few aluminium ship-type details have been tested, thus, there would be significant uncertainty in determining which reference detail to use. However, the hot-spot stress approach has been discussed extensively in fatigue literature in general, and marine fatigue literature in particular. Partanen and Niemi[208] argue the hot-spot approach is more accurate than the nominal stress approach. Many of the published aluminium ship detail fatigue tests include hot-spot stress analysis, allowing the hot-spot stress theory to be compared with experiments. As fewer S-N curves need to be developed for the hot-spot approach, the relatively small amount of aluminium ship detail tests available is not as much of a disadvantage as it is for the nominal stress approach. The notch stress approach was also investigated, however , current uncertainties in determining the weld SCF made the notch stress approach less attractive than the hot-spot stress approach. Therefore, the hot-spot approach was selected for use in this work.

4.4.1 Selection of the Limit State Functions

The first step in developing a reliability-based fatigue model is to express the fatigue failure as a limit-state equation, or an equation which represents structural failure when the equation's output is less than zero, and structural safety when the limit state equation is greater than zero. For fatigue in the S-N approach, failure is defined as the presence of a significant crack in the structure, typically of several centimeters in length. As such, this represents a service limit state, not an ultimate limit state such as those reviewed in Chapter 3. Normally, this limit state equation will contain several random variables relating to material properties, expected loadings, and structural properties of the detail under consideration. For fatigue loadings on high-speed vessels, the limit state equation must be able to handle variable-amplitude loading, which suggests a Miner-Palmgren approach. Two previously proposed limit states have been investigated in this study. The first is an equation proposed by Jensen[78]:

$$G(\mathbf{X}) = D_{cr} - D \qquad \textit{Equation 52}$$

Where **X** is a vector of random variables, D_{cr} is the Miner-Palmgren cumulative damage index which would cause failure, and D is the damage index at any point in the

vessel's life. In this limit state, failure is taken when the G(X)≤ 0, or the calculated damage is more than the damage assumed at failure.

Jensen[78] further developed this equation for load spectrums that can be expressed by a two-parameter Weibull distribution, as this distribution has been shown to be a good fit for many vessel's long-term loadings. Using the expression for the expected moment of a Weibull distribution to represent the variable stress range acting on the detail, the following limit state equation results:

$$G(\mathbf{X}) = D_{cr} - \frac{(2\alpha_w)^m \cdot N}{A}\Gamma\left(1+\frac{m}{\beta_w}\right) \qquad \textit{Equation 53}$$

Where α_w and β_w are the Weibull distribution scale and slope parameters of the stress amplitude distribution, Γ(.) is the Gamma function, and all other variables are as defined previously. Jensen proposes that all variables except N could be treated as stochastic. The Jensen limit state function was used in the initial study on the Safety@Speed project, as tools were being developed to express the long-term loading on HSV in terms of a Weibull distribution.

The second limit state function investigated is that proposed by de Souza and Ayyub[41]. In this form of the limit state equation, the number of stress cycles that the structural detail can withstand is calculated and compared to the number of stress cycles applied in service. Additionally, the stress range can be left as a summation from the stress histogram, without fitting any probability distribution to it:

$$G(\mathbf{X}) = \frac{A \cdot D_{cr}}{k_s^m \cdot \sum_{i=1}^{n} S_i^{\,m}} - N \qquad \textit{Equation 54}$$

This limit state includes a stress uncertainty factor k_s which multiplies the cumulative stress range, S, itself a stochastic variable. All other variables are as above. Unlike Jensen's limit state, de Souza and Ayyub treat the S-N slope parameter, m, as constant. Comparing these two limit state expressions to each other, it is apparent that the only significant difference is the representation of the stress range acting on the structural detail. Otherwise, the limit states are just algebraic manipulations of each other, with Jensen's limit state measuring damage allowable vs. damage applied in service, and de Souza and Ayyub's limit state measuring cycles allowable vs. cycles applied in service. However, the accuracy of simplified reliability methods may differ when applied to these two limit states, based on their different handling of the stress range. In the de Souza and Ayyub limit, the stress range is treated as a single stochastic variable, however in the Jensen limit state uncertainties in the Weibull shape parameter, β, and the S-N curve slope will effect the equivalent stress range via the highly non-linear gamma function, possibly adding increased non-linearity to the

solution. Wirsching's approach[179] could also have been used as a limit state, it is attractive as it does not require a FOR solution, and has fewer random variables to determine from the experimental results. However, it does lack the flexibility to directly model the uncertainty in the Weibull distribution as Jensen's limit state does, or to use distributions other than the lognormal distribution, and it was not developed further in this work.

Both limit state equations require the long-term loading at the detail in question to be determined. Based on the level of analysis, this could be done in several ways while still using these two limit states. For preliminary design, the long-term loading could include global bending moments and contribution from shell pressure by classification society rules, or predictive formulas such as those discussed in Chapter 2. Alternatively, the loading could be developed from a full spectral analysis of the loading on the vessel, potentially including non-linear effects such as springing and whipping. As the focus of this chapter is on the fatigue side of the prediction, the loading used will be that discussed in Chapter 2, although the shortcomings of the current loading tools, also discussed in Chapter 2, should be born in mind.

4.4.2 Determination of the Fatigue Capacity

4.4.2.1 Review of Previous Test Programs

With the limit states set up, establishing a suitable fatigue capacity model was the next requirement. As the hot-spot stress approach has been selected, the fatigue capacity model consists of three parameters: the S-N curve constant A, the S-N curve slope parameter m, and the cumulative damage index Dcr. The associated uncertainty in each these parameters must also be determined. An extensive literature search was carried out to locate applicable design codes and published experimental fatigue tests of aluminium ship-type structural details. By comparing these sources, estimates were made for the mean fatigue capacity of aluminium structural details and the level of uncertainty in these values.

Before proceeding with the development of the fatigue capacity model, the underlying principles of the hot-spot stress procedure will be presented. This is intended as an brief review of the subject, for more information the reader is referred to the large body of literature on using the hot-spot stress analysis method for marine details[85, 173, 209]. For welded marine details, hot-spot stresses are the stresses at the detail in question arising from the structural configuration of the detail, but not from the weld itself. They are also referred to as geometric stresses or structural stresses. They differ from notch stresses, or total stresses, which include the stress-raising effect of the weld itself. This is illustrated below in Figure 46.

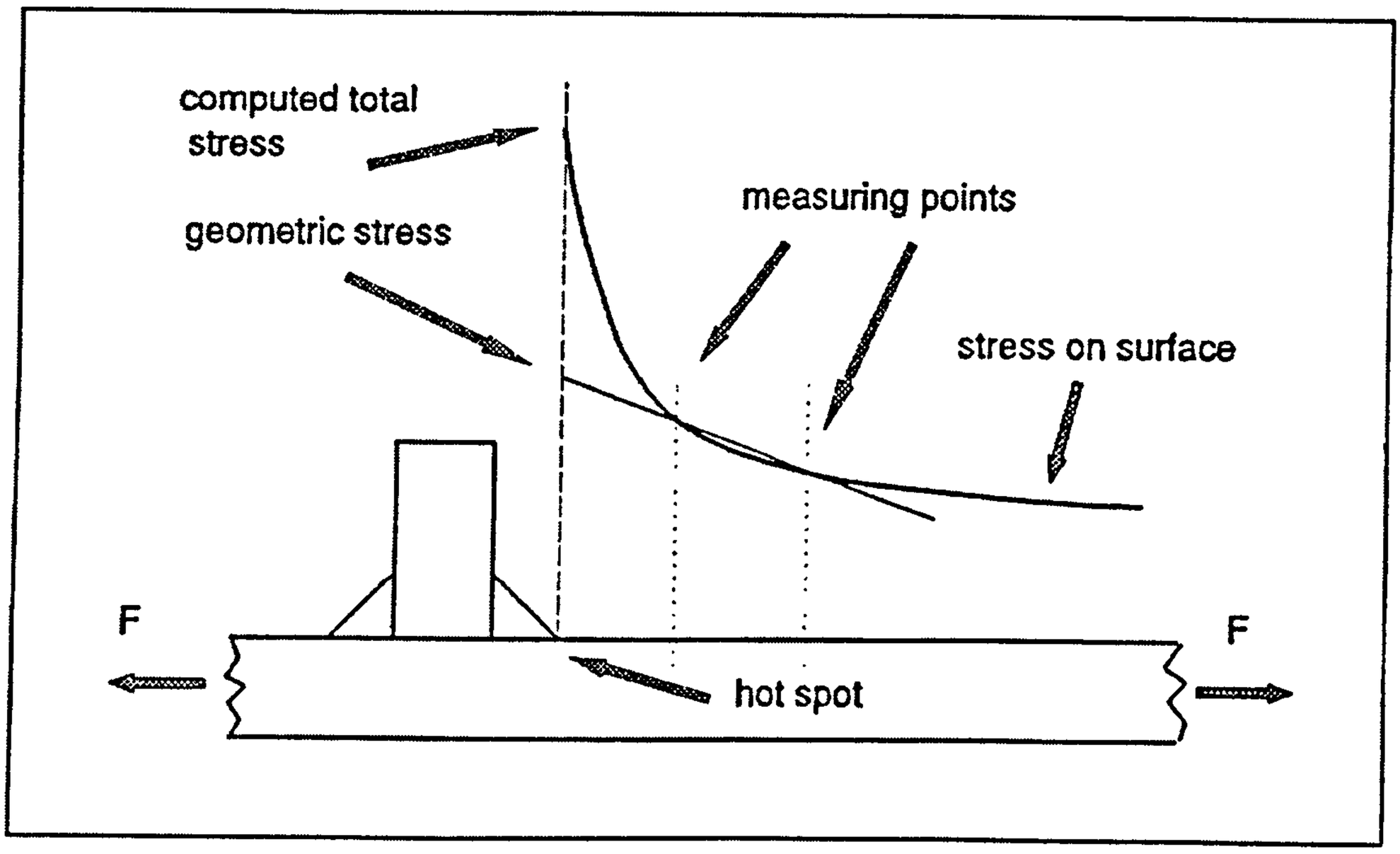

Figure 46: Stresses at a Typical Detail[207]

Fine-mesh finite element models are used to calculate the hot-spot stress for a particular detail. As the structural discontinuity in most details causes elastic finite-element models to predict infinite stress at the hot-spot, typically an extrapolation procedure is used to predict the hot-spot stress from calculated stresses some distance away from the discontinuity. A linear extrapolation is shown in Figure 46 above, using two points labelled "measuring points". Various extrapolation procedures have been proposed, Tveiten[209] reviews several of these for ship structural details and proposes a new method. Additionally, many classification societies, including ABS[171] and DNV[98] have issued guidelines on determining the hot-spot stress from finite-element models. It is important to note that there is some uncertainty in method for determining the hot-spot stress, in a review of the various classification-society methods for one detail, the hot-spot SCF, K_g, ranged from 1.47 to 2.15[205].

As the stress-raising effect of the weld itself is not included in the determined hot-spot, or geometric, stress range, this effect needs to be built into the hot-spot S-N curve. Theoretically, a hot-spot S-N curve should be defined for every type of weld and the base material. However, in practice it is common to use one hot-spot S-N curve for most common welds. In developing a hot-spot stress procedure for aluminium, Sharp et al.[176] showed that the fatigue data for groove welds, fillet welds, and unloaded appendages would fall on a common S-N curve when the stress-range was expressed in terms of a hot-spot stress,

although some scatter appeared at shorter fatigue lives. This result was partially built on the work of Sharp and Nordmark[210] on tubular aluminium trusses. In this study, Sharp and Nordmark were able to demonstrate that the fatigue lives of large-scale truss joints were equal to the fatigue lives of a small double-strap fillet welds if hot-spot stresses were used in place of nominal stresses. Partanen and Niemi[208] reviewed a wide-range of MIG-welded small-scale aluminium joints, and were able to form a common hot-spot S-N curve for a variety of welds, including butt welds, transverse fillet welds, gusset welds, and lap welds. This seems to indicate that the stress concentrating effect of most common welds is roughly similar, or at least within the data scatter of most fatigue tests, although the author is aware of no published statistical tests to back up this approach.

However, a common curve is most likely not suitable for un-welded base material, which would be expected to have different notch stress SCFs for different surface finishes resulting from different manufacturing techniques-e.g. thermal cutting, laser cutting, machine cutting, etc. Additionally, if a shipyard invested in post-weld treatment, such as profile grinding, or a radically different welding technology, such as friction stir welding, a new hot-spot S-N curve would be required.

As many of the fatigue-prone structural details in aluminium HSC are welded details, determining the welded hot-spot S-N curve constants A and m was a logical place to start. There are several published aluminium fatigue codes, including the Eurocode 9[60], and the U.S. Aluminum Association Aluminum Design Manual [53]. Additionally, the International Institute of Welding has issued a set of recommendations for the fatigue analysis of welded joints[207]. The latter two references specify single-slope S-N curves, while Eurocode 9 specifies a two-slope S-N curve with an infinite-life region under variable amplitude loading. Of these, only the Eurocode 9 has an established hot-spot S-N curve for aluminium joints. Sharp et. al[176, 211] developed a hot-spot procedure from the data within the Aluminum Design Manual. However, both of these sources use design curves, which are formed from the mean curve determined in the fatigue tests minus two standard deviations, or a similar safety margin. This is not acceptable for a reliability analysis, where the mean curve is required. Sharp[176] does include expressions to convert the Aluminum Association design curves to mean curves, however there is still some uncertainty around these curves as the slope can be quite different from the Eurocode 9 recommendation. Therefore, a further literature search was carried out to locate experimental test results for welded aluminium details in the hope that these test results could be compared with the various recommended curves, and a suitable hot-spot curve developed.

At first, a broad literature review was conducted for aluminium weldment fatigue tests that could be investigated in terms of hot-spot stress. However, it quickly became apparent that an enormous number of small-scale tests had been conducted, and to review them all would not be possible. Furthermore, because many of the specimens were small, the residual stresses in the these specimens were not expected to be equal to that of larger ship-type details, where there may be more restraint against shrinkage. Additionally, there was no guarantee that a consistent level of construction quality would be maintained between the different testing programs. However, one notable paper was located which is worth of review here. Partanen and Niemi[208] reviewed the fatigue lives of 87 MIG-welded aluminium joints tested at Lappeenranta University in Finland with the aim of developing a hot-spot S-N curve for welded aluminium joints. While most of the specimens tested were fairly small-scale, and only plate thicknesses of 3mm-6mm were investigated, these test results are a useful reference when developing a ship-detail hot-spot S-N curve. Hot-spot S-N curves were determined at two slopes, and both mean values and characteristic(design) values corresponding to the mean value at 75% confidence minus 1.64 standard deviations, or roughly a 98% probability of survival. More details can be found in Partanen and Niemi[208]. Their experimental results are summarized in Table 24 below.

Table 24: Partanen and Niemi[208] Hot-Spot S-N Curve Results
Each Curve is Single-Slope for all Cycles

Description	*Slope, m*	*FAT Class (Stress at $2*10^6$ Cycles)*
Mean value	*3.5*	*69.1 MPa*
Characteristic value	*3.5*	*45.5 MPa*
Mean value	*3.0*	*63.0 MPa*
Characteristic value	*3.0*	*39.5 MPa*

To avoid the problems encountered with the small-scale tests, the focus of the investigation shifted to larger-scale, ship-specific detail tests. These tests were fewer in number than the small-scale detail tests so it was possible to review them and use the test results to help determine the fatigue properties for welded aluminium ship details. This approach also has the advantage that short-range residual stresses and average workmanship should be reflected in the test results, as most of the test specimens were fabricated by shipyard personal, or by using shipyard techniques. An overview of each test program is given below.

Four significant test programs which included hot-spot analysis were located by the literature search. The earliest program tested a deck-to-side-wall connection for an aluminium surface-effect-ship was tested as part of the Brite Euram project MATSTRUTSES[212]. Two identical specimens were tested, under constant-amplitude

loading, with the hot-spot stresses determined through extrapolation of strain gauge readings. Material was 5083 alloy for the plating, and 6082 for the stiffeners. Cracks appeared at the connection of the haunch bracket to the side wall. This test involved an extremely large section of structure, with plating up to 20mm thick, as a result the fatigue crack was able to propagate to lengths exceeding one meter before the tests were stopped. When used in the present study, the cycles to failure were adjusted to correspond to a through-thickness crack of several centimetres in length, consistent with other tests review.

As part of his PhD thesis, Tveiten investigated two connecting bracket designs between longitudinal bulb stiffeners and a bulkhead[209]. Type "A" featured a straight bracket, while type "B" feature a radius bracket. Material was 5083 alloy for the plating, and 6082 for the stiffener. The specimen was loaded in bending, with a force applied in the plane of the bulkhead, and the stiffener ends simply-supported roughly 900mm from the bulkhead. The hot-spot stresses were determined by FEA, using a new extrapolation technique proposed by Tveiten.

As part of the Danish SASAK project, fatigue tests were carried out on six double bottom type connections, featuring a bottom longitudinal to web frame connection constructed out of 5083-W23 aluminium. The specimens were loaded under bending normal to the bottom shell plating, similar to Tveiten's experiments above. Five specimens were tested under constant amplitude loading, and one under variable amplitude loading. Hot-spot stresses were determined by FEA. The results are summarized in Jensen et al.[213] and more information is presented in Sears and Birk-Sørensen[214].

Additionally, Lloyds Register presented the results of fatigue tests on the connections of transverse bottom to side frames and tee section longitudinals to web frames[204]. Four transverse bottom frames to side frame connections were tested, for these specimens all material was 5083-0 alloy. The loading was constant-amplitude loading, and the hot-spot stresses were determined by FEA. Two of the specimens failed at non-welded locations, so these have been excluded from the current analysis. Eight tee longitudinal connections were tested, however, each specimen contained three longitudinals, and it was often possible to repair the first longitudinal that cracked so that additional test data could be generated. Two different types of welds were used for the longitudinals, type I had welds across the entire top of the longitudinal flanges, while in type II the welds stopped short of the edge of the flange. The specimens had 5083-0 alloy plate and 6082-T6 alloy stiffeners. They were tested under constant-amplitude tests, and hot-spot stresses were determined by FEA.

4.4.2.2 Combination of Test Program Data

The test results discussed above were entered into a common table, Table 25, and plotted on a combined S-N curve, Figure 47. In doing this, it became apparent that a common failure point needed to be defined before the various test results could be plotted on a common graph. This emerged as the MATSTRUTSES test specimens were large enough that they did not fail until the primary fatigue crack had grown to over 1m in length. On the other hand, in the SASAK specimens, the fatigue crack grew though an l-profile stiffener that was only 40mm deep, limiting the maximum crack length to only 40mm. Therefore, a common failure point was defined as a through-thickness crack of several centimetres(≈ 4 cm – 7 cm) in length, this is the conventional failure definition for Miner-Palmgren sum approaches of large ship details[85]. Assuming that most of the fatigue life is spent at very short crack lengths, the difference in life for a 4cm and 7cm crack is judged to be small. Therefore, of the experimental results, only the MATSTRUTSES results need to be adjusted. This was done by using the table of crack growth vs. cycles included in the MATSTRUTSES results. The compiled results are shown below in Table 25.

After compiling a table of results, the next step is to analyze the results, which is normally done through statistical methods. Several standards and recommendations have been published which give guidelines on interpreting S-N test results such as these, including ASTM E 739[215] and British Standard 3518[216]. Huther[167] gives recommendations on the statistical analysis of fatigue data. Additionally, when combining multiple sets of fatigue data, statistical checks should be made to ensure that all of the data belongs to the same population. This will be discussed in more detail after determining the appropriate regression line. The recommended approach is to fit a regression line to the S-N data using a least-squares fitting routine. It is important to perform the regression so that fatigue life(cycles to failure) is treated as the dependent variable, even though fatigue life is conventionally plotted on the horizontal axis of the S-N diagram. ASTM E 739 recommends first determining the estimated slope of the regression line from least squares, which fixes the slope coefficient m, and then determining the mean value of the intercept, which fixes the value of A. Alternatively, the slope of the regression line can be fixed ahead of time, and the value of the intercept determined from the mean values. Huther[167] recommends doing this when the fatigue data points form a cloud and accurate determinations of the slope are difficult. Furthermore, the International Institute of Welding is investigating fixing the slope of all welded joint fatigue tests at m=3.00[208]. Compared to the Eurocode 9 and the Aluminum Design Manual, a slope value of 3 seems a bit low for many aluminium welds. Further adjustments must be made if the plot of the data points reveals that a piecewise

linear approach must be taken, as illustrated in Figure 45. However, the scatter of the current data made it impossible to detect any such change-in-slope. For the ship-detail data presented in Table 25, a range of regressions techniques were carried out, first a free-slope regression was carried out, and then the regression was repeated with fixed slopes of m=3.00, 3.50, 4.00, and 4.50 for the entire range of life values(N). The results are presented in Figure 47 and Table 26 below.

The regression equation used in investigating these results took the form:

$$\log(N) = \log(A) - m\log(\Delta\sigma_{HS})$$

Where :

N : Number of Cycles to Failure

A : S - N Curve Constant

m : S - N Curve Slope

$\Delta\sigma_{HS}$: Hot - Spot Stress Range (MPa)

Equation 55

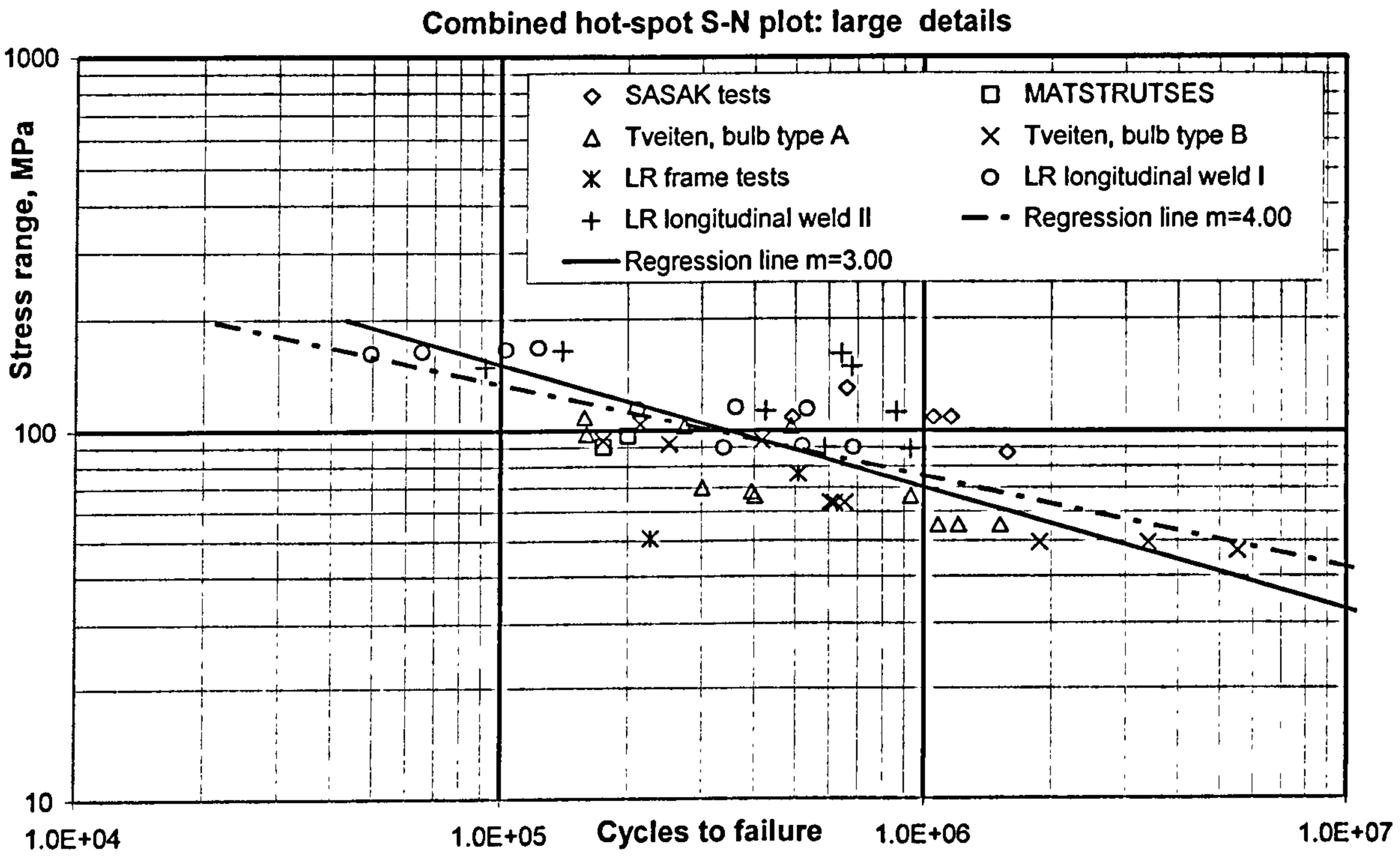

Figure 47: S-N plot of all large detail tests

As can be seen from Table 26, the free slope regression results in a slope far below the typical slopes for aluminium welded joints, which typically range around three to four. This erroneous slope value was attributed to the "clouding" of the data points between 10^5 and 10^6 cycles, and 50-110 MPa stress range. Enforcing a higher slope raises the standard deviation of Log(A), but does not noticeably effect the coefficient of variation(COV) in Log space.

Table 25: Compiled S-N Test Results from Reviewed Fatigue Projects

Project Name	Test Specimen --	Cycles to Failure --	Cycles to Common Failure Point	Hot Spot-Stress Range MPa	Load Ratio, R --	Log_{10} Stress Range Log(Mpa)	Log_{10} Cycles --
SASAK	1B-3	660000	660000	130.5	≈0.1	2.116	5.820
	1B-5	1055000	1055000	108.7	≈0.1	2.036	6.023
	2A-1	1161000	1161000	108.7	≈0.1	2.036	6.065
	2A-2	491000	491000	108.7	≈0.1	2.036	5.691
	2A-4	1572000	1572000	87.0	≈0.1	1.940	6.196
MAT.	1	640138	175000	90.5	0.10	1.957	5.243
	2	764275	200000	96.7	0.10	1.985	5.301
Tveiten, Bulb Stiffener Connections, Type A	A4	272288	272288	103.2	0.44	2.014	5.435
	A9	157895	157895	108.7	0.44	2.036	5.198
	A1	488431	488431	103.2	0.44	2.014	5.689
	A2	159782	159782	97.9	0.44	1.991	5.204
	A5	401392	401392	66.4	0.44	1.822	5.604
	A7	300626	300626	70.0	0.44	1.845	5.478
	A8	932751	932751	66.4	0.44	1.822	5.970
	A6	394363	394363	68.2	0.44	1.834	5.596
	A3	1083774	1083774	55.3	0.44	1.742	6.035
	A10	1209699	1209699	55.3	0.44	1.742	6.083
	A11	1518356	1518356	55.3	0.44	1.742	6.181
Tveiten, Bulb Stiffener Connections, Type B	B9	214191	214191	104.1	0.44	2.018	5.331
	B2	174563	174563	93.8	0.44	1.972	5.242
	B4	416149	416149	93.8	0.44	1.972	5.619
	B5	250900	250900	92.2	0.44	1.965	5.400
	B8	605712	605712	63.7	0.44	1.804	5.782
	B7	653355	653355	63.7	0.44	1.804	5.815
	B6	619470	619470	63.7	0.44	1.804	5.792
	B3	1879326	1879326	49.4	0.44	1.694	6.274
	B11	3396009	3396009	49.4	0.44	1.694	6.531
	B10	5515418	5515418	46.9	0.44	1.671	6.742
LR Frm.	1	226856	226856	50.7	0.10	1.705	5.356
	2	508352	508352	76.3	0.10	1.883	5.706
LR Bulb Stiffener, Weld Type I	1	49532	49532	162.8	0.10	2.212	4.695
	2	65267	65267	164.5	0.10	2.216	4.815
	3	102608	102608	166.3	0.10	2.221	5.011
	4	122422	122422	168.0	0.10	2.225	5.088
	5	210225	210225	114.5	0.10	2.059	5.323
	6	337873	337873	89.9	0.10	1.954	5.529
	7	361001	361001	115.8	0.10	2.064	5.558
	8	531177	531177	114.7	0.10	2.060	5.725
	9	519583	519583	90.9	0.10	1.959	5.716
	10	684642	684642	90.0	0.10	1.954	5.835
LR Bulb Stiffener, Weld Type II	1	91888	91888	148.8	0.10	2.173	4.963
	2	139755	139755	164.7	0.10	2.217	5.145
	3	425984	425984	113.5	0.10	2.055	5.629
	4	586639	586639	90.0	0.10	1.954	5.768
	5	932499	932499	89.2	0.10	1.950	5.970
	6	863182	863182	112.5	0.10	2.051	5.936
	7	677128	677128	149.2	0.10	2.174	5.831
	8	640780	640780	161.7	0.10	2.209	5.807

Table 26: Summary of Regression Results for Alternative Slope Values

Welded Hot-Spot S-N Curve Summary Table				
Description	**Slope, m**	**Mean Log(A)**	**St. Dev Log(A)**	**COV Log(A)**
Free slope	1.72	9.021	0.326	0.036
Fixed slope	3.00	11.540	0.384	0.033
Fixed slope	3.50	12.524	0.431	0.034
Fixed slope	4.00	13.507	0.485	0.036
Fixed slope	4.50	14.491	0.547	0.038

Before mixing fatigue data from many experiments, it is advisable to check that they are all representative of the same phenomenon, meaning they all share the same mean value and standard deviation[167]. If the distributions are not equivalent in this way, the S-N curve will be less precise and will have more scatter than a series of separate curves for each distribution . This can be done by several statistical tests such as the ANOVA test if the distributions are known to be normal, or the Kruskal-Wallis test if the distributions are not normal. As the distribution of fatigue test results is typically log-normal, the latter test was performed on the gathered fatigue data. To perform the test, all the points were moved to a common hot-spot stress range of 100 MPa via Equation 49 using imposed slopes with constants m=3 and m=4. As there were only two data points in the Lloyd's Register frame connection group and the MATSTRUTSES group, these groups were not included in the statistical test. The statistical test results for the remaining 44 data points in 5 groups are shown below in Table 27.

Table 27: Kruskal-Wallis test result, 5 groups of data

S-N slope, m	$H_{Kruskal\text{-}Wallis}$	$\chi^2_{(0.01,4)}$
3	*27.8*	*13.28*
4	*31.6*	*13.28*

As the Chi-squared values at p=0.01 are less than half the values obtained from the test, regardless of which slope is used, there is strong evidence that equivalence seems to be violated in this case. This is not a surprising conclusion, inspection of the various test programmes suggest the following reasons:

- **Differences not accounted for by the hot-spot method:** The Lloyd's Register longitudinal tests included two different welding configurations that would be expected to have the same or closely similar hot-spot stresses, yet different fatigue strengths. This will results in different mean values for the two sets of data.

- **Differences in load ratio, R, at the hot-spot:** This difference comes from two sources. First, the applied loading R was not the same for all the test programmes. Additionally, the residual stresses from fabrication would be expected to be different at the hot-spot for the different details tested, based on both the configuration of the detail, quality of welding, and level of restraint in the manufacturing process.

- **Differences in hot-spot estimation technique:** Different hot-spot estimation techniques were used by the various programmes. Some used linear extrapolations from strain gauges, others finite element models, and Tveiten used his own proposed singularity-check method.

- **Possible thickness effect:** The thicknesses of the different specimens ranged from plate 5mm thick to plates 20mm thick, although not all programmes published full dimensional information. While conventional steel classification rules do not consider thickness effects until the thickness exceeds 25mm[98], the Eurocode 9 specifies different hot-spot S-N curves for thickness of < 4mm, 4-10mm, 10-15mm, 15-25mm, 25-40mm, > 40mm, suggesting some dependence on specimen thickness.

- **Multiple failure sites:** Both the Lloyd's Register bracket test and the Tveiten bulb stiffener tests had multiple potential failure sites. As the tests were conducted until one of these sites experienced a fatigue failure, the tests have a conservative bias, Tveiten[209] discusses this with respect to another test program not presented here. This should not effect the Lloyd's Register longitudinal tests, which tested three identical details with one failure site in each specimen, as in this case testing could continue after the failure of one detail until the other details failed.

A case can be made that at the preliminary design stage the first three factors mentioned above are unknown to the designer, and furthermore largely uncontrollable by the designer. If this argument is accepted, then in a reliability setting the hot-spot S-N curve should attempt to include the scatter that these factors cause. However, when the full set of data was investigated in this way, the coefficient of variation in the S-N intercept parameter A was greater than one, indicating an unacceptably large amount of scatter. Therefore, it was necessary to attempt to reduce the amount of scatter by examining the various experimental programs and attempting to select a sub-set that minimizes the sources of variation mentioned above.

Examining the assembled experimental data in Table 25 above, the Tveiten bulb test results appear to be the best choice to use as a subset. At 21 test points, they are a substantial proportion of the entire data, they all were tested under the same R ratio, and had the same thickness. This data set should also be a conservative selection, as it was tested under the highest R ratio of any of the test programs, and the test results are for the weakest location out of two possible locations. These test generally form the lower band of fatigue results in Figure 47. Additionally, the hot-spot stress was determined by the same method for all of the specimens. Originally, this experimental data was entered with hot-spot stresses determined by Tveiten's proposed hot-spot extrapolation method, and it was anticipated that the uncertainty introduced by different hot-spot extrapolation procedures would be included in the uncertainty in the S-N curve. However, as only Tveiten's data will now be used, this needs to be re-examined. Many classification societies and design codes specify how the hot-spot extrapolation procedure is to be carried out, and they largely specify linear extrapolation; therefore it is perhaps best that the S-N curve be derived from linearly-extrapolated hot-spot data. Tveiten included the hot-spot SCF determined by both the IIW linear extrapolation procedure and the DNV linear extrapolation procedure. For the bulb-stiffener specimens, the SCFs determined by these two methods are virtually the same. The IIW SCF was selected, which lead to the set of reduced data shown in Table 28.

The same regression techniques used on the full set of data was applied to this data. For the Tveiten tests alone, the free-slope regression yields a slope value of 3.06, which is very close to the IIW recommendation of a fixed slope 3.0 for welded joints. With an enforced slope of 3.0, the mean Log(A) value works out to 11.47. The Kruskal-Wallis test was carried out again on this data, converted to number of cycles at a hot-spot stress range of 100 MPa with the slope set equal to 3. An H value of 0.045 was obtained from this, which compares favourably to the Chi-squared distribution(at one degree of freedom, and a

probability value of 0.05) of 3.84. This indicates that the two Tveiten test sets can be mixed with a good degree of confidence.

Table 28: Reduced S-N Data

Tveiten Only Data, IIW Linear Ext. SCF						
Project Name	Test Specimen --	Cycles to Common Failure Point	Hot Spot-Stress Range MPa	Load Ratio, R --	Log_{10} Stress Range Log(Mpa)	Log_{10} Cycles --
Tveiten, Bulb Stiffener Connections, Type A	A4	272288	117.1	0.44	2.068	5.435
	A9	157895	123.4	0.44	2.091	5.198
	A1	488431	117.1	0.44	2.068	5.689
	A2	159782	111.1	0.44	2.046	5.204
	A5	401392	75.4	0.44	1.877	5.604
	A7	300626	79.5	0.44	1.900	5.478
	A8	932751	75.4	0.44	1.877	5.970
	A6	394363	77.4	0.44	1.888	5.596
	A3	1083774	62.7	0.44	1.797	6.035
	A10	1209699	62.7	0.44	1.797	6.083
	A11	1518356	62.7	0.44	1.797	6.181
Tveiten, Bulb Stiffener Connections, Type B	B9	214191	113.2	0.44	2.054	5.331
	B2	174563	102.0	0.44	2.009	5.242
	B4	416149	102.0	0.44	2.009	5.619
	B5	250900	100.2	0.44	2.001	5.400
	B8	605712	69.2	0.44	1.840	5.782
	B7	653355	69.2	0.44	1.840	5.815
	B6	619470	69.2	0.44	1.840	5.792
	B3	1879326	53.8	0.44	1.730	6.274
	B11	3396009	53.8	0.44	1.730	6.531
	B10	5515418	51.0	0.44	1.708	6.742

4.4.2.3 Development of Mean Curve and Uncertainty Values

In order to develop an appropriate design curve for the hot-spot reliability method, the Tveiten S-N data was plotted and compared to several S-N curves. This is shown in Figure 48 below. Four S-N curves were used for comparison, the first was a regression curve with the slope fixed at m=3.00, as this was almost identical to the free-slope regression curve. The second curve was the Aluminum Association category "B" mean curve, Sharp et al.[211] recommend the design version of this curve for hot-spot design of aluminium welded connections. Appendix A of Sharp et al.[176] gives an expression which converts the Aluminum Association design curves to mean-value curves, this correction factor was applied to plot the mean curve. The final two curves were the Partanen and Niemi[208] mean curves with m=3.0 and 3.5 discussed above.

All curves compare well with the data points. The Partanen and Niemi curves seem slightly higher than the rest of the curves. This could be caused by several factors. First, the Partanen and Niemi test specimens were smaller and in many cases simpler than the large-scale ship details plotted here. This means that achieving good alignment during fabrication may have been easier. Also, the residual stresses from fabrication may have been smaller as the less complex specimen geometry may not restrain the welds to the same degree as the ship details.

Unfortunately, measurements of alignment and residual stresses have not been widely reported in the open literature, so it is impossible to confirm that this is the case. Additionally, the Partanen and Niemi test were carried out at a variety of R ratios, while the Tveiten tests were all carried out at a high R ratio. The U.S. Aluminium Association curve seems to be a reasonable fit, although its higher slope constant means that it becomes more optimistic at higher cycles than the other curves and the Tveiten data seem to indicate.
The issues of curve slope must also be addressed. At the current time, there is not enough high-cycle($N > 5 * 10^6$) fatigue data to investigate using a two-slope S-N curve, therefore, a single slope curve must be adopted. The International Institute of Welding recommendations[207] use a standard slope of m=3.0 for all welded joints. However, both the U.S. Aluminium Association and the Eurocode 9 recommendations allow for different slopes for different weld and joint configurations. The U.S. Aluminum Association category "B" curve which Sharp et al.[211] suggest as a hot-spot curve corresponds to a groove or fillet weld running in the direction of the applied stress, or to a groove weld ground flush transverse to the applied stress. The recommend slope is 4.84. For similar welds, Eurocode 9 recommends slopes between 4 and 5. The current data suggests a slope of 3, but neither the Aluminum Association category "B" curve with m=4.84 or the Partanen and Niemi curve with m=3.5 looks completely off. At the current time, a fixed slope of 3.00 with a mean Log(A) value of 11.47 seems to be best S-N curve. In terms of the IIW FAT classification, this corresponds to a FAT class of 52.8, indicating a hot-spot stress range of 52.8 MPa at a life of 2 million cycles.

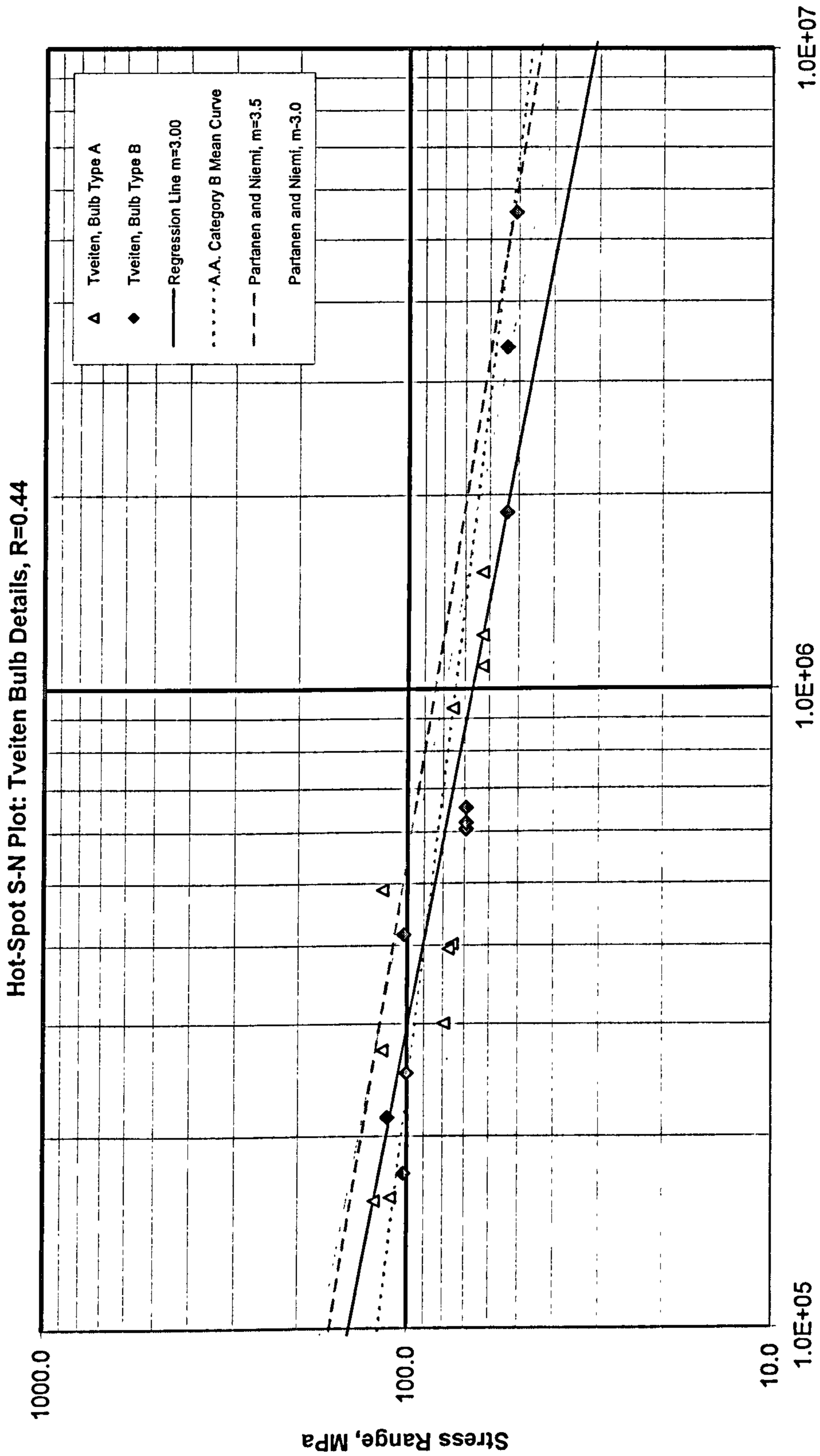

Figure 48: Combined S-N Plot

The recommended S-N curve developed in the paragraph above may not be the best way to model fatigue capacity in a reliability-based setting. As the slope value m has been fixed, it seems best to treat this as a deterministic variable, not a stochastic variable. This leaves only the intercept value, A, as a stochastic variable. This variable is typically assumed to follow a log-normal distribution[40, 41]. With the S-N curve slope fixed at 3.00, the value of the intercept parameter A was calculated for each of the 21 test points. The mean and standard deviation of these points were then calculated. The mean value of A determined this way does not correspond to the mean value of Log(A) determined in the S-N curve, because the log of the mean of the data does not equal the mean of the logs of the individual data points. The mean value of A was $3.31 * 10^{11}$, and the log of this value is 11.52. This correspond to a FAT class of 54.9 MPa, slightly higher than the 52.8 MPa reported above, but not a large move given the scatter shown in Figure 48. This raises the question of which one is the best to use. For the S@S study, the mean value of the individual points of A was selected. Assuming that the linear model fits the data well, which it appears to, one can view the 21 tests as 21 trials which can be used to define the statistical parameters of A. Adopting this approach only measures the variability in the fatigue data, not the variability between the actual fatigue data and the assumption of a linear relationship in log stress-log cycles space. If the variability from the log-linear assumption is to be included, then another factor or method of determining the C.O.V. must be adopted.

To test the assumption that the values of A follows a lognormal distribution, the natural log of this data was entered into the Minitab statistical software to investigate the normality of the natural log of the data. This was done by plotting a histogram of the data, and seeing how well the data seemed to fit a normal curve. Additionally, the Ryan-Joiner normality test was performed. The results are shown in Figure 49 and Figure 50 below:

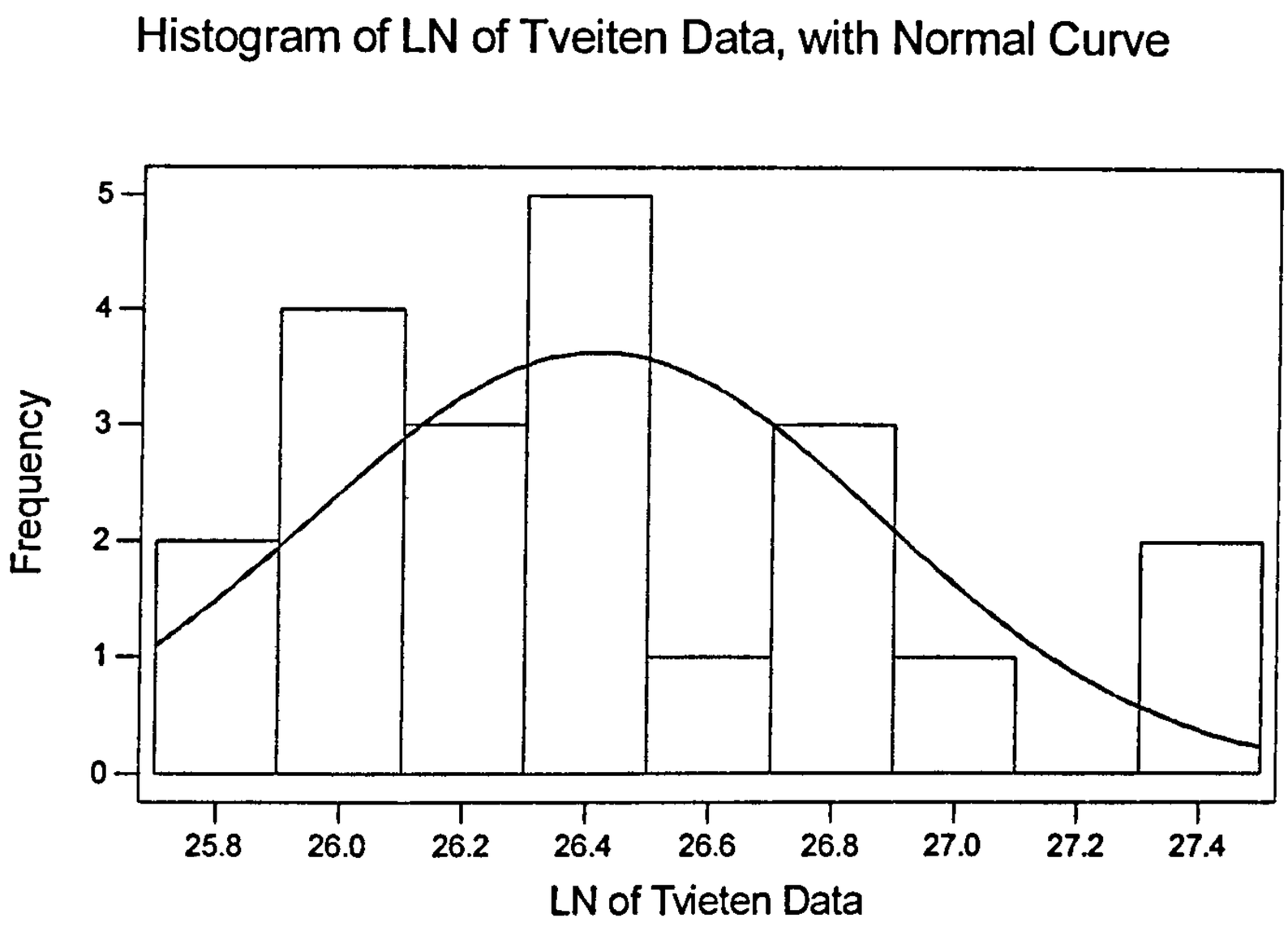

Figure 49: Histogram of Hot-Spot S-N Data

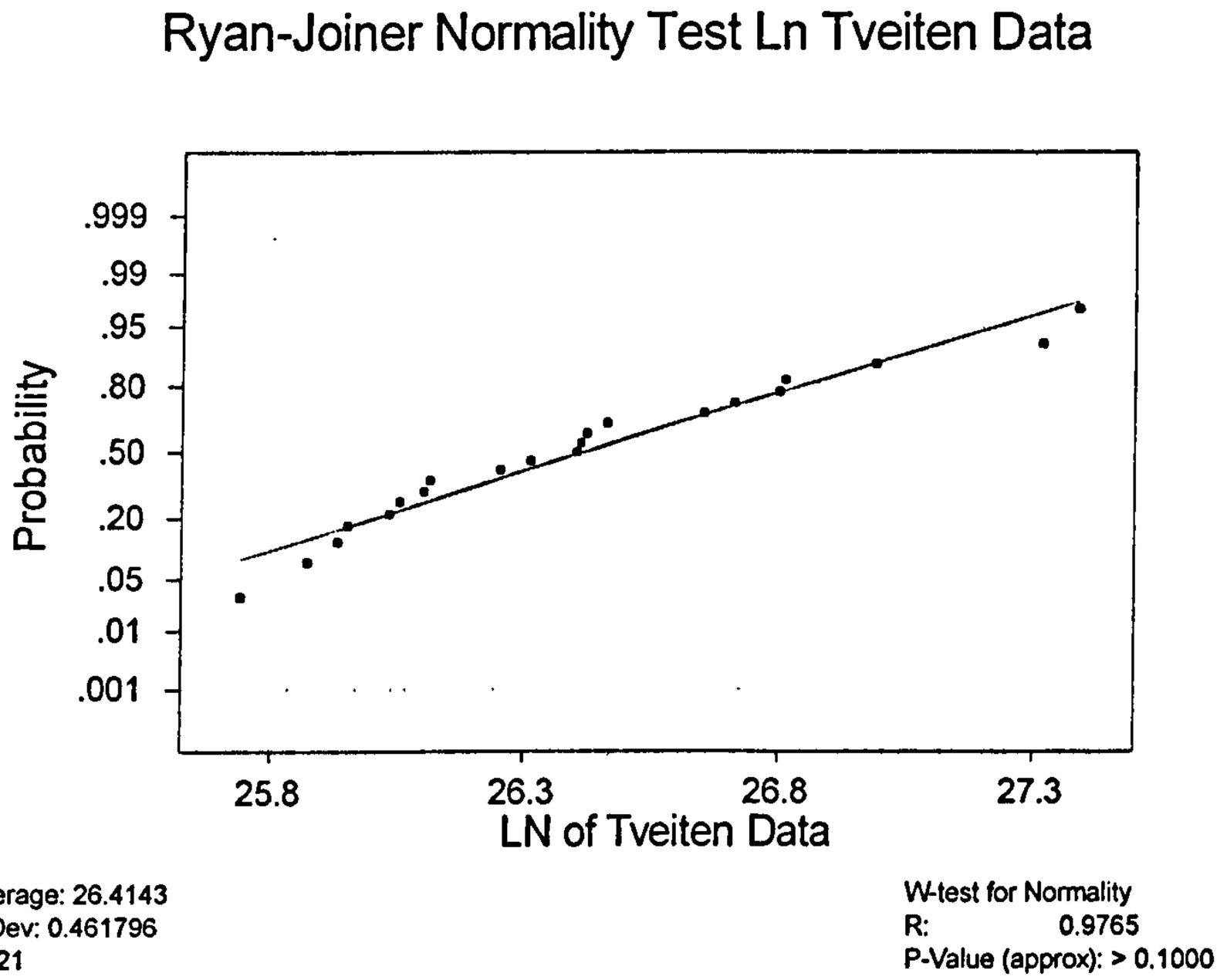

Figure 50: Normal Probability Plot

Because there are only 21 data points, it is hard to make strong conclusions about the log-normality of this data. However, based on the above tests, there is no reason to conclude that the data is not log-normally distributed. When the entire data set of 48 points was

investigated, the data was more strongly normal. However, as mentioned above, the scatter in this data was extremely large. With the current distribution, the reported means and coefficient of variation(based on sample standard deviation) of the A values are $3.31 * 10^{11}$ with a COV of 0.53. Unfortunately, no other published COV were found for aluminium welded joints, however this value agrees well with data for steel joints, in a survey of statistical data relating to 11 steel S-N curves, Ayyub et al.[40] reported COV of A between 0.43 and 1.36, with nine of the values falling between 0.43 and 0.63. Thus, this uncertainty measure seem reasonable.

4.4.2.4 Potential Modifications Required to the Mean S-N Curve

Many previous studies have indicated that the mean stress, corrosion, alloy, and plate thickness can all have an effect on S-N curves. With this in mind, an investigation was made into the effects these elements may have on the hot-spot S-N curve determined above. Mean stress can come from still-water bending loads and from residual stresses from the construction of the vessel. While the local residual stresses from the weld should be included in the fatigue test data itself, the longer-range residual stress present in the hull structure from assembling large structural components will not, which could influence the mean stress level. Any still-water bending moment that is fairly constant would also influence the mean stress. As the final S-N curve in this study was determined from the Tveiten tests which combined both typical welding residual stresses and were performed at a high R ratio, it seems likely that no further mean stress effects need to be accounted for.

Thickness effects were discussed briefly above. At the current time, only the Eurocode 9 specifies different S-N curves for hot-spot stresses when the thickness of the individual elements are below 25mm. Hobbacher[207] recommends considering thickness effects for plates thicker than 25mm in both steel and aluminium. There is also the difficulty in determining the thickness of certain components, such as the flange region of a bulb-profile stiffener, for either hot-spot stress extrapolation, or accounting for thickness effects[172]. Therefore no thickness effects will be considered. At the current time, there is also no information to indicate that the different marine alloys of aluminium have different fatigue strengths in the welded condition. The Aluminum Association, Hobbacher, and the Eurocode 9 all make no adjustment for differences between the 5000 and 6000 series alloys in the welded condition. However, developing fatigue-resistant alloys is a current area of research, so this topic may need to be revisited in the future.

The effects of corrosion also need to be considered. All of the test data described above was gathered under laboratory conditions. However, for use with HSVs, the S-N curve must address the issue of the marine environment. This could mean either

atmospheric changes such as saltwater spray, or the possibility of the specimen being fully immersed in seawater. Sharp et al.[176] presents the results of several investigations into welded joints in both the seacoast environment and immersed in saltwater. For transverse fillet welds exposed for one year in seacoast and industrial environments, the fatigue test results were roughly equivalent to specimens tested in laboratory conditions. Sharp et al. [176] concludes that there are not statistically significant differences for butt and fillet weld joints in the common marine alloys in marine atmospheres. However, Sharp et al. [176] report that there is a reduction in fatigue strength for joints immersed in salt water. The observed reduction was greater for butt welds than fillet welds, and painting seemed to improve the situation.

These conclusions are supported by Eurocode 9, which specifies reductions in fatigue strength depending on alloy and environmental conditions. For "moderate" marine environments, Eurocode 9 specifies no reduction for 5000, 6000, or 7000 alloys. For "severe" marine environments, Eurocode 9 specifies that the 5000-series alloys should move closer to a single-slope S-N curve, while the same changes should be made for 6000 and 7000 series alloy plus reducing the S-N curve capacity by one and two curve classes respectively. For the curves provided with Eurocode 9, each class is separated from its neighbours by about 10%, or roughly 5-6 MPa around FAT Class 50. For immersion in saltwater, all alloys should move closer to a single-slope curve with reductions of one, two and three curve classes for 5000, 6000, and 7000 series alloys respectively.

Based on these sources of information, it seems reasonable to use the mean curve identified without modification in this comparison study. For typical HSV structural details that are not immersed in salt water, it seems that thickness, mean stress, and corrosion concerns should be broadly equivalent to the test data used to generate the mean curve. However, for wider design considerations, the effect of thickness, corrosion, mean stress, and alloy should still be evaluated, as these assumptions may break down in other fatigue-prone areas, e.g. water jet ducts.

4.4.2.5 Miner-Palmgren Damage Summation

With the mean S-N curve and the associated uncertainties established, the last area of fatigue capacity which has to be examined is the Miner-Palmgren sum at failure. Similar to the mean S-N curve, this parameter must be treated as a stochastic variable, as previous results have shown that the Miner's sum at failure can vary widely. This is partially a result of the large amounts of scatter in fatigue properties, as discussed above, and partially a result of the simplified empirical nature of the Miner-Palmgren damage rule. The Miner-Palmgren damage rule ignores effects such as load sequencing, which do affect the rate of damage

accumulation. However, as Sharp et al.[176] noted, the Miner-Palmgren rule is still widely applied as it combines reasonable accuracy with attractive simplicity, and a better alternative has yet to be found.

To determine the appropriate statistical parameters for the Miner's sum at failure, a literature survey was carried out for aluminium variable-amplitude test programs. Table 29 presents a summary of the information located in the search. Tveiten's[209] fatigue studies include variable-amplitude testing of a flat bar with non-load carrying plate attachments, these were tested under a Weibull spectrum with a shape parameter equal to 1.19. Twelve specimens were included in the Miner's sum analysis. The Miner's sum was carried out with a nominal stress approach based upon S-N curves developed from constant-amplitude testing of this particular detail. Conservative Miner's sum predictions were observed, when using a fixed-slope S-N curve with m=3.00. Tveiten also compared his results to the tests of a similar program carried out by Orjasaeter. Unfortunately, the full results from the Orjasaeter tests were not available, so Tveiten's summary was used. This programme consisted of a series of butt and fillet weld joints tested under two different types of spectrums, log-linear and Rayleigh. This corresponds to Weibull spectrums with shape parameters of 1.0 and 2.0 respectively. For these specimens, non-conservative life predictions resulted, with a mean damage at failure between 0.6 and 0.7. Unfortunately, the S-N curved used in the analysis and the C.O.V. of the results were not reported in Tveiten's summary, so it is impossible to determine if the variability is in the Miner-Palmgren summation or in the S-N curve.

In a study of variable-amplitude fatigue predictions, Wirsching et al.[217] summarized the statistical properties of a wide variety of aluminium fatigue tests. These tests appear to be mainly from aerospace sources, and thus would be expected to include both non-marine alloys and non-welded connections. It is interesting to note that this review compared both mean and median values of damage at failure, and in many cases the mean values were significantly above the median values, indicating skewed distributions This review also compared data for other materials, and overall recommended a median value of 1.00 with a C.O.V. of 0.65. The exact type of load spectrums and connections tested are not known for this review.

James et al.[218] present the variable-amplitude fatigue life of welded beam cover plates from a series of experiments conducted in South Africa. Two-level loading was used(i.e. two stress ranges), and the number of high-low cycles was varied over a wide range. Different welding techniques were used, and heat-treatment and stress relief were also studied. The result was a wide range of Miner's sums at failure, ranging from 0.31 to

15.42, though most results were much closer to 1. On the whole, James et al. commented that Miner's sum was usually conservative, and the non-conservative predictions occurred in two groups, one group of samples with a specific welding technique, and one group of samples subjected to vibratory stress relief. Only summary results were presented, so it was not possible to determine the C.O.V. from the presented information.

In addition to the variable-amplitude aluminium tests reviewed above, recent proposals for fatigue reliability in steel vessels were also reviewed. Three recent papers present statistical information on the Miner's sum at failure. Ayyub et al.[40] presented some recent research on reliability-based guidelines for fatigue, and recommend a median value of 0.9 and a C.O.V. of 0.48 for steel ship structures. In a similar study de Souza and Ayyub[41] used a mean value of 1.0 with a C.O.V. of 0.48 when comparing fatigue reliability calculations by the S-N curve and by the fracture mechanics approach. More recently, in developing a new set of guidelines for high-tensile steel vessels, Folsø et al.[206] used a reliability model to calibrate the new guidelines. For the reliability model, the Miner's sum was treated as having a median value of 1.00 with a C.O.V. of 0.3. These results are also presented in Table 29 below.

Table 29: Survey of Aluminium Variable-Amplitude Fatigue Experiments and Recent Proposals for Steel Structural Details

Name	*Material*	*Type of Detail*	*Type of V.A. Loading*	*Damage at Failure*	*C.O.V. of Damage at Failure*	*Source*
Tveiten's flat bar test	*Alum.*	*Fillet welds*	*Weibull distribution*	*1.869*	*0.25*	*[209]*
Orjasaeter tests	*Alum.*	*Fillet and butt welds*	*Log-linear and Rayleigh*	*0.6-0.7*	*Not Available*	*[209]*
ASCE survey	*Alum.*	*Mixed*	*Mixed*	*1.33*	*0.65*	*[217]*
James et al. tests	*Alum.*	*Fillet welds*	*Two-Block*	*0.31-15.42, most < 5*	*Not Available*	*[218]*
Ayyub et al. paper	*Steel*	*N/A*	*N/A*	*0.9*	*0.48*	*[40]*
de Souza and Ayyub paper	*Steel*	*N/A*	*N/A*	*1*	*0.48*	*[41]*
Foslø et al. paper	*Steel*	*N/A*	*N/A*	*1.0*	*0.3*	*[206]*

As can be seen from Table 29, many different values of Miner's sum have been suggested for aluminium. From the previously proposed values, it seem appropriate to select a mean value of 1.0, and a C.O.V. of 0.48 for the fatigue capacity mode. As negative values do not make sense for Miner's sum, a lognormal distribution is recommended. With

the mean value and uncertainty determined for the Miner-Palmgren damage sum, as well as the S-N curve parameters A and m in the previous section, the fatigue capacity model is complete for both the Jensen and de Souza and Ayyub limit states. The next step is to test the proposed method against the reference vessels and existing design codes, to see how suitable these mean values and uncertainties are.

4.5 Analysis of the Proposed Method

In the development of the S-N reliability method above, it was clear that previous studies have produced a wide range of mean values and uncertainties for fatigue capacity. Furthermore, the literature review revealed that comparison studies between fatigue methods, such as the ISSC study of the container ship coaming pad, often reveal large discrepancies in predicted fatigue life. As a number of the values for mean strength and uncertainty were selected based on limited information, it is important to compare the proposed method to existing design codes and recommendations, to see if the overall method developed produces reasonable results. Furthermore, for the method to be of practical use for designers, a means of evaluating the reliability of limit state needs to be developed. In Chapter 3, the fast and simple first-order reliability(FOR) method was used with high accuracy to evaluate the compressive collapse limit state. The simplicity of this method makes it useful for practical reliability evaluation, and it would be ideal to apply it to the fatigue limit state as well. However, both the fatigue limit states proposed here(Equation 53 and Equation 54) are much more non-linear than the compressive collapse limit state. Furthermore, the uncertainty of the variables in the limit state are also much higher for fatigue than for compressive collapse. For example, two of the variables for fatigue, A and Dcr, have COVs around 0.5. Thus, the accuracy of the first-order reliability method must be re-examined for this limit state before the use of the FOR approach is recommended.

To cover these issues, three different investigations will be made of the proposed S-N curve and both the Jensen and de Souza and Ayyub limit states. First, a hypothetical application to a midship detail in the 150m reference vessel (discussed in Chapter 2) will be made. This will allow mean values and uncertainties to be determined for the loading side of the limit state, and give an initial indication of the suitability of the method. Second, the accuracy of the FOR approach will be assessed by comparing the FOR results to those from a Monte Carlo simulation for both limit state equations. This comparison will use the reference vessel case as a base case, and then vary the parameters of the limit state from this base case to assess the accuracy of the FOR approach over a wide range of values. Finally, the proposed method will be applied to details in the International Institute of Welding

(IIW)[207]and Aluminum Association Specification[53] fatigue design codes, to see what safety index corresponds to the allowable stresses in the code.

4.5.1 Application to a Reference Vessel

The first step in the analysis is to determine a base case by applying the method to a hypothetical fatigue location in the midship section of 150m reference vessel, which was presented in Chapter 2. This will yield mean values of loading that should be roughly typical of actual details on HSVs, and allow us to determine the uncertainty associated with this loading. This reference vessel is a a hypothetical monohull high-speed craft with a design length of 150m, based on model 5, from Table #2 of Blok and Beukelman[101]. The vessel's required section modulus was estimated by the DNV HSLC Rules[102], again considering global loading only. Using the simplified loading sheet proposed by Jensen and Mansour[91], a long-term estimate was made for the global vertical bending load, as discussed in Chapter 2. This method produced a Weibull long-term bending moment distribution with a scale factor of 72.2 MNm and a shape parameter of 1.26. To convert the bending moment distribution to a hot-spot stress distribution, the required deck section modulus from the HSLC Rules was used, along with a hypothetical non-load bearing attachment with a nominal to hot-spot stress concentration factor of 1.4. This would be representative of the stress distribution of a detail such as a bracket or similar support, on the main deck of the vessel near centerline, where both lateral loading and horizontal bending are small and can be excluded. With these assumptions, the resulting stress distribution has a scale parameter, α_w, of 4.7 MPa, with a shape parameter, β_w, of 1.26. This value of β_w is at the high end of the range for normal commercial vessels, and may be a reflection of the operating restrictions on high-speed craft which compress the exposure into a smaller range of sea-states.

This Weibull distribution is sufficient for the Jensen limit state, however, for the de Souza and Ayyub limit state an equivalent stress range is required. This stress range was found by equating the m^{th} expected moment of the Weibull distribution to the stress term in the de Souza and Ayyub limit state:

$$(2\alpha_w)^m \Gamma\left(1+\frac{m}{\beta_w}\right) = (k_s)^m \sum_{i=1}^{n} S_i^m \qquad \textit{Equation 56}$$

With the slope of the S-N curve set at 3, and k_s taken as 1(see discussion below), the single-block(n=1) equivalent stress range of the Weibull distribution worked out to 13.47 MPa.

The final issue which must be addressed with respect to loading is the uncertainty which should be associated with the combined stress distribution. Unfortunately, as determining the hydrodynamic loading itself is still an area of research on high-speed craft, almost no information exists about uncertainties. Given this situation, a literature review was made of previous fatigue work for steel craft and large commercial craft, to determine what sorts of uncertainties are typically employed. Munse et al.[79] addressed uncertainties when developing a probabilistic fatigue damage model, using a coefficient of variation(COV) of 0.1 to account for uncertainties in the stress determination. More recently, both de Souza and Ayyub[41] and Ayyub et al.[40] considered the COV of the total stress range acting on a structural detail as 0.1, but also multiplied this stress range by the uncertainty factor k_s discusses above, assigning a mean value of 1.0 and a COV of 0.1 to this parameter. Similarly, in a fatigue reliability study on an aluminum catamaran, Song and Moan[219] assumed that natural log of the Weibull scale parameter would be normally distributed with a COV of 0.1. The Weibull slope was taken as fixed, but a stress uncertainty factor with a mean of 1.0 and a COV of 0.1 was also applied.

No firm recommendations can be made from these studies for monohull high-speed craft, this is an area for further research. It was decided to pick reasonable values of uncertainties for the base case in the study, and then let them vary as part of the study to see the effect of this variation on both the resulting safety index and the accuracy of the first-order reliability method. To be comparable to previous studies, it is proposed that a COV of 0.1 is associated with both the Weibull shape and scale parameter, and that lognormal distribution is used for α_w and a normal distribution for β_w . Following the approach adopted by de Souza and Ayyub, for their limit state the stress range, S, will be treated as a lognormal parameter with a COV of 0.1, while k_s is normally distributed and has a mean of 1.0 and a COV of 0.1. There is strong grounds to argue that the Weibull scale and shape parameters should not be allowed to vary independently, as there is a relation between these parameters. However, given the current lack of data on the uncertainty in high-speed craft loading, a more likely design approach will be to treat one of these variables as deterministic, not stochastic, and to assign all the uncertainty in the loading to the other variable. With this end use in mind, it was decided to model these variables as independent, and see the effect of varying the COV of each. This leads to the base case shown below in Table 30.

Using the values in Table 30, Monte Carlo simulation was used to determine corresponding safety index, β; this was established as 1.56 for both the Jensen and de Souza and Ayyub limit states. Given that no efforts have been made to adjust the mean values and uncertainties in this limit state to agree with previous design codes, this seems a fairly

reasonable safety index for a fatigue failure. Mansour et al.[22] recommends target safety indexes for fatigue failures which range from two to four, depending upon the seriousness of the failure. These recommendations were used by Ayyub et al.[40]. In a recent study, Folsø et al.[206] reported safety indexes between 1.2 to 2.3 for an existing tanker designed to RINA, BV, and GL classification rules. Thus, the initial application of the methodology yields encouraging results.

Table 30: Base Case for the Limit States

Jensen Limit State				*de Souza and Ayyub Limit State*			
Variable	*Mean Value*	*COV*	*Distribution*	*Variable*	*Mean Value*	*COV*	*Distribution*
α_w	*4.7MPa*	*0.10*	*Lognormal*	*S*	*13.47 MPa*	*0.10*	*Lognormal*
β_w	*1.26*	*0.10*	*Normal*	*ks*	*1.0*	*0.10*	*Normal*
Dcr	*1.0*	*0.48*	*Lognormal*	*Dcr*	*1.0*	*0.48*	*Lognormal*
M	*3.0*	*--*	*Fixed*	*M*	*3.0*	*--*	*Fixed*
A	$3.31*10^{11}$ MPa^3	*0.53*	*Lognormal*	*A*	$3.31*10^{11}$ MPa^3	*0.53*	*Lognormal*
N	$3.2*10^7$	*--*	*Fixed*	*N*	$3.2*10^7$	*--*	*Fixed*

4.5.2 Accuracy of First-Order Reliability Methods for S-N Design

The second step in the analysis of the proposed fatigue reliability formulation is to determine the accuracy of the FOR method for evaluation the reliability of the two fatigue limit states proposed. While the initial application to the 150m reference vessel seems successful, the safety index for this vessel was determined by Monte Carlo simulation, which is inefficient and impractically slow for engineering work. Thus, it is important to establish if the FOR reliability method is acceptably accurate when applied to the fatigue limit state equations. As discusses above, there are two main reasons for concern in applying the FOR method to these limit states:

- Both the de Souza and Ayyub and Jensen limit states are highly non-linear compared to the limit states investigated previously. The FOR first-order approach relies on a linearization of the limit state about an appropriate point, it may produce large errors when the limit state is highly non-linear. Furthermore, the two limit state equations handle the loading differently, and thus the FOR method may be better with one than the other.
- The uncertainty in the variables in the fatigue limit state, especially those with non-normal distributions, is much higher than in the limit states studied

previously. As the FOR approach is approximating these distributions, this may lead to errors

Because of these concerns, a comparison study between the FOR approach and the Monte Carlo simulation results was undertaken for both the Jensen and de Souza and Ayyub limit state equations. This study used the 150m reference vessel case above as a base case, but then varied the mean value and uncertainty of each variable in the limit state in turn to cover a wide range of possible input parameter. For each case, the safety index was determined by the FOR and Monte Carlo approach, as outlined in Chapter 2. The Monte Carlo approach used the convergence formula, Equation 5 shown in Chapter 2, to estimate the coefficient of variation of the simulation result. The simulations were run until the number of cycles and number of observed failures were sufficient to yield a COV of the result less than 0.03.

The non-linear nature of the limit state equations was felt immediately when the FOR approach was applied. Applying the Rackwitz and Fiessler method to solve the Jensen limit state equation lead to numeric instabilities for certain mean values. The large values of the derivatives of the equation could result in large swings in the checking point between iteration steps in the Rackwitz and Fiessler method, leading to non-convergence in either the method as a whole, or domain errors in the numeric formulations used. A fairly simple method of solving this problem was discovered, instead of starting the Rackwitz and Fiessler algorithm at the mean values of the variables, the starting point of the variables A and Dcr were reduced by multiplying by a factor of 0.1 to 0.01. This lead to stability over a wide range of safety indexes (roughly $|\beta| < 5$ on the Safety@Speed project), which covers the range of interest to practical engineering problems.

With the FOR solver stabilized, a wide range of comparison studies were undertaken. In general, the agreement between the FOR approximation and the Monte Carlo simulation was quite good. Varying the mean value of the parameters results in safety index values between roughly one and four. For each of these cases, the relative error in the predicted safety index was determined by the following formula:

$$Error = \frac{\beta_{FORM} - \beta_{MONTE\_CARLO}}{\beta_{MONTE\_CARLO}} \qquad \textit{Equation 57}$$

This yields negative errors when the FOR prediction is conservative, and positive errors when the FOR approach over-predicts the safety index. Over this range, the magnitude of the relative error in the predicted safety index between the FOR approximation and the Monte Carlo simulations were generally less 5%, as summarized in Table 31. The one

exception occurred when the value of k_s in the de Souza and Ayyub limit states was reduced to 0.7 or below, in which case the errors were between 6% and 11.2%. Interestingly, the Jensen limit state trends less conservative as the safety index decreases, while the de Souza and Ayyub limit state trends more conservative as the safety index decreases. However, the absolute magnitude of the errors were so small in most cases that side which the error fell on would be insignificant for practical applications. The results from the variation in the damage summation at failure, Dcr, which were typical of the overall results are presented below in Figure 51. This plot shows how the magnitude of the error increases as the safety index decreases. Some exploratory cases were studied with safety indexes approaching 0, which would indicate a 50% probability of failure, which confirmed that the trend of increasing errors continued as the safety index decreased. For these cases, the relative error fell between 10%-20%, and although the absolute error generally grew along with the relative error, , the absolute error was still quite small, in all cases less than 0.07.

Table 31: Comparison between FOR and Monte Carlo Solutions As Mean Values Vary

Jensen Limit State							
Variable	*Base Value*	*Max Value*	*Min Value*	*β @ Max*	*β @ Min*	*Error @ Max*	*Error @ Min*
α_w	*4.7MPa*	*5.50MPa*	*2.00MPa*	*0.97*	*4.81*	*-0.1%*	*-5.2%*
β_w	*1.26*	*3.00*	*1.05*	*3.12*	*0.81*	*0.0%*	*4.4%*
Dcr	*1.0*	*10.00*	*0.55*	*4.49*	*0.79*	*-4.3%*	*2.1%*
M	*3.0*	*3.15*	*2.40*	*0.95*	*4.12*	*0.8%*	*-1.0%*
A	$3.31*10^{11}$ MPa^3	$4.00*10^{12}$ MPa^3	$2.25*10^{11}$ MPa^3	*4.73*	*1.07*	*-5.0%*	*-0.4%*
N	$3.2*10^7$	$6.0*10^7$	$3.0*10^6$	*0.75*	*4.57*	*2.3%*	*-4.4%*
de Souza and Ayyub Limit State							
Variable	*Base Value*	*Max Value*	*Min Value*	*β @ Max*	*β @ Min*	*Error @ Max*	*Error @ Min*
S	*13.47 MPa*	*15.50MPa*	*7.00MPa*	*1.04*	*4.06*	*-1.6%*	*-0.3%*
Ks	*1.0*	*1.15*	*0.53*	*1.05*	*3.57*	*-3.1%*	*11.2%*
Dcr	*1.0*	*7.00*	*0.70*	*4.03*	*1.12*	*-0.2%*	*-1.6%*
M	*3.0*	*3.15*	*2.30*	*1.06*	*4.10*	*-0.2%*	*-1.5%*
A	$3.31*10^{11}$ MPa^3	$2.20*10^{12}$ MPa^3	$2.20*10^{11}$ MPa^3	*3.97*	*1.05*	*-0.3%*	*-1.6%*
N	$3.2*10^7$	$5.0*10^7$	$4.50*10^6$	*1.00*	*4.05*	*-1.7%*	*-0.2%*

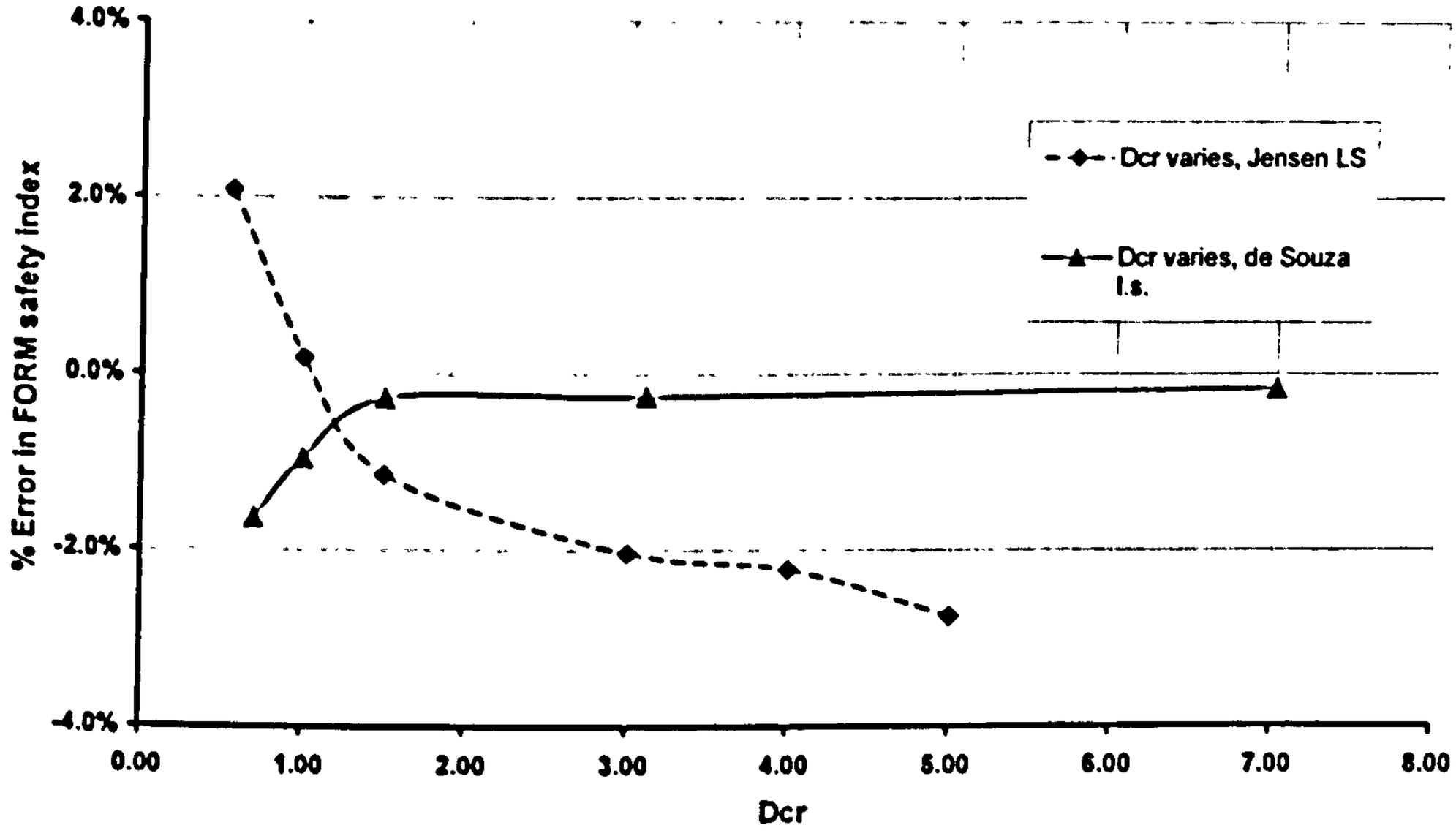

Figure 51: Typical Error Between FOR and Monte Carlo Methods

After varying the mean value of the input parameters, the COV of the input parameters was varied to see how that affected the accuracy of the FOR predictions. For the vast majority of the variables, the results were quite similar to the variations in the mean value of the variables. These results are summarized in Table 32 and Figure 52 below. The one exception was the β_w parameter in the Jensen limit state, where increasingly larger deviations were seen as the COV increased. This parameter is inside the argument of the Gamma function in the Jensen limit state, and consequently the limit state would be expected to be very non-linear in respect to this parameter. To avoid encountering very low safety indexes as the COV of β_w increased, the base case was modified when studying the COV of β_w, by reducing α_w to 2.7 MPa from 4.7 MPa.

Table 32: Comparison between FOR and Monte Carlo Solutions As COV Values Vary

Jensen Limit State							
Variable	*Base COV*	*Max COV*	*Min COV*	*β @ Max*	*β @ Min*	*Error @ Max*	*Error @ Min*
α_w	0.1	0.50	0.05	0.96	1.65	1.0%	-0.7%
β_w*	0.1	0.50	0.00	1.18	3.92	-20.8%	0.1%
Dcr	0.48	1.50	0.2	0.58	1.97	2.3%	-1.6%
m*	0.00	0.40	0.00	1.76*	4.11*	-62.9%	-7.7%
A	0.53	0.70	0.10	1.31	2.21	0.5%	-3.1%
*-Indicates that base case was adjusted to prevent running into very low safety indexes as the COV increased.							
de Souza and Ayyub Limit State							
Variable	*Base COV*	*Max COV*	*Min COV*	*β @ Max*	*β @ Min*	*Error @ Max*	*Error @ Min*
S	0.1	0.50	0.00	0.98	1.67	-1.0%	-0.9%
ks	0.1	0.50	0.00	0.79	1.67	4.5%	0.0%
Dcr	0.48	1.0	0.10	0.95	2.04	-1.4%	-0.8%
m*	0.00	0.30	0.00	2.47*	4.13*	-58.3%	-0.3%
A	0.53	0.80	0.15	1.19	2.13	-1.2%	-0.7%
*-Indicates that base case was adjusted to prevent running into very low safety indexes as the COV increased.							

This finding raised interest in investigating the accuracy of the FOR approximation if the S-N curve slope parameter, m, was allowed to vary as well. This analysis was carried out assuming that m followed a normal distribution. Additionally, the base case was modified so that a higher safety index was obtained when the COV of m was 0, to prevent running into very low safety indexes as the COV was increased. The COV of the intercept parameter, A, was also set to 0 to avoid the need to consider A and m correlated. Experimentation with alternative base cases showed that the error between the FOR and Monte Carlo methods seem to be primarily affected by the COV of m, with the parameters of the base case having a smaller influence. The results for the variation in β_w and m are plotted in Figure 52. This graph shows that the FOR approximation is significantly in error when there is any uncertainty in the S-N slope, m, or a COV greater than 0.1 for β_w. The errors are all conservative, but are of such a magnitude that the FOR approximation is not useful for engineering work in these situations.

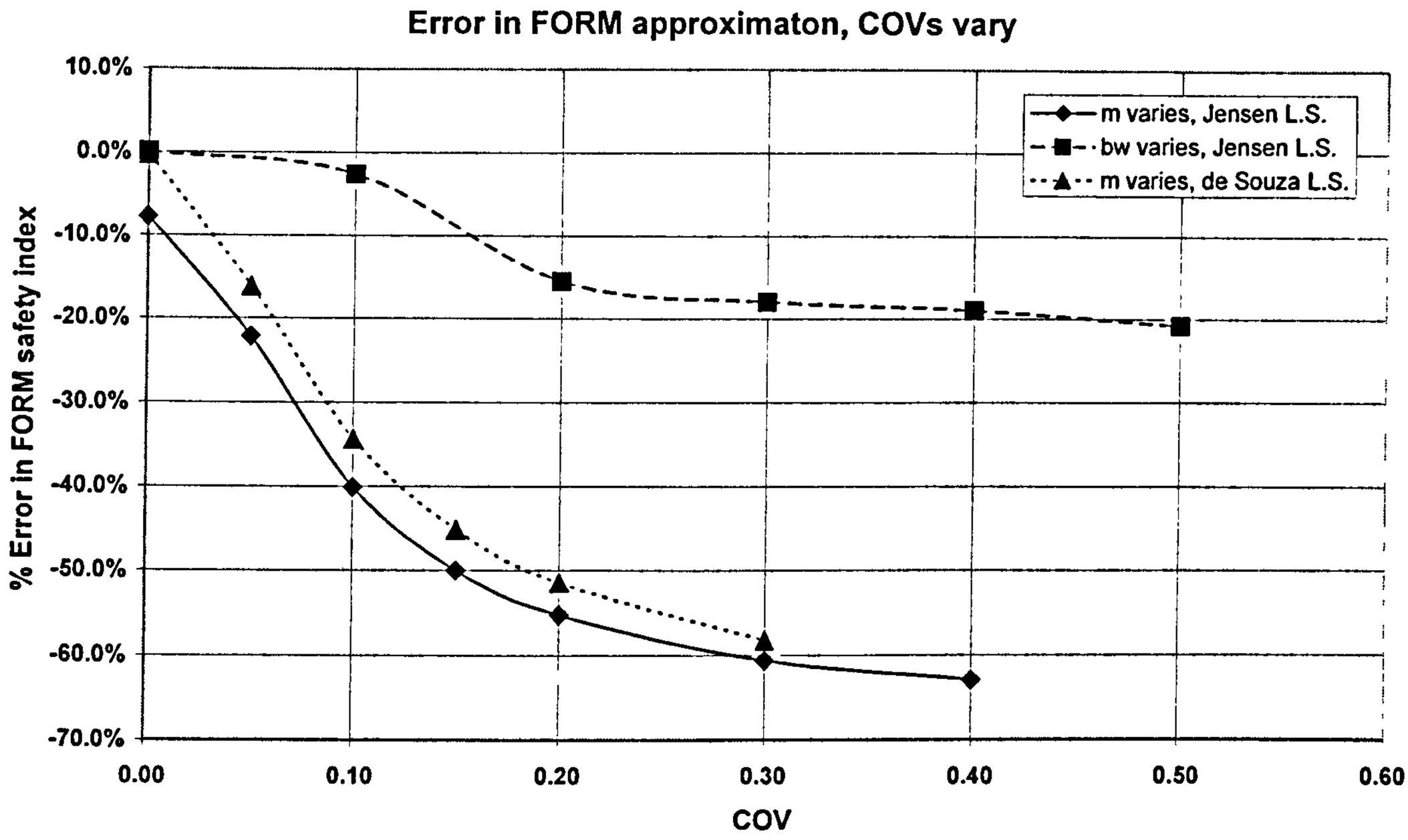

Figure 52: Errors with Increasing Uncertainty in m and β_w

With the current method, where the S-N slope is treated as constant, and the COV of β_w equal to 0.1, the FOR method will not suffer these large errors. However, in developing future methods in which m could be considered a stochastic variable, these differences between the FOR approximation and the Monte Carlo results should be considered. In such cases, a second-order method or a response surface method may be needed to produce accurate estimates of the probability of failure in an efficient manner. Similar conservative predictions occur when the COV of β_w is larger than 0.1. This finding should be borne in mind when using the FOR approximation of this limit state in situations where the long-term stress range is not known with high confidence. Overall, if m is treated as a deterministic variable, the FOR approximation of both limit states is quite good over a range of safety indexes likely to be encountered in design work. Observing the restrictions on the uncertainty of m and β_w, the FOR approach was used to compare the proposed to S-N curve and reliability formulation to existing design codes.

4.5.3 Comparison of the Proposed Method Against existing Approaches

4.5.3.1 Overview

The third and final step in the analysis of the proposed fatigue reliability method is to compare the results of the method to current fatigue design codes or recommendations. The

goal of such a comparison is to shed more light on what values of safety index should be considered "acceptable" for the new method. The application of the proposed method to the 150m reference vessel in Section 4.5.1 gave a rough idea of what type of safety index would be acceptable, however, as this reference vessel is not a complete design and as not all sources of loading were available for the vessel, it is hard to draw firm conclusions from this case. Therefore, in this section a comparison will be made with the IIW fatigue recommendations[207] and the U.S. Aluminum Association's(A.A.) *Specification for Aluminum Structures*[53]. These standards cover a wide range simple welded joints acting under a single type of loading, the simplicity of these joints makes them ideal candidates for comparison.

To compare the proposed methodology to the standards, the allowable stress range and number of cycles were computed for several structural details covered by these standards. These allowable stresses and number of cycles to failure were used as inputs to the proposed method along with the S-N curve values and uncertainties presented above in Table 30. The safety index was then determined by the FOR method. The resulting safety indexes give a measure of the safety index implied in the current fatigue design standards, which can then be used as a basis for assessing "acceptable" values for the safety index. Such an approach has been used before in developing partial-safety factors for load factor resistance design(LFRD), see for example Melchers[81] for a general discussion or Folsø et al.[206] for a recent example dealing with fatigue from the marine industry. In general, when performing such code calibration, it is necessary to obtain a "complete" engineering design for the detail by the code so that all of the partial safety factors specified on both the load and resistance side of the limit state in the code are included. In this respect, the two codes investigated here a special cases, in that the *Specification* specifies that unfactored stresses shall be used in the fatigue evaluation and the IIW leaves the partial safety factors on the load side up to the national code bodies to specify. For this analysis, a partial safety factor of 1.0 was used for IIW recommendations so that it would be in line with the *Specification* approach. Current marine design practice with the spectral approach to fatigue is similar in that any safety factors present tend to appear in the S-N curve itself, or the Miner-Palmgren damage summation at failure[85] However, were higher partial safety factors specified, the resulting safety indexes in this section would have been higher as well.

Four details were selected for the comparison study. The first detail is a simple butt weld. The second detail is a lap connection, typical for the ending of a long doubler plate investigated in Doerk et al.[220] in Section 3.1 of that reference. The third is a non-load bearing longitudinal attachment investigated in Fricke and Petershagen[221]. Finally, a

cantilever beam attached by load-bearing fillet welds is considered, also investigated in Doerk et al.[220], in Section 3.4 of that reference. These details were selected as they represent a broad range of structural connections typically found aboard HSV. They are shown in Figure 53.

As both the IIW recommendations and the *Specification* are based on the nominal stress approach, a hot-spot stress concentration factor had to be determined for each of these details. This data was largely available from previous studies, though some care is needed in order to obtain a consistent set of hot-spot stress concentration factors. Recently, there have been extensive studies of the effect of hot-spot stress analysis procedures on the resulting SCF[220, 222].

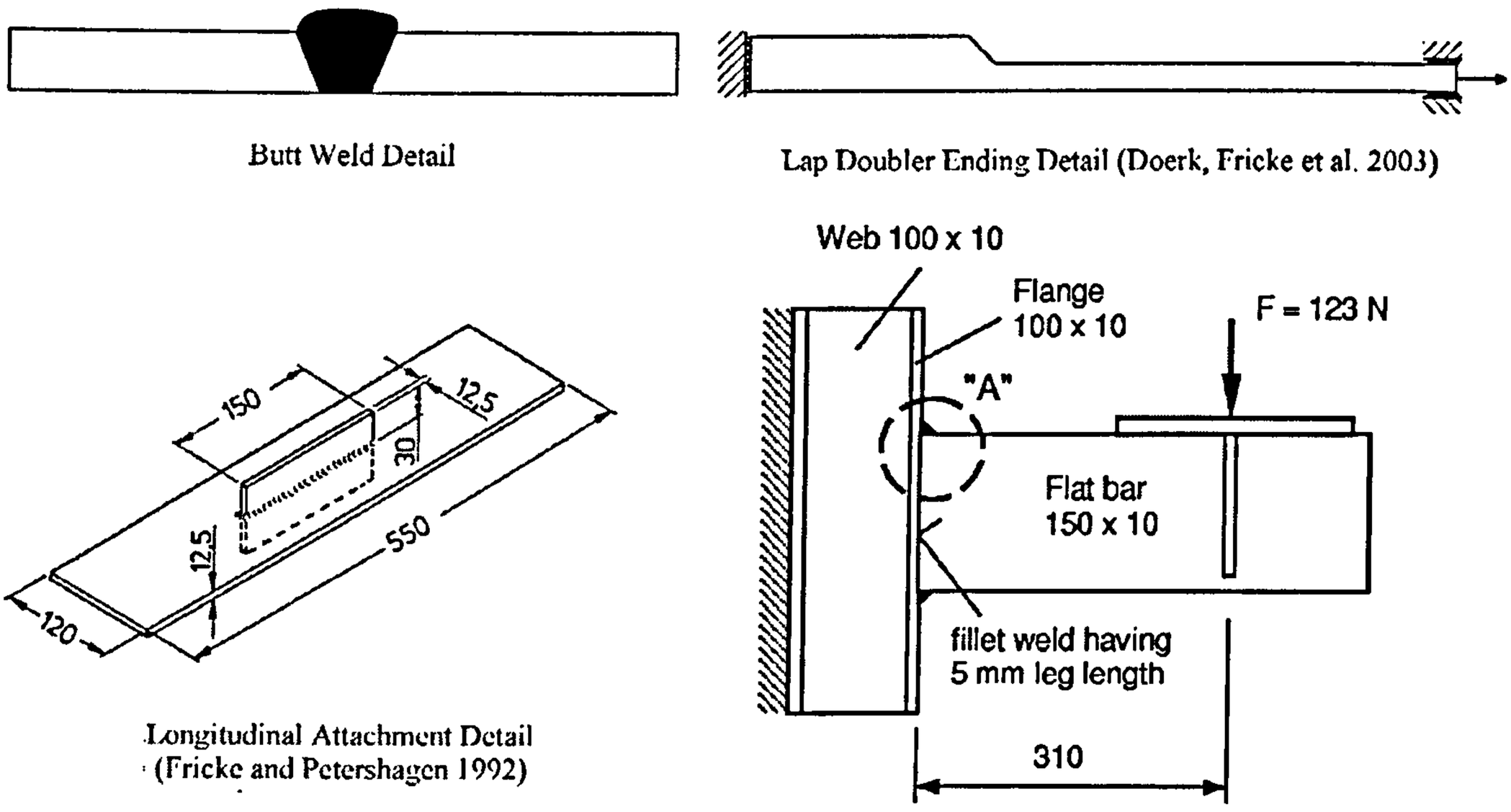

Figure 53: Details Selected for Comparison

In order to provide a consistent basis the SCF resulting from the IIW extrapolation was whenever available. For the butt weld, the SCF is equal to 1.0 as all the stress concentration is in the weld profile itself. Based on the current IIW recommendations (See Doerk, Fricke et al.[220] for example), the lap joint SCF would be determined by linear extrapolation while the cantilever connection would be determined by quadratic extrapolation. Quadratic extrapolation was also used by Fricke and Petershagen for the longitudinal attachment with good results, although current IIW recommendations would use linear extrapolation for such a joint today. However, based on the results of Fricke and Petershagen's study, it was decided to use their original quadratic extrapolation method. The hot-spot stress concentration factor for each detail is shown in Table 33 below.

Table 33: Hot Spot Stress Concentration Factors

Detail	*Hot-Spot SCF*
Butt Weld	*1.0*
Lap Doubler Ending	*1.19*
Longitudinal Attachment	*1.40*
Cantilever Attachment	*1.77*

With the hot spot stress concentration factors determined, the next step is to determine the safety factor of each detail for the allowable stresses in the IIW and Aluminum Association design standards. The results of these two comparisons will be presented in turn.

4.5.3.2 IIW Results

The first code comparison was made with the International Institute of Welding fatigue recommendations published by Hobbacher[207]. These recommendations are based on the experiences of the IIW and have formed the basis of several fatigue studies in recent years. They include both steel and aluminium details, and are based on the nominal stress approach. To predict the fatigue strength of a structural detail, the detail is first matched to a reference detail in the standard. Each reference detail in the standard has its fatigue strength expressed in terms of FAT curve. The value of the FAT curve is the nominal stress fatigue strength in MPa at a life of 2 million cycles. For all the welded aluminium joints in the standard, the slope constant of the S-N curve is 3.00. For the four details used in the comparison study, the corresponding reference detail and FAT curve are listed below in Table 34. One of the disadvantages of the nominal stress approach is that there is often difficulty matching the details in question to reference details in the standard, and this study was no exception. The standard contains several different butt weld details, some with requirements for non-destructive testing, some without, some single-sided and some double sided. All of the welds have a hot-spot concentration factor equal to 1.0, but different fatigue strengths. A double-sided butt weld without any non-destructive testing requirement was settled on for this study; however, if a single-sided weld had been selected the butt weld safety indexes below would have been higher, while if a double-sided weld with non-destructive testing had been selected they would have been lower. As similar difficulty was encountered with the longitudinal attachment. The longitudinal attachment has a length of 150mm which places it right on the cut-off between two FAT classes in the IIW recommendations. Had this detail been slightly shorter, it would have had a FAT class

of 25 MPa, resulting in lower safety indexes than those reported below. This source of variability should be kept in mind when reviewing the results below.

With the reference details decided upon, the next step was to convert the reference detail allowable stresses range into the form required for the two limit state equations. For the de Souza and Ayyub limit state, no modifications are required. For the Jensen limit state the relation is expressed in Equation 56 , it is possible to construct an infinite number of α_w and β_w combinations which would correspond to Weibull distributions with the same 3rd moment as the constant-amplitude stresses from the fatigue recommendations. To get around this problem, three values for β_w were assumed, 0.8, 1.0, and 1.2, as previous studies have shown that the long-term stress distribution for ships typically has a Weibull shape parameter in this range. Then the corresponding α_w values were computed. The IIW recommendations use a S-N curve with a m value of 3.00, the same as the hot-spot S-N curve used in the proposed reliability method. This slope means that for the IIW allowable stresses, the safety index resulting from the reliability model will be invariant with the number of cycles. With the loading determined, the safety indexes were found via the FOR approach and are listed below in Table 34. The fatigue resistance and all the uncertainties were kept the same as in the 150m reference vessel study, and are listed in Table 30.

Table 34: Results from IIW Comparison

	Butt Weld	*Lap Doubler Ending*	*Longitudinal Attachment*	*Cantilever Attachment*
IIW reference detail		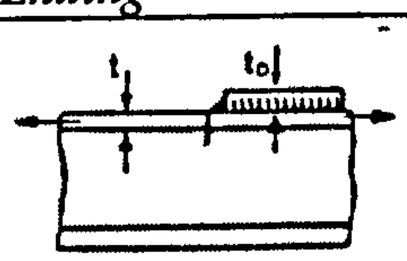	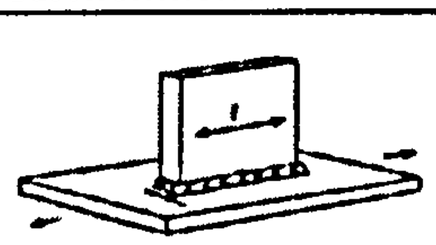	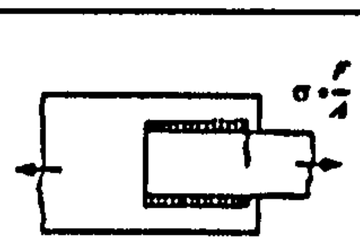
IIW reference detail number	*213*	*711*	*521*	*612*
FAT class	*FAT 32*	*FAT 18*	*FAT 20*	*FAT 18*
Safety Index, Jensen, β_w=0.8	*1.46*	*2.54*	*1.84*	*1.47*
Safety Index, Jensen, β_w=1.0	*1.65*	*2.94*	*2.10*	*1.67*
Safety Index, Jensen, β_w=1.2	*1.76*	*3.21*	*2.25*	*1.78*
Safety Index, De Souza & Ayyub	*1.77*	*3.30*	*2.28*	*1.79*

The safety indexes fall between 1.46-3.30, which is a rather large spread. However, a large part of this spread appears to be the result of the difficulty in matching the details under comparison to reference details in the code. Note that the butt weld, which had the lowest safety indexes could have returned higher values if a single-sided weld had been

chosen for the reference detail. The average value of safety index is 2.11, slightly higher than the safety index for the 150m reference case. These results will be reviewed further, along with the results from the Aluminum Association in Section 4.5.3.4.

4.5.3.3 Aluminum Association Results

The U.S. Aluminum Association's *Specification for Aluminum Structures*[53] contains a similar fatigue design standard to that of the IIW. The nominal stress approach is used again, although there are fewer reference details and only six S-N curves, compared to the 15 FAT classes of the IIW recommendations. Furthermore, the S-N curves of the *Specification* have different slopes, covering a range from 6.85 to 3.42. This means that when comparing to the proposed reliability method, which uses a fixed slope constant of 3.0 for all joints, the safety index will vary with the number of applied cycles as well as the detail under consideration. Therefore, the comparison between the proposed method and the *Specification* was made at both 10^6 and 10^8 cycles, which should roughly be indicative of the number of cycles expected in service for wave loading on high-speed vessels. It must be noted that Tveiten's S-N tests, on which the proposed S-N curve is based, only covered up to $5x10^6$ cycles, so applying the method at 10^8 cycles is somewhat speculative. The reference details, reference curve letters, reference curve slopes, and results from the FOR comparison with the Specification are presented below in Table 35, in a similar format to the IIW comparison discussed above. As with the IIW comparison, the fatigue resistance and all the uncertainties were kept the same as in the 150m reference vessel study, which are listed in Table 30.

The impact of the Specification using reference curves with a slope constant higher than three is immediately apparent in the table of results. These higher slope constants translate into increased allowable stresses at longer lives compared to the proposed reliability method. When these higher stresses are entered into the reliability method, the resulting safety indexes are very low, as low as 0.49 for the butt weld at 10^8 cycles. As the present study includes no fatigue data in this high-cycle range, it is impossible to say if the current method is too conservative, or if the Aluminum Association recommendations are too optimistic at high cycles. Based on the available test result, the Aluminum Association "B" curve appeared to be increasingly optimistic at high cycles(see Figure 48). The IIW recommends a slope of 3.0 for welded joints in aluminium under variable amplitude loading, regardless of the number of applied cycles. However, the experimental justification for either the Aluminum Association or the IIW curves in this high-cycle region are not known. This is particularly troubling, as many high-speed vessels details would be expected to be subjected to 10^7 to 10^8 cycles.

Table 35: Results from Aluminum Association *Specification* Comparison

		Butt Weld	*Lap Doubler Ending*	*Longitudinal Attachment*	*Cantilever Attachment*
A.A. reference detail		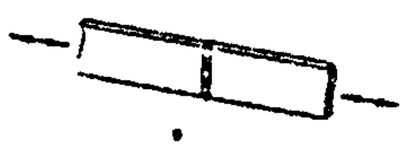	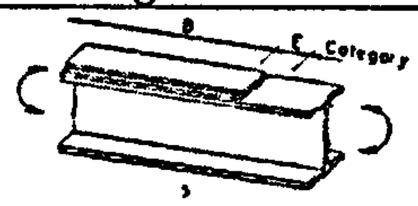	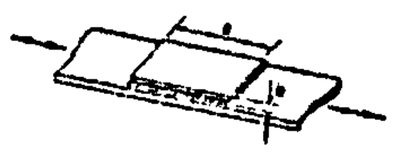	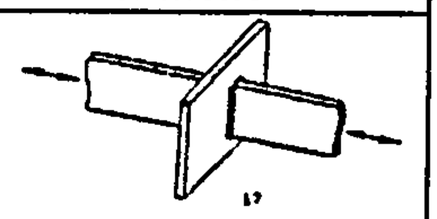
A.A. reference detail number		*9*	*5*	*20*	*17 or 18*
Reference curve letter and slope		*C/3.64*	*E/3.45*	*E/3.45*	*E/3.45*
10^6 cycles	*Safety Index, Jensen, β_w=0.8*	*1.76*	*3.11*	*2.74*	*2.16*
	Safety Index, Jensen, β_w=1.0	*1.86*	*3.56*	*3.11*	*2.38*
	Safety Index, Jensen, β_w=1.2	*1.89*	*3.86*	*3.32*	*2.50*
	Safety Index, De Souza & Ayyub	*1.52*	*3.77*	*3.15*	*2.26*
10^8 cycles	*Safety Index, Jensen, β_w=0.8*	*0.96*	*2.65*	*2.25*	*1.60*
	Safety Index, Jensen, β_w=1.0	*0.94*	*3.00*	*2.50*	*1.72*
	Safety Index, Jensen, β_w=1.2	*0.89*	*3.20*	*2.62*	*1.76*
	Safety Index, De Souza & Ayyub	*0.49*	*3.01*	*2.39*	*1.50*

The comparison at 10^6 cycles is broadly similar to the IIW results above. The range of the safety indexes reported is 1.52 to 3.86, compared to 1.46 to 3.30 for the IIW recommendations, with the butt weld being the lowest and the lap doubler ending being the highest. The average safety index is slightly higher, 2.68 for the results at 10^6 cycles compared to 2.11 for the IIW results. Overall, for both 10^6 and 10^8 cycles the average safety index for the comparison to the *Specification* is 2.33. The increased variability the Specification result may also be a result of there only being six reference S-N curves to cover

all the detail types, this leads to the lap double ending, the longitudinal attachment, and the cantilever attachment all using the "E" curve, though the hot-spot stress concentration factor varies from 1.19 to 1.77 for these details.

4.5.3.4 Summary of Code Comparison

The proposed FOR reliability method, including both the Jensen and de Souza and Ayyub limit states was compared to the IIW and Aluminum Association fatigue design standards. Overall, the results of the comparison showed safety index values ranging between 0.49 and 3.86, though many were in the range of 1.5-3.0 when high-cycle fatigue is excluded. Including both low and high cycle fatigue, the mean values of the safety index corresponding to the IIW recommendations was 2.11 and for the Aluminum Association recommendations was 2.33. If the variability is temporarily excluded, the mean values seem to agree well with previous studies. Mansour et al.[22] recommends target safety indexes for fatigue failures which range from two to four, depending upon the seriousness of the failure. These recommendations were used by Ayyub et al.[40]. In a recent study, Folsø et al.[206] determined the safety index for a range of fatigue details in ships designed to RINA, BV and GL classification society rules. The resulting values fell between 1.2 and 2.4, and Folsø et al. established 1.5 as a target safety index for new design guidelines. This agrees well with the results in the tables above. Many authors also used a C.O.V. of 0.3, not 0.48 on the Miner's sum damage at failure. While the recent research suggests a C.O.V. closer to 0.5, if a C.O.V. of 0.3 had been adopted, higher safety indexes would have resulted. It is also interesting to note in passing that many non-reliability based fatigue design recommendations instruct engineers to make their best estimate of applied loadings, and then use a S-N curve equal to approximately two standard deviations from the mean curve[98], implying a probability of failure equal to a safety index of two, which is again in agreement with these results.

The high variability that marked the results seems to be largely a result of the difficulties of the nominal stress approach, where obtaining exact matches between the detail in questions and the reference details in the design standard is difficult. Additionally, some design standards, such as the Aluminum Association *Specification*, use very few reference S-N curves, which results in details with different hot-spot stress concentration factors being assigned to the same S-N curve and end up with the same fatigue lives. When such approaches are compared to a hot-spot approach, where each individual hot-spot stress concentration factor is used in the calculation, scatter is inevitable. One of the potential advantages of the hot-spot approach is that, at least theoretically, it should be able to achieve a more consistent level of safety than the nominal stress approach.

However, the hot spot approach itself is also responsible for some of this scatter as well. This could be seen with the butt weld results. The hot-spot method implicitly assumes that the fatigue properties of each type of weld are similar enough to be represented by a common S-N curve, which only needs to be modified by the hot-spot stress concentration to account for the effect of the local structural arrangement. Thus in the hot-spot approach all butt welds would be treated the same. This is not the case in the design recommendations, the IIW fatigue recommendations assign fatigue classes of FAT 18 to FAT 50 to different type of butt welds, depending on the joint type and non-destructive testing used. While a FAT 32 weld was chosen for this comparison, the safety indexes for the butt weld could have been raised or lowered significantly by adopting a FAT 18 or a FAT 50 weld instead. This supports the notion that some restriction should be placed on type of weld each hot-spot method is applicable to. For example, the curve developed here was based on Tveiten's experiments with fillet welded joints, so perhaps this method should be limited to fillet-welded connections. Such an approach may have removed some of the variability from the results.

A more alarming conclusion from the comparison study was the variability of the safety index in the high-cycle fatigue region between the two design standards used for comparison. This is the region in which most details on HSVs will be designed. While the proposed reliability method and the IIW fatigue recommendations both use a S-N curve slope constant of three, the Aluminum Association *Specification* uses a higher slope constant, leading to more optimistic fatigue predictions at longer lives. If the *Specification* is correct, designing using the proposed reliability method or the IIW recommendations would lead to significantly over-designed structures, with a corresponding weight, performance, and cost penalty. On the other hand, if the IIW approach is correct, a vessel designed to the *Specification* would suffer extensive cracking before it service life was completed, requiring costly repairs and down time. The current experimental evidence cannot resolve this discrepancy, as none of the fatigue test programs reviewed in Section 4.4 above tested at or above 10^7 cycles. However, to test details in the range of 10^7 to 10^8 cycles is usually an undertaking that will take weeks or months on the test rig, and thus is not always practical.

Overall, the proposed reliability method compared well with established design codes, suggesting a safety factor in the region of two would be appropriate. As at present, only a few comparisons have been made, further comparisons are required before using the developed fatigue reliability method in a design setting. The method shows potential for reducing the variability in safety margin that can result from using the nominal stress

approach. While the current data used in this method should be further verified in the high cycle fatigue region, the basic mechanics of the method appear sound.

4.6 Conclusions

This chapter reviewed the current situation in aluminium fatigue, specifically for marine HSV applications, constructed an aluminium-specific fatigue reliability method using hot-spot stress approach, and analyzed the accuracy and suitability of the new approach. The S-N approach using the Miner-Palmgren damage summation was selected for the reliability methodology, as this method is widely used and researched in the marine industry. A hot-spot stress analysis approach was selected for the analysis as the current situation in aluminium fatigue means that this approach has several advantages over the nominal stress and notch stress approaches. Two limit states, one proposed by Jensen and one proposed by de Souza and Ayyub were used in the reliability formulation. The mean fatigue capacity of aluminium welded connections was represents by a S-N curve derived from previously published test results on large aluminium structural details typical of HSV construction. The published test results had wide scatter, and could not all be combined into the final curve. Test results from Tveiten's experimental program were selected, yielding a S-N curve with a fixed slope constant of 3.0 and intercept parameter of 3.31×10^{11} MPa^3 with a COV of 0.53. A Miner-Palmgren damage summation of 1.0 was used, with a COV of 0.48

The proposed reliability method was applied to the 150m reference vessel from Chapter 2, using estimated long-term loading and uncertainties. Both the Jensen and the de Souza and Ayyub limit states performed well, and an initial safety index value of 1.56 was obtained. Because of the high level of non-linearity and uncertainty in the fatigue reliability formulation, an extensive comparison study was undertaken between the FOR reliability method and Monte Carlo simulations to determine if the FOR approach is adequate for use with the fatigue limit state. With the exception of variable S-N curve slope constants, or high variability in the Jensen limit state Weibull stress distribution shape parameter, the FOR method performed very well, with typical error magnitudes less that 5%. Both the Jensen and de Souza and Ayyub limit states performed similarly. The proposed reliability method was compared to existing fatigue design recommendations, to determine what value of safety index would correspond to the level of safety in existing design standards. Comparison to the IIW standards and the Aluminum Association *Specification* showed that a safety index value of roughly 2.0-2.5 is appropriate. This value was in good agreement with previous studies. The comparison showed a high variability in safety indexes for different joint configurations, this variability seemed to be related to the difficulties inherent in the nominal stress approach of the existing design standards, and also partly difficulties of

represent different weld types in the hot-spot approach. The two design standards did not agree in the high-cycle fatigue region where most high-speed vessel designs will operate, and the published test programs did not include any data in this region to shed light on which standard might be more realistic. While the mechanics of the proposed reliability appear sound from the comparison, the problem with data in the high-cycle region should be born in mind when reviewing the methodology for application to design. This disagreement and range of scatter are not unique in marine fatigue predictions, similar examples of scatter for large steel commercial vessels were presented in the literature review.

Overall, the proposed hot-spot S-N fatigue reliability model works well and represents a worthwhile extension of the existing S-N fatigue design method. Use of a reliability model such as this one will allow designers to better understand the actual risk of fatigue failures occurring in service. As with the ultimate strength reliability model, the uncertainty values can be adjusted to reflect the designer's confidence in the strength and loading estimates. If the uncertainty values are restricted so that the FOR evaluation method can be used, the reliability calculation is not much more computationally complex than the existing S-N fatigue calculation. Further comparison studies and more high-cycle S-N data should be incorporated before this method is used for design.

CHAPTER

5

"Fatigue is an important design consideration in most aluminum structures, and the most difficult problem to resolve" [9 page 223]

Initiation-Propagation Fatigue Formulations: An Initial Review

5.1 Overview of Initiation-Propagation Approaches

Chapter 4 showed that a conventional S-N fatigue approach can be successfully recast into a reliability based fatigue formulation; however, as a limit state equation the basic S-N approach leaves something to be desired. From a reliability standpoint, one of the most significant limitations of the S-N fatigue approach is the feedback the method gives the engineer about the seriousness of the fatigue failure. Failure in the S-N approach is the Palmgren-Miner index reaching unity, which indicates that a crack is present in the structure. However, the method gives the engineer no information on the size or seriousness of this crack. In this sense, the failure predicted by the Palmgren-Miner index is a serviceability limit state, not an ultimate limit state, as typical HSV structure has sufficient redundancy to accept further loading even with several small cracks present. Thus, the engineer cannot directly compare the safety index calculated in Chapter 3 for ultimate strength with that in Chapter 4 for fatigue failure, there are simply too many unanswered questions. How big a crack will exist in the detail? How fast will it grow? What will happen to the surrounding structure when it grows? Philosophically, the S-N fatigue formulations are simply not compatible with reliability-based ultimate limit state design for HSV as they do not address an ultimate limit state.

To investigate and understand the significance of a potential fatigue crack on the safety of the overall structure requires going beyond the pass-fail S-N approach, and constructing a fatigue model capable of predicting the size of the crack in the structure at any time. This information can then be used to examine the impact of the crack on the structure over time, including final fracture or collapse of the crack-weakened section. Fatigue models capable of predicting both the initiation and growth of a crack are known as initiation-propagation(I-P) models, and form one of the *local approaches* to fatigue life prediction[223].

Typically these models use a stress or strain life approach to determine the initiation period where the material is being loaded cyclically but has not yet developed a single dominate crack . Once such a crack forms, its growth is estimated by a fracture mechanics model. By doing so, the I-P fatigue approach is a useful engineering improvement on the S-N fatigue approach as it more closely approximates the physical process of fatigue. The I-P approach gives additional useful information about the structure's safety to the engineer. It is important to stress from the outset that the I-P approach is still an engineering approximation, and is not a true physical model for the process of fatigue. Radaj[223] has depicted this point graphically:

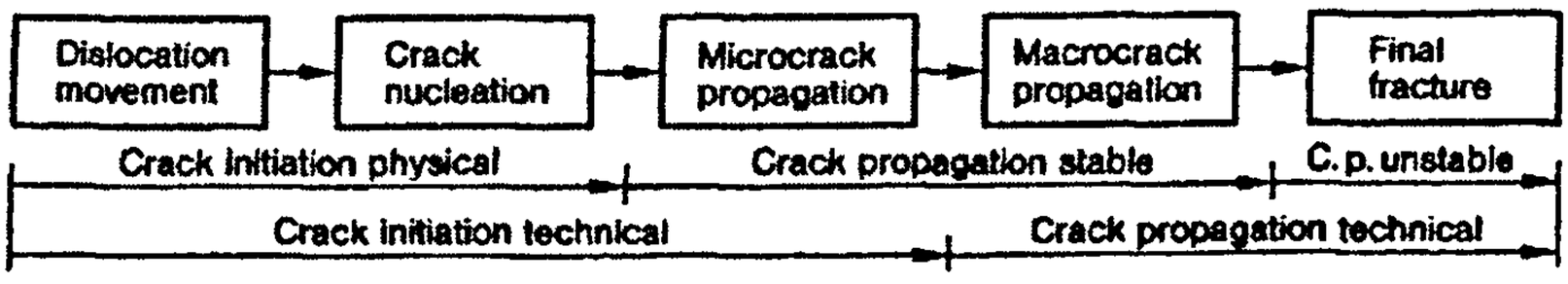

Figure 54: Fatigue Process Radaj[223]

In Figure 54 the current understanding of the physical process of fatigue is shown in the uppermost level of rectangles. Two levels of engineering approximation are shown below, the I-P approach is equivalent to the bottom line, consisting of two phases, initiation and propagation. In the S-N approach, the entire process would be viewed as one phase, ignoring the details of initiation and final fracture. While the I-P produces more information than the S-N approach, the complexities of modelling the physical processes of dislocation, nucleation, and micro-crack propagation have been removed. The I-P model therefore consists of two distinct stages. The first is the technical initiation period for the crack, this represent the time required for dislocations to nucleate into micro-cracks, and for these micro-cracks to grow and combine into a dominate crack which is large enough to be modelled by traditional engineering fracture mechanics. Typically this is taken to be a crack with a depth on the order of 0.25mm-0.5mm. The second phase is the crack propagation phase, where traditional engineering fracture mechanics approaches are used to determine the crack size as it grows towards final fracture. The total fatigue life is taken as the sum of these two periods.

This approach can be rendered into a stochastic framework by considering both the initiation period and the growth rate as stochastic variables. Thus, the model will account for the uncertainty in fatigue predictions by calculating both the probability of initiation and the probability density function of crack size at any time instead of a deterministic crack size.

This approach is fairly advanced in the aerospace industry, and some initial attempts have been made in the marine field as well. The approach is depicted graphically in Figure 55.

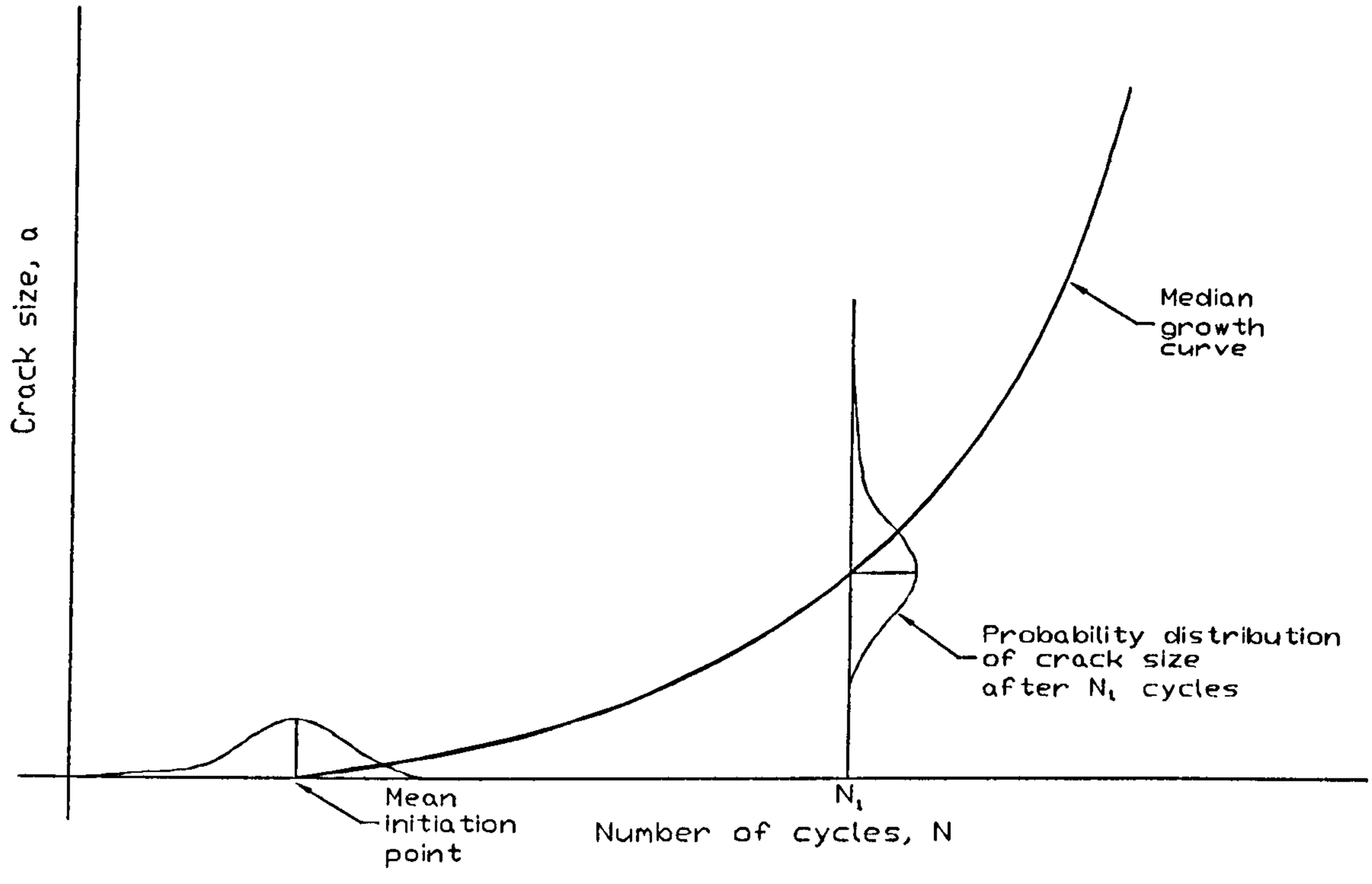

Figure 55: Mean and Probabilistic Initiation-Propagation Fatigue Modelling

Unlike the S-N approach which is now fairly well standardised, there are many different approaches to the individual components of the I-P model which have not yet been formalised into a recommended approach[223]. Probabilistic models have been proposed for specific instances, but are in general even less formalised. In the next section, a literature review will be presented on the different aspects of, and approaches to, the I-P fatigue model. This will include marine papers which deal with components of the I-P approach or the overall approach. Then, the mechanics of one particular implementation of the I-P model will be discussed in some detail. This will be followed by a trial application to the fatigue life of aluminium butt welds. Unfortunately, sufficient experimental data and time were not available to generate a full stochastic model for HSV-type details, however possible extensions of the model developed will be discussed.

5.2 Literature Review

The I-P fatigue model is typically composed of an initiation period which is modelled by a strain-life or stress-life approach, followed by a fracture mechanics crack growth period. Similar to the S-N approach, an enormous amount of material has been published on the initiation-propagation approach and its components. To keep this literature review manageable, attention will be focused on the key papers that set up the framework and

components of the I-P approach, recent marine applications of the approach, and efforts to implement the approach in a stochastic or reliability-based framework. The fundamentals of the strain-life, stress-life, and fracture mechanics approaches can be found in any reference book on fatigue. Sharp, Nordmark, and Menzemer's *Fatigue Design of Aluminum Components and Structures*[176] is a useful book focusing on aluminium, while Stephens et al.'s *Metal Fatigue in Engineering*[169] is an excellent general reference on all three of these prediction methodologies. To move beyond the fundamentals into the details of the numerous strain-life, stress-life, fracture mechanics, and I-P models proposed to date, Radaj and Sonsino's work *Fatigue Assessment of Weld Joints By Local Approaches*[224] is an invaluable reference. Not all of these local approaches will be covered in this section, more information can be found in Radaj and Sonsino's book. The Eurocode 9[60] and the IIW Fatigue Recommendations[207] contain limited discussion on fracture mechanics approaches.

The I-P model is usually implemented as a combination of a strain-life approach to crack initiation and a fracture mechanics approach to crack growth. The strain-life approach to fatigue is based upon the well-known Manson-Coffin relationship proposed in 1962[225], where the fatigue life of a specimen is expressed in terms of strain amplitude:

$$\varepsilon_a = \frac{\sigma_f'}{E}(2N_f)^b + \varepsilon_f'(2N_f)^c$$

Where:

ε_a Applied strain amplitude

N_f Number of cycles to failure

σ_f' Fatigue strength constant

E Elastic modulus

b Fatigue strength exponent

ε_f' Fatigue ductility constant

c Fatigue ductility exponent

Equation 58

This approach is able to predict the formation of cracks over a wide range of fatigue conditions, from high cycle fatigue to low cycles fatigue. Once the crack is formed, its development is modelled by fracture mechanics. The modern basis for the vast majority of fracture mechanics formulations stems from work conducted in the 1950s and 1960s on modelling crack propagation. At this time a relationship proposed by Paris[226, 227] emerged as the most rational and consistent over a broad range of experimental data. This was demonstrated in a landmark paper published by Paris and Erdogan[228] , and has lead to this relationship being termed the Paris Law or the Paris-Erdogan Law:

$$\frac{da}{dN} = C(\Delta K)^m$$

Where:

$\frac{da}{dN}$ Crack growth rate per load cycle

C Crack growth constant

ΔK Applied crack tip stress intensity factor range

m Crack growth exponent

Equation 59

Fracture mechanics has remained an area of active research since this time, and improvements and refinements to the relationship proposed by Paris have been put forward from all quarters, with significant work on improving the predictions for short cracks, determining the threshold below which cracks do not propagate, and examining the influence of cycle-to-cycle interaction on the rate of fatigue crack growth. For further discussion on these topics and additional sources of reference the reader is referred to the texts of Stephens et al.[169] and Barsom and Rolfe[175] for general fracture mechanics review, and that of Sharp et al.[176] for aluminium-specific data and considerations. The work of Barlsom and Rolfe also includes an interesting marine case study on applying fracture mechanics to oil tankers in the Trans Alaska Pipeline Service. An recent historical review and commentary on fracture mechanics has been published by Paris[229].

Lawrence et al.[230] suggested combining the initiation life and the propagation life of a weld to obtain the total fatigue life. Each of these lives could be calculated independently, and Lawrence et al. demonstrated the use of the strain-life technique to estimate the initiation life of welds in several materials. This includes analytical methods for approximating the strain at the root of a weld notch, based on the Neuber and Peterson equations, which will be reviewed in Section 5.3. Lawrence et al. coupled the initiation life and the propagation life by assuming that the end of the initiation life represented a crack of 0.25mm in size, an approach that has been widely adopted since. This approach has become known as the Lawrence approach[224]. Socie et al.[231] applied a similar approach to fatigue in steel and aluminium, but constructed an analytical model for the transition between initiation and propagation life where the material at the fatigue initiation location is subdivided into several elements which can fail by initiation or propagation. The transition from initiation to propagation is made when the rate of advance by propagation exceeds that from initiation.

Sakai et al.[184] carried out an extensive study on the fatigue of annealed 5083 aluminium stiffened panel structures for the construction of SPB-type LNG tanks, including both local fatigue life and crack propagation. While they did not attempt to couple their

analysis into an I-P model, their work represents a valuable source of data for crack initiation and growth in marine-type structures made of 5083 alloys. Ho and Lawrence[232] presented further analysis of the Lawrence approach for cruciform and lap welds under high-cycle and variable-amplitude fatigue. Ho and Lawrence simplified the Mason-Coffin relationship for long fatigue lives by assuming the elastic component of the relationship will be dominant, and can be used alone. With this simplification, good agreement was seen between the experimental and predicted fatigue lives. Ho and Lawrence note that with their model, the fatigue crack initiation period can be significant in the long fatigue life region, despite the common assumption that welds have negligible fatigue crack initiation lives. They also note that bending stresses from joint distortion and incorrect alignment of the joint components may significantly influence the calculated fatigue life.

As these through-life fatigue models developed, interest grew in combining them with reliability approaches to handle the large scatter observed in fatigue experiments. A significant stochastic fracture mechanics model is the lognormal random process model which was developed in the aerospace world. While this model does replaces the initiation life with a pre-existing initial flaw based on the limits of the inspection given the structure, it models the crack growth life in a stochastic manner. The initial applications of this model was in the analysis of jet engine components[233]. However, the majority of the subsequent development was focused on fatigue of aerospace aluminium alloys, which was presented as part of a volume on probabilistic fracture mechanics[234]. The basic premise of the model is that a deterministic crack growth law, L(ΔK, …) which could be any of the crack growth laws such as the Paris-Erdogan law, can be randomized by multiplying it by non-negative random process with a median value of one, X(t). This process is initially taken as a stationary lognormal random process:

$$\frac{da(t)}{dt} = X(t)L(\Delta K,...) \qquad \textit{Equation 60}$$

Where the crack growth is now expressed against time instead of cycles. This has the significant advantage that existing (and perhaps quite complex) deterministic crack growth rate procedures can continue to be used, as long as a method of determining the appropriate characteristics of X(t) are available from test data. Further, if Z(t) is defined as

$$Z(t) = \log(X(t)) \qquad \textit{Equation 61}$$

Z(t) will be a stationary normal random process. Because the median value of X(t) is unity, the mean of Z(t) is 0.0. Therefore, Z(t) can be described by its autocorrelation function, R_{zz}, alone. From previous measurements and observations of fatigue striations left in the wake of propagating fatigue cracks, Yang et al. note that the distance between these

striations is correlated, and that this correlation decreases with increasing distance along the crack path. Based on this observation, Yang et al. hypothesized that the autocorrelation function for Z(t) could be adequately represented by an exponential decay function of τ, where τ is the time difference used to compute the correlation:

$$R_{zz}(\tau) = \sigma_z^2 e^{-\xi|\tau|} \qquad \textit{Equation 62}$$

Yang et al. considered three potential cases, first when ξ goes to infinity, when ξ is zero, and when ξ is between infinity and zero. The first case, there is no correlation unless τ=0, and the process is the white noise process. This leads to the smallest predicted scatter of crack length, and Yang et al. term this the most un-conservative and unrealistic model. If ξ goes to zero, the autocorrelation function becomes the variance of the process, and the process is completely correlated. Thus, a crack which starts out with growing quickly will always have a fast growth rate. This is conservative with the highest scatter, but has the advantage that the lognormal random process X(t) reduces to a simple lognormal random variable X, allowing analytical expressions to be developed for the distribution of time to reach a particular crack size, or the distribution of crack size at a particular time. In the third case, x was estimated from experimental results, and a Monte Carlo simulation was used to predict the distribution of crack lengths after different time intervals as no analytical solution was available. Either treating ξ as 0 or estimating it from experimental results produced good agreement between the model and the observed crack growth rates from experiments. Yang et al. developed these expressions for power crack growth law that was shown to be a good match for cracks growing from rivet holes.

Yang and Manning[235] extended the lognormal variable simplification of the lognormal random process model into a non-stationary approach, by dividing the crack growth curve into a series of segments, each with its own value of X, X_j. This retains the advantage of keeping the deterministic crack-growth calculations separate from the stochastic modelling, while further refining the stochastic model. Yang and Manning also discuss how to incorporate uncertainties from stress analysis and applied loading, in addition to the material variability in the distribution of X. Finally, the resulting method, using Equation 62 was applied to a series of bolt-hole fatigue tests on 7475-T7351 aluminium specimens, with good agreement being observed. However, allowing the standard deviation of X to vary over the crack growth process resulted in only small improvements in accuracy, leading the authors to conclude that in practical applications, a constant standard deviation may still be applied.

Yang and Manning[236] expanded upon their previous work by developing an analytical approach that can handle the lognormal random process model with variable

correlation. In their previous work, only the lognormal random variable model could be solved analytically, and the lognormal random process model required Monte Carlo simulation. However, the first two moments of the integral of the lognormal random process can be determined, and by assuming that this integral will follow a lognormal distribution it is possible to develop analytical expressions for the crack size distribution at any time. The effect of varying the correlation was examined by using the model to investigate a series of aluminium fastener hole tests. The approach was not extended to include probabilistic initial flaw sizing as information did not exist about distribution of initial flaw sizing.

The approach of Yang and Manning was further studied by Wu and Ni[237], who tested a measured the crack growth in 30 2024-T351 aluminium crack specimens as part of a study on the reliability of aging aircraft made of 2024-T351. Wu and Ni reported good agreement using Yang and Manning's approach with the Paris-Erdogan crack growth law. Similar to Yang and Manning, they concluded that treating randomizing factor is simple a lognormal random variable was sufficiently accurate.

Similar work was ongoing in the offshore industry. Shetty and Bakler[238] presented the reliability of an offshore tubular joint in fatigue. The crack growth relation was again expressed in a deterministic form, however the inputs to this relationship were treated as stochastic variables, and the FOR approach was used to calculate the safety index for fatigue limit states involving the crack growing through the tube wall and from fracture. This method assumed a stochastic initial flaw size, but no initiation period. Lecsek et al.[239] using Monte Carlo simulation to estimate mean fatigue life and uncertainty in the fatigue life of thick T-joints representative of tubular connections on offshore structures. The methodology adopted followed the general structure of Lawrence's approach, with both the initiation and propagation lives treated stochastically. The model include the effects of multiple potential initiation sites and multiple cracks occurring simultaneously. The simulation produced mean values and uncertainties close to experimental results. The initiation period was underestimated, but was found to be only 10%-20% of the total fatigue life at the stress ranges considered, which lead to fatigue lives of 10^5 to 10^6 cycles.

For large steel vessels, Guedes Soares and Garbatov[43] have also developed a fracture mechanics model, which they have used to examine the time-variant reliability of large steel commercial ships. Their approach used a fracture mechanics approach based upon a application of the Paris-Erdogan equation, which includes threshold effects below which the crack will not grow.

$$\frac{da}{dN} = C\Delta K^m, \Delta K > K_{Th}$$

$$\Delta K = \Delta\sigma Y(a)\sqrt{\pi a}$$

Where :

K_{TH} Threshold SIF which must be crossed for growth

$\Delta\sigma$ Applied stress range

$Y(a)$ Crack geometry factor

a Crack size

Equation 63

Using the assumption that Y could be treated as constant, Guedes Soares and Garbatov developed equations for the expected crack size and variance of the expected crack size over time. This was done by first integrating the crack growth law to yield the crack size at any time:

$$a(t) = \left[a_0^{1-m/2} + \left(1-\frac{m}{2}\right)C\Delta\sigma^m Y^m \pi^{m/2} N(t)\right]^{1/(1-m/2)}$$

Equation 64

An incomplete gamma function is used to obtain the m^{th} moment of a stress spectrum define by the Weibull distribution, excluding the stresses which produce ΔK values beneath the threshold:

$$\Delta\sigma^m = \alpha^m \Gamma\left[1+\frac{m}{\beta};\left(\frac{\Delta\sigma_{th}}{\alpha}\right)^\beta\right]$$

Equation 65

In this approach, the initial crack size a_0, the Paris- Erdogan constant C, and the stress range $\Delta\sigma$ were treated as stochastic variables. The distribution of crack size at any time was estimated through a second-moment approach using a Taylor-series expansion of the crack size at the mean values of a_0, C, and $\Delta\sigma$. Thus, the accuracy of this approximation will decrease as the COVs of the variables involved increases. The stress range is characterized by a mean up-crossing rate and the expected moment of the stress range, a simplification which ignores the distribution of the cycles over time. Additionally, treating the geometry factor Y as a constant is a significant simplification which is generally not strictly valid.

However, the resulting model is quite straightforward and is capable of treating the initial crack size as a random variable. The crack initiation period was modelled as a fixed percentage of the total mean propagation time. This crack growth model was used to predict the midship section modulus over time, accounting for lost effective areas as the cracks grew. The initial paper concentrated on predicting the time-variant section modulus accounting for the potential for cracks in all plate and stiffener elements. Later work refined and extended this model, including the effects of inspection and repair[240], combined local and global

loading and tee section stiffeners[241, 242], and the combined effects of corrosion and fatigue[243, 244].

In 1996, Radaj published a significant review paper of the various local approaches proposed to date[223], these approaches are further elaborated in his book with Sonsino[224] discussed above. Further work on fracture mechanics was done as part of the Ship Structural Maintenance Project at the University of California at Berkeley. Xu[200] presents a summary of this work, which was written up extensively in two Ship Structures Committee reports, SSC-386 and SSC-395. Using the Paris-Erdogan equation and the simplifications that load sequences effects are ignored, and the assumption that the slope of the crack growth curve is the same as the inverse slope of the S-N curve, Xu demonstrates how "cracked S-N curves" can be developed to predict the life remaining in a structural detail until a critical crack size is reached. Xu also presents a simple load-shedding model for a longitudinal connection based upon modifying the stress intensity acting on the crack.

Several other authors have also addressed fracture mechanics in the marine industry. In a work on reliability methods in the marine industry, Chang[245] presented a brief review of applying fracture mechanics to marine structures, including crack growth laws and methods to determine the stress intensity factors of the crack tips. As part of a larger study of the reliability analysis of fatigue locations in FPSOs, Kaminski and Krekel[246] constructed a simple reliability model using a fracture mechanics limit state function based on the Paris-Erdogan approach. In the offshore world, Lanning and Shen[42] investigated the reliability of offshore structure T-joints using a combination of the Paris-Erdogan approach and FOR techniques. The cracks investigated were semi-elliptical crack, and stress intensity factor were found though approximate analytical solutions. A limit state function was written and evaluated assuming that the initial crack size and material properties were random variables. Failure through both fracture and elastic-plastic action were considered. The approach is an interesting complement to that of De Souza and Ayyub discussed below

Fracture mechanics has also been examined for HSVs. Di et al. [247] present an overview of applying fracture mechanics to aluminium catamarans, including a case study on a 68m catamaran using the Paris-Erdogan equation linked to a finite element models of the vessel. Berkovits et al.[248] discuss the effect of welding residual stress on fatigue cracking, and demonstrate that a fracture-mechanics approach without any crack initiation time gives lower, and in their opinion, more accurate fatigue life predictions than the S-N approach. Spyker, Kelly and Chowdhury[249] also examined an aluminium catamaran using a Paris-Erdogan law approach while accounting for the threshold value of ΔK. The authors briefly discuss determining load sequences from long-term Weibull distributions which do

not have sequence information, recommending applying stress spectrums representing one year of service, with the highest stresses in the middle of the spectrum. Song and Moan[219] investigated the fatigue reliability of a large aluminium catamaran. The reliability calculations used a similar limit state function to Kaminski and Krekel, expanded to include the effects of crack initiation time. The material parameters in this model were estimated by calibrating against existing S-N curves. The overall reliability of the vessel was determined through series reliability estimates, using various simplified formulas. The effects of inspection and repair were included in the model, and a review of the sensitivity of the reliability index to the various stochastic variables was conducted.

A significant aluminium I-P fatigue model was created by Brandt, Lawrence, and Sonsino[250, 251] for 5083 aluminium butt welds for use in road vehicles. This model was validated against test results for 5mm and 25mm thick plates, with complete and incomplete joint penetration. In the original study, the Lawrence model was used to estimate the fatigue life, using measured strain parameters for crack initiation, and measured crack propagation parameters for crack growth. The strain parameters were measured for a crack depth of 0.5mm, but the crack growth was assumed to start at a depth of 0.25mm. The effect of load ratio was shown to have a strong impact on the relative importance of initiation and propagation life, with initiation life dominating under mean stress (R=0) conditions, and propagation dominating under reversed loading(R=-1). Additionally, the effect of bending from joint angular misalignment was shown to be significant for predicting the lives of the 5mm welds. These results were further investigated by a number of different approaches[252] which show promise for future development.

There has also been extensive recent work on steel commercial ships. Fricke and Muller-Schmerl[253] also used a Paris-Erdogan approach in examining the crack propagation behaviour for fatigue cracks initiating at notches of different radii. The stochastic properties of crack growth were accounted for by using Monte Carlo simulations, which determined the probability of a crack growing to a critical size from a given notch without being detected through inspection intervals. Sun and Bai[254, 255], and Sun et al. [256] investigated the time-variant reliability of an FPSO and bulk carrier using the same fracture mechanics expressions as Guedes Soares and Garbatov above for the crack size, however, they used different ultimate strength and through-life reliability models. Terai et al.[257] presented a similar Paris-Erdogan approach using an effective stress intensity factor range in evaluating the fatigue life of a 210,000 DWT bulk carrier. Additionally, the structural stress concentration factor at the detail under consideration was allowed to vary as the crack grew. The paper was notable for developing a simulation-based loading procedure, which

accounted for several different storm and heading models, as well as investigating the effect of alternating stillwater stresses. Considerable difference in predicted fatigue life was observed depending upon the loading model and the mean stress, indicating that these factor will be important for predicting crack growth accurately.

De Souza and Ayyub[41] extended the fracture mechanics approach to include the effects of residual stresses. A Paris-Erdogan approach similar to that used by Kaminski and Krekel or Guedes Soares and Garbatov was adopted, and developed into a limit state function based on the growth a flaw from a stochastic initial size to a stochastic critical size. This limit state function was modified to include the effects of the stress ratio, R, thus including the effects of residual stresses. The authors compared the fracture mechanics approach to the S-N approach for two sample joints, and investigated potential applications of fracture mechanics to ship design and maintenance. Akpan et al.[258] studied the time-variant reliability of the hull girder under corrosion and fatigue. While they examined the simplified crack propagation model proposed by Yang and Manning, a Paris-Erdogan approach was finally settled upon as data for the constants in Yang and Manning's formula are not readily available for marine structures and materials. The crack growth model incorporated stochastic initial crack dimensions and material properties, however, all the cracks in the structure were assumed to propagate simultaneously. Both the instantaneous reliability and the time-variant reliability of the overall structure were examined.

Cui[259] presents a feasibility study of using fracture mechanics for the fatigue life of marine structures. A procedure for cycle-by-cycle integration of the load history is presented. Cui also presents a review of several refinements to the Paris-Erdogan crack growth equation, including several recent ideas which account for mean stresses, crack opening, and similar concepts. A demonstration application of a selected group of these approaches is made, and potential problems are discussed. Cui also presents the results of a Monte Carlo simulation of fatigue crack growth under random loading sequences whose stochastic properties are known.

Taking a different approach to the crack growth problem, Lassen [260] presented a Markov model developed directly from experimental test programs for offshore T-joints. The measured crack depth during laboratory fatigue tests was used to create a Markov chain model, where the various steps in the chain relate to specific crack depths as the crack grows. This model can then be scaled to the stress ranges expected in service, and when additional uncertainty is incorporated to account for errors in real-world stress prediction, a very simple tool results for investigating fatigue reliability without explicitly using any fracture

mechanics approaches. However, the reliance on test data makes this approach currently impractical for HSV construction where the details have not yet been experimentally tested.

5.3 Mechanics of the Initiation-Propagation Approach

Regardless of the type of fatigue location to be examined, or the I-P model selected, the I-P fatigue life prediction follows a common structure. In this section, the major steps of the I-P model will be presented, using Lawrence's model[224, 230, 232]. The basic approach is to divide the fatigue life of the detail into two distinct regions, initiation and propagation, and calculate the life of each separately before combining them to determine the total life.

$$N_{Total} = N_i + N_p$$

Where:

N_{Total} Total life

N_i Crack initiation life

N_p Crack growth life

Equation 66

In the sections which follow, the initiation and propagation lives will be presented separately.

5.3.1 Modelling of the Initiation Life

The initiation life is typically modelled with a strain-life approach, which allows for an accurate determination of fatigue life even at a low number of applied cycles. The complete strain life equation is given in Equation 58, which combines plastic and elastic strains to determine the total fatigue damage. If the overall fatigue life is expected to be relatively long, the plastic contribution to the fatigue damage can be assumed small, and only the elastic portion of the curve retained[224, 251]. Ho and Lawrence[232] suggest doing this when the initiation life is over 10^5 cycles, which would seem to include details on HSVs where the total life should be two to three orders of magnitude higher than this. The resulting equation can then be solved directly for the initiation life in terms of the remote applied stress, leading to the Basquin equation, which can be further modified by the Morrow approach to include non-zero mean strain:

$$N_i = \frac{1}{2}\left(\frac{\Delta\sigma_a K_f}{\sigma_f' - \sigma_m}\right)^{\frac{1}{b}}$$

Where:

$\Delta\sigma_a$ Remote (nominal) applied stress amplitude

K_f Fatigue notch factor

σ_m Mean stress

All other variables as in complete strain life equation

Equation 67

For variable amplitude loading, a linear damage summation such as the Miner-Palmgren rule is typically employed. This approach also introduces a fatigue notch factor which converts from nominal stress to the strain at the notch at which point the fatigue crack is predicted to initiate, in this case typically the toe of the weld. The worse-case fatigue notch at a weld toe is difficult to define; an approach which has been widely adopted in implementing the Lawrence approach is Peterson's equation[230, 232, 250, 251], where the fatigue notch factor can be estimated in terms of a notch radius and a material parameter:

$$K_f = 1 + \frac{K_t(r) - 1}{1 + \frac{a}{r}}$$

Where:

K_f Fatigue notch factor

$K_t(r)$ Elastic stress concentration factor for notch radius, r

r Notch radius

a Microstructural support parameter

Equation 68

For typical welds, Ho and Lawrence[232] proposed that the elastic stress concentration factor can be expressed in terms of the notch radius, plate thickness, and a constant that is determined by the weld geometry and type of loading.

$$K_t = 1 + \alpha\sqrt{\frac{t}{r}}$$

Where:

K_t Elastic stress concentration factor for notch radius, r

α Weld constant

r Notch radius

t Plate thickness

Equation 69

Values for the constant α can be found in Ho and Lawrence's paper or the work of Radaj and Sonsino[224]. However, the notch radius still needs to be selected. Ho and Lawrence note that many values of notch radius can be measured at the toe of a weld, and propose that the most damaging notch radius be used in the determination of the fatigue notch factor. By

substituting the elastic stress concentration factor into Peterson's equation and finding the maximum by differentiation, the worse case is found to be when the notch radius equals the microstructural support parameter, a. Thus, the worse case fatigue notch factor is found to be:

$$K_{f\_MAX} = 1 + \frac{K_t(a) - 1}{2}$$ *Equation 70*

With the fatigue notch factor defined, the only remaining parameter to determine is the mean stress. For a welded joint in a HSV, a rough approximation of the mean stress might be the residual stress in the weld[224], however, this is a simplification of a complex stress state that would be expected to be multi-axial and influenced by plasticity. Determining the actual mean stress in the notch is therefore not straightforward. Lawrence recommends considering a "set-up" cycle to determine the mean stress based on the local cyclical stress-strain curve at the notch root including plasticity. Radaj and Sonsino[224] note that this seems at odds with the assumption that the elastic portion of the strain-life equation dominates, and for shorter cycle fatigue Lawrence himself often used the full strain-life equation for initiation. The problem is illustrated graphically in Figure 56, if the initial mean stress is already near the yield or proof stress in the notch, and then a large alternating fatigue stress is added to the specimen, the notch will deform plastically. This is shown for aluminium (5183 weld metal), mild steel (ASTM A36), and high-strength steel (ASTM 514) in Figure 56. Each of the metals is under high residual stress (σ_{kr}) before the fatigue load is applied. The initial application of the fatigue load takes the stress-strain response along the plastic part of the stress strain curve until the peak fatigue load is reached. Then as the fatigue stress decreases the material will unloaded elastically and follow the hysteresis loops shown in the figure, which have a very different mean stress than the initial residual stress. For constant-amplitude fatigue loading as shown in this figure, if the hysteresis loops are stable the mean stress can be calculated once, however, for variable amplitude loading the mean stress may change cycle to cycle, depending on the amplitude of each cycle and the cycles that came before it. It is also not clear how significant this effect will be for the loading on HSV. The vast majority of the fatigue loading cycles applied to the detail would be expected to be much smaller in amplitude than the residual stress from welding, which is typical on the order of the yield stress of the material. In such case, the hysteresis loops will be much smaller vertically, and the mean stress may not change significantly, though this cannot be accurately evaluated without a cycle-by-cycle investigation with an actual HSV load history. For a soft metal such as aluminium, using the full residual stress seems a conservative approach.

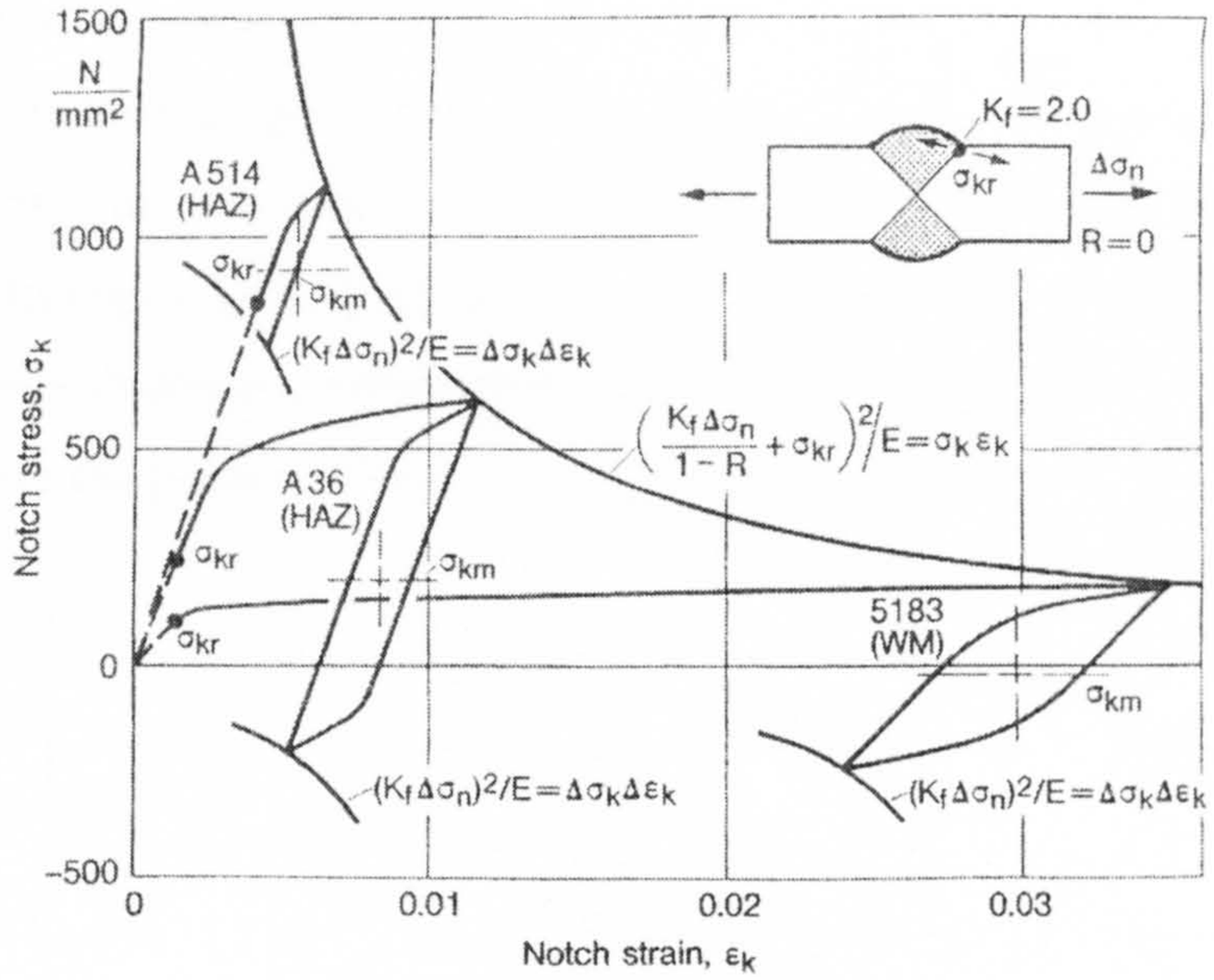

Figure 56: Influence of Plasticity on the Mean Stress[224]

Provided a reasonable estimate of mean stress is available, or a conservative estimate is made, determining the initiation life is not much more complex than determining S-N life of the fatigue location. After the initiation life has been consumed, a small crack will exist at the weld notch, and its growth can be modelled by fatigue crack propagation.

5.3.2 Modelling of the Propagation Life

After the initiation period is over, the crack is large enough that is growth can be predicted by considering the crack in homogenous material. The most common type of fracture mechanics used for crack propagation modelling is linear elastic fracture mechanics(LEFM), which assumes that the material will behave in primarily a linear elastic manner. While for the final fracture of aluminium under extreme loading this might be a poor approximation, for the stable growth of cracks under normal service loading this approximation is typically quite good. For crack propagation, LEFM will be used in this study. LEFM mechanics relies on the crack trip stress intensity factor, K, which in turn depends on the applied loading, crack size, and the geometry of the crack location. Thus the major tasks in the fracture mechanics phase of the modelling are: determining the relation between crack growth and K, determining the initial crack size, and determining the K value for the particular geometry of the problem.

For a perfectly elastic material, the stress around the tip of a long crack can be described in terms of relative position to the crack tip in polar coordinates and a scalar factor, which is the crack tip stress intensity factor, K[169]. Thus, for several different cracks, the stress at the same point relative to the crack tip will depend solely on K. The basis of the

fracture mechanics models used today is an observation that the crack growth rate per cycle is linearly related to the change in the crack tip stress intensity factor, ΔK, for a range of ΔK values in log space. This was proposed by Paris[226, 227] and is shown as region II (R II) in Figure 57 below. In region I, the crack growth rate slows to a threshold value of ΔK, below which no crack growth occurs and in region III where the crack growth rate accelerates as the loading approaches the point at which the material will fracture.

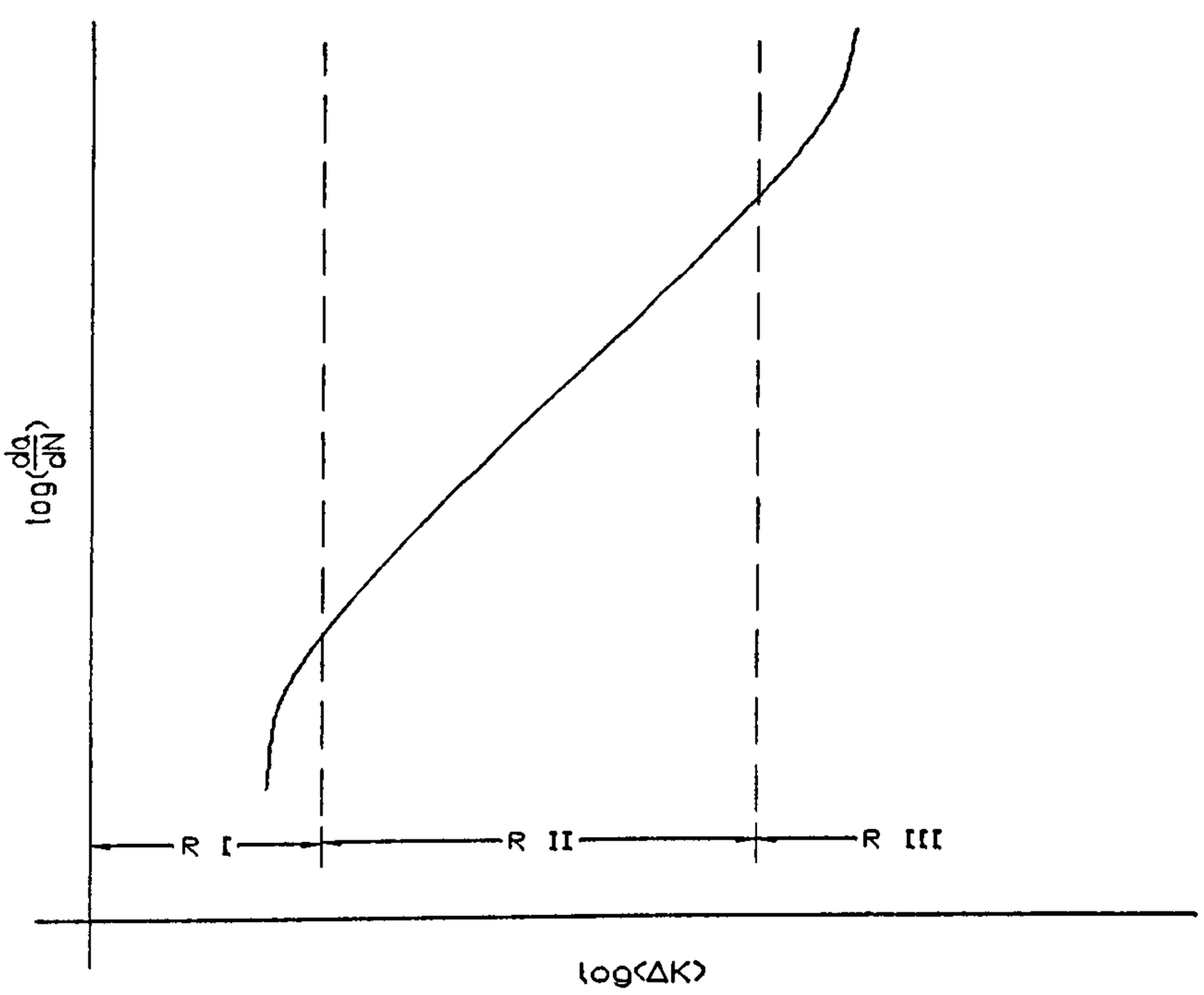

Figure 57: Crack growth relation

These observation was first made in the late 1950s and early 1960s, and has resulted in a variety of crack-propagation models sharing the following basic form:

$$\frac{da}{dN} = C(\Delta K)^m$$

$$\Delta K = \Delta\sigma \cdot Y(a)$$

Where:

$\frac{da}{dN}$ Crack growth rate per load cycle

C Crack growth constant

ΔK Applied crack tip stress intensity factor range

m Crack growth exponent

$\Delta\sigma$ Applied stress range

$Y(a)$ Geometry function

Equation 71

The most famous of the these models is the Paris-Erdogan law, named after the authors' 1963 paper[228], which follows the form of Equation 71. Many following authors have offered refinements to this law, incorporating factors such as mean stress, threshold behaviour, closure of the crack under compressive loads, and cycle-to-cycle interaction.

Many of the most widely used laws are presented in textbooks covering fatigue, including *Metal Fatigue in Engineering*[169], further references can be found on in several review works on the subject[259, 261].

The crack growth rate is determined by the changed in the crack tip stress intensity factor, K, which is in turn a function of the crack geometry and the applied loading. The geometry function, Y, will typically including both the crack size and the local geometry of the problem. Theoretical solutions for Y are generally restricted to a few simple but important cases, such as a two-dimensional edge or centre crack in a finite sheet. For more complex geometry including the stress concentration influence of weld profiles, Y can be determined by linear finite element analysis. For many common engineering cracks such as those near welds, empirical expressions are available based on finite element analysis of three-dimensional cracks. These have been tabulated into handbooks[262], and for welded joints British Standard 7910[263] contains many useful expressions.

The initial crack size must also be determined, this is where initiation ends and propagation begins. Several potential approaches could be taken for doing this. One approach is to use the crack depth observed at the end of the strain-life experiment as the initial value of crack depth. Another is to assume a size, this is typically taken as 0.25mm in the Lawrence approach[232, 250, 251]. In general, the current uncertainty in initial crack size is unsatisfactory, as the propagation life it highly dependent on the on initial crack size. Thus, a larger initial crack size in generally conservative and may be the best way forward. An alternative approach to the initial crack size problem is to ignore the initiation life period for welded joints entirely, and calibrate the initial crack size so that the total life obtained by the fracture mechanics approach is equal to the fatigue life observed experimentally. Strong philosophical objections have been raised against this approach, as the initial crack size which must be assumed is often so small that LEFM cannot be reasonably applied, see for example the discussion in Chapter 7 of Radaj and Sonsino[224]. Given the lack of correlation between the model and the physical reality, using the simpler S-N approach may be more appropriate.

As a further complication for aluminium structures, Sharp et al.[176] note that the ΔK-dA/dN relationship for aluminium alloys may not be adequately fitted by a single straight line, a finding supported by several experimental studies[264, 265]. In this case the constants C and m in Equation 71 will take on several values over Region II, which are typically represented by a piecewise-linear plot. This may add complication to the model, but does not change any of the fundamentals of the model. If appropriate values can be found for the range of applied stress intensity factors, the initial crack size, and the crack

growth constants C and m, the crack propagation life can be found by integrating Equation 71. In doing so, numerical integration is typically used. A common simplification is to apply the stress in blocks to the crack, calculating the geometry factor Y at the beginning of the block and taking it constant over the block. This is an un-conservative approach that would be expected to accumulate larger and larger errors as the fatigue life progresses, as Y generally increases with crack size. However, the rate of change of Y is usually small enough that these errors are not large if a sufficient number of stress block are used. British Standard 7910 recommends using blocks smaller than 0.1% of the total life, and ensuring that the change in crack size is less than 0.5% per block[263]. Tying in this fracture mechanics approach with the initiation approach discussed previously, the presence of a crack and the crack size can be determined at any point in the fatigue life of a structural detail.

5.4 Trial Application to Aluminium Butt Weld Connections

To evaluate the practicality of using the I-P model in place of the S-N model, a trial application was made to transverse aluminium butt welds in tension. Using the I-P approach, a S-N curve was simulated for the transverse welds, and compared with the experimental results. This application focused on predicting the mean strength of these welds, stochastic characteristics of the growth was not yet considered. A group of small-scale transverse weld test results were assembled from open literature. Crack initiation and growth data from the studies of Brandt et al.[250, 251] was used along with approximate solutions for the stress intensity factor of welded joints.

The progression of the fatigue failure of the butt weld is shown in three phases in Figure 58. In the initial phase, phase one, a crack will initiate at the toe of the weld where the stress concentration is highest. Once a crack starts, it will initially grow as a "thumbnail" crack down through the plate, as shown in phase two. Finally, the crack will penetrate through the full thickness of the plate, and grow rapidly to final fracture, as shown in phase three. Each of these phases will be examined in an I-P fatigue approach.

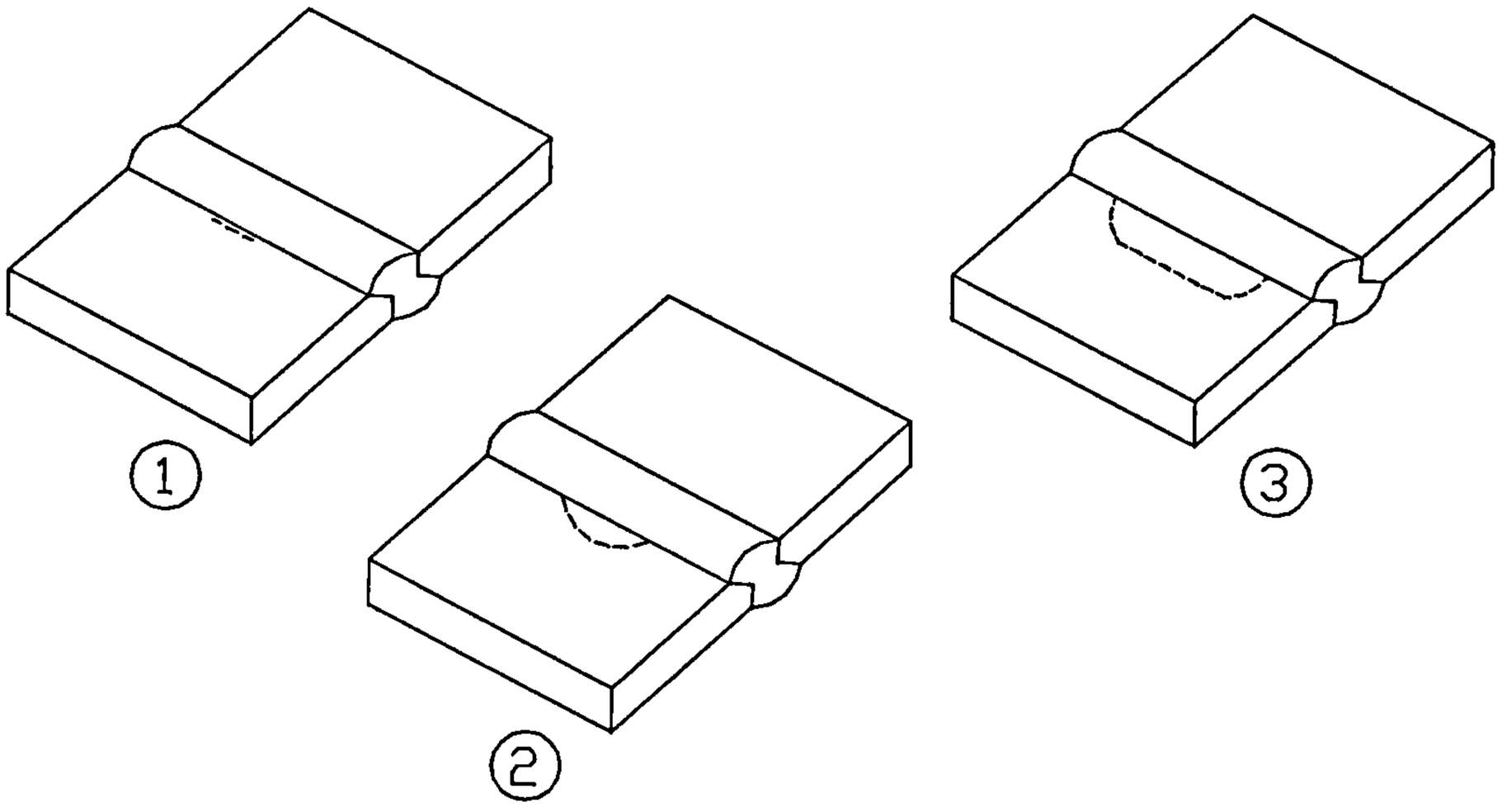

Figure 58: Fatigue Life Phases of Small Butt-Weld Specimen

5.4.1 Sample Data

For a trial application, a simple fatigue case was desirable. A transverse butt weld was selected, as this is a joint common in HSVs, but also simple to model. Several experimental programs which tested this sort of weld were located. Mindlin[69] reported on a series of butt weld fatigue tests in 5083-H113 plate of varying thickness and joint configurations. Nordmark and Clark[266] present the results for a wide range joints, including bolts, rivets, and welds in 6061-T6 aluminium, similar to the 6082-T6 alloy used in marine applications. Further results with joining 5083 to 6061 material were reported by Person[267]. Similar to the Tveiten tests discussed in Chapter 4, the test results under a high mean stress (R=0.5) were selected as most representative of larger details in HSVs, where the methodology tested here would hopefully be applicable. The results from the test programs were plotted on a common axis, along with a free-slope regression line. For comparison, two hot-spot curves are included in the plot as well, the U.S. Aluminum Association category "B" mean curve, and final mean S-N curve developed in Chapter 4 for reliability analysis. The results are shown in Figure 59.

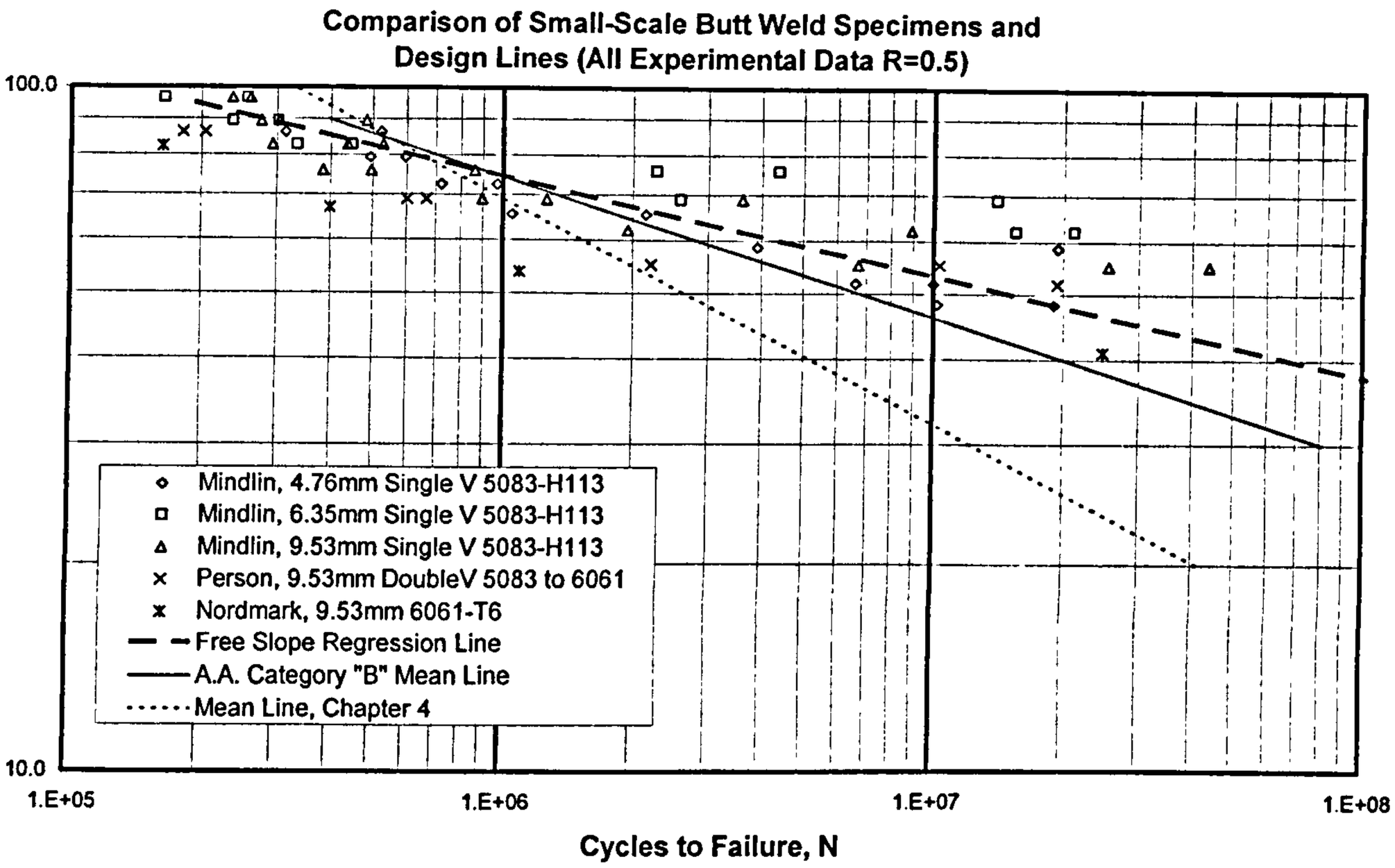

Figure 59: Small-Scale Butt Weld Data

The free-slope regression came out with a very high slope, approximately 6.8, although this was most likely influenced by the high-cycle fatigue results where an endurance limit effect may have been encountered, as these were constant-amplitude tests. The Aluminum Association category B curve looks to be almost as good a fit as the regression line if an endurance limit is assumed at 5 million cycles. The mean curve proposed in Chapter 4 has a much lower slope, and is significantly conservative in the high-cycle region. This curve was based on fillet-welded connections, even though the curve represents hot-spot stresses, it does not include in the stress concentration of the weld itself. It is likely that the weld stress concentration factor of a fillet weld is higher than a butt weld. Additionally, this curve was designed for variable-amplitude loading where there would be no endurance limit.

5.4.2 Initiation Life

The initiation life was modelled by Equation 67 above, which required determining the material constants, the mean stress, and the fatigue notch factor. The material constants were taken from the published weld metal strain tests by Brandt et al[250] and are summarized in Table 36. Plotting the relative importance of the plastic and elastic components of this data confirmed that the behaviour was primarily elastic in the high-cycle region, which is the region of interest for HSVs. The fatigue notch factor was determined though an equation proposed by Ho and Lawrence[232] for axial loading of butt welds:

$$K_t = 1 + 0.27(\tan(\theta))^4 \sqrt{\frac{t}{r}}$$

Where :

K_t Elastic stress concentration factor for notch radius, r

θ Weld flank angle

r Notch radius

t Plate thickness

Equation 72

Flank angles of 30 degrees and 45 degrees were assumed, to cover a range of potential weld profiles. As required by the approach, the notch radius is assumed equal to the microstructural support parameter, a, which was taken as 0.25mm. As the majority of the plates tested were 3/8" or 9.5mm in thickness, this value was used for the thickness in determining the fatigue notch factor. In lieu of a set-up cycle analysis, it was decided to use two values of mean stress, 0 MPa and 125 MPa, which should bracket the actual mean stress at the fatigue location. 125 MPa was selected as it is roughly 90% of the welded yield stress of 5083 and 6082 alloys. The variation in weld flank angle and mean stress leads to a total of four combinations to be considered:

Table 36: Initiation Life Conditions

Parameter	*Condition 1*	*Condition 2*	*Condition 3*	*Condition 4*
Plate thickness, mm	*9.5*	*9.5*	*9.5*	*9.5*
Weld flank angle, θ	*30*	*30*	*45*	*45*
K_t	*2.45*	*2.45*	*2.67*	*2.67*
K_{fmax}	*1.73*	*1.73*	*1.83*	*1.83*
σ_f' MPa	*791*	*791*	*791*	*791*
B	*-0.15*	*-0.15*	*-0.15*	*-0.15*
Mean stress, MPa	*0*	*125*	*0*	*125*

5.4.3 Propagation Life

Once the crack initiates, it will grow as a semi-elliptical surface crack as shown in phase two of Figure 58. This phase of the crack growth was modelled by Equation 71, ignoring any threshold behaviour. The required material constants were taken from a previous study by Brandt et al[250]. The initial crack depth was taken as 0.5mm, which corresponds to the crack depth at the end of the strain life data used in the previous section, although Brandt et al.[250] also suggest using an initial crack depth half this size, which has been used elsewhere in the Lawrence I-P model. The initial parameters at the start of the crack propagation phase of the model are summarized in Table 37.

Table 37: Crack Growth Parameters

Parameter	*Value*
C	$1.24 * 10^{-14}$
m	*4.01*
Initial depth	*0.5mm*
Initial aspect ratio	*15*

To implement the growth prediction routine for this crack, an expression is needed to determine the crack tip stress intensity factor range, ΔK, from the applied loading. As the crack grows both along the weld and through the thickness of the plate, two values of ΔK are needed, one for the deepest point of the semi-elliptical crack, and one for the surface. While standard solutions are available for such a crack growing in a plate, the situation is further complicated in this example by the presence of the weld toe, which adds an additional stress-concentration factor. To model the stage of the crack growth, the standard Newman-Raju[268] surface crack equation is adopted, with modifications to account for the local stress concentration of the weld toe.

The Newman-Raju surface crack equation is the result of extensive study of the semi-elliptical surface crack in a finite sheet, a problem which is not amenable to exact solutions by theoretical tools of elasticity. The basic problem is shown in Figure 60 where the principle dimensions are labelled.

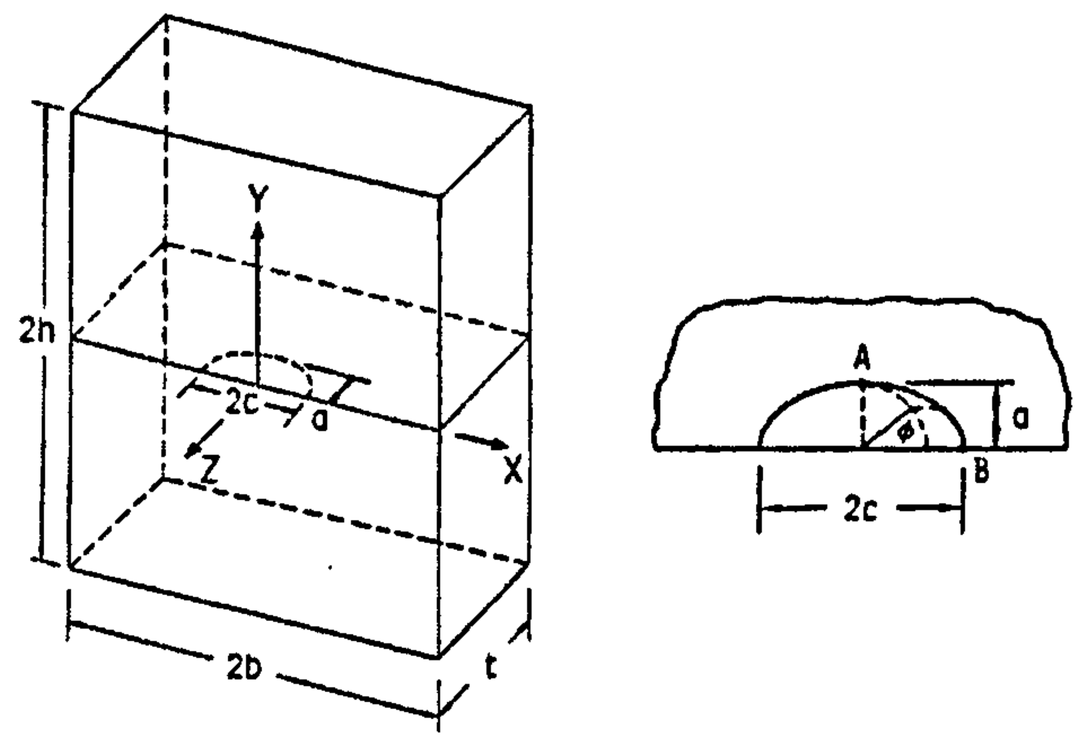

Figure 60: Newman-Raju Elliptical Surface Crack Dimensions[268]

Newman and Raju calculated the crack tip stress intensity factor along the curved crack front for wide range of geometry by detailed finite-element models. The crack front curvature is parameterized in terms of the angle ϕ, which is related to the position on the elliptical crack front through circles whose diameters are the major and minor dimensions of the ellipse as shown in the right-hand side of Figure 60. The geometric parameters varied by Newman and Raju included $0 < a/c \leq 1.0$, $0 \leq a/t < 1.0$, $c/b < 0.5$, and $0 \leq \phi \leq \pi$. Both tension

and bending loads normal to the crack plane were investigated. After completing the finite element analysis, Newman and Raju fitted the result with an empirical equation, which relates applied stress to the crack tip stress intensity factor anywhere along the crack front:

$$K = (\sigma_t + H\sigma_B)\sqrt{\pi \frac{a}{Q}} F\left(\frac{a}{t}, \frac{a}{c}, \frac{c}{b}, \phi\right)$$

Where:

σ_t, σ_b : Remote tension and bending stress respectively

H, F : Fitting functions

a, t, c, b : Geometric dimension as in figure above

Q : Shape factor $\approx 1 + 1.464\left(\frac{a}{c}\right)^{1.65}, \frac{a}{c} \le 1, 1 + 1.464\left(\frac{c}{a}\right)^{1.65}, \frac{a}{c} > 1$

Equation 73

The fitting function, F, handles tension loading:

$$F = \left[M_1 + M_2\left(\frac{a}{t}\right)^2 + M_3\left(\frac{a}{t}\right)^4\right] f_\phi \cdot g \cdot f_w$$

$$M_1 = 1.13 - 0.09\left(\frac{a}{c}\right)$$

$$M_2 = -0.54 + \frac{0.89}{0.2 + (a/c)}$$

$$M_3 = 0.5 - \frac{1.0}{0.65 + (a/c)} + 14\left(1.0 - \frac{a}{c}\right)^{24}$$

Equation 74

$$f_\phi = \left[\left(\frac{a}{c}\right)^2 \cos^2\phi + \sin^2\phi\right]^{\frac{1}{4}}$$

$$g = 1 + \left[0.1 + 0.35\left(\frac{a}{t}\right)^2\right](1 - \sin\phi)^2$$

$$f_W = \sqrt{\sec\left(\frac{\pi c}{W}\sqrt{\frac{a}{t}}\right)}$$

The fitting function for bending is similar:

$$H = H_1 + (H_2 - H_1)\sin^p\phi$$

$$p = 0.2 + \frac{a}{c} + 0.6\left(\frac{a}{t}\right)$$

$$H_1 = 1 - 0.34\left(\frac{a}{t}\right) - 0.11\left(\frac{a}{c}\right)\left(\frac{a}{t}\right)$$

$$H_2 = 1 + G_1\left(\frac{a}{t}\right) + G_2\left(\frac{a}{t}\right)^2$$

Equation 75

$$G_1 = -1.22 - 0.12\left(\frac{a}{c}\right)$$

$$G_2 = 0.55 - 1.05\left(\frac{a}{c}\right)^{\frac{3}{4}} + 0.47\left(\frac{a}{c}\right)^{\frac{3}{2}}$$

The Newman-Raju equation above is sufficient to determine the ΔK, and thus the crack growth, both at the surface ($\phi=0$) and at the deepest point of the crack($\phi=\pi/2$). This then needs to be modified to account for the stress concentration effect of the weld toe at the edge of the crack. The effect of the weld toe stress concentration factor has been previously examined along a similar approach to the Newman-Raju finite element regression equations, which can be combined with the ΔK value found by the Newman-Raju approach. In this work, the stress concentration factors recommended in Appendix M, Section M5.1.3, of British Standard 7910[263] were used. These factors are based on three-dimensional finite element modelling of cracks originally presented by Bowness and Lee[269], although in the British Standard implementation the weld flank angle is fixed at 45 degrees.

Once the crack has grown through the thickness of the plate, the behaviour becomes more complex. There are now two cracks, one on each side of the plate, and a curved crack front connecting the two. This geometry cannot be treated by standard two-dimensional crack formulas, which implicitly assume the same crack length on both sides of the plate. This problem has been investigated previously to support leak-before-break design of pressure vessels and hazardous cargo tanks. Leak before break design requires any fatigue cracks in a tank to grow through the thickness of tank without an unstable fracture occurring. When the crack grows through the tank, the tank will start to leak, alerting the operator to the presence of a crack. In these situations, it is desirable for fatigue cracks propagate stably for a short time after penetration so that there is adequate time for inspection and repair of the tank[270]. In this vein, Ando et al. [270] developed expressions for the crack tip stress intensity factors for both sides of the plate after an elliptical surface crack penetrates the back surface a plate. Initially, this was developed for tension loading only, however, it was later expanded to include bending loads[271], local stress concentrations[272, 273], and aluminium-specific plates[274]. The method is simple yet has agreed well with test data, making it excellent for the current purposes.

The method develops crack tip stress intensity factors based upon assumed crack-opening displacements, and the ability to treat the top and bottom surfaces as 2-dimensional through crack problems, tied together by the crack opening displacements. The method requires several assumptions, which are listed below[270]:

(1): After a crack through thickness occurs, the crack opening displacement in the centre of the crack, that is, on line BB' in Figure 61, is assumed to be equal on the top and back sides and at the centre of the thickness of the plate.

(2): After penetration through the plate, the crack is assumed to retain its semi-elliptical shape, and it is also assumed that the surface crack, a_s, is the major axis of an ellipse. As a result, the crack length, a_e, at the centre of the thickness of the plate can be expressed as follows:

$$a_e = \frac{\sqrt{3a_s^2 + a_b^2}}{2}$$ *Equation 76*

(3): The crack opening displacement $\delta(a_e)$ at the centre of the crack of Figure 61 is assumed to be equal to the crack opening displacement at the centre of a two-dimensional crack through thickness with a length 2ae in the plate whose width is 2W. As a result, $\delta(a_e)$is expressed as follows:

$$\delta(a_e) = \frac{4\sigma a_e(1-\upsilon^2)}{E} V(\eta)$$

Where:

ν: Poisson's ratio

E: Young's modulus *Equation 77*

$$\eta = \frac{a_e}{W}$$

$$V(\eta) = -0.071 - 0.535\eta + 0.169\eta^2 + 0.029\eta^3 - 1.071\left(\frac{1}{\eta}\right)\log(1-\eta)$$

(4): The stress intensity factor at points A and D of Figure 61 after a crack through thickness is assumed to be equal to the stress intensity factor, whereby the crack opening displacement at the centre of a two-dimensional $2a_s$ or $2a_b$ long crack through thickness in a 2W wide plate is exposed to a uniform stress equal to $\delta(a_e)$

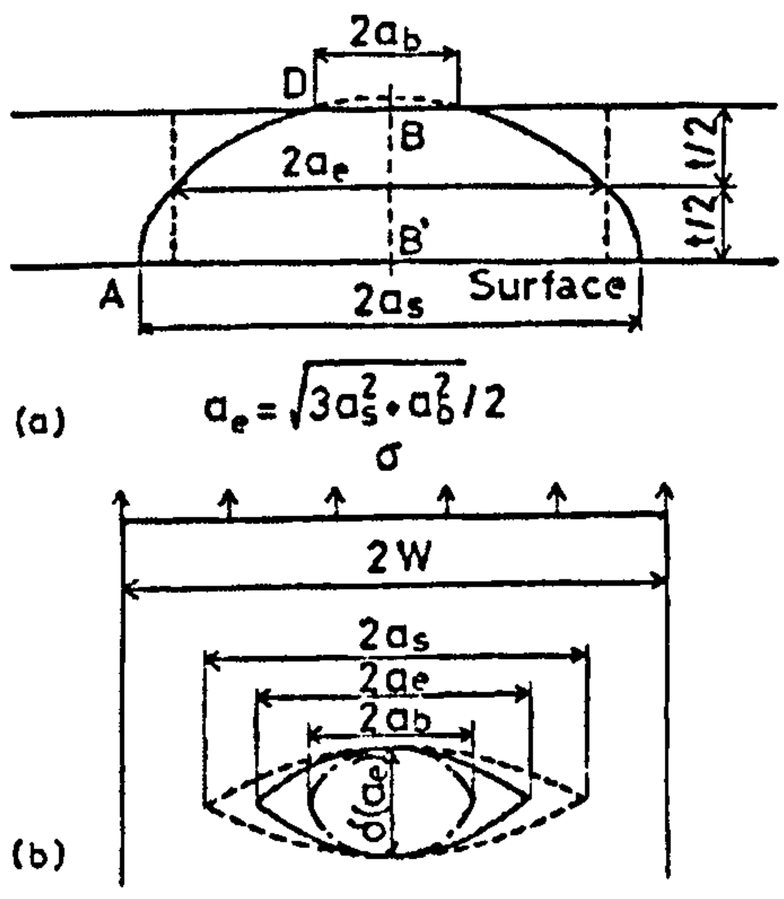

Figure 61: Dimensions for Ando et al. method[270]

Based on these four assumptions, the crack tip stress intensity factor at points A and D can be expressed as a modification to the two-dimensional crack tip stress intensity formula as follows:

$$K_A^e = \frac{\delta(a_e)}{\delta(a_s)}\sigma\sqrt{\pi a_s}F(\eta_s)$$

$$K_D^e = \frac{\delta(a_e)}{\delta(a_b)}\sigma\sqrt{\pi a_b}F(\eta_b)$$

Where:

$\delta(a_s), \delta(a_b)$: Crack displacement functions found by substituting a_s and a_b in the formulas of assumption 3 above

σ : Applied stress

$$\eta_s = \frac{a_s}{W}, \eta_b = \frac{a_b}{W}$$

$$F(\eta) = \frac{1 - 0.5\eta + 0.370\eta^2 - 0.044\eta^3}{\sqrt{1-\eta}}$$

Equation 78

To validate the assumptions made in developing this formula, Ando et al. compared experimental crack growth and crack opening to that predicted by the formula, using both mild and high-tensile steel, with good agreement shown. One such comparison graph is presented below, where the da/dN vs. ΔK plot was constructed using the Newman-Raju crack tip stress intensity equation before the crack penetrated the plate(the B.T.T. symbols), and the new proposal after (the A.T.T. and back symbols). As can be seen from the plot, all of symbols fall on a straight line, indicated that both the Newman-Raju equation and the new expression for crack tip stress intensity factor both work well for this case.

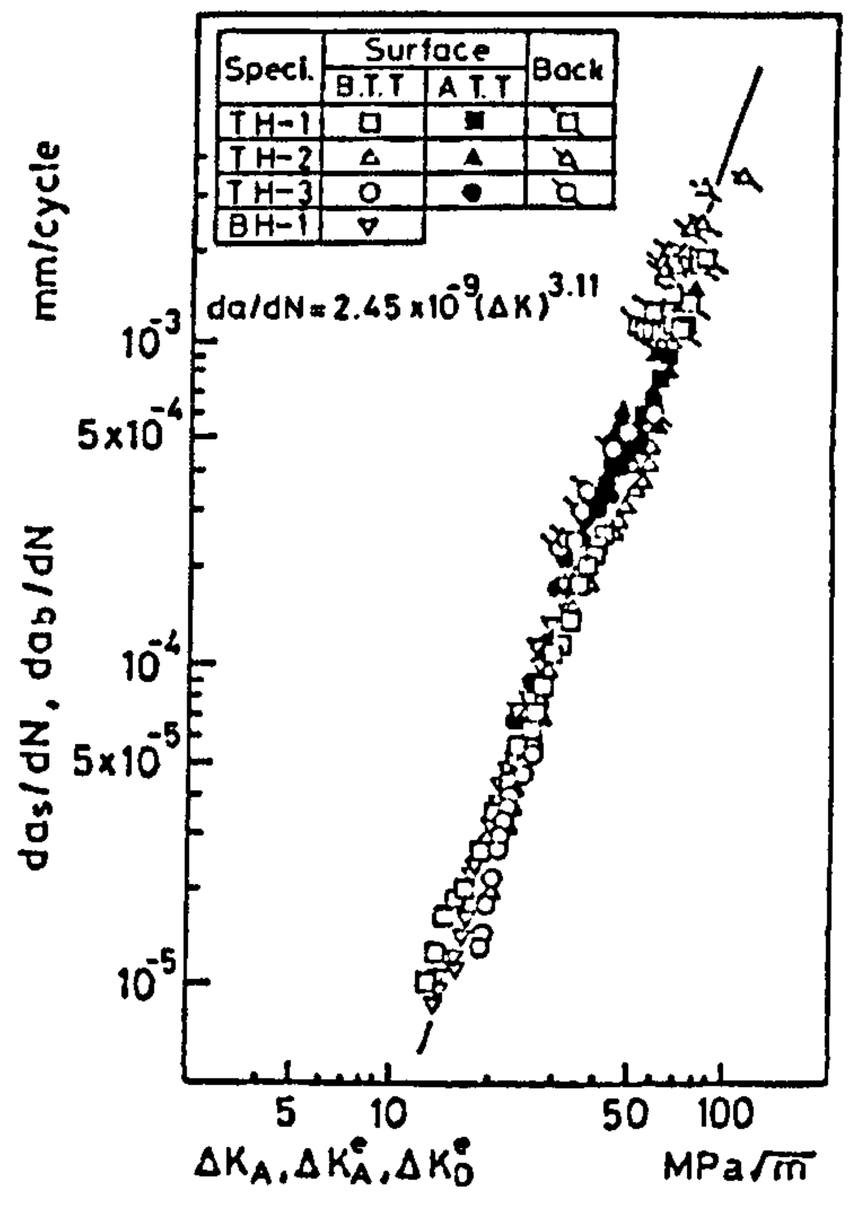

Figure 62: Surface and thru-thickness crack growth[270]

Several years later, Nam et al.[274] conducted a similar study for 5083-0 aluminium alloy, and found good agreement as well, as shown below in Figure 63. The results on this graph correspond to both the Newman-Raju equation and the thru-thickness equation of Ando et al. Again, all the points fall on a straight line, indicating that the equations work well. This simple equation can be used to address the phase three crack growth from Figure 58.

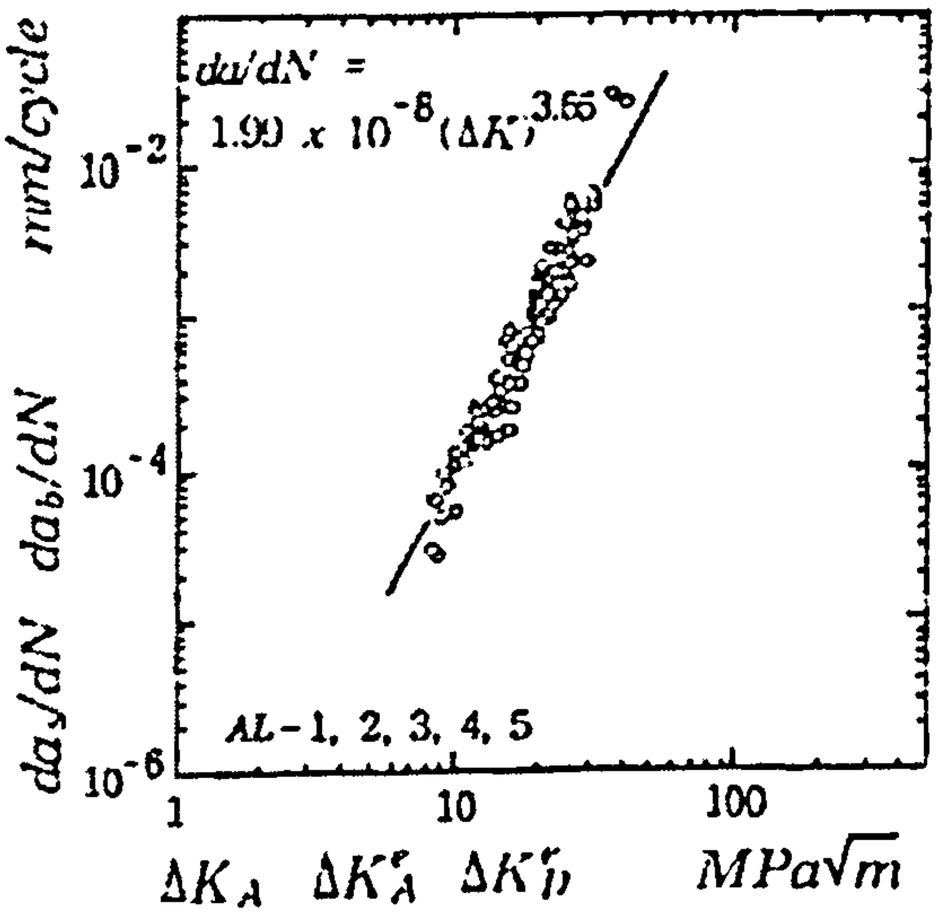

Figure 63: 5083-0 Aluminium results, surface and thru-thickness cracks[274]

After developing relations for the crack tip stress intensity factors for a crack growing through the thickness of a plate under pure tensile , the authors expanded their research to include local stress concentrations. Local stress concentrations were examined as these are likely sites for cracks to appear. Nam et al.[272, 273] studied cracks growing at the base of fillets of various radii with stress concentration factors between 1.15 and 1.75. While the stress concentration did effect the aspect ratio of the crack as it grew before penetrating the thickness of the plate, the stress concentration did not appear to significantly affect the growth once the crack was through-thickness crack. Based on these findings, Nam et al. neglected the stress concentration factor when computing the crack growth after penetration. For the purposes of the current study, this means that the stress concentration factor caused by the weld bead can be neglected once the crack has penetrated through the thickness of the shell plating. After the crack penetrated the thickness of the plate, it was allowed to grow until the upper portion of the crack spanned the entire specimen side-to-side, which was taken as the failure point. As the actual specimen widths varied in the study, a mean value of approximately 45mm was used for the width. At this value of width, the through-crack growth portion of the life was generally very small.

5.4.4 Results

The initiation and propagation approaches described in Sections 5.4.2 and 5.4.3 were used to simulate the small butt weld S-N data. The four initiation parameter combinations presented in Table 36, along with the crack propagation approach. The resulting data points were used to construct S-N curve which were then plotted with the experimental data discussed in Section 5.4.1. The four total life plots are shown, along with a separate plot of the crack propagation life, as seen in Figure 64. It is clear from this figure that the current I-P model is overly optimistic, although the predicted lines do pass through the upper portions of the data points, and the slope of the line is well predicted.

The mean stress and the weld angle significantly effect the prediction line, especially at long lives where the fatigue crack propagation is a comparatively short part of the overall life, this was noted early by Ho and Lawrence[232]. This is also similar to the result of Brandt et al.[250], who showed initiation was a significant portion of the total fatigue lifetime of aluminium butt welds under mean stress load(R=0). Interestingly, if the loading was fully reversed(R=-1), initiation became a negligible part of the overall lifetime. Thus, the amount of residual stress acting on a joint in a HSV may be significant in determining the relative importance of the initiation and propagation phases.

The propagation phase could also be extended if a more advanced crack growth relationship was used, perhaps considering threshold effects and crack closure. At shorter lives, the fatigue crack propagation phase is a much longer part of the overall life, roughly 10%-20% of the overall life. For larger structures, where multiple load paths could lead to load shedding as the crack grows, the propagation life may be much larger proportionately. A smaller initial crack size would also have increased the propagation time .

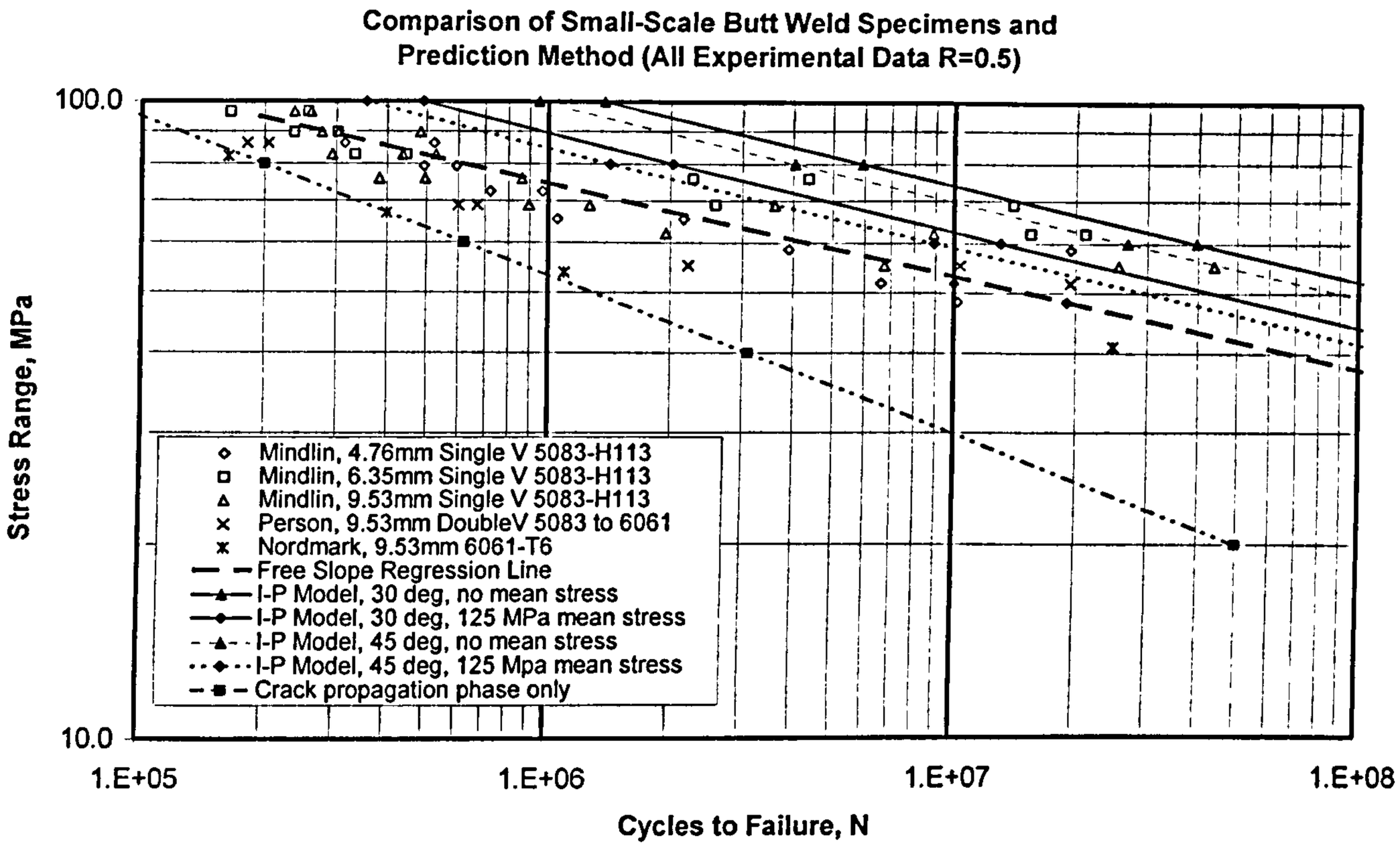

Figure 64: I-P Model Predictions and Test Data

A possible reason for the over prediction is angular miss-alignment of the butt weld, which can introduce secondary bending stresses. Previous studies[250, 251] showed that as little as one degree in 5mm plate could lead a noticeable reduction in the strength of the joint. The effect of this misalignment increases with decreasing plate thickness, so for the 9.5mm plate considered here, the reduction might be slightly less, but would move curve in the correct direction. Another potential reason is improvements in welding and weld metal used for the test programs, which were mostly conducted in the 1950s and 1960s, and the more recent initiation and growth data that was determined some 40 years later.

It is clear from these results that the local geometry and material properties may have a significant impact on the predicted initiation life, and thus need to be considered in using the I-P fatigue model. Unfortunately, in this regard, the small-scale specimens are likely to differ significantly from the details in HSVs, and little data is available at the moment on the weld angle, misalignment, and residual stresses resulting from HSV construction.

Additionally, as the mean stress does seem to have a significant impact on the prediction results, a proper cycle-by-cycle estimation of the mean stress under variable amplitude loading may be required.

5.5 Conclusions

The initiation-propagation fatigue model was presented as a way of extending the existing S-N fatigue approaches. The S-N approach cannot give the engineer feedback on

the seriousness of the fatigue failure. Thus the S-N approach can be used to evaluate service limit states, but not the impact of fatigue on the ultimate limit state. By modelling fatigue as a two-part process, crack initiation and then crack propagation, the I-P approach can describe the size of the crack present in the structure at any point in time. This size information could then be used to evaluate the impact of the crack on the structure's ultimate limit states. Previous studies have extended aspects of the I-P model, especially the propagation part, into stochastic approaches which could be adapted for structural reliability formulations. A trial application with the Lawrence I-P model was made for a series of simple butt-weld test specimens. Initiation and crack propagation data were taken from a recent study on similar welds. The prediction results captured the trend of the data, however, they were non-conservative on life predictions. Crack initiation life was the major component of the overall specimen life. The results were significantly influence by mean stress and weld flank angles, and local bending stresses may have also contributed to the optimistic prediction. Trying to accurately model these local conditions for joints on aluminium HSVs is difficult at the moment as published data is scarce.

All of these concerns make the I-P model significantly more difficult to apply at the current time than the S-N model, and therefore less attractive from an engineering perspective. From the designer and operators standpoint, the primary interest is in determining how likely a crack is to occur, and once it occurs, how long is there until it becomes a major safety hazard. Therefore, it may be possible to construct a simpler I-P model that would be more suitable for application with the current level of knowledge. An adjusted version of the S-N curve presented in Chapter 4 could be used as an initiation curve, though the point of initiation would be assumed to be a much larger crack than in the Lawrence I-P model, perhaps a through-thickness crack several centimetres in length. This crack growth could be modelled with a Paris law approach, accounting for load shedding to the surrounding structure. Such an approach would eliminate the need to consider the local details of the fatigue initiation site beyond the hot-spot stress, yet could still give information on the probability of crack occurring, and the relative consequence of crack propagation in different locations of the vessel. Such an approach is similar to the approach taken by Guedes Soares and Garbatov[43], with a more rational approach to estimating the initiation period. The difficulty would be in obtaining a rational transition crack size from the S-N approach to the fracture mechanics approach.

CHAPTER

6

"A conclusion is the place where you got tired thinking."
Martin Henry Fischer

Conclusions and Recommendations for Future Work

6.1 Conclusions

The use of aluminium in HSV construction has expanded rapidly over the past 15 years, with a steady progression of larger and faster HSVs coming into service in more challenging roles and environments. This rapid development in vessel application has outstripped the engineering approaches for designing such vessels, making weight optimization difficult and leading to worrying failures in service. This thesis investigated the options for predicting the ultimate and fatigue strength and the associated reliability of aluminium stiffened panels, which form the majority of the structure on HSVs. In addressing this problem, this thesis set out to achieve four objectives:

1. To review and benchmark existing methods for predicting the compressive strength and reliability for secondary and tertiary response of aluminium structures.
2. To develop an improved approach to determine the tension and compression stress-strain relationship of aluminium stiffened panels, accounting for the differences between aluminium and steel.
3. To develop a reliability-based fatigue approach extending the existing S-N design approach.
4. To investigate a fracture-mechanics based approach for estimating the impact of fatigue on the panel's ultimate limit states.

The work presented in Chapters 2 through 5 addressed each of these objectives, allowing several conclusions to be made about the responses of these panels.

6.1.1 Ultimate Strength

The ultimate strength investigation of aluminium un-stiffened plates revealed that the existing ultimate strength prediction methods worked well for the type of plates common on aluminium HSVs. The different stress-strain properties of the 5000 and 6000 series alloys

were significant in predicting the response of the plates, and methods which did not account for this difference did show a logical bias towards one alloy or the other. An approximate method for estimating the stress-strain curve of an aluminium plate in compression was developed, based on the ultimate strength predicted by any of the simplified methods. This approach showed good agreement with the experimental results, considering the simplicity of the approach.

The tensile ultimate strength behaviour of aluminium un-stiffened plates showed that strain concentration in the transverse HAZ at the loaded plate boundaries has a significant effect on the strength and ductility of the plate. The 6000-series alloys, which have a lower fracture strain and a lower rate of strain-hardening in the HAZ, were particularly susceptible to suffering failure by fracture at relatively low overall strains.

A similar comparison study was carried out for stiffened panels showed that aluminium prediction methods gave good prediction results overall. The design codes were conservative, and all the methods having more variability than similar studies have shown with steel panels. The amount of experimental test data available was quite limited, and not necessarily fully representative of typical HSV construction. When rendered material-independent by using the non-dimensional slenderness parameters β and λ, steel methods also showed good agreement with the test data. Because of the small data set, it was difficult to detect any difference between 5000 and 6000 series alloy behaviour in these tests. Additionally, none of the tested panels had a transverse weld away from the loaded edges, which could significantly effect the results.

Methods capable of generating the entire stress-strain curve of a panel in compression were also examined, including a method modified to include the new approximate method for determining the stress-strain response of aluminium plates. None of these methods proved particularly reliable in predicting the peak strength value accurately, but the proposed modified method capture the shape of the stress-strain curve. A similar tensile response study was carried out for stiffened panels, which showed the same potential for strain concentration as the un-stiffened plates.

To evaluate the effect of the limited ductility in tension that the 6000-series plates and panels displayed, the response of a simple aluminium box girder was studied by a Smith-type progressive collapse analysis. When the box girder was of similar scantlings all around, there was no effect from strain concentration. When the compressive flange was relatively stocky, the tension flange of the girder was required to achieve higher strain rates to develop the ultimate strength of section. In the case of a 6000-series tension flange, and small HAZ breadths, it is possible that strain concentration would prevent the tension flange from

having sufficient ductility to achieve the ultimate strength. A simple limit state equation and FOR approach was investigated to determine the reliability of aluminium stiffened panels. For such applications, the FOR approach appeared entirely adequate.

6.1.2 Fatigue Strength

The initial fatigue strength investigation was a hot-spot S-N approach, based on previously published data. Combining previously-published hot-spot test results into a common mean strength curve is not recommended as an approach, as in this analysis the different data sets did not share a common distribution. This banding was felt to be a result of different experimental and analysis assumptions made by the different test programs. It was possible to combine a subset of the data representative of two different details from a single test program.

Experience with two S-N fatigue limit state functions and a mean fatigue strength curve from a single experimental program demonstrated that it is possible and worthwhile to combine hot-spot S-N analysis with reliability approaches. This method was shown to give reasonable safety index values when applied to a reference vessel, and when compared to existing fatigue design codes for four common details. Comparison to existing nominal-stress design codes showed some variability as the design codes often mapped details with different hot-spot stresses to a common S-N curve.

The FOR reliability approach appears sufficiently accurate for engineering work when applied to the non-linear S-N fatigue limit state functions as set up in this study. Typical errors between the FOR safety index and Monte Carlo simulations were on the order of 5%. If the S-N curve slope parameter is taken as stochastic, the FOR approach is no longer accurate, and large errors are possible. These errors are also possible if the uncertainty in the Weibull shape parameter is quite large, in the Weibull loading limit state equation proposed by Jensen.

The S-N fatigue approach only addresses a service limit state and does not give information about the seriousness of the fatigue failure. The initiation-propagation fatigue model was proposed as a potential way to obtain such information. However, the Lawrence initiation-propagation approach used in this study was shown to be highly sensitive to local weld parameters including flank angle and mean stress. In a trial application for butt welds the initiation-propagation approach yielded results which captured the trend of the data adequately, but were overly optimistic. Given the difficulty in obtaining accurate data for the local weld parameters, the initiation-propagation approach appears much more difficult to apply to HSVs at this time than the S-N approach.

A general conclusion drawn from both the S-N fatigue approach and the initiation-propagation approach is the difficulty in working with several sets of previously published test data. Often, it is not possible to quantify all the test parameters or analysis assumptions in each test program, and given the highly non-linear nature of fatigue, these differences can lead to data scatter that makes it difficult to validate new approaches or identify their areas of weakness. In this regard, it would seem desirable to perform the final verification of new approaches to fatigue on HSVs with a large fatigue test program, similar to that of Tveiten, specifically designed for such validation.

6.2 Recommendations for Future Work

This thesis performed a fairly broad analysis of both strength and reliability of stiffened panels, so it is not surprising that many areas were identified for future work during the course of this research. With the continued growth in aluminium HSV applications for monohull, catamaran, and trimaran hullforms serving a wide variety of roles, there are many areas which deserve further attention.

6.2.1 Ultimate Strength

To allow for the broad overall scope of this thesis, several restrictions had to be made at the outset of this thesis. Perhaps the most restrictive of these was the concentration on axial loading only. In many HSVs, such as in the cross-decks of catamarans and trimarans, aluminium stiffened panels would be expected to undergo biaxial loading, with shear and lateral pressure loads likely as well. A useful expansion of this work would be to investigate ultimate strength formulations for these other types of loading, and possible interaction equations as well. The work done in the aerospace industry and the work of Kristensen[46] on the un-stiffened plates would be good starting points.

Several simplifications also had to be made to in modelling the material response of aluminium. While the Ramberg-Osgood relation was used to represent the stress-strain curve, several simplifications were still made. In general, aluminium exhibits different Ramberg-Osgood curve exponents in tension and compression, and extrusions may also be marked by anisotropic properties related to the direction of the extrusion[63]. Furthermore, the shape of the stress-strain curve seems to vary significantly from specimen to specimen, based on the results presented by Mofflin[45] and Zha and Moan[62]. These type of properties can typically be modelled with finite-element analysis. Finite-element analysis can in turn be combined with reliability approaches by using response-surface techniques. This would allow a sensitivity study to be made on the ultimate strength of aluminium plates or panels to see how important the currently excluded material characteristics are in

determining the reliability of the plate or panel. If the excluded parameters are shown to be significant, the strength formulations could be expanded to include them.

A third simplification that was made was that transverse welds at mid-panel length were excluded from this study. These welds clearly have the ability to reduce the strength of the panel, and methods are required to evaluate their effects on the ultimate limit state of the panel. Such behaviour could be included as part of a more advanced beam-column approach to modelling the stress-strain curves.

Producing an improved beam-column approach for the collapse of aluminium stiffened panels is an area worthy of more research. A simple extension of the modified Gordo and Faulkner approach presented here would be to switch the plate and column curves used in the approach from the U.S. Aluminum Association formulae to the equivalent Eurocode 9 formulae. For the A.R.E. test results which the models were compared to, the Eurocode 9 was much more consistent in its prediction than the prediction made from Aluminum Association formulae. In a similar vein, the maximum stress could be modified to including tripping as a failure mode, perhaps first examining the elastically-supported compression flange approximations presented by Sharp[9], or the elastic formulations discussed by Faulkner[162].

The modified approach presented here which was based on Faulkner's and Gordo's method has several significant limitations inherent to the approach it adopts. As it relies on existing column curves, it is not capable of including lateral pressures, nor is it capable of explicitly modelling the initial deflection of the panels. Adopting an approach based upon Hughes'[21] beam-column methods that include these effects would be a worthwhile extension. An additional shortcoming of the current approach is that the column curves are restricted to either modelling the behaviour of 5000 series alloys or 6000 series alloys, panels with 5000 series alloy plate and 6000 series alloy stiffeners can not be modelled. Again, a more detailed beam-column approach may be able to include this effect. Finally, as noted in the discussion in Chapter 3, there are some theoretical shortcomings in the tangent effective width relations in the Gordo approach which may be able to be treated more rigorously in a beam-column approach.

In a similar vein, the simple effective breadth expression used in this work for the response of plates should be examined. While the method gives reasonable results, it is not capable of including the effect of the Ramberg-Osgood exponent on the shape of the effective width curve. A more advanced formulation could be made attempting to include the Ramberg-Osgood exponent in the effective width relation. In developing such a formulation it would be useful to supplement Mofflin's test results with additional finite element

simulations. Little[132] and Kristensen[46] also reported good results in normalizing plate behaviour based on the stress at which point the elastic and plastic strains are equal, not the 0.2% offset proof stress. It would be worth re-examining the effective width approach using this value as the basis for normalization. The simple spring model developed for the tensile response of plates and panels could also be confirmed with non-linear finite element solutions.

6.2.2 Fatigue Strength

Similar to ultimate strength formulations, there is considerable scope for future research on fatigue formulations. The S-N approach presented here appeared to give reasonable values when compared to existing design codes, although the predicted safety indexes at a higher number of cycles were strongly dependent on the slope of the S-N curve used. Further comparisons at long lifetimes would be a valuable extension to this work, and benchmarking the reliability formulation against HSV designs which have proven acceptable in service and those that have not, would shed further light on what should be considered an acceptable value of the safety index for this method. Adapting Wirsching's lognormal fatigue reliability model for aluminium would also be interesting extension, especially as the information on uncertainties for HSVs are currently sparse enough that a simpler model such as the lognormal model may not end up being restrictive.

While the FOR approach proved accurate for most cases with the S-N fatigue limit state, an interesting extension would be to compare second-order and response surface techniques to see if they would be acceptably accurate for the cases of stochastic slope parameter where the FOR approach was not adequate.

Further fatigue tests of details common to high-speed craft would also be useful. Based on the experiences in this work of attempting to formulate design recommendations from a variety of data sources, it would seem favourable to conduct relative few but large test programs incorporating several specimens and a variety of load cases. As there is little fatigue data in the high-cycle region for ship structures, generating such data would be a worthwhile area of research. This may require different testing techniques to avoid the lengthy experimental times required to reach 10^7 or 10^8 cycles when testing at 1-10Hz. Further studies of variable-amplitude fatigue would also be useful, using accurate time-histories of the type of loads experienced on high-speed craft. In doing such experimental studies, consideration should be given to generating the necessary data for initiation-propagation fatigue approaches; including the number of cycles to crack initiation, and the local material and geometric properties at the initiation site.

There are many potential improvements that could be made to the initiation-propagation model proposed in this thesis. Examining the local strain cycling at the fatigue notch would be useful for quantifying the mean stress to be used in the initiation model. Additionally, comparisons with other initiation models than the Lawrence model used here would be valuable, alternative approaches are discussed in Sonsino et al.[252] and Radaj and Sonsino[224]. Effective methods must be developed for variable-amplitude loading, where calculating the local strain cycling on a cycle-by-cycle basis may prove too costly. Due consideration should also be given to more advanced fracture-mechanics growth relation than the simple Paris-Erdogan law used in this work. The loading on HSVs will be both variable amplitude and reversed loading consisting of alternation tension and compression, so the effects of residual stresses, threshold behaviour, and crack closure may be important in the fracture mechanics models. Many crack growth relations have been proposed that can include some or all of these effects. Expanding the initiation-propagation model to a stochastic formulation is a worthy research goal as well, though it seems logical to first concentrate efforts on improving the prediction performance for the mean growth curve.

Investigating a simpler I-P model where a S-N curve is used to predict a crack of several centimetres in length in the structure and fracture mechanics is used to model the growth of this crack, would also be an interesting research goal. Such an approach would avoid attempting to model the local properties of the fatigue notch beyond the hot-spot stress. Obtaining accurate data and prediction techniques for these properties seems to be one of the larger barriers in implementing the initiation-propagation approach. A key problem in attempting to create such a model would be rationally determining the crack length at the transition between the S-N approach and the fracture mechanics approach. Such a model also has the inherent difficulty that the initiation and small-crack growth periods have been combined into the S-N curve. As these are different physical processes, combining them may make generating a single S-N curve that would be valid for many different details difficult.

References

1. Moan, T. "Towards Structural Design of High-Speed Craft Based on Direct Calculations". in *FAST 2001*. 2003. Ischia, Italy. Keynote Lectures: 31-50.
2. Smith, C.S. "Influence of Local Compressive Failure on Ultimate Longitudinal Strength of a Ship's Hull". in *PRADS 77,*. 1977. Tokyo. 73-79.
3. Rutherford, S.E. and J.B. Caldwell. "Ultimate Longitudinal Strength of Ships". in *SNAME Annual Meeting 1990*. 1990. 14-1-14-26.
4. Collette, M., "Report on the Structural Inspection of the M/V SuperSeaCat 3", *Safety@Speed*, 2002, Report: S103.10.13.066.001(confidential).
5. Thomas, G., et al. "Transient Dynamic Slam Response of Large High Speed Catamarans". in *FAST 2003*. 2003. Ischia, Italy. Session B1 1-8.
6. Mansour, A.E., et al., "Structural Safety of Ships", *SNAME Transactions*, 1997. 105: 61-98.
7. Ayyub, B.M., et al., "Methodology for Developing Reliability-Based Load and Resistance Factor Design (LRFD) Guidelines for Ship Structures", *Naval Engineers Journal*, 2002. 114(2): 23-41.
8. Muckle, W., *The Design of Aluminium Alloy Ships' Structures*. 1963, London: Hutchinsons & Co. (for the Aluminium Development Association).
9. Sharp, M.L., *Behavior and Design of Aluminum Structures*. 1993, New York: McGraw-Hill.
10. Phillips, S., "Fast Ferry Safety Statistics", *Fast Ferry International*, 2004. 43(7): 35-36.
11. Austal Inc., *Auto Express 126*, <http://www.austal.com/datasheets/ae127-H260-Trimaran.pdf>, accessed 3 February 2005.
12. Austal Inc., *Auto Express 101*, <http://www.austal.com/datasheets/ae101-euroferry.pdf>, accessed 3 February 2005.
13. INCAT, *INCAT-Generations*, <http://www.incat.com.au/fleet_fs.html>, accessed 3 February 2005.
14. Rodriquez Cantieri Navali SpA, <http://www.rodriquez.it/fastferry/download/TMV%20115.pdf>, accessed March 27, 2005.
15. Fincantieri, "MDV 1200 Pegasus A.A. Fast Ferry: Final Stability Booklet", *Fincantieri*, 1999, GZ8350010M(Confidential).
16. Anon, *HSV 4676 WestPac Express*, <http://www.globalsecurity.org/military/agency/navy/hsv-4676.htm>, Global Security, accessed March 27, 2005.
17. Anon, *IX 532 / HSV 4676 Joint Venture HSV-X1/ HSV Austal Westpac Express*, <http://www.globalsecurity.org/military/systems/ship/hsv.htm>, accessed March 27 2005.
18. "The X-Craft- A Potential Solution to Littoral Warfare Requirements", *Warship Technology*, 2005(January): 9-12.
19. Cooper, M., et al., "Confirmation of Main Causes, Deliverable 3.1", *Safety@Speed*, 2001, S103.10.06.054.001(Confidential).
20. Paik, J.K. and A. Thayamballi, *Ultimate Limit State Design of Steel-Plated Structures*. 2003, London: John Wiley & Sons.
21. Hughes, O.F., *Ship Structural Design*. 1988, Jersey City, New Jersey: The Society of Naval Architects and Marine Engineers.
22. Mansour, A.E., et al., "Probability Based Ship Design: Implementation of Design Guidelines", *Ship Structure Committee*, 1996, SSC-392.
23. Joint Tanker Project, "Draft Common Structural Rules for Double Hull Oil Tankers", *Joint Tanker Project(ABS, DNV, and Lloyd's Register)*, 2004, June 2004.
24. Jensen, J.J. and et. al., *Report of Committee III.1, "Ductile Collapse"*, in *Proc. 12th International Ship and Offshore Structures Congress*, N.E. Jeffery and A.M. Kendrick, Editors. 1994. p. 229-387.

25. Mansour, A.E. and R.C. Ertekin, eds. *Proceedings of the 15th International Ship and Offshore Structures Congress*. 2003, Elsevier: San Diego.
26. Moan, T. and S. Berge, eds. *Proceedings of the 13th International Ship and Offshore Structures Congress*. 1997, Pergamon: Trondheim, Norway.
27. Ohtsubo, H. and Y. Sumi, eds. *Proceedings of the 14th International Ship and Offshore Structure Congress*. 2000, Elsevier: Nagasaki.
28. Caldwell, J.B., "Ultimate Longitudinal Strength", *Transactions of the Royal Institution of Naval Architects*, 1960. **107**: 411-430.
29. Paik, J.K. and A.E. Mansour, "A Simple Formulation for Predicting the Ultimate Strength of Ships", *Journal of Marine Science and Technology* 1995. **1**(1): 52-62.
30. Rahman, M.K. and M. Chowdhury, "Estimation of Ultimate Longitudinal Bending Moment of Ships and Box Girders", *Journal of Ship Research*, 1996. 40(3): 244-257.
31. Gordo, J.M. and C.G. Soares, "Approximate Method to Evaluate the Hull Girder Collapse Strength", *Marine Structures*, 1996. 9: 449-470.
32. Nielsen, L.P., *Structural Capacity of the Hull Girder*, PhD. Thesis, Department of Naval Architecture and Offshore Engineering, Technical University of Denmark, 1998.
33. Boote, D. and M. Figari. "Stress Distribution at Collapse for Fast Mono Hull Vessels". in *FAST 2001*. 2001. 153-161.
34. Lewis, E.V., ed. *Principles Of Naval Architecture*. Vol. I,II,III. 1988, The Society of Naval Architects and Marine Engineers: Jersey City, New Jersey.
35. Paik, J.K. and A. Thayamballi. "An Empirical Formulation for Predicting the Ultimate Compressive Strength of Stiffened Panels". in *7th International Offshore and Polar Engineering Conference (ISOPE)*. 1997. Honolulu: The International Society of Offshore and Polar Engineers. 328-338.
36. Rutherford, S.E., "Stiffened Compression Panels the Analytical Approach (Revision 2)", *Lloyd's Register of Shipping*, 1984, 82/26/R2. April 1984.
37. Steen, E., et al. "Computerized Buckling Models for Ultimate Strength Assessment of Stiffened Ship Hull Panels". in *Practical Design of Ships and Other Floating Structures (PRADS 04)*. 2004. Luebeck-Travemuende: Schiffbautechnische Gesellschaft. 235-242.
38. Paik, J.K. and A. Duran, "Ultimate Strength of Aluminum Plates and Stiffened Panels for Marine Applications", *Marine Technology*, 2004. **41**(3): 108-121.
39. Rigo, P., et al., "Sensitivity Analysis on Ultimate Strength of Aluminium Stiffened Panels", *Marine Structures*, 2003. **16**(6): 437-468.
40. Ayyub, B.M., et al., "Reliability-Based Design Guidelines for Fatigue of Ship Structures", *Naval Engineers Journal*, 2002. **114**(2): 113-138.
41. de Souza, G.F. and B.M. Ayyub, "Probabilistic Fatigue Life Prediction for Ship Structures Using Fracture Mechanics", *Naval Engineers Journal*, 2000. **112**(4): 375-397.
42. Lanning, D. and M.-H.H. Shen, "Reliability of Welded Structures Containing Fatigue Cracks", *Journal of Offshore Mechanics and Arctic Engineering, Transactions of the ASME*, 1996. **118**(4): 300-306.
43. Guedes Soares, C. and Y. Garbatov, "Fatigue reliability of the ship hull girder", *Marine Structures*, 1996. 9(3-4): 495-516.
44. Kissel, J.R. and R.L. Ferry, *Aluminum Structures: A Guide to Their Specifications and Design*. 2002, New York: John Wiley & Sons, Inc.
45. Mofflin, D.S., *Plate Buckling in Steel and Aluminium*, Phd Thesis, University of Cambridge, 1983.
46. Kristensen, O.H.H., *Ultimate Capacity of Aluminium Plates Under Multiple Loads, Considering HAZ Properties*, Department of Marine Structures, Norwegian University of Science and Technology, 2001.
47. Allday, W.J. "Methods of Avoiding Common Problems with Aluminium Structures". in *FAST 1991*. 1991. Trondheim, Norway. 765-780.
48. Adley, B., "Aluminium Alloys-Design For Fatigue", *Ship and Boat International*, 1993. September: 25-27.

49. Kissell, J.R. and R.L. Ferry, *Aluminum Structures: A Guide to Their Specifications and Design.* 2002, New York: John Wiley & Sons, Inc.
50. Mazzolani, F.M., *Aluminium Alloy Structures, 2nd Ed.* 1995, London: E & FN Spon.
51. Van Horn, K.R., ed. *Aluminum.* 1967, American Society for Metals: Metals Park, Ohio.
52. Mathers, G., *The Welding of Aluminium and Its Alloys.* 2002, Cambridge, England: Woodhead Publishing Limited.
53. The Aluminum Association, *Aluminum Design Manual: Specification for Aluminum Structures - Load and Resistance Factor Design Specification.* 7th ed. 2000, Washington, D.C: Aluminum Association.
54. "Aluminium Debacle Shakes US Shipbuilders", *Ship and Boat International,* 2002(July-August): 32-35.
55. "Aluminium and the Sea", *Pechiney/Rhenalu,* 2001,
56. Skillingberg, M., "The Aluminium Industry Continues Support for the Marine Market New Temper Definitions Published", *The Aluminum Association,* 2004, September 15, 2004.
57. *AEC General FAQs,* <http://www.aec.org/resources/faqgen.html>, accessed March 30, 2005.
58. *Friction Stir Welding,* <http://www.hma.hydro.com/hydro/ham/hamweb.nsf/all/96F1627732FFFFCBC125685F004A697F?OpenDocument>, Hydro Marine Aluminium, accessed March 30, 2005.
59. Aalberg, A., M. Langseth, and P.K. Larsen, "Stiffened Aluminium Panels Subjected to Axial Compression", *Thin-Walled Structures,* 2001. 39(10): 861-885.
60. European Committee for Standardization (CEN), *Eurocode 9: Design of Aluminium Structures.* 1998, Brussels: European Committee for Standardization (CEN). ENV 1999-1-1: 1998 E.
61. British Standards, *BS 8118: Structural Use of Aluminium.* 1991, London: BSI British Standards.
62. Zha, Y. and T. Moan, "Ultimate Strength of Stiffened Aluminum Panels with Predominantly Torsional Failure Modes", *Thin-Walled Structures,* 2001. 39(8): 631-648.
63. Moen, L.A., O.S. Hopperstad, and M. Langseth, "Rotational Capacity of Aluminum Beams Under Moment Gradient I: Experiments", *Journal of Structural Engineering,* 1999. 125(8): 910-920.
64. Hill, H.N., J.W. Clark, and R.J. Brungraber, "Design of Welded Aluminum Structures", *Journal of the Structural Division, Proceedings of the ASCE,* 1960. 86(ST6): 101-124.
65. DNV, *Rules for Classification of High Speed, Light Craft and Naval Surface Craft.* 2003, Hϕvik, Norway: Det Norske Veritas.
66. Hval, M., et al., "Numerical Modeling of Ductile Fracture Behavior in Aluminum Weldments", *Welding Journal Research Supplement,* 1998. 77(5): 208s-217s.
67. Övreas, L., C. Thaulow, and M. Hval. "Effect of Geometry and Size on the Mechanical Properties of AlMgSi1 Weldments". in *Proceedings of the 5th International Conference on Aluminium Weldments (INALCO).* 1992. 10.1.1-10.1.8.
68. Matusiak, M. and P.K. Larsen. "Strength and Ductility of Welded Connections in Aluminium Alloys". in *Joints in Aluminium - INALCO 98.* 1998. Cambridge. 299-310.
69. Mindlin, H., "Fatigue of Aluminum-Magnesium Alloys", *Welding Journal Research Supplement,* 1963. 42(6): 276s-281s.
70. Hval, M., R.H. Johnsen, and C. Thaulow. "Strength and Deformation Properties of Welded Aluminium Structures With Reference to Local Design and Material Properties". in *Proceedings of the 6th International Conference on Aluminium Weldments (INALCO).* 1995. 167-182.
71. Feng, F. and Z. Li. "The Effect of Post-Weld Heat Treatment on the Mechanical Properties of AA6082 T6 Welds". in *Aluminum 2001 - Proceedings of the TMS 2001 Aluminum Automotive and Joining Sessions.* 2001. 129-138.

72. Strombeck, A.v., et al. "A Comparison Between Microstructure, Properties And Toughness Behaviour of Power Beam and Friction Stir Welds in Al Alloys". in *Aluminum 2001 - Proceedings of the TMS 2001 Aluminum Automotive and Joining Sessions*. 2001.
73. Freudenthal, A.M., "Safety and the Probability of Structural Failure", *ASCE Transactions*, 1956. **121**: 1337-1397.
74. Assakkaf, I., et al., "Reliability-Based Load and Resistance Factor Design(LRFD) Guidelines for Stiffened Panels and Grillages of Ship Structures", *Naval Engineers Journal*, 2002. **114**(2): 89-111.
75. Haldar, A. and S. Mahadevan, *Reliability Assessment Using Stochastic Finite Element Analysis*. 2000, New York: John Wiley & Sons, Inc.
76. Downes, J. and Y. Pu, "Reliability-Based Sensitivity Analysis of Ships", *Proceedings of the Institution of Mechanical Engineers, Part M: Journal of Engineering for the Maritime Environment*, 2005. **In Press**.
77. Hess, P.E., et al., "Uncertainties in Material and Geometric Strength and Load Variables", *Naval Engineers Journal*, 2002. **114**(2): 139-165.
78. Jensen, J.J., *Load and Global Response of Ships*. Ocean Engineering Series, ed. R. Bhattacharyya and M.E. McCormick. Vol. 4. 2001, Oxford: Elsevier.
79. Munse, W.H., et al., "Fatigue Characterizations of Fabricated Ship Details for Design", *Ship Structure Committee*, 1982, SSC-318.
80. Haldar, A. and S. Mahadevan, *Probability, Reliability, and Statistical Methods in Engineering Design*. 2000, New York: John Wiley & Sons, Inc.
81. Melchers, R.E., *Structural Reliability Analysis and Prediction*. 2nd ed. ed. 1999, Chichester, England: John Wiley & Sons Ltd.
82. Press, W., et al., *Numerical Recipes in C*. 2nd edition ed. 1992, Cambridge: Cambridge University Press.
83. *The World-Wide Web Virtual Library: Random Numbers and Monte Carlo Methods*, <http://random.mat.sbg.ac.at/links/rando.html>, accessed April 1, 2005.
84. Rackwitz, R. and B. Fiessler, "Structural Reliability Under Combined Random Load Sequences", *Computers and Structures*, 1978. 9(5): 484-494.
85. Glen, I.F., et al., "Fatigue-Resistant Detail Design Guide for Ship Structures", *Ship Structure Committee*, 1995, SSC-405.
86. Kramer, R.K., B. Rampolla, and A. Magnusson, "Fatigue of Aluminum Structural Weldments", *Ship Structure Committee*, 2000, SSC-410. May 2000.
87. Friis Hansen, P., J. Juncher-Jensen, and P. Terndrup-Petersen. "Long Term Springing and Whipping Stresses in High-Speed Vessels." in *FAST 95*. 1995. Lubeck, Germany: Schiffbautechnische Gesellschaft. 473-485.
88. Jensen, J.J. and P.T. Pedersen, "Wave-Induced Bending Moments in Ships-A Quadratic Theory", *Transactions of the Royal Institution of Naval Architects*, 1979. **121**: 151-165.
89. Friis Hansen, P., J.J. Jensen, and P.T. Pedersen. "Wave-Induced Springing and Whipping of High-Speed Vessels". in *International Conference on Hydroelasticity in Marine Technology*. 1994. Trondheim, Norway: A.A. Balkema. 191-204.
90. Faltinsen, O.M. and R. Zhao, "Numerical Predictions of Ship Motions at High Forward Speed", *Philosophical Transactions of the Royal Society, Series A*, 1991. **A334**.
91. Jensen, J.J. and A.E. Mansour, "Estimation of Ship Long-Term Wave-Induced Bending Moment Using Closed-Form Expressions", *Transactions of The Royal Institution of Naval Architects Part B*, 2002. **144**: 41-55.
92. Sikora, J., A. Dinsenbacher, and J. Beach, "A Method For Estimating Lifetime Loads and Fatigue Lives For SWATH and Conventional Monohull Ships", *Naval Engineers Journal*, 1983. **May**: 63-85.
93. Sikora, J.P. and J.E. Beach. "Automated Method for Predicting Maximum Lifetime Loads and Fatigue Lives of Ships". in *9th Annual Energy Sources Technology Conference*. 1986. New Orleans. 267-277.

94. Sikora, J.P., R.W. Michaelson, and B.M. Ayyub, "Assessment of Cumulative Lifetime Seaway Loads for Ships", *Naval Engineers Journal*, 2002. **114**(2): 167-180.
95. Heggelund, S.E., B.W. Tveiten, and T. Moan. "Fatigue Analysis of High Speed Aluminium Catamarans". in *3rd International Forum on Aluminium Ships*. 1998. Haugesund, Norway.
96. Sikora, J.P. "Cumulative Lifetime Loadings For Naval Ships". in *ASME 1998 International Mechanical Engineering Congress and Exhibition-Recent and Advances in Mechanics of Aerospace Structures and Materials*. 1998. Anaheim, CA: ASME. 299-312.
97. Collette, M., "Investigation of Simplified Hull-Girder Ultimate Strength Methods for Aluminium Hulls", *Safety@Speed*, 2003, Report: S103.23.13.058.003c. January 2003.
98. DNV, "Fatigue Assessment of Ship Structures Class Note 30.7", *Det Norske Veritas*, 2001, Class Note 30.7. January 2001.
99. Jensen, J.J. and A.E. Mansour. "Estimation of Impulsive Wave-induced Loads on a FPSO". in *ICOSSAR 2005*. 2005. Rome, Italy. mini symposium ms-c2, paper 8.3.
100. Mansour, A.E. and A. Thayamballi, "Probability-Based Ship Design Loads and Load Combinations", *Ship Structure Committee*, 1993, SSC-373.
101. Blok, J.J. and W. Beukelman, "The High-Speed Displacement Ship Systematic Series Hull Forms-Seakeeping Characteristics", *SNAME Transactions*, 1984. **92**: 125-150.
102. DNV, *Rules for Classification of High Speed, Light Craft and Naval Surface Craft*. 2001, Hϕvik, Norway: Det Norske Veritas.
103. Collette, M., "Review of Simplified Ultimate Strength Methods for Aluminium Stiffened Panels", *Safety@Speed*, 2002, Report: S103.32.13.058.002a. December 2002.
104. Collette, M. and A. Incecik. "An Investigation of the Options for Evaluating the Compressive Strength and Reliability of Aluminium Stiffened Panels". in *FAST 2003*. 2003. Ischia, Italy. Session B2, 17-24.
105. Galambos, T.V., ed. *Guide to Stability Design Criteria for Metal Structures*. 4th Edition ed. 1988, John Wiley & Sons: New York.
106. Vasta, J., "Lessons Learnt from Full-Scale Ship Structural Tests", *SNAME Transactions*, 1958. **66**: 165-243.
107. Lang, D.W. and W.G. Warren, "Structural Strength Investigation of Destroyer Albuera", *Transactions of the Royal Institution of Naval Architects*, 1952. **94**: 243-286.
108. Seide, P., "The Effect of Longitudinal Stiffeners on One Side of A Plate on the Compressive Buckling Stress of the Plate-Stiffener Combination", *National Advisory Committee for Aeronautics (NACA)*, 1953, NACA Technical Note 2873. 1953.
109. Stowell, E.Z., "Compressive Strength of Flanges", *National Advisory Committee for Aeronautics (NACA)*, 1951, Report 1029 (Supercedes Technical Note 2020). 1951.
110. Anderson, R.A. and M.S. Anderson, "Correlation of Crippling Strength of Plate Structures with Material Properties", *National Advisory Committee for Aeronautics (NACA)*, 1956, Technical Note 3600. January 1956.
111. Muckle, W., "Resistance to Buckling of Light-Alloy Plates", *Transactions North East Coast Institution of Engineers and Shipbuilders*, 1948. **64**: 223-269.
112. Snaith, G.R., "A Note on the Comparative Buckling Properties of Mild-Steel and Aluminium-Alloy Plating", *The Shipbuilder and Marine Engine-Builder*, 1958(September).
113. Clark, J.W. and R. Rolf, "Buckling of Aluminum Columns, Plates, and Beams", *Journal of the Structural Division, Proceedings of the ASCE*, 1966. **92**(ST3): 17-38.
114. Chapuis, J. and T.V. Galambos, "Reliability of Aluminium Beam-Columns", *ASCE Journal of the Structural Division*, 1982. **108**(ST4): 709-727.
115. Galambos, T.V., "Load and Resistance Factor Design for Aluminum Structures", *Washington University*, 1979, Report No. 54. May 1979.
116. Herzog, M.A.M., "Simplified Design of Unstiffened and Stiffened Plates", *Journal of Structural Engineering*, 1987. **113**(10): 2111-2124.

117. Murray, N.W., "Buckling of Stiffened Panels Loaded Axially and in Bending", *Structural Engineer*, 1973. 51(7): 285-301.
118. Horne, M.R. and R. Narayanan, "Ultimate Capacity of Stiffened Plates Used in Girders", *Proc. Inst. of Civil Engineers*, 1976. 61(Part 2): 253-280.
119. Horne, M.R., P. Montague, and R. Narayanan, "Influence on Strength of Compression Panels of Stiffener Section, Spacing, and Welded Connection", *Proc. Inst. of Civil Engineers*, 1977. 63(Part 2): 1-20.
120. Faulkner, D., *Compression Test on Welded Eccentrically Stiffened Plates Panels*, in *Steel Plated Structures*, P. Dowling et al., Editor. 1977, Crosby Lockwood Staples: London. p. 581-617.
121. Smith, C.S., "Compressive Strength of Welded Steel Ship Grillages", *Transactions of the Royal Institution of Naval Architects*, 1975. 117: 325-359.
122. Faulkner, D., "A Review of Effective Plating For Use in the Analysis of Stiffened Plating in Bending and Compression", *Journal of Ship Research*, 1975. 19(1): 1-17.
123. Faulkner, D., et al., "Synthesis of Welded Grillages To Withstand Compression and Normal Loads", *Computers and Structures*, 1973. 3: 221-246.
124. Faulkner, D., *Compression Strength of Welded Grillages*, in *Ship Structural Design Concepts*, J.H. Evans, Editor. 1975, Cornell Maritime Press, Inc: Cambridge, Maryland.
125. Murray, N.W., "Analysis and Design of Stiffened Plates for Collapse Load", *The Structural Engineer*, 1975. 53(3): 153-158.
126. Adamchak, J.C., "ULTSTR: A Program for Estimating the Collapse Moment of a Ship's Hull Under Longitudinal Bending", *DTNSRDC Report 82/076 Oct.*, 1982, 82/076. October.
127. Dow, R.S., et al. "Evaluation of Ultimate Ship Hull Strength". in *SNAME Extreme Loads Response Symposium*. 1981. Arlington, Virginia. 133-148.
128. Dow, R.S., "N106C: A Computer Program for Elasto-Plastic, Large Deflection Buckling and Post-Buckling Behaviour of Plane Frames and Stiffened Panels", *AMTE(S)*, 1980, R80726. July, 1980.
129. Chen, Y.K., et al., "Ultimate Strength of Ship Structures ", *SNAME Transactions* 1983. 91: 149-168.
130. Udea, Y., S. Rashed, and J.K. Paik, "Plate and Stiffened Plate Units of the Idealized Structural Unit Method", *Journal of the Society of Naval Architects of Japan*, 1984. 156: 366-376.
131. Little, G.H., "Collapse Analysis of Plates With Strain Hardening", *International Journal of Mechanical Sciences*, 1981. 23(9): 561-576.
132. Little, G.H., "Collapse Behaviour of Aluminium Plates", *International Journal of Mechanical Sciences*, 1981. 24(1): 37-45.
133. Clarke, J.D. and J.W. Swan, "Interframe Buckling of Aluminium Alloy Stiffened Plating", *Admiralty Research Establishment Dunfermline*, 1985, AMTE(S) R85104. October, 1985.
134. Clarke, J.D. "Buckling of Aluminium Alloy Stiffened Plate Ship Structure". in *Aluminium Structures: Advances, Design, and Construction. Proceedings of International Conference on Steel and Aluminium Structures*. 1987. Cardiff: Elsevier Applied Science. 81-92.
135. Gordo, J.M. and C.G. Soares. "Approximate Load Shortening Curves for Stiffened Plates Under Uniaxial Compression". in *Integrity of Offshore Structures-5*. 1993. Glasgow: EMAS Publishers. 189-211.
136. Gordo, J.M., C.G. Soares, and D. Faulkner, "Approximate Assessment of the Ultimate Longitudinal Strength of the Hull Girder", *Journal of Ship Research*, 1996. 40(1): 60-69.
137. Yao, T. and P. Nikolov, "Progressive Collapse Analysis of a Ship's Hull under Longitudinal Bending", *Journal of the Society of Naval Architects of Japan*, 1991. 170: 449-461.
138. Yao, T. and P. Nikolov, "Progressive Collapse Analysis of a Ship's Hull Under Longitudinal Bending", *Journal of the Society of Naval Architects of Japan*, 1992. 172: 437-446.

139. Dow, R.S. "Testing and Analysis of 1/3 Scale Welded Steel Frigate Model". in *Proceedings of the International Conference on Advanced Marine Structures*. 1991. ARE, Dunfermline, Scotland.
140. Yao, T. "Ultimate Longitudinal Strength of Ship Hull Girder: Historical Review and State of the Art". in *Eighth ISOPE Proceedings, Montreal*. 1998. 1-10.
141. Hopperstad, O.S., M. Langseth, and L. Hanssen, "Ultimate Compressive Strength of Plate Elements in Aluminium: Correlation of Finite Element Analyses and Tests", *Thin-Walled Structures*, 1998. 29(31-46).
142. Kristensen, O.H.H. and T. Moan. "Ultimate Strength of Aluminium Plates Under Biaxial Loading". in *FAST 99*. 1999. Seattle: Society of Naval Architects and Marine Engineers. 1-15.
143. Herrington, P.D. and R.G. Latorre, "Development of an Aluminum Hull Panel for High-Speed Craft", *Marine Structures*, 1998. 11(1-2): 47-71.
144. Tanaka, Y. and K. Matsuoka. "Buckling Strength of Lightened Aluminum Hull Structures". in *Proceedings of the 1997 7th International Offshore and Polar Engineering Conference Vol 4*. 1997. Honolulu. 790-797.
145. Zha, Y. and T. Moan, "Experimental and Numerical Prediction Collapse of Flatbar Stiffeners in Aluminum Panels", *Journal of Structural Engineering*, 2003. 129(2): 160-168.
146. Zha, Y., T. Moan, and E. Hanken. "Experimental and Numerical Studies of Torsional Buckling of Stiffeners in Aluminium Panels". in *ISOPE*. 2000. Seattle. 249-255.
147. Abildgaard, P.M., P.W. Hansen, and B.C. Simonsen. "Ultimate Strength of Welded Aluminium Structures". in *HIPER 2001*. 2001.
148. Xiao, Y. and C.C. Menzemer, "Ultimate Compressive Strength of Aluminum Plate Elements", *Journal of Structural Engineering*, 2003. 129(11): 1441-1447.
149. Setta, K., D. Yanagihara, and F. Masahiko. "Buckling/Plastic Collapse Behaviour and Estimation of Ultimate Strength of Aluminium Stiffened Plate". in *Proceedings of the Twelfth International Offshore and Polar Engineering Conference, Vol 4*. 2002. 636-643.
150. Mofflin, D.S. and J.B. Dwight. "Buckling of Aluminium Plates in Compression". in *Behaviour of Thin Walled Structures*. 1984: Elsevier. 399-427.
151. Paik, J.K., A. Duran, and D.H. Lee. "Ultimate Strength Formulae for Aluminum Plates and Stiffened Panels Under Axial Compressive Loads". in *RINA International Conference on Advanced Marine Materials*. 2003. London: RINA.
152. Bulson, P.S., "The Treatment of Thin-Walled Aluminium Sections in Eurocode 9", *Thin-Walled Structures*, 1997. 29(1-4): 3-12.
153. Cobden, R., "TALAT Lecture 1501: Aluminium:Physical Properties, Characteristics, and Alloys", in *TALAT CD-ROM*. 1994, European Aluminium Association.
154. Lin, Y.T., *Ship Longitudinal Strength Modeling. PhD. Thesis*, Department of Naval Architecture and Ocean Engineering, University of Glasgow, 1985.
155. Faulkner, D., *Compression Tests on Welded Eccentrically Stiffened Plate Panels*, in *Steel Plated Structures*, P.A. Frieze, Editor. 1977, Crosby Lockwood Staples: London. p. 581-617.
156. Niho, O., *Ultimate Strength of Plated Structures*, Department of Naval Architecture and Ocean Engineering, University of Tokyo. (in Japanese), 1978.
157. Yao, T., *Ultimate Compressive Strength of Ship Plating*, Department of Naval Architecture and Ocean Engineering, Osaka University. (in Japanese), 1980.
158. Murray, N.W., "The Behaviour of Thin Stiffened Steel Plates", *IABSE Proceedings*, 1973. 33(1): 191-201.
159. Murray, N.W., "Das Stabilitatsverhalten von Axial Belasteten, in Langsrichtung Ausgesteiften Platten im Plastischen Bereich", *Stahlbau*, 1973. 42(12): 372-379.
160. Sharp, M.L., "Longitudinal Stiffeners for Compression Members", *Journal of the Structural Division, Proceedings of the ASCE*, 1966. 96(ST 5): 187-211.
161. Chatterjee, S. and P. Dowling. "The Design of Box Girder Compression Flanges". in *Steel Plated Structures: An International Symposium*. 1977. London: Crosby Lockwood Staples.

162. Faulkner, D. "Toward a Better Understanding of Compression Induced Tripping". in *Steel and Aluminium Structure*, 3. 1987: Elsevier Applied Science. 159-175.
163. Guedes Soares, C. and A.P. Teixeira, "Structural Reliability of Two Bulk Carrier Designs", *Marine Structures*, 2000. 13(2): 107-128.
164. Pohler, C.H., et al., "A Technology Base for Aluminum Ship Structures", *Naval Engineers Journal*, 1979(October): 33-43.
165. Collette, M., "Fatigue and Longevity Model: Deliverable No. D3.2.4", *Safety@Speed*, 2002, S103.24.13.051.001A(Confidential). September 2002.
166. Collette, M. and A. Incecik, "An Approach for Reliability-Based Fatigue Design of Welded Joints on Aluminum High-Speed Vessels", *Accepted for Publication in the Journal of Ship Research.*
167. Huther, M. "Fatigue Testing and Evaluation of Data for Design". in *IIS/IIW-Committee XIII Meeting*. 2002. Tokyo.
168. Shigley, J. and C. Mischke, *Mechanical Engineering Design*. 5th ed. ed. 1989, New York: McGraw-Hill, Inc.
169. Stephens, R.I., et al., *Metal Fatigue in Engineering*. 2nd Edition ed. 2001, New York: John Wiley & Sons, Inc.
170. Violette, F.L.M., et al. "Basic Parameters Governing the Fatigue of Aluminum Ships". in *3rd International Forum on Aluminium Ships*. 1998. Haugesund, Norway.
171. ABS, "ABS Rules for Building and Classing Steel Vessels 1998-1999: Appendix 5/2AA-Fatigue Strength Assessment of Tankers". 1999, American Bureau of Shipping: New York.
172. Tveiten, B.W. and T. Moan. "Fatigue Assessment of Welded Aluminum Ship Details". in *FAST 99*. 1999. Seattle: Society of Naval Architects and Marine Engineers. 1-18.
173. Fricke, W., "Fatigue Analysis of Welded Joints: State of Development", *Marine Structures*, 2003. 16(3): 185-200.
174. Maddox, S.J., "Review of fatigue assessment procedures for welded aluminium structures", *International Journal of Fatigue*, 2003. 25(12): 1359-1378.
175. Barsom, J.M. and S.T. Rolfe, *Fracture and Fatigue Control in Structures : Applications of Fracture Mechanics*. 1999: ASTM.
176. Sharp, M.L., G.E. Nordmark, and C.C. Menzemer, *Fatigue Design of Aluminum Components and Structures*. 1996, New York: McGraw-Hill.
177. Jordan, C.R. and C.S. Cochran, "In-Service Performance of Structural Details", *Ship Structures Committee*, 1978, SSC-272.
178. Jordan, C.R. and C.S. Cochran, "Further Survey of In-Service Performance of Structural Details", *Ship Structures Committee*, 1980, SSC-294.
179. Wirsching, P.H., "Fatigue Reliability of Offshore Structures", *Journal of Structural Engineering*, 1984. 110(10): 2340-2356.
180. Argy, G., P.C. Paris, and F. Shaw, *Fatigue Crack Growth and Fracture Toughness of 5083-0 Aluminum Alloy*, in *Properties of Materials for Liquefied Natural Gas Tankage, STP 579*, J.G. Kaufman, Editor. 1975, ASTM: Philadelphia. p. 96-137.
181. Kaufman, J.G. and R.A. Kelsey, *Fracture Toughness and Fatigue Properties of 5083-O Plate and 5183 Welds for Liquefied Natural Gas Applications*, in *Properties of Materials for Liquefied Natural Gas Tankage, STP 579*, J.G. Kaufman, Editor. 1975, ASTM: Philadelphia. p. 138-158.
182. Kelsey, R.A., R.H. Wygonik, and P. Tenge, *Crack Growth and Fracture of Thick 5083-0 Plate Under Liquefied Natural Gas Ship Spectrum Loading*, in *Properties of Materials for Liquefied Natural Gas Tankage, STP 579*, J.G. Kaufman, Editor. 1975, ASTM: Philadelphia. p. 44-79.
183. Person, N.L. and G.C. Wolfer, *Fatigue Crack Growth Rate of Thick 5083-0 Plate at Room and Low Temperatures*, in *Properties of Materials for Liquefied Natural Gas Tankage, STP 579*, J.G. Kaufman, Editor. 1975, ASTM: Philadelphia. p. 80-95.

184. Sakai, K., et al., "A Study on Fatigue Evaluation of A5083-0/A5183 Stiffened Plate Structure", *International Institute of Welding*, 1983, IIW Document XIII-1096-83.
185. Fujitani, T., et al. "IHI SPB LNG carrier - fatigue strength, quality control and recent design development". in *Gastech 84 LNG/LPG Conference.* 1985. Amsterdam, Neth: Gastech Ltd, Rickmansworth, Engl. 232-255.
186. Chu, H.P., "Fatigue crack propagation in a 5456-H117 aluminum alloy in air and seawater", *Journal of Engineering Materials and Technology, Transactions of the ASME*, 1974. 96-H(4): 261-217.
187. Chu, H.P., J.A. Hauser, and J.P. Sikora, "Fatigue Crack Growth in Stiffened Panels under Pressure Loading", in *Design of Fatigue and Fracture Resistant Structures, ASTM STP 761*, P.R. Abelkis and C.M. Hudson, Editors. 1982. 345-372.
188. Birmingham, J.T., et al. "Development of a Fatigue Lifetime-Load Spectrum for a Large-Scale Aluminum Ship Model". in *Service Fatigue Loads Monitoring, Simulation, and Analysis, ASTM STP 671.* 1979. Philadelphia: American Society for Testing and Materials. 121-143.
189. Johnson, R.E. and J.E. Beach, "The Aluminum Ship Evaluation Model (ASEM) Static Test Results", *David Taylor Naval Ship Research and Development Center*, 1983, DTNSRDC-83/079. December 1983.
190. Wirsching, P. and Y.-N. Chen, "Considerations of Probability-Based Fatigue Design for Marine Structures", *Marine Structures: Design Constrution and Safety*, 1988. 1(1): 23-45.
191. May, R. and N. Barltrop, "Fatigue in Fast Craft", *Ship and Boat International*, 1993. **September**: 35-37.
192. Olkinuora, P., et al. "Structural Design of an Aluminium Missile Boat". in *FAST 91.* 1991. Trondheim, Norway. 727-741.
193. Taliva, J. and R. Wiefelsputt. "Offshore Measurements on Large Scale Model and Investigation of Structural Response Aspects of Slamming Loads for High-Speed Monohulls". in *FAST 1991.* 1991. Trondheim, Norway. 797-809.
194. Hermundstad, O.A., M. Wu, and T. Moan. "Hydroelastic Response Analysis of a High-Speed Monohull". in *Hydroelasticity in Marine Technology.* 1994. Trondheim, Norway. 245-259.
195. Faltinsen, O. and R. Zhao, "Numerical Predictions of Ship Motions at High Forward Speed", *Phil. Trans. R. Soc. London*, 1991. **A 334**: 241-257.
196. Jensen, J.J. and P.T. Pedersen, "Wave Induced Bending Moments in Ships-a Quadratic Theory", *Transactions-RINA*, 1979. **121**: 151-165.
197. Jensen, J.J. and M. Dogliani, "Wave-induced Ship Hull Vibrations in Stochastic Seaways", *Marine Structures*, 1996. 9(4): 353-387.
198. Friss-Hansen, P., "On Combination of Slamming and Wave Induced Responses", *Journal of Ship Research*, 1994. 38(2): 104-114.
199. Friis Hansen, P. and A.K. Thayamballi, "Fatigue Damage Considering Whipping Arising From Slamming", *OMAE 95 Vol II*, 1995: 155-163.
200. Xu, T., "Fatigue of Ship Structural Details-Technical Development and Problems", *Journal of Ship Research*, 1997. 41(4): 318-331.
201. Frediksen, A. "Fatigue Aspects of High Speed Craft". in *Fast '97.* 1997: Baird Publications. 217-224.
202. Skjelby, T., M. Lindgren, and A. Kjeldaas. "Fatigue Evaluations for High-Speed Light Craft Based on Direct Load Transfer Procedures". in *FAST 99.* 1999. Seattle: Society of Naval Architects and Marine Engineers. 673-682.
203. Donovan, J. and R. Humphrey, "The Evaluation of Fatigue Performance of Aluminum High Speed Craft", *HIPER 99*, 1999.
204. Polezhaeva, H. and W. Malinowski. "Fatigue Strength of Aluminum Structural Details of Special Service Craft". in *Fast 2001.* 2001. London: RINA. 135-142.

205. Fricke, W., et al., "Comparative Fatigue Strength Assessment of a Structural Detail in a Containership Using Various Approaches of Classification Societies", *Marine Structures*, 2001(15): 1-13.
206. Folsø, R., S. Otto, and G. Parmentier, "Reliability-Based Calibration of Fatigue Design Guidelines for Ship Structures", *Marine Structures*, 2002. 15(6): 627-651.
207. Hobbacher, A., *Fatigue Design of Welded Joints and Components: Recommendations of IIW Joint Working Group XIII-XV*. 1996, Cambridge: Abington.
208. Partanen, T. and E. Niemi, "Hot Spot S-N Curves Based on Fatigue Tests of Small Mig-Welded Aluminium Specimens", *Welding in the World*, 1999. 43(1): 16-22.
209. Tveiten, B.W., *Fatigue Assessment of Welded Aluminium Ship Details*, PhD Thesis, Department of Marine Structures, Norwegian University of Science and Technology, 1999.
210. Sharp, M.L. and G.E. Nordmark, "Fatigue Strength of Welded Tubular Aluminum Truss", *Journal of the Structural Division, Proceedings of the ASCE*, 1977(August): 1619-1629.
211. Sharp, M.L., G.E. Nordmark, and C.C. Menzemer. "Hot-Spot Design of Aluminum Joints". in *Materials for the New Millennium*. 1996. Washington, D.C.: ASCE. 1027-1036.
212. Dijkstra, O.D., et al. "Fatigue Testing of Large Scale Details of a Large Size Aluminium Surface Effect Ship". in *PRADS 1998*. 1998: Elsevier Science B.V. 865-872.
213. Jensen, J.J., R. Tornqvist, and P.-E.W. Nielsen. "Fatigue Damage Predictions in Aluminium Structures". in *Fatigue 2002*. 2002. Stockholm. 3253-3260.
214. Sears, M. and M. Birk-Sorensen, "Aluminium Fatigue Tests", *Knud E. Hansen*, 2000, SASAK-RAP-LE-AKS-KEH-0006-03. September 2000.
215. ASTM, *ASTM Standard E 739-91: Standard Practice for Statistical Analysis of Linear of Linearized Stress-Life and Strain-Life Fatigue Data*, in *2000 Annual Book of ASTM Standards*. 2000, ASTM. p. 631-637.
216. BSI, "BS 3518-5:1996 Methods of Fatigue Testing- Part 5 Guide to the Application of Statistics". 1999, British Standards Institute.
217. Wirsching P.H. et al., "Fatigue Reliability: Variable Amplitude Loading", *Journal of the Structural Division, Proceedings of the ASCE*, 1982. 108(ST1): 47-69.
218. James, M.N., A.E. Paterson, and N. Sutcliffe, "Constant and Variable Amplitude Loading of 6261 Aluminium Alloy I-Beams with Welded Cover Plates--Influence of Weld Quality and Stress Relief", *International Journal of Fatigue*, 1997. 19(2): 125-133.
219. Song, R. and T. Moan. "Fatigue Reliability of Large Catamaran Considering Inspection Updating". in *ISOPE 98*. 1998. 412-419.
220. Doerk, O., W. Fricke, and C. Weissenborn, "Comparison of Different Calculation Methods for Structural Stresses at Welded Joints", *International Journal of Fatigue*, 2003. 25(5): 359-369.
221. Fricke, W. and H. Petershagen. "Detail Design of Welded Ship Structures Based on Hot-Spot Stresses". in *PRADS '92*. 1992. Newcastle. 2.1087-2.1100.
222. Fricke, W. "Recommended Hot Spot Analysis Procedure for Structural Details of FPSOs and Ships Based on Round-Robin FE Analyses". in *ISOPE 2001*. 2001. Stavanger, Norway. 89-96.
223. Radaj, D., "Review of fatigue strength assessment of nonwelded and welded structures based upon local parameters", *International Journal of Fatigue*, 1996. 18(3): 153-170.
224. Radaj, D. and C.M. Sonsino, *Fatigue Assessment of Welded Joints by Local Approaches*. 1999, Norwich, New York: William Andrew Publishing.
225. Tavernelli, J.F. and L.F. Coffin Jr., "Experimental Support for Generalized Equation Predicting Low Cycle Fatigue, plus discussion by S.S. Manson", *Transactions of the ASME, Journal of Basic Engineering*, 1962. 84(4): 533-537.
226. Paris, P.C., *The Growth of Fatigue Crack Due to Variations in Load*, Phd. Thesis, Lehigh University, 1962.

227. Paris, P.C., M.P. Gomez, and W.E. Anderson, "A Rational Analytic Theory of Fatigue", *The Trend in Engineering at the University of Washington*, 1961. **13**(1): 9-14.
228. Paris, P.C. and F. Erdogan, "A Critical Analysis of Crack Propagation Laws", *Journal of Basic Engineering, Transactions of the ASME*, 1963. **85**: 528-534.
229. Paris, P.C., "Fracture Mechanics and Fatigue: A Historical Perspective", *Fatigue and Fracture of Engineering Materials & Structures*, 1998. **21**(5): 535-540.
230. Lawrence, F.V., et al. "Estimating the Fatigue Crack Initiation Life of Welds". in *ASTM STP 648, Fatigue Testings of Weldments Symposium*. 1978. Toronto: ASTM. 134-158.
231. Socie, D.F., J. Morrow, and W.-C. Chen, "A Procedure for Estimating the Total Fatigue Life of Notched and Crack Members", *Engineering Fracture Mechanics*, 1979. **11**: 851-859.
232. Ho, N.-J. and J. Lawrence, F. V., "Constant amplitude and variable load history fatigue test results and predictions for cruciform and lap welds", *Theoretical and Applied Fracture Mechanics*, 1984. **1**(1): 3-21.
233. Yang, J.N., G.C. Salivar, and C.G. Annis Jr., "Statistical Modeling of Fatigue-Crack Growth in a Nickel-Base Superalloy", *Engineering Fracture Mechanics*, 1983. **18**(2): 257-270.
234. Yang, J.N., et al., *Stochastic Crack Growth Models for Applications to Aircraft Structures*, in *Probabilistic Fracture Mechanics and Reliability*, J.W. Provan, Editor. 1987, Martinus Nijhoff: Dordrecht.
235. Yang, J.N. and S.D. Manning, "Stochastic Crack Growth Analysis Methodologies for Metallic Structures", *Engineering Fracture Mechanics*, 1990. **27**(5): 1105-1124.
236. Yang, J.N. and S.D. Manning, "A Simple Second Order Approximation for Stochastic Crack Growth Analysis", *Engineering Fracture Mechanics*, 1996. **53**(5): 677-686.
237. Wu, W.F. and C.C. Ni, "A Study of Stochastic Fatigue Crack Growth Modeling Through Experimental Data", *Probabilistic Engineering Mechanics*, 2003. **18**(2): 107-118.
238. Shetty, N.K. and M.J. Bakler. "Fatigue Reliability of Tubular Joints in Offshore Structures: Reliability Analysis". in *Proceedings of the International Offshore Mechanics and Arctic Engineering Symposium (OMAE)*. 1990. Vol 2 231-239.
239. Lecsek, R.L., et al., "Probabilistic model for initiation and propagation of surface cracks in welded joints", *Fatigue and Fracture of Engineering Materials & Structures*, 1995. **18**(7-8): 821-831.
240. Guedes Soares, C. and Y. Garbatov. "Influence of Inspection and Repair on the Fatigue Reliability of Oil Tankers". in *Offshore Mechanics and Arctic Engineering (OMAE)*. 1996: ASME. 245-254.
241. Garbatov, Y. and C. Guedes Soares. "Fatigue Reliability of Maintained Welded Joints in the Side Shell of Tankers". in *Offshore Mechanics and Arctic Engineering (OMAE)*. 1997: ASME. 219-228.
242. Guedes Soares, C. and Y. Garbatov, *Reliability Based Fatigue Design of Maintained Welded Joints in the Side Shell of Tankers*, in *Fatigue Design and Reliability*, G. Marquis and J. Solin, Editors. 1999, Elsevier: Amsterdam. p. 13-28.
243. Guedes Soares, C. and Y. Garbatov, "Reliability of Corrosion Protected and Maintained Ship Hulls Subject to Corrosion and Fatigue", *Journal of Ship Research*, 1999. **43**(2): 65-78.
244. Guedes Soares, C. and Y. Garbatov, "Reliability of Maintained Ship Hulls Subjected to Corrosion and Fatigue Under Combined Loading", *Journal of Constructional Steel Research*, 1999. **52**(1): 93-115.
245. Chang, P.Y., "A State-of-the-Art Review of the Reliability Approach and Methodology for the Design of Aerospace and Ocean Systems", *Marine Technology*, 1990. **27**(5): 300-320.
246. Kaminski, M. and M. Krekel. "Reliability Analysis of Fatigue Sensitive Joints in FPSO". in *OMAE 95*. 1995. 175-186.

247. Di, S., et al. "Development of a Generic Ship Model for the Study of Fatigue in Welded Aluminium Catamaran". in *FAST 97*. 1997. Sydney. 629-636.
248. Berkovits, A., D.W. Kelly, and S. Di, "Considerations of the effect of residual stresses on fatigue of welded aluminum alloy structures", *Fatigue and Fracture of Engineering Materials & Structures*, 1998. **21**(2): 159-170.
249. Spyker, R., D. Kelly, and M. Chowdhury. "Fatigue Analysis of Ship Structures Using Fracture Mechanics". in *Sea Australia 2000*. 2000. Sydney, Australia. Session 23, Paper 23.1.
250. Brandt, U., F.V. Lawrence, and C.M. Sonsino, "The Fatigue Behaviour of 5 and 25mm 5083 Aluminium Alloy Weldments", *International Institute of Welding*, 1998, IIW Document XIII-1718-98.
251. Brandt, U., F.V. Lawrence, and C.M. Sonsino, "Fatigue crack initiation and growth in AlMg4.5Mn butt weldments", *Fatigue and Fracture of Engineering Materials and Structures*, 2001. **24**(2): 117-126.
252. Sonsino, C.M., et al., "Fatigue assessment of welded joints in AlMg 4.5Mn aluminum alloy (AA 5083) by local approaches", *International Journal of Fatigue*, 1999. **21**(9): 985-999.
253. Fricke, W. and Muller-Schmerl, *Consideration of Crack Propagation Behaviour in the Design of Cyclic Loaded Structures*, in *Fatigue Design and Reliability*, G. Marquis and J. Solin, Editors. 1999, Elsevier: Amsterdam. p. 163-172.
254. Sun, H.H. and Y. Bai. "Reliability Assessment of a FPSO Hull Girder Subjected to Degradations of Corrosion and Fatigue". in *ISOPE 2000*. 2000. Seattle, WA, USA: ISOPE. 355-363.
255. Sun, H.H. and Y. Bai, "Time-Variant Reliability Assessment of FPSO Hull Girders", *Marine Structures*, 2003. **16**(3): 219-253.
256. Sun, H.H., G.-H. Liao, and Y. Bai, "Reliability Analysis of Ship Hull Girders Considering the Degradations of Corrosion and Fatigue", *Key Engineering Materials*, 2000. **183**: 1023-1028.
257. Terai, K., et al. "Fatigue Design Method of Ship Structural Members Based on Fatigue Crack Growth Analysis". in *ISOPE 2001*. 2001. Stavanger, Norway. 5899-594.
258. Akpan, U.O., et al., "Risk Assessment of Aging Ship Hull Structures in the Presence of Corrosion and Fatigue", *Marine Structures*, 2002. **15**(3): 211-231.
259. Cui, W., "A Feasible Study of Fatigue Life Prediction for Marine Structures Based on Crack Propagation Analysis", *Engineering for the Maritime Environment, Proceedings of IMechE*, 2003. **217**(Part M): 11-23.
260. Lassen, T. "Damage tolerance assessment of welded joints subjected to fatigue crack growth". in *ISOPE 98*. 1998. Montreal: The International Society of Offshore and Polar Engineers. 27-32.
261. Miller, M.S. and J.P. Gallagher. "Further Review of Fracture Mechanics Crack Growth Laws". in *ASTM STP 738, Fatigue Crack Growth Measurement and Data Analyses*. 1981: ASTM. 205-251.
262. Tada, H., P.C. Paris, and G. Irwin, *The Stress Analysis of Cracks Handbook, 3rd Ed.* 2000, New York: ASME.
263. British Standards, *BS 7910:1999 Guide On Methods for Assessing the Acceptability of Flaws in Metallic Structures*. 1999, London: British Standards.
264. Graf, U. and D. Kosteas. "Data Basis for Fracture Mechanics Analysis of Aluminium Weldments". in *Third International Conference on Aluminium Weldments*. 1985. Munich. IV.6.
265. Paauw, A.J. and E. Bardahl. "Fatigue Crack Growth in Aluminium Alloy AlMgSi1 in Air and Saltwater". in *Third International Conference on Aluminium Weldments*. 1985. Munich, Germany. Paper V.9.
266. Nordmark, G.E. and J.W. Clark, "Fatigue of Joints in Aluminum Alloy 6061-T6", *Journal of the Structural Division, Proceedings of the ASCE*, 1964. 90(ST6): 35-50.

267. Person, N.L., "Fatigue of Aluminum Alloy Welded Joints", *Welding Journal Research Supplement*, 1971. 50(2): 77s-87s.
268. Newman Jr., J.C. and I.S. Raju, "An empirical stress-intensity factor equation for the surface crack", *Engineering Fracture Mechanics*, 1981. 15(1-2): 185-192.
269. Bowness, D. and M.M.K. Lee, "Prediction of Weld Toe Magnification Factors for Semi-Elliptical Cracks in T-butt Joints", *International Journal of Fatigue*, 2000. 22(5): 389-396.
270. Ando, K., et al., "Fatigue life and fatigue crack through-thickness behavior of a surface-cracked plate (For the case of tensile load)", *JSME International Journal*, 1987. 30(270): 1898-1905.
271. Nam, K.W., et al., "Fatigue life and penetration behaviour of a surface-cracked plate under combined tension and bending", *Fatigue and Fracture of Engineering Materials & Structures*, 1994. 17(8): 873-882.
272. Nam, K.W., et al., "Fatigue life and fatigue crack through-thickness behavior of a surface-cracked plate (Effect of stress concentration)", *JSME International Journal Series I*, 1988. 31(2): 272-279.
273. Nam, K.W., K. Ando, and N. Ogura, "Surface fatigue crack life and penetration behavior of stress concentration specimen", *Engineering Fracture Mechanics*, 1995. 51(1): 161-166.
274. Nam, K.W., K. Iwase, and K. Ando, "Fatigue life and surface crack penetration behaviour of an aluminium alloy", *Fatigue and Fracture of Engineering Materials & Structures*, 1995. 18(2): 179-187.

Appendix A: Computer Programs

Overview of Software: AluShip

As part of the research work on this thesis, an extensive range of calculation techniques were investigated, including hydrodynamic, structural, and reliability assessment. Initially, several small programs, Mathcad documents, and Excel spreadsheets were used for these calculations. However, as the research progressed, it was clear that there was an advantage in tying together many of these methods into a single program. This was done in the AluShip program, which aims for automated analysis of aluminium ships. The program was designed as a piece of research code, and was structured using an object-oriented approach, to make it easier to modify and extend in the future. At the moment, the code is not complete in the sense that not all the methods explored in the thesis have been implemented, but substantial progress has been made. The code has been released under the GPL open-source licence for use by other researchers. The code is research code and has been in continual development for the past three years, and no guarantee is made of the accuracy, stability, or suitability of the code for any purpose. The code is suitable for further development, but not yet ready to run as a design tool. This appendix is aimed to give an overview and initial guide to the code for researchers who wish to extend it.

AluShip currently models a transverse cross-section of a high-speed craft which can be built up from various aluminium materials, plates, and stiffeners. Ultimate strength, load-shortening curve predictions, and Smith-type progressive collapse are all currently implemented, long-term loading calculations and S-N fatigue reliability predictions are coded as objects, but not tied into calculation procedures yet. The material, components, and section are all specified in a XML-formatted input file, and the output is written to a similar file. However, the size of the output file makes reading it by hand difficult, and a database or filtering approach would be beneficial for interpreting the large amounts of data available. The code has been written entirely in C++, making extensive use of the open-source GNU Scientific Library[1] and the TinyXML[2] XML parser and document object model. The source code has been documented using the Doxygen[3] system so that a user guide to the code can be automatically created, as discussed further under the source code and documentation section.

As of the end of this thesis, the following functionality is available in AluShip:

---

[1] Available at: http://sources.redhat.com/gsl/

[2] Available at: http://www.grinninglizard.com/tinyxml/

[3] Available at: http://www.stack.nl/~dimitri/doxygen/

- **Materials:** Aluminium-type materials can be entered with different uniaxial properties in tension, compression, and in the HAZ. A Ramberg-Osgood model is used for the material properties in each direction/condition
- **Stiffeners:** Flat bar, angle bulb, tee-stiffeners, and generic stiffeners defined only by their overall geometric properties and HAZ extents are allowed. Some calculation methods will not work on the generic stiffeners, however the result returning system in AluShip ensures that this results in a controlled error situation and not a terminal crash for the program.
- **Plates and Panels:** Both un-stiffened plates and stiffened plates can be specified. Stiffened plates are allowed to have any type of stiffener
- **Sections:** Vessel cross-sections can be built up form any arbitrary combination of plates and stiffened panels. Entire panels can be entered in the XML input file, these will be broken down into individual stiffener and plate combinations automatically, with any leftover material added to un-stiffened plate equally distributed at the panel edges.
- **Calculation methods:** For plates and panels, Paik and Duran's method, Paik and Thayamballi's method, Herzog's method, and the U.S. Aluminium Association method are fully implemented. The Eurocode 9 is only implemented for un-stiffened plates at the moment. The modified Gordo/Faulkner stress-strain method is fully implemented for plates and tee-stiffened panels in both tension and compression. A Smith-type progressive collapse approach is also implemented. S-N calculations and long-term loading calculations are also implemented, including calculating the response in any sea state, and determining the long-term distribution from a scatter diagram and operational profile. However, these two calculation methods are not yet linked to the XML input file, so can only be called by hard coding. Likewise, limited ability to export plates and tee-stiffened panels to the ANSYS finite-element packaged is included, though not yet linked to the XML input file.

Reliability-methods have not yet been introduced into the AluShip code, although source code for these methods is also available, see the final section of Appendix A for more information.

Program Structure

AluShip has been designed as a C++ object-oriented program, making use of multiple inherence, virtual classes, and class templates, making the program structure hard to decipherer from the sources file alone. In this section, the various components of the

program will be described, starting with the geometry modelling, the calculation procedures modelling, the result reporting, the loading calculations, testing procedures, and the XML parsing and integrating objects. The online documentation generated by Doxygen and included with the source code on the CD may be useful in determining further details for any of the methods or objects discussed in this section.

The geometrical modelling is comprised of several classes, as shown in Figure A-1. At the highest level is the AluMat object, which represents the material properties of one particular type of aluminium. Derived from the AluMat object are the Plate object, which adds plate geometry and property functions to the AluMat object, and the virtual stiffener object that defines the properties which each stiffener type must add to the AluMat object. Four types of stiffeners are modelled at the moment, tee stiffener, flat bars (FB), angle bulbs (AB), and generic stiffeners which are only defined in terms of the overall geometric properties. Derived from the plate object is a plate component object (PlateComp) which adds functionality for being incorporated into a structural cross section, this includes the ability to contain a stress-strain curve, fatigue details, and centeriod and area information. At the lowest level is a stiffened panel template (SPanel). This is not an object per say, but rather a set of instructions to the complier to tell it how to generate a stiffened panel object from a plate component and any stiffener object. This allows the code that calculates the properties of a stiffened panel to be written once for all type of panels, instead of requiring a separate stiffened panel object for each type of stiffener.

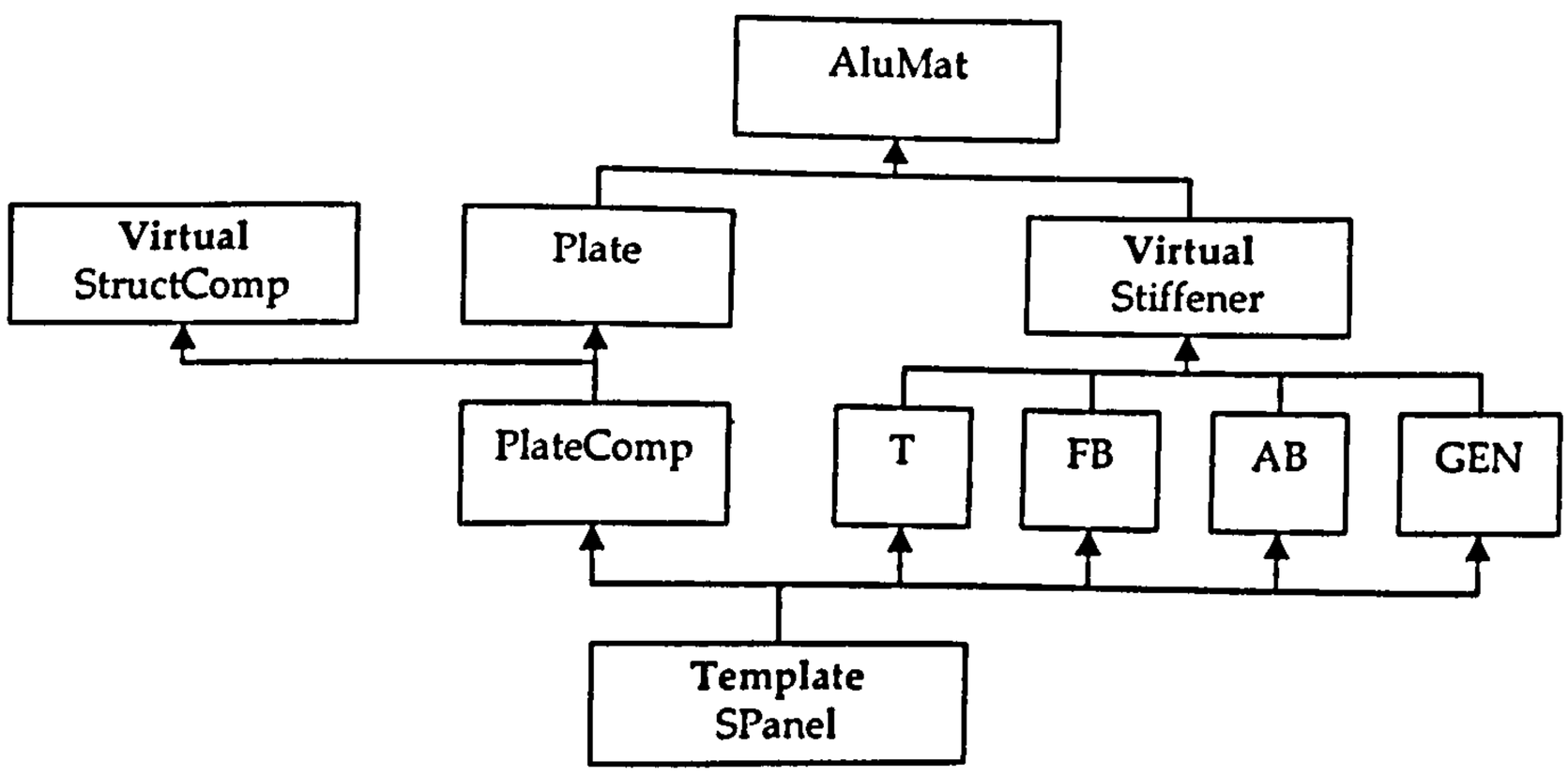

Figure A-1: Class Inheritance for Geometric Modelling

Hull cross sections are a separate objects which are not derived from any of the objects above. Instead they keep track of a list of pointers to objects that are derived from the virtual StructComp base class. Thus, at the moment, a section could include plates or stiffened panels, however, future extension to include alternative structures such as hollow

extruded decks can be made without re-writing the section object, so long as all new structural components are derived from the virtual StructComp base class.

The virtual StructComp base class also defines a "dispatchTo" method which allows the object to dispatch itself to any calculation method derived from a calculation virtual base class, vCalcMethod. This is a double-dispatch system, and allows the code for applying calculation methods to be written in general terms for all calculation methods that apply to structural components. Thus, a calculation technique can be passed to a Section object, which will in turn apply the method correctly to all the objects in the section. The Aluminum Association code, the Eurocode 9, Paik and Duran's method, Paik and Thayamballi's method, the Herzog method, and the modified Gordo method were all implemented as derived classes from the vCalcMethod class.

To keep track of the output from multiple calculation methods, a results tracking system was derived. A class was implemented that represents the results of any type of calculation, CalcResult. This class has provisions for recording the type of calculation result, reporting errors, storing a single output value or a table of output values, and recording the intermediate steps of the calculation. This class could be better implemented using an XML document object model directly for the results storage, however, at the moment it stores the data in its own internal form, and can return XML-formatted text string representing the internal results. As more than one calculation result can be assigned to one piece of structure, a ResultSet object was also created that manages a list of CalcResult objects. This object was incorporated into the PlateComp object(and thus the SPanel template) and the Section object by inheritance.

The loading calculation consists of several different objects. There is a RAO object, which allows for spline interpolation of RAO data, and allows certain description data to be appended to the RAO. A collection of RAOs can be stored in the Response object, which can return an RAO for a given speed/heading combination. Bretschneider and Pierson-Moskowitz wave spectra are currently defined, these are both derived from a virtual spectrum base class object, vSpectrum. All RAO integrations are defined in terms of vSpectrum, so additional spectra can be added to the program without rewriting any of the load calculation procedures. Operational profile and scatter diagram data are stored in the OpProfile and ScatDia classes respectively. The LoadPredict object contains functions for doing short-term and long-term load predictions from the various load definition objects. This includes a two-dimensional minimization routine to fit a Weibull distribution to the calculated long-term probabilities.

All the objects discussed above are tested individually. The test procedures have been bundled into a testing object, called test. This object controls the test accuracy required, and will log the results to a text file. A self-test on all the objects can be run automatically from the input file, which is useful for regression testing to ensure any future improvements and extensions to the code do not break existing objects.

The XML input and output files are parsed by the controller object, this uses the TinyXML library to read in the XML input file and load it into memory as a document object model(DOM). Then, the controller pareses the XML nodes, building the materials, components, and sections, and collecting them in memory. This includes breaking up large stiffened panels into their component stiffener-plate combinations. The controller then builds the calculation objects with the options specified in the XML input file, and applies them to the structural objects in memory. Finally, the output XML file is assembled and written.

Input and Output File Formats

The input and output files are both XML-formatted files, and as such are largely decipherable by eye. Four sample input files are included with the source code distribution in this thesis, a self-test file (testonly.xml) that writes a stlog.txt file containing the self-test results, Mofflin's plates (plates.xml), the collected stiffened panels (exppanels.xml) and the box girder collapse tests (boxgirder.xml). By running AluShip, the corresponding three sample output files can be generated, alternatively, they are available on the CD-ROM as the files above, with "out" added to the end. Note that some runs may take a minute or two, as the amounting of processing is quite large. Because of the length of the input and output files, only a high-level description will be given in this appendix, the sample input files and source code can be referred to for more information. The input file format is divided into the following tags:

```
<ALUSHIPRUN>
    <MATERIAL_LIST></MATERIAL_LIST>
    <STIFFENER_LIST></STIFFENER_LIST>
    <SECTION_LIST></SECTION_LIST>
    <COMMAND_LIST></COMMAND_LIST>
</ALUSHIPRUN>
```

The first section of the input file is the material list, which contains a nested list of aluminium material properties for different alloys. The preferred form of entering this information is via the "ALUMAT_T" tag, which contains separate tensile and compression material properties, however, the simpler "ALUMAT" tag can also be used containing only compression material properties, in this case, the tension and compression responses are assumed identical. Note that the material names must be unique, and will be used later to

build plates and stiffeners. Also note that at the current moment, strict ordering of the property sub-tags is necessary, as the parser does not match sub-tag name against a predefined list, it only checks that the correct number of tags have been specified. The stiffener list follows a similar form, with tags for entering flat bar, angle bulb, tee, and generic stiffeners. Examples of most of these can be found in the three sample input files. Note that each stiffener must refer to a previously-defined material. The section list is build up in a similar way, as a series of un-stiffened and stiffened plates or panels. Note that the overall breadth of the panels may be entered here, the program will automatically divide the panels into individual plate/stiffener combinations, inserting extra un-stiffened plates if the panel length can not be evenly divided into whole stiffener bays. Also note that these extra plates are not included in any individual ultimate strength calculations, and are assigned the same stress-strain curve as the rest of the panel in section ultimate strength calculations. There is no restriction on panels overlapping or their location, thus it is possible to create a "fictitious" section when only individual ultimate strength properties are of interest. This was done in the exppanels.xml and plates.xml input files, where all panels started at the origin and were of one stiffener bay in breadth.

The final section of the input file is the command list, where the various individual ultimate strength and section ultimate strength commands can be given. Individual ultimate strength commands are applied to all objects created, while section ultimate strength commands are applied to sections by name. Each command has a series of options that can be specified within the command tag, further information on these options is available in the source code.

The output file is divided into the following sections:

```
<ALUSHIP_RESULTS>
      <INPUT_ECHO_PROCESS></INPUT_ECHO_PROCESS>
      <RESULTS></RESULTS>
</ALUSHIP_RESULTS>
```

The first section is an echo of the input process as the items are built, including their geometric properties. This is useful for error-checking and being sure that the input is correct. The "RESULTS" tag contains all of the CalcResult objects created during the program run, sorted by structural component. This section of the output file is truly huge, checking it by hand is very difficult. Ideally, the output file would be loaded into an additional post-processing program which would allow the key results to be extracted and presented in tabular format, with the additional detail of the individual calculation steps available if requested, however, this program has not been written yet. A simple program

which extracts the method name, the error code, and the result value or table is discussed in the additional programs section below.

Running The Program

The current compiled AluShip executable can be found in the AluShip\bin directory of the CD-ROM included with this thesis. It runs on any 32-bit Windows machine. AluShip is run from the command line by calling the program with three arguments, the input XML *file, the desired name of the output XML file, and the name of a log file:*

```
AluShip <Input.XML> <Ouput.XML> <Log.txt>
```

Note that the output and log file will be overwritten if they exist already without warning. The log file will follow the execution of the program, noting as each object is built and as each command is processed. Error messages regarding the format of the input file will be written to the log file. Additionally, as the text log file is written as commands execute, it is the first place to look for errors as particularly bad problems may prevent the output XML file from executing correctly.

Source Code and Documentation

The source code to the AluShip project is available on the CD-ROM under the directory AluShip\src. Note that the project was assembled using the Dev-Cpp[4] C++ IDE, which is a front end to the MinGW compiler, itself a port of the GNU C++ compiler from Linux. The code should be OS-independent and should be able to be recompiled to run under Unix/Linux without any changes. There is a Dev-Cpp project file included with the source code which will allow the project to be loaded into Dev-Cpp. Note that the GNU Scientific Library(GSL) must be available in precompiled form in the Dev-Cpp installation for the program to be recompiled, GSL is available freely as noted on the first page of this appendix. The libraries are provided in binary form for Windows 32-bit applications in the GSL directory of the CD-ROM, otherwise, they can be built with the MSYS extension to MinGW.

The source code documentation is available in HTML and RTF format in the AluShip\doc directory. Documentation is provided for just about every public member of every class. Private members are documented in the source code itself, but are not documented publicly. The HTML documentation is the most useful for using on-line while browsing the source code. This documentation can be loaded into any web browser by loading the index.html file from the HTML documentation directory. Note that there is as of

[4] Available at: http://www.bloodshed.net/dev/devcpp.html

yet no user manual, as the program is not polished enough to be used without understanding the source code structure yet.

Additional Programs

Three additional programs are also include on the CD-ROM. Most of these programs are not as advanced or as rigorously reviewed as the AluShip code, they most likely have been verified for their applications in this thesis only. AluOut, in the AluOut directory of the CD-ROM is a simple program which reads through a AluShip output file, and converts the results list to a simpler text format, listing the structural component, the name of the calculation method, the error code (0 indicating no errors) and the numeric value or values table for the results. The simple text format allows these values to be easily extracted or copy and pasted into Excel or other software. It is a simple program that can be launched from the command line, and then it will ask for the input file and the output file.

As the reliability code has not been incorporated into AluShip, some of the to-be incorporated code has been added to the CD-ROM. The FOR reliability approach for the ultimate strength limit state in including in the FOR directory. This is a simple program that does not take any user input, instead, the code must be changed to run different limit states. One bug in this code is that each stochastic variable is assigned two parameters, which are noted in some output as Mean and COV, however, for non-normal distributions these values may not follow the strict definition of mean and COV, being rather, parameters related to these values, such as the X and σ terms in the Gumbel distribution. The current state of the Monte Carlo simulation code is contained in the MONTE directory, this code is currently being worked into a library. At the moment, the code is not complete, although the initial version of the library and the checking program so far are included.